

**INVESTIGATION INTO SNAP LOADING OF CABLES  
USED IN MOORED BREAKWATERS**

by

Anthony Lee Farmer

Thesis submitted to the Faculty of the  
Virginia Polytechnic Institute and State University  
in partial fulfillment of the requirements for the degree of

MASTER OF SCIENCE  
IN  
CIVIL AND ENVIRONMENTAL ENGINEERING

Approved by:

---

Raymond H. Plaut, Chairman

---

Siegfried M. Holzer

---

Kamal B. Rojiani

November, 1999  
Blacksburg, Virginia

Key Words: breakwater, snap loading, mooring lines, nonlinear dynamics, vibration

# **INVESTIGATION INTO SNAP LOADING OF CABLES USED IN MOORED BREAKWATERS**

by

Anthony Lee Farmer

Raymond H. Plaut, Chairman

Civil and Environmental Engineering

(ABSTRACT)

A two-dimensional, nonlinear dynamic analysis is conducted on a moored breakwater configuration to investigate snap loads in mooring lines. Breakwaters are structures used to attenuate or eliminate waves and protect shorelines, harbors, and other natural and man-made marine structures from wave damage. The breakwater in this investigation is modeled both as a point mass and as a rigid body. Both models are subjected to free undamped motions and forced undamped wave motion. Energy is dissipated through the use of a coefficient of restitution applied when a mooring line becomes taut (i.e., reaches its natural length). The mooring line is modeled as an inextensible cable with no axial or bending resistance when slack. Snap loading arises when a mooring line transitions suddenly from a slack condition to a taut condition. The analysis was conducted on a breakwater configured upside down and hanging by two mooring lines. The length of the mooring lines, coefficient of restitution, size and shape of the breakwater, initial position of the breakwater, amplitude of wave forcing, ratio of vertical to horizontal forcing, and frequency of forcing were all varied in the analysis. The results show that the rotations of the rigid body and the wave forcing have a significant role in the analysis, indicating that a rigid-body model for a moored breakwater under wave forcing is the more accurate model.

## Acknowledgements

I would first like to thank Dr. Raymond H. Plaut for being very supportive of me during my undergraduate years at Virginia Tech and for providing me with interesting research in my years as a graduate student. He opened my eyes to a whole new way of looking at structural problems, which are problems that do not remain static. I also would like to acknowledge Dr. Siegfried M. Holzer and Dr. Kamal B. Rojiani who have given me a tremendous amount of knowledge and guidance throughout my graduate studies and who aided me greatly as members of my graduate committee. I also appreciate the assistance in FORTRAN given to me by Dr. Raul Andruet and the research help I received from Juan Archilla. I appreciate the financial support given me for this research from the National Science Foundation Grant No. BES-9521425 and the support of the College of Engineering in the form of a Graduate Teaching Assistantship.

I would especially like to thank my parents, Calvin and Octavia Farmer, and my sister, Teresa, for all of their love and support throughout my years growing up and through my many years in college. I would like to thank all of my friends in Orange, who stuck by me during the best and worst times of my life. I would like to thank all of the interesting people I have met while at Virginia Tech and in its graduate program. The friends I have made throughout my life have been very special to me and I hold them dear to my heart. I would like to acknowledge the following people who have assisted me in my life and my studies: Bill Budd, Mark Campbell, Travis Chewing, Liz and Nate Cluff, Amy Dalrymple, Stacie Darrow, Thomas Gibson, Shelley Henkell, Andre Jackson, Rob Liberatore, Laura Miller, Bill Mack, Rich Meyerson, Mike Neubert, John Ryan, Rob Schottler, Phillip, Helen, and Leigh Skipper, Mike Sladki, Anthony Temeles, NuRocha Williams, and Chane Williamson. Finally, but most importantly, I would like to thank God for all of the blessings He has bestowed upon me during my life.

# Table of Contents

<b>Chapter 1: Introduction and Literature Review .....</b>	<b>1</b>
1.1 Introduction.....	1
1.2 Literature Review.....	1
1.2.1 Floating Breakwaters.....	1
1.2.2 Mooring Systems.....	6
1.2.2.1 Materials.....	6
1.2.2.2 Cables .....	7
1.2.2.3 Analysis of Cables .....	8
1.2.3 Snap Loading .....	10
1.3 Need for Further Research .....	13
1.4 Scope of Research.....	14
<b>Chapter 2: Problem Formulation .....</b>	<b>16</b>
2.1 Assumptions.....	16
2.2 Point-Mass Model .....	17
2.2.1 Geometrical Configuration.....	17
2.2.2 Boundaries.....	18
2.2.3 Analogy.....	19
2.3 Nondimensionalization .....	20
2.4 Equations of Motion.....	21
2.4.1 Equations of Motion at Impact .....	21
2.5 Impact .....	22
2.5.1 Definition of Impact .....	22
2.5.2 Impact Response when $g_1=0$ .....	23
2.5.2.1 Angle $\phi$ .....	23

2.5.2.2 Normal and Tangential Velocities at $g_1=0$ .....	24
2.5.3 Impact Response when $g_2=0$ .....	25
2.5.3.1 Angle $\psi$ .....	25
2.5.3.2 Normal and Tangential Velocities at $g_2=0$ .....	26
2.5.4 Snap Loading Response .....	27
2.6 Convergence to a Boundary .....	28
2.7 Solution Procedure .....	29
2.8 Development of Alternate Modeling Program .....	30
2.8.1 Numerical Modeling Program .....	30
<b>Chapter 3: Free Motions of a Point-Mass Breakwater .....</b>	<b>31</b>
3.1 Introduction.....	31
3.2 Equations of Motion.....	31
3.3 Analyzed Cases .....	31
3.3.1 Standard Case.....	33
3.4 Analysis of Data.....	33
3.4.1 Types of Graphs .....	33
3.4.2 Observations.....	34
3.5 Verification of Computer Modeling Techniques .....	40
3.5.1 Analytical vs. Numerical Solution.....	40
3.5.2 Verification of Impact Times.....	40
3.5.3 Verification of Rebound Angles .....	45
3.5.4 Verification of Impact Conditions .....	47
<b>Chapter 4: Forced Motions of a Point-Mass Breakwater .....</b>	<b>48</b>
4.1 Introduction.....	48
4.2 Wave Forcing.....	48
4.2.1 Forcing Equations .....	49
4.2.2 Analytical Solution.....	51
4.3 Analyzed Cases .....	52

4.3.1 Standard Case.....	54
4.4 Analysis of Data.....	54
4.4.1 Observations.....	55
4.4.2 Critical Force.....	62
4.4.3 Norms.....	65
4.5 Special Cases .....	67
4.5.1 No-Gravity Case.....	67
4.5.1.1 No-Gravity Case Formulation.....	68
4.5.1.2 No-Gravity Case Results .....	69
4.5.2 Harmonic Motion Case.....	72
4.5.2.1 Harmonic Motion Case Formulation .....	72
4.5.2.2 Harmonic Motion Case Results .....	73
<b>Chapter 5: Free Motions of a Rigid-Body Breakwater .....</b>	<b>80</b>
5.1 Introduction.....	80
5.2 Rigid-Body Model and Configuration.....	80
5.2.1 Rigid-Body Breakwater Shape .....	82
5.2.2 Boundary Equation Formulation .....	82
5.2.2.1 Upper Boundary Restriction .....	84
5.2.2.2 Rotation Restriction .....	85
5.3 Nondimensionalization .....	85
5.4 Equations of Motion.....	86
5.5 Rigid-Body Impact.....	87
5.5.1 Definition of Rigid-Body Impact.....	87
5.5.2 Formulation of Impact Response.....	87
5.5.3 Impact Response when $g_1=0$ .....	88
5.5.3.1 Normal and Tangential Velocities at $g_1=0$ .....	89
5.5.3.2 Impact Solution for $g_1=0$ .....	89
5.5.4 Impact Response when $g_2=0$ .....	91

5.5.4.1 Normal and Tangential Velocities at $g_2=0$ .....	92
5.5.4.2 Impact Solution for $g_2=0$ .....	92
5.6 Convergence to a Boundary .....	94
5.7 Analyzed Cases .....	95
5.7.1 Standard Case.....	98
5.8 Analysis of Data.....	99
5.8.1 Observations.....	99
5.8.2 Point-Mass Case.....	105
<b>Chapter 6: Forced Motions of a Rigid-Body Breakwater .....</b>	<b>107</b>
6.1 Introduction.....	107
6.2 Equations of Motion.....	107
6.3 Analyzed Cases .....	107
6.3.1 Stopping Criteria .....	108
6.3.2 Standard Case.....	112
6.4 Analysis of Data.....	112
6.4.1 Observations.....	113
6.4.2 Critical Force.....	125
6.4.3 Norms.....	130
6.5 Special Cases .....	137
6.5.1 Sliding Case .....	137
6.5.1.1 Sliding Case Formulation .....	138
6.5.1.2 Sliding Case Results .....	145
6.5.2 Rocking Case .....	149
6.5.2.1 Rocking Case Formulation .....	149
6.5.2.2 Rocking Case Results .....	152

<b>Chapter 7: Summary, Conclusions, and Recommendations.....</b>	<b>156</b>
7.1 Summary and Conclusions.....	156
7.2 Recommendations.....	162
<b>References .....</b>	<b>165</b>
<b>Appendix .....</b>	<b>171</b>
A.1 Other Types of Graphs .....	171
<b>Vita.....</b>	<b>180</b>

## List of Figures

Figure 2.1	Breakwater Configuration .....	16
Figure 2.2	Dimensional Parameters.....	17
Figure 2.3	Breakwater at Equilibrium State.....	18
Figure 2.4	Breakwater on Left Boundary, Right Cable Taut .....	18
Figure 2.5	Boundary with Radius Inside the Supports.....	19
Figure 2.6	Boundary with Radius Outside the Supports .....	19
Figure 2.7	Bouncing-Ball Analogy.....	19
Figure 2.8	Breakwater Configuration with Nondimensionalized Parameters .....	20
Figure 2.9	Axes at a Point on $g_1=0$ .....	24
Figure 2.10	Differential Triangle ( $dx<0, dy>0$ ).....	24
Figure 2.11	Velocity Vectors at a Point on the $g_1=0$ .....	25
Figure 2.12	Normal and Tangential Velocity Vectors .....	25
Figure 2.13	Axes at a Point on the $g_2=0$ .....	26
Figure 2.14	Differential Triangle ( $dx>0, dy>0$ ).....	26
Figure 2.15	Velocity Vectors at a Point on the $g_2=0$ .....	27
Figure 2.16	Normal and Tangential Velocity Vectors .....	27
Figure 3.1	Typical Trajectory Plot, Standard Case .....	35
Figure 3.2	Typical Normal Velocity Before Impact vs. Time Plot, Standard Case... 35	35
Figure 3.3	$y$ vs. $x$ , Case 194611 ( $r=1.5$ ).....	36
Figure 3.4	$y$ vs. $x$ , Case 294611 ( $r=2.5$ ).....	36
Figure 3.5	$v_n^-$ vs. $t$ , Case 194611 ( $e=0.9$ ).....	37
Figure 3.6	$v_n^-$ vs. $t$ , Case 174611 ( $e=0.7$ ).....	37
Figure 3.7	$v_n^-$ vs. $t$ , Case 154611 ( $e=0.5$ ).....	37
Figure 3.8	$y$ vs. $x$ , Case 114611 ( $e=1.0$ ).....	38

Figure 3.9	y vs. x, Case 194611 ( $v_x=0.6, v_y=-0.1$ ).....	39
Figure 3.10	y vs. x, Case 194010 ( $v_x=0.0, v_y=0.0$ ).....	39
Figure 3.11	Breakwater Striking Boundary Upwards.....	45
Figure 3.12	Breakwater Striking Boundary Downwards.....	45
Figure 3.13	y vs. x, Standard Case (Case 194611).....	47
Figure 3.14	y vs. x, Mirror of Standard Case.....	47
Figure 4.1	Breakwater with Horizontal and Vertical Forces.....	48
Figure 4.2	Horizontal Sinusoidal Forcing.....	50
Figure 4.3	Vertical Sinusoidal Forcing.....	50
Figure 4.4	Combined Elliptical Forcing.....	50
Figure 4.5	Comparison of $r=1.5$ and $r=2.5$ Areas.....	56
Figure 4.6.a	y vs. x, Case 190010-559, $0 \leq y \leq h_{1.5}=1.118$ .....	56
Figure 4.6.b	y vs. x, Case 190010-559, $0 \leq y \leq 0.1$ .....	56
Figure 4.7	y vs. x, 290010-559, $0 \leq y \leq h_{2.5}=2.291$ .....	56
Figure 4.8	y vs. x, Case 110010-559 ( $e=1.0$ ).....	57
Figure 4.9	y vs. x, Case 1950010-559 ( $e=0.95$ ).....	57
Figure 4.10	y vs. x, Case 190010-559 ( $e=0.9$ ).....	57
Figure 4.11	y vs. x, Case 180010-559 ( $e=0.8$ ).....	57
Figure 4.12	y vs. x, Case 170010-559 ( $e=0.7$ ).....	57
Figure 4.13	$v_n^-$ vs. t, Case 110010-559 ( $e=1.0$ ).....	58
Figure 4.14	$v_n^-$ vs. t, Case 1950010-559 ( $e=0.95$ ).....	58
Figure 4.15	$v_n^-$ vs. t, Case 190010-559 ( $e=0.9$ ).....	58
Figure 4.16	$v_n^-$ vs. t, Case 180010-559 ( $e=0.8$ ).....	58
Figure 4.17	$v_n^-$ vs. t, Case 170010-559 ( $e=0.7$ ).....	58
Figure 4.18	y vs. x, Case 190010-555 ( $\Omega=0.5$ ).....	60
Figure 4.19	y vs. x, Case 190010-5575 ( $\Omega=0.75$ ).....	60
Figure 4.20	y vs. x, Case 190010-559 ( $\Omega=0.9$ ).....	60
Figure 4.21	y vs. x, Case 190010-5515 ( $\Omega=1.5$ ).....	60

Figure 4.22	y vs. x, Case 190010-5520 ( $\Omega=2.0$ ).....	60
Figure 4.23	$v_n^-$ vs. t, Case 190010-555 ( $\Omega=0.5$ ) .....	61
Figure 4.24	$v_n^-$ vs. t, Case 190010-5575 ( $\Omega=0.75$ ) .....	61
Figure 4.25	$v_n^-$ vs. t, Case 190010-559 ( $\Omega=0.9$ ) .....	61
Figure 4.26	$v_n^-$ vs. t, Case 190010-5515 ( $\Omega=1.5$ ) .....	61
Figure 4.27	$v_n^-$ vs. t, Case 190010-5520 ( $\Omega=2.0$ ) .....	61
Figure 4.28	y vs. x, Case 190010-359 ( $f_o=0.3$ ).....	63
Figure 4.29	y vs. x, Case 190010-559 ( $f_o=0.5$ ).....	63
Figure 4.30	y vs. x, Case 190010-7559 ( $f_o=0.75$ ).....	63
Figure 4.31	y vs. x, Case 190010-1059 ( $f_o=1.0$ ).....	63
Figure 4.32	y vs. x, Case 190010-1559 ( $f_o=1.5$ ).....	63
Figure 4.33	Critical Force vs. e .....	64
Figure 4.34	Critical Force vs. $\Omega$ .....	64
Figure 4.35	$y_{max}$ vs. $f_o$ , Norm Plot .....	66
Figure 4.36	$\rho_1$ and $\rho_2$ vs. $f_o$ , Norm Plots.....	66
Figure 4.37	$\rho_3$ vs. $f_o$ , Norm Plot .....	67
Figure 4.38	y vs. x, Case 110010-01575ng ( $f_o=0.01$ ) .....	70
Figure 4.39	y vs. x, Case 110010-02575ng ( $f_o=0.02$ ) .....	70
Figure 4.40	y vs. x, Case 110010-03575ng ( $f_o=0.03$ ) .....	70
Figure 4.41	y vs. x, Case 110010-04575ng ( $f_o=0.04$ ) .....	70
Figure 4.42	y vs. x, Case 110010-05575ng ( $f_o=0.05$ ) .....	70
Figure 4.43	y vs. x, Case 115302-04575ng (Centered Ellipse).....	70
Figure 4.44	y vs. x, Case 110010-02175ng ( $\nu=0.1$ ).....	71
Figure 4.45	y vs. x, Case 110010-022575ng ( $\nu=0.25$ ).....	71
Figure 4.46	y vs. x, Case 110010-02575ng ( $\nu=0.5$ ).....	71
Figure 4.47	y vs. x, Case 110010-021075ng ( $\nu=1.0$ ).....	71
Figure 4.48	y vs. x, Standard Case with Errors (Case fspstd).....	76
Figure 4.49	y vs. x, Standard Case (Case fspstd).....	76
Figure 4.50	$v_n^-$ vs. t, Case fspo3 .....	76

Figure 4.51	y vs. x, Case fspe95 ( $e=0.95$ ) .....	76
Figure 4.52	y vs. x, Case fspstd ( $\Omega=1.5$ ) .....	77
Figure 4.53	y vs. x, Case fspo2 ( $\Omega=2.0$ ).....	77
Figure 4.54	y vs. x, Case fspo3 ( $\Omega=3.0$ ).....	77
Figure 4.55	y vs. x, Case fspo4 ( $\Omega=4.0$ ).....	77
Figure 4.56	y vs. x, Case fspo5 ( $\Omega=5.0$ ).....	77
Figure 4.57	y vs. x, Case fspstd ( $y_o=0.1$ ).....	78
Figure 4.58	y vs. x, Case fspy2 ( $y_o=0.2$ ).....	78
Figure 4.59	y vs. x, Case fspy3 ( $y_o=0.3$ ).....	78
Figure 4.60	y vs. x, Case fspy4 ( $y_o=0.4$ ).....	78
Figure 4.61	x Impact Poincaré Plot, Case fspo3 .....	79
Figure 4.62	y Impact Poincaré Plot, Case fspo3 .....	79
Figure 5.1	Dimensional Parameters.....	80
Figure 5.2.a	Rigid-Body Breakwater Shape, Circular .....	82
Figure 5.2.b	Rigid-Body Breakwater Shape, Square .....	82
Figure 5.2.c	Rigid-Body Breakwater Shape, Rectangular .....	82
Figure 5.3	Dimensions with RBBW Moved in Positive Directions.....	83
Figure 5.4	Right Cable Taut with RBBW Moved in Positive Directions.....	90
Figure 5.5	Left Cable Taut with RBBW Moved in Positive Directions.....	93
Figure 5.6	y vs. x, Case 1910121100 ( $r=1.5, a=0.1, b=0.0$ ).....	101
Figure 5.7	y vs. x, Case 2910121100 ( $r=2.5, a=0.1, b=0.0$ ).....	101
Figure 5.8	y vs. x, Case 1911121100 ( $r=1.5, a=0.1, b=0.1$ ).....	101
Figure 5.9	y vs. x, Case 2911121100 ( $r=2.5, a=0.1, b=0.1$ ).....	101
Figure 5.10	y vs. x, Case 1921121100 ( $r=1.5, a=0.2, b=0.1$ ).....	101
Figure 5.11	y vs. x, Case 2921121100 ( $r=2.5, a=0.2, b=0.1$ ).....	101
Figure 5.12	$\theta$ vs. t, 1911121100 ( $a=0.1, b=0.1$ ).....	102
Figure 5.13	$\theta$ vs. t, 1921121100 ( $a=0.2, b=0.0$ ).....	102

Figure 5.14	$\theta$ vs. $t$ , 1931121100 ( $a=0.3, b=0.1$ ).....	102
Figure 5.15	$v_n^-$ vs. $t$ , Case 1110121100 ( $e=1.0$ ).....	103
Figure 5.16	$v_n^-$ vs. $t$ , Case 1910121100 ( $e=0.9$ ).....	104
Figure 5.17	$v_n^-$ vs. $t$ , Case 1710121100 ( $e=0.7$ ).....	104
Figure 5.18	$v_n^-$ vs. $t$ , Case 1510121100 ( $e=0.5$ ).....	104
Figure 5.19	$y$ vs. $x$ , PMBW-Case 194611 .....	105
Figure 5.20	$y$ vs. $x$ , RBBW-Case 1900461100.....	105
Figure 6.1	$y$ vs. $x$ , Case 191000100-359 ( $r=1.5, a=0.1, b=0.0$ ).....	115
Figure 6.2	$y$ vs. $x$ , Case 2910001000-359 ( $r=2.5, a=0.1, b=0.0$ ).....	115
Figure 6.3	$y$ vs. $x$ , Case 1911001000-359 ( $r=1.5, a=0.1, b=0.1$ ).....	115
Figure 6.4	$y$ vs. $x$ , Case 2911001000-359 ( $r=2.5, a=0.1, b=0.1$ ).....	115
Figure 6.5	$y$ vs. $x$ , Case 1921001000-359 ( $r=1.5, a=0.2, b=0.1$ ).....	115
Figure 6.6	$y$ vs. $x$ , Case 2921001000-359 ( $r=2.5, a=0.2, b=0.1$ ).....	115
Figure 6.7	$y$ vs. $x$ , Case 2921001000-359 ( $r=2.5, a=0.2, b=0.1$ , twice scale) .....	116
Figure 6.8	$\theta$ vs. $t$ , Case 1911001000-359 ( $a=0.1, b=0.1$ ).....	117
Figure 6.9	$\theta$ vs. $t$ , Case 1921001000-359 ( $a=0.2, b=0.1$ ).....	117
Figure 6.10	$\theta$ vs. $t$ , Case 1931001000-359 ( $a=0.3, b=0.1$ ).....	117
Figure 6.11	$v_n^-$ vs. $t$ , Case 1110001000-359 ( $e=1.0$ ).....	119
Figure 6.12	$v_n^-$ vs. $t$ , Case 1910001000-359 ( $e=0.9$ ).....	119
Figure 6.13	$v_n^-$ vs. $t$ , Case 1710001000-359 ( $e=0.7$ ).....	119
Figure 6.14	$v_n^-$ vs. $t$ , Case 1510001000-359 ( $e=0.5$ ).....	120
Figure 6.15	$y$ vs. $x$ , Case 1110001000-359 ( $e=1.0$ ).....	120
Figure 6.16	$\theta$ vs. $t$ , Case 1110001000-359 ( $e=1.0$ ).....	120
Figure 6.17	$\theta$ vs. $t$ , Case 1910001000-355 ( $\Omega=0.5$ ).....	123
Figure 6.18	$\theta$ vs. $t$ , Case 1910001000-3575 ( $\Omega=0.75$ ).....	123
Figure 6.19	$\theta$ vs. $t$ , Case 1910001000-359 ( $\Omega=0.9$ ).....	123
Figure 6.20	$\theta$ vs. $t$ , Case 1910001000-3515 ( $\Omega=1.5$ ).....	123
Figure 6.21	$\theta$ vs. $t$ , Case 1910001000-3520 ( $\Omega=2.0$ ).....	123

Figure 6.22	$v_n^-$ vs. $t$ , Case 1910001000-355 ( $\Omega=0.5$ ) .....	124
Figure 6.23	$v_n^-$ vs. $t$ , Case 1910001000-3575 ( $\Omega=0.75$ ).....	124
Figure 6.24	$v_n^-$ vs. $t$ , Case 1910001000-359 ( $\Omega=0.9$ ) .....	124
Figure 6.25	$v_n^-$ vs. $t$ , Case 191001000-3515 ( $\Omega=1.5$ ) .....	124
Figure 6.26	$v_n^-$ vs. $t$ , Case 191001000-3520 ( $\Omega=2.0$ ) .....	124
Figure 6.27	Critical Force vs. $e$ ( $r=1.5$ ) .....	128
Figure 6.28	Critical Force vs. $\Omega$ ( $r=1.5$ ) .....	128
Figure 6.29	Critical Force vs. $e$ ( $r=2.5$ ) .....	129
Figure 6.30	Critical Force vs. $\Omega$ ( $r=2.5$ ) .....	129
Figure 6.31	$ \theta _{\max}$ vs. $f_o$ , Norm Plot ( $r=1.5$ ) .....	133
Figure 6.32	$y_{\max}$ vs. $f_o$ , Norm Plot ( $r=1.5$ ) .....	133
Figure 6.33	$\rho_1$ and $\rho_2$ vs. $f_o$ , Norm Plot ( $r=1.5$ ) .....	134
Figure 6.34	$\rho_3$ vs. $f_o$ , Norm Plot ( $r=1.5$ ) .....	134
Figure 6.35	$ \theta _{\max}$ vs. $f_o$ , Norm Plot ( $r=2.5$ ) .....	135
Figure 6.36	$y_{\max}$ vs. $f_o$ , Norm Plot ( $r=2.5$ ) .....	135
Figure 6.37	$\rho_1$ and $\rho_2$ vs. $f_o$ , Norm Plot ( $r=2.5$ ) .....	136
Figure 6.38	$\rho_3$ vs. $f_o$ , Norm Plot ( $r=2.5$ ) .....	136
Figure 6.39	Right Cable Taut with Dimensions in Terms of $\alpha$ and $\beta$ .....	140
Figure 6.40	Left Cable Taut with Dimensions in Terms of $\alpha$ and $\beta$ .....	141
Figure 6.41	Left Cable Taut with Forces and Virtual Displacements Shown .....	141
Figure 6.42	Breakwater with One Cable Taut (Sliding) Being Pushed by Waves .....	146
Figure 6.43	$y$ vs. $x$ , Case 1910001000-2759, Plot Showing Sliding .....	148
Figure 6.44	Circular RBBW Rocking Configuration.....	150
Figure 6.45	$y$ vs. $x$ , Case 1910001000-159, Plot Showing Rocking .....	155
Figure A.1	$x$ vs. $t$ , PMBW Standard Case .....	172
Figure A.2	$y$ vs. $t$ , PMBW Standard Case .....	172
Figure A.3	$v_x$ vs. $x$ , PMBW Standard Case .....	174

Figure A.4	$v_y$ vs. $y$ , PMBW Standard Case .....	175
Figure A.5	$v_\theta$ vs. $\theta$ , PMBW Standard Case .....	175
Figure A.6	$x$ Impact Poincaré Plot, PMBW Standard Case .....	176
Figure A.7	$y$ Impact Poincaré Plot, PMBW Standard Case .....	177
Figure A.8	$\theta$ Impact Poincaré Plot, PMBW Standard Case .....	177
Figure A.9	Total Energy vs. $t$ , PMBW Case .....	178
Figure A.10	Kinetic Energy vs. $t$ , PMBW Standard Case .....	179

## List of Tables

Table 3.1	Parameters and Initial Conditions for Free Motions of a PMBW .....	32
Table 3.2	Comparison of Impact Times Calculated by Different Methods .....	44
Table 3.3	Verification of Striking and Rebound Angles.....	46
Table 4.1	Parameters and Initial Conditions for Forced Motions of a PMBW .....	53
Table 4.2	Initial Conditions for Harmonic Motions of a PMBW .....	75
Table 5.1	Parameters and Initial Conditions for Free Motions of a RBBW.....	97
Table 5.2	Moments of Inertia for Different Shapes .....	103
Table 5.3	Comparison of PMBW Solution with the RBBW Solution .....	106
Table 6.1	Parameters and Initial Conditions for Forced Motions of a RBBW.....	111
Table 6.2	Critical Force Results of Different Size RBBW's with Different $r$ Values and Same Standard Conditions .....	126

# Nomenclature

## (Definitions of Symbols and Terms)

A,a:	horizontal dimension of breakwater, from center to edge
$a_{mn}$ :	entry in velocity matrix
B,b:	vertical dimension of breakwater, from center to edge
$b_{mn}$ :	entry in impact condition matrix
C:	center of mass of breakwater
$c_n$ :	various constants of integration
$CV_x$ :	distance from C to V in x direction
$CV_y$ :	distance from C to V in y direction
$CW_x$ :	distance from C to W in x direction
$CW_y$ :	distance from C to W in y direction
e:	coefficient of restitution
$f_{cr}$ :	critical force
$f_o$ :	amplitude of harmonic forcing function
$F_x, f_x$ :	harmonic force applied in x direction
$F_y, f_y$ :	harmonic force applied in y direction
g:	gravitational acceleration
$g_1$ :	circular arc defined by right cable being taut
$g_2$ :	circular arc defined by left cable being taut
H,h:	height of region U
$I_c$ :	mass moment of inertia about its center
J:	left connection of cable to breakwater
$JV_x$ :	distance from J to V in x direction
$JV_y$ :	distance from J to V in y direction
K:	right connection of cable to breakwater

KE:	kinetic energy
$KW_x$ :	distance from K to W in x direction
$KW_y$ :	distance from K to W in y direction
L:	Lagrangian
m:	mass of breakwater
PE:	potential energy
$Q_q$ :	generalized force for coordinate q
q:	coordinate (x, y, $\theta$ , $\alpha$ , or $\beta$ )
R/r:	length of cable (radius of $g_1$ or $g_2$ circular arc)
S,s:	spacing between centerline of the symmetric configuration and a support
T,t:	time
$T_x, t_x$ :	phase for harmonic horizontal force component $F_x$
$T_y, t_y$ :	phase for harmonic vertical force component $F_y$
U:	valley-shaped region defined by circular arcs $g_1$ and $g_2$
V:	left support of cable to breakwater
$v_n$ :	normal velocity
$v_t$ :	tangential velocity
$v_x$ :	velocity in x direction
$v_y$ :	velocity in y direction
W:	right support of cable to breakwater
X,x:	horizontal direction
$\dot{x}$ :	velocity in x direction
$\ddot{x}$ :	acceleration in x direction
Y,y:	vertical direction
$\dot{y}$ :	velocity in y direction
$\ddot{y}$ :	acceleration in y direction
$\alpha$ :	angle from vertical to taut mooring line

$\beta$ :	angle from vertical to line between connection points
$\gamma$ :	incoming and rebound angle
$\delta$ :	virtual displacement
$\delta W$ :	virtual work
$\theta$ :	angle of rotation of breakwater measured about its centroid
$\dot{\theta}$ :	angular velocity of breakwater measured about its centroid
$\ddot{\theta}$ :	angular acceleration of breakwater measured about its centroid
$\lambda, \lambda_1, \lambda_2$ :	Lagrange multipliers
$v$ :	ratio of amplitude of $f_y$ to amplitude of $f_x$
$\phi$ :	angle measured from horizontal to tangent line at point on $g_1$ circular arc
$\psi$ :	angle measured from horizontal to tangent line at point on $g_2$ circular arc
$\Omega$ :	frequency of harmonic forces

Note:

- upper case letters represent dimensional parameters
- lower case letters represent nondimensional parameters
- subscript (i) indicates a variable at time of impact or new initial condition after impact
- subscript (m) integer indicates column position in matrix
- subscript (n) integer indicates row position in matrix
- subscript (x) indicates a variable in the horizontal direction
- subscript (y) indicates a variable in the vertical direction
- subscript ( $\theta$ ) indicates a rotational variable
- superscript (-) indicates a variable just before impact
- superscript (+) indicates a variable just after impact
- dot ( $\bullet$ ) indicates a derivative
- subscript (o) indicates an initial condition
- hat ( $\wedge$ ) indicates impulsive action

# Chapter 1

## Introduction and Literature Review

### 1.1 Introduction

Breakwaters are structures used to attenuate or eliminate waves. They help prevent damage to shorelines, harbors, and other natural or man-made marine structures. There are two types of breakwaters; one is a fixed barrier structure and the other is a moored floating type. Several different forms of floating breakwaters have been investigated and used for various applications in the past. Now inflatable floating breakwaters are being investigated for potential use and are the focus of this research. However, the primary motivation of this research is to investigate a simple model of snap loading that occurs in the cable mooring system of a breakwater and investigate fatigue of the cables due to snap loading.

The purpose of this research is to investigate the mooring system of a floating breakwater which moves about a region, causing its mooring cables to transition between slack and taut conditions. The breakwater will be modeled as a point mass and a rigid body, both of which will be subjected to free and forced motions. The analysis will be performed in two dimensions and the snap loading in the mooring system will be monitored.

### 1.2 Literature Review

#### 1.2.1 Floating Breakwaters

Little attention was paid to the use of floating or transportable breakwaters until the necessity arose of landing men and materials during the Normandy invasion of World

War II. Two types of breakwaters were used during this event. The first were fixed breakwaters that were barges floated from Great Britain positioned just off shore and sunk. The second were actual floating breakwaters of cruciform cross section (Hales 1981). These “Bombardon” floating breakwaters were steel structures arranged in two lines along the Normandy coast. The controversial decision to use this floating breakwater was made after theoretical analyses and hydraulic model testing were conducted by Great Britain (Tsinker 1995). These breakwaters both served their purpose to dissipate the waves of the English Channel and provide shelter for invading troops and their materials during the crucial invasion. The “Bombardon” breakwaters were successful during the invasion, but they later failed during a storm which created stresses eight times larger than those for which they were designed.

Use of floating breakwaters declined over the following years until the 1950’s, when the U.S. Navy saw the potential of these structures to protect small craft and marine structures from open-ocean waves (Hales 1981). As people started moving towards the coasts during the 1960’s, the need to protect boats and structures increased. Later, studies were performed on the use of breakwaters to protect beaches, harbors, pleasure craft, and other important natural and man-made marine structures from the effects of waves. Some of these studies are Carver et al. (1987), Gaythwaite (1987), and Mays (1997, 1999).

Thus, over the years, many different types of floating breakwaters have been developed and many conclusions have been made as to their effectiveness. Some of the advantages of floating breakwaters include the following:

1. Floating breakwaters are less expensive than fixed structures in deeper water (depths greater than 10 feet) (Hales 1981).
2. Floating breakwaters can effectively attenuate moderate wave heights (less than about 6.5 feet) (Tsinker 1995).

3. Poor soil conditions may make floating breakwaters more feasible to use than heavy rubble fixed breakwaters (McCartney 1985).
4. Floating breakwaters produce minimal interference on water circulation, sediment transport, and fish migration (Kelly 1999).
5. Floating breakwaters can be easily moved and rearranged in different layouts or transported to another site (Hales 1981).
6. If ice formation presents a problem, floating breakwaters can be removed from the site (McCartney 1985).
7. Floating breakwaters are not as obtrusive as fixed breakwaters and can be more aesthetically pleasing (McCartney 1985).

Some of the disadvantages of floating breakwaters are the following:

1. Floating breakwaters are less effective in reducing wave heights for slow waves than fixed structures are; a practical upper limit for the design wave period is in the range of 4 to 6 seconds (equal to a minimum frequency of 1.0 rad/s to 1.6 rad/s) (Tsinker 1995).
2. Floating breakwaters are susceptible to structural failure during catastrophic storms (Tsinker 1995).
3. If the structure fails and is detached from its moorings, the breakwater may become a hazard (Kelly 1999).
4. Relative to common fixed breakwaters, floating breakwaters require a high amount of maintenance (Tsinker 1995).

Advantages and disadvantages of the use of inflatable breakwaters came up during a discussion with Mr. Howard Kelly of the Naval Facilities Engineering Command in Norfolk, Virginia in July of 1999. Mr. Kelly stated that some potential advantages to using inflatable structures as breakwaters include the following:

1. As opposed to a rigid breakwater, which absorbs wave energy by its mass and mooring system, inflatable breakwaters may absorb energy through the structure's deformations as well.

2. When the breakwater is not required, it may be deflated and stored efficiently.
3. The breakwater may be inflated onshore or on a ship.
4. Moorings could be left in place and structures floated to the site when needed.

Some disadvantages may include the following:

1. Inflating and towing would require higher labor costs than structures which are left in place.
2. The structure has the possibility of becoming punctured.

There are an extensive number of different types of floating breakwaters in existence today. The types of floating breakwaters may be seen as combinations of variations of materials, breakwater shape, its mooring system (including configuration), and its function. These variables generate a large list of possible floating breakwaters; however, they can be divided into four basic groups: box, pontoon, mat, and tethered float (McCartney 1985).

Most box-type breakwaters are reinforced concrete, rectangular-shaped modules that may be flexibly or rigidly connected to other modules to make a larger breakwater. Box breakwaters may also be constructed of steel or even barges. These structures have proved to be effective and have several uses, including recreational and temporary boat moorage. The main disadvantages for these structures are that they are considerably more expensive than mat types and require higher maintenance. One parameter that restricts the design of these structures is the  $L/W$  (wavelength-to-breakwater width) ratio. McCartney (1985) shows that as this value increases, the wave transmission coefficient decreases. The wave transmission coefficient is the ratio between the wave height after striking the breakwater and the incident wave height. For design purposes, the wave transmission coefficient should be as low as possible for the given case; this indicates that the wave heights are being decreased.

Pontoon types include several different models, such as the ladder type, catamaran type, sloping-float (inclined pontoon), and a frame type. This group of breakwaters has been investigated extensively by experimentalists and theorists. These prismatic structures are ideal for other uses such as floating walkways, storage, boat moorings, and fishing piers (Hales 1981). Pontoon types are generally less expensive than box types and have similar advantages and disadvantages to the box type. Attention must be paid to the L/W parameter, to control deformation, as it was in the box type (McCartney 1985).

An interesting way of dealing with the ever-increasing number of old tires is to bind a group of them together to create a floating breakwater. There are three basic designs for tire mat breakwaters; these are known as Wave Maze, Goodyear, and Wave-Guard (Hales 1981). The many advantages and disadvantages were discussed by DeYoung (1978) and McCartney (1985). Some advantages of the tire mat breakwater include low cost, simple design and construction, portability, low anchor loads, and greater effectiveness than box and pontoon types. Disadvantages include lack of buoyancy, 15-20 year design life, they do not effectively damp long wave lengths, they cannot be moored year round because of icing effects, and they can break apart if not constructed adequately and then they would create floating debris.

The last type of floating breakwater is the subject of this thesis, the tethered (moored) floating breakwater. Unlike the other types of breakwaters, which use their mass to attenuate waves, the tethered floating breakwater uses its mooring system to dissipate wave energy. This is accomplished by restricting the motions of the breakwater by use of a mooring system. Waves move the breakwater around until the mooring system restricts its motion; then wave energy is transferred to the anchors and ultimately the sea floor, dissipating the wave height. Work involving this type of breakwater has been performed by Mays (1997, 1999) and Archilla (1999); however, this type of breakwater is still under investigation and there is not a significant amount of information on these moored breakwaters to make any conclusive remarks. Thus, the remainder of this literature

review will cover the theoretical and limited experimental research completed on these types of breakwaters, along with a review of applicable mooring systems and slack/taut behavior of cables.

## **1.2.2 Mooring Systems**

Several reviews of mooring systems have been conducted. There are several types of systems used to moor a breakwater to the sea floor. Some of these are piling, mass anchors and line, and stake piles and line (McCartney 1985). The choice of a mooring system depends on the type of breakwater to be used and the site conditions where it is to be placed. This investigation will be concerned with the lines used in a mooring system and not the anchors. McCartney (1985) discusses further about the configuration of mooring lines and types of materials used.

### **1.2.2.1 Materials**

There are several types of materials, mooring line setups, and configurations that have been discussed in the literature. McCartney (1985) and Skop (1988) both discuss the material and mechanical properties and characteristics of different material types used for mooring lines. A wide variety of available materials were covered, such as synthetic line, chain, and wire ropes or cables. Sensibly, the mooring system must possess a high resistance to corrosion and wear due to the harsh environment in which it is exposed. The offshore industry is starting to use synthetic materials in mooring systems because they are corrosion resistant and are lighter than the steel materials commonly used. Several types of synthetic materials are available for mooring systems; these materials include nylon, dacron, polyester, polypropylene, polyethylene, and kevlar. Ansari (1980) discusses how sometimes a mooring system may be segmented in a multicomponent setup with a combination of materials used in one single line. For example, steel chain is commonly connected to the anchor (to provide extra weight and abrasion resistance) and the floating body (to provide extra strength and weight for added stability), with a different material in between for economic, mechanical, and property reasons. Other

papers dealing with mooring systems include Gaythwaite (1987), Chaplin and Del Vecchio (1992), D'Souza et al. (1993), Dercksen and Hoppe (1994), Bernitsas et al. (1996), and Szelangiewicz (1996). Whatever the material used, the mooring system must be designed adequately to resist the mooring forces induced by the absorbed wave energy.

### **1.2.2.2 Cables**

This investigation will consider a non-segmented homogeneous mooring line. String, rope, wire, chain links, and cables are all members of a family known as tension members. A tension member has the interesting property of being able to resist tensile forces but poorly resists flexure and compression. A cable is typically known and referred to as a steel member either in strand or wire rope form used to transfer tensile forces. Cables, in one form or another, have been used for centuries as structural components. Many ancient civilizations, like the Chinese and Incas, constructed suspension bridges to span rivers and gorges. Handmade forms of cables date back to Babylonian and Roman times. Not until 1834 did a German, A. Albert, first produce wire rope mechanically. The methods he used to produce this early cable are still used today (Scalzi et al. 1969). Applications of cables in structures include suspension bridges, marine anchoring systems (e.g., buoy anchors), wind-resisting systems in buildings (e.g., lateral X bracing), construction applications (e.g., cranes), towing and securing of objects (e.g., tugboats and mooring), and even in space as tethering components. Cables are everywhere and it is hard not to see a use for them as structural components.

The major disadvantage of cables is that they lack rigidity in bending and compression and are useful only when a member in a structure is designed to carry tension or when a component must have little resistance to bending. This property makes cables ideal for use in mooring systems. Leonard (1988) states some of the advantages of cable members for use as structural components:

1. They are lightweight and collapsible, and therefore easy to transport and erect.
2. They can be prefabricated in a factory, have low installation costs, and are potentially relocatable.
3. Loads can be efficiently carried by direct stress without bending.
4. They are load-adaptive in that the members change geometry to better accommodate changes in load patterns and magnitudes.

Also, cables can be quite pleasing aesthetically when left exposed to the public eye. An excellent example of this is the Brooklyn Bridge in New York City with its diagonal cable stays. With these considerations in mind, an engineer can easily take advantage of the properties of cables in order to design a safe and economic structure.

### **1.2.2.3 Analysis of Cables**

In order for engineers to design an adequate cable component, they must analyze it for static and dynamic loads. As seen in texts such as those by Irvine (1981) and Leonard (1988), there has been much research and analysis on cable configurations under static conditions. These texts give standard equations for various geometric configurations of cables under different loading conditions. Using geometric and trigonometric principles and basic laws of statics, one can analyze a cable structure under static loads fairly easily.

The primary focus of recent research has been the response of cables under dynamic loading conditions. The two chief dynamic responses of cables include free movement and vibration. Free movement is the behavior of a cable as it moves freely in space. Irvine (1981) discusses the vibration analysis of cables. Time-varying forces such as wind, wave action, and earthquake loading may cause these vibrations. Bathe (1982) states that if time-varying forces shake a structure at less than one-third of the lowest natural frequency of vibration for the structure, the response is essentially static in nature and dynamic motions and stresses can be considered to be negligible. At higher frequencies the inertial forces on the structural components are mobilized and dynamic

motions become important. For extremely high frequencies, greater than four times the highest natural frequency of vibration for the structure, there is insufficient time for the structure to respond to the load before the direction of load reverses, and therefore the dynamic motions may be small.

Leonard (1988) states that in tension structures, the stiffness is relatively small compared to other structural components, but their mass may be large because of attached components or cladding. Since natural frequencies are proportional to the square root of the stiffness-to-mass ratio, the natural frequencies of tension structures can be expected to be smaller than for most other structural types. Dynamic responses to time-varying loads are more significant for tension structures in that dynamic stresses superposed on loading may lead to failure of members as a result of overstressing or fatigue. Leonard (1988) continues to say that stiffness is proportional to cable tension, that is, if a tensile component is overstressed by an applied load, the natural frequency will drop, because frequency is proportional to stiffness, making the component more susceptible to dynamic load responses.

Hence, since cables have little stiffness, thus producing low natural frequencies, and due to the fact that natural frequency and load are related, dynamic analysis of tension structures is vital. Dynamic analysis should be considered on a case-by-case basis, since some structures are more susceptible to dynamic load conditions (like suspension bridges) than others (like a wind-resistant component of a building). As a result, from these basic facts, much research has been done in the area of dynamic effects on cable components and cable systems involved in structures.

The major types of dynamic response phenomena associated with flexible systems are forced vibrations, self-induced vibrations (self-excitation), and flutter. Forced vibrations of flexible components and systems come from such time-varying external loads as wind, waves, or earthquakes. Structures have the ability to damp these oscillations out over

time. When a structure goes through some displacement or deformation and then returns to its original configuration, the internal forces that return it are known as self-induced internal forces or self-excitation. Flutter is a vibration associated with a fluid moving across a flexible member (e.g., wind and water) and may cause failure of the structure (Scalzi et al. 1969).

These effects occur frequently in marine anchoring systems, since wave action tends to toss objects around easily, causing the mooring cables to transition between slack and taut conditions repeatedly. Therefore, mooring cable dynamics is another topic in which much research has been performed. The need for adequate marine anchoring systems for many offshore and subsea engineering projects is obvious. Researchers like Liu (1973), Lo (1982), Brekke and Gardner (1988), Niedzwecki and Thampi (1991), and Huang and Vassalos (1993, 1995, 1996) investigated many different topics involved in the area of marine cable anchorage, suggesting design criteria and methods of analysis. The development of analytical methods for nonlinear marine cable analysis has met with much difficulty since researchers were unable to solve the highly nonlinear governing equations involved in finite deformation analysis, and the stress-strain relationships for inelastic materials were not well established. But perhaps the most important reason is that the interest in such analysis was not stimulated until the widespread use of cables as structural elements occurred. Students of mechanics and applied mathematics have known small-deflection, isotropic, linearly elastic solutions for cables for many years. However, the applicability of linear solutions is limited because nonlinear effects are generally predominant in anchoring systems (Lo 1982).

### **1.2.3 Snap Loading**

“Snap loading” and “snatch loading” are terms used to describe a dynamic response which arises when a cable goes through a transition from a slack condition to a taut condition suddenly (i.e., over a small interval of time). “Taut” in the sense of this thesis means that the cable has been stretched out and has reached its natural length. Similar

but slightly different definitions will be discussed later. This phenomenon of becoming taut suddenly is like an impact and may be very violent. Because snap loading may be several orders of magnitude greater than static or simple dynamic loading, where the tension member stays taut in both cases, cables usually exhibit a jerk, accompanied by impulsive forces. This phenomenon may be attributed to the high tensile capacity but low compressive and flexural resistance of cables. Snap loading is very significant to the life of a cable, because cables are susceptible to fatigue when subjected to cyclic loading. This phenomenon has applications to other cable structures, such as suspension and cable-stay bridges, cable-suspended roof systems, and moored marine structures, all of which undergo dynamic loading. This thesis will investigate snap loading in the cables of a floating breakwater mooring system.

In Juan Archilla's Master's thesis (1999), for example, mooring lines were modeled as compressionless springs. When a line was slack (i.e., the distance between its ends was smaller than its natural length), it was assumed that the line had no effect on the breakwater. When a line was taut, it acted like a linear spring. During motions in which a line became alternately slack and taut, large tension loads (snap loads) occurred in the line during the taut phases. Here a simpler model is considered. Instead of being extensible, the lines are assumed to be inextensible. When a line becomes taut, it is assumed to instantaneously rebound and become slack again. This can be related to the motion of a bouncing ball. The objective of this thesis is to examine the behavior of mooring lines using this simple model.

Several researchers performed investigations into the phenomenon of snap loading. Snap loading is defined by the researchers as sudden re-tensioning of a slack cable, producing a spike in the tension of the member. However, not everyone described the same conditions under which this phenomenon arose. Some papers regarding this topic are summarized below. Goeller and Laura (1971) and Laura and Goeller (1971) considered experimental and analytical studies of a vertically hanging segmented cable system. The

top portion is composed of steel and the bottom segment is composed of nylon. The cable was analyzed as a structure used to deliver or recover a payload from the sea floor. Forced oscillations were imposed on the system, and it was found that “snap loading” conditions occurred in the steel portion of the cable before resonance was achieved. “Snap loading” in this sense was defined as occurring when one section or both became slack and then taut all of a sudden. Impact loads from the cable becoming taut suddenly were found to be up to nine times the static payload. Such high impact loads or “snap loads” can cause catastrophic failure.

Huang and Vassalos (1993, 1995, 1996) performed a significant amount of research in determining methods for solving the highly complex dynamics of cables when used in anchoring systems. They derived mathematical models for the geometric motions of the marine cables and the forces that cables experience. Their models include allowances for the following:

1. Three-dimensional motion.
2. Large displacements. No linearization is made based on a small-amplitude motion assumption.
3. Inclusion of forces due to the weight of the cable, buoyancy, drag, and inertia of the fluid.
4. Non-uniform cables. Their approach has the capacity to include any subsystems, such as hanging weights on the cable.
5. Bi-linear axial stiffness of the cable operating in alternating taut-slack conditions.

Their models are a powerful means of solving for the dynamic responses of cables, like forces and motions. Their theoretical results were confirmed by previous experimental research. In the analyses described, they define snap loading as occurring when a portion of a cable, modeled as lumped masses connected by massless springs, becomes slack and then taut suddenly while the rest stays taut.

Liu (1973) looked at how surface waves affected the cables in mooring systems as well as when packages are being lowered to the sea floor. Liu defined three different types of tension loads on the mooring lines: static tension load, dynamic tension load, and snap load. The static tension load was simply the initial weight of the cable system. The dynamic tension load was defined as the maximum increase or decrease in tension from the static load. Snap load was defined, in this case, as the sudden tensioning of a slack cable system after a state of zero tension and is a special type of dynamic loading. It was found that this load usually occurred for very short periods of time, but was often orders of magnitude greater than static and dynamic tension loads, and would significantly impact the design of the mooring system.

The work of other authors in this area includes Suhara et al. (1981), who performed a similar analysis to Huang and Vassalos, but investigated the dynamic behavior and tension force of oscillating mooring chains. They describe snap loading as when the chain slacks and becomes taut in a short interval of time. Niedzwecki and Thampi (1991) expanded on the investigations into the dynamic response of cables when packages were being delivered to the seabed, defining snap loading as a severe impact upon re-tensioning which is several orders of magnitude larger than normal static and dynamic loads. More papers available on the slack/taut behavior of cables and mooring lines are Brekke and Gardner (1988), Milgram et al. (1988), Shin (1991), Driscoll and Iggins (1993, 1996), Patel et al. (1994), and Patel and Park (1995).

All of these investigations show that the dynamic analysis of cables is important and that the effects of snap loading should play a significant role in the design of a mooring system in marine situations. Although these authors looked at different applications of cables, they all investigated the dynamic response of these cables to external and internal effects. Their results give good insight into cable dynamics, as they propose methods for analysis and design of cable systems in marine applications especially relevant to the mooring system of a breakwater.

### **1.3 Need for Further Research**

Most previous research studies, as seen in the previous discussion, dealt with slack/taut conditions in cables where “taut” was defined as “positive tension,” and some have talked of “snap loads” when a cable exhibits a transition from zero to positive tension in a small interval of time. Souza de Cursi (1992) defines another concept of “taut:” when a cable reaches its “natural length.” Therefore, when the distance between the ends is less than its “natural length,” the cable is thought to be slack, and conversely, when the distance between its ends is equal to its “natural length,” then it is considered to be taut. When a cable goes from a slack to a taut condition suddenly, a jerk is felt in the cable, which is analogous to an impact with some loss of energy. This situation is defined as snap loading and produces a spike in the tension of the member. This loading is considered as being felt throughout the cable and is not localized as others might suggest. Whatever the situation, when the tension peaks suddenly, this has a significant effect on the life of a cable and should be of interest. This concept has not been investigated in detail in the literature; thus, this definition of “taut” in association with the term “snap loading” will be investigated in detail in this thesis.

### **1.4 Scope of Research**

This thesis will investigate a simple model of snap loading that occurs in the cable mooring system of a breakwater and investigate fatigue of the cables due to snap loading. Four problems were investigated. Each consisted of several cases, which were created by varying parameters and initial conditions for those cases. The basic formulation of these problems is discussed in Chapter 2. The motions of the breakwater will be studied in a two-dimensional vertical plane.

The first problem investigated is discussed in Chapter 3. This problem had the breakwater modeled as a point mass which would undergo free vibration. Free motions are where the only forces acting on the breakwater are buoyancy and gravity.

The second problem investigated is discussed in Chapter 4. This problem still had the breakwater modeled as a point mass, but it was subjected to sinusoidal horizontal and vertical forcing which when combined form an ellipse. This elliptical forcing is a mathematical model of natural wave forcing.

The third problem investigated is discussed in Chapter 5. This problem investigated free motions like the first problem, but now the point-mass breakwater is given dimensions and becomes a rigid-body breakwater with free motions.

The fourth problem and final problem investigated is discussed in Chapter 6. This problem investigated a rigid body undergoing forced wave motions. The third and fourth problems are very similar to the first and second except that angular positions and velocities of the breakwater are added. These angular variables modify the breakwater's response when a cable becomes taut; however, the solution procedure stays the same.

## Chapter 2

### Problem Formulation

#### 2.1 Assumptions

Before beginning to formulate the mathematics of the problems to be investigated, certain assumptions will be made in order to simplify the analysis. For the analysis, the breakwater will be investigated in a planar fashion and is modeled in cross-section. Normally a breakwater would float in a body of water that would give an upward buoyant force greater than the downward gravitational force. However, in this project the breakwater is considered upside-down with the net buoyant force equal to the gravitational force, and it could also represent an object hanging by two cables (Fig. 2.1).

Further assumptions are that the mooring cables are inextensible and the weight, inertia, bending resistance, and axial resistance in compression of the cables are neglected. During an “impact,” when a cable becomes taut, the cable will dissipate some energy and this will be accounted for in a coefficient of restitution,  $e$ , which will be explained in more detail later. Finally, no other “damping” is considered in the system; this includes any damping that would come from the surrounding fluid, and internal dissipation of energy in the cables.

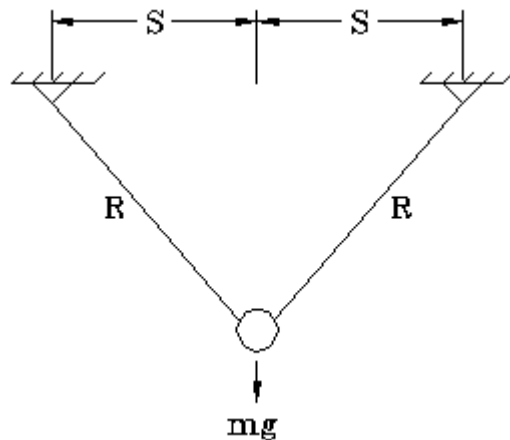


Fig. 2.1 Breakwater Configuration

## 2.2 Point-Mass Model

During the first part of this investigation, the breakwater will be modeled as a point mass. Free vibrations are considered first, followed by the response to harmonic forcing. The following formulation is for the point-mass configuration under free motions.

### 2.2.1 Geometrical Configuration

In this formulation, the breakwater has no dimension so it is seen as infinitesimally small and is treated as a point mass. The geometric configuration of the breakwater and its mooring system is arranged in such a manner that the components are symmetric. The two cables are of equal length and are suspended from the same height. The configuration of the moored breakwater, with its dimensional parameters, can be seen in Fig. 2.2. This figure also shows

that the origin of the global X-Y axes is located at the center of the breakwater when it is at its lowest point, its equilibrium state with both cables taut. The coordinates  $x$  and  $y$  define the position of the point mass. Figure 2.2 shows the separation length of the supports as  $2S$ , and the “taut” (natural) length

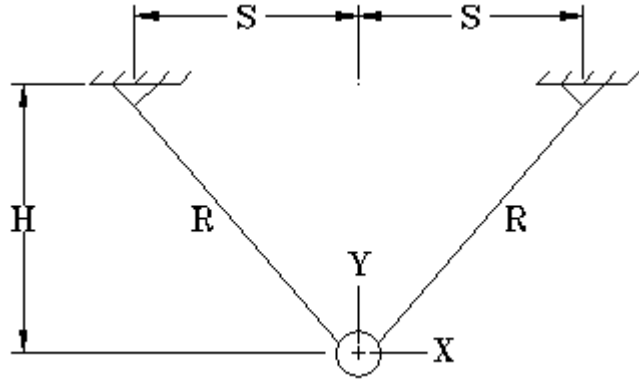


Fig. 2.2 Dimensional Parameters

of each cable as  $R$ . “Taut” in this sense means the cable has been stretched out and has reached its natural length. In order for the breakwater to float, the following condition must be satisfied:

$$R > S \quad (2.1)$$

With these dimensions, the distance,  $H$ , from the supports to the breakwater’s lowest point in its equilibrium state may be defined by

$$S^2 + H^2 = R^2 \quad (2.2)$$

Further restrictions are placed on the breakwater of mass  $m$ . Motions of the mass must remain below the height of the supports (i.e., the breakwater not hitting the sea floor) and at or above the equilibrium position shown in Fig. 2.2. Therefore the following restriction on  $Y$  must be met:

$$0 \leq Y \leq H \quad (2.3)$$

There are two degrees of freedom in this system:  $X(T)$ ,  $Y(T)$ , where  $T$  = time.

### 2.2.2 Boundaries

As stated before, the extreme vertical limits are the lowest point being  $Y=0$ , with both cables taut (Fig. 2.3), and the highest being  $Y=H$ , the sea floor. Now the horizontal limits must be defined. If the breakwater moves with one cable being taut, as shown in Fig. 2.4, one can see that a boundary is formed where that cable can be extended no further than its natural length. A left boundary,  $G_1=0$ , is formed when only the right cable is taut, and a right boundary,  $G_2=0$ , is formed when only the left cable is taut.



Fig. 2.3 Breakwater at Equilibrium State

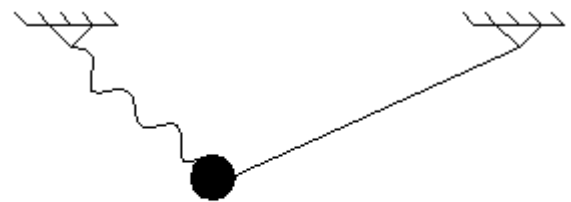


Fig. 2.4 Left Boundary, Right Cable Taut

The boundaries form circular arcs (Figs. 2.5 and 2.6 in nondimensional form) with the radius being the length of the cable and the limits being  $Y=0$  (equilibrium state) and  $Y=H$  (sea floor). Two cable lengths were investigated, one length where the breakwater would stay inside its supports (Fig. 2.5) and one where it could go outside of its supports (Fig. 2.6). If the right cable is taut, the left circular boundary,  $G_1=0$ , may be defined by

$$(X-S)^2 + (Y-H)^2 = R^2 \quad (2.4)$$

If the left cable is taut, the circular boundary,  $G_2=0$ , may be defined by

$$(X+S)^2 + (Y-H)^2 = R^2 \quad (2.5)$$

Thus the motion of the breakwater mass must remain in the region U (Figs. 2.5 and 2.6)

where

$$0 \leq Y \leq H: \quad (X-S)^2 + (Y-H)^2 - R^2 \leq 0 \quad (G_1 \text{ equation}) \quad (2.6)$$

$$(X+S)^2 + (Y-H)^2 - R^2 \leq 0 \quad (G_2 \text{ equation}) \quad (2.7)$$

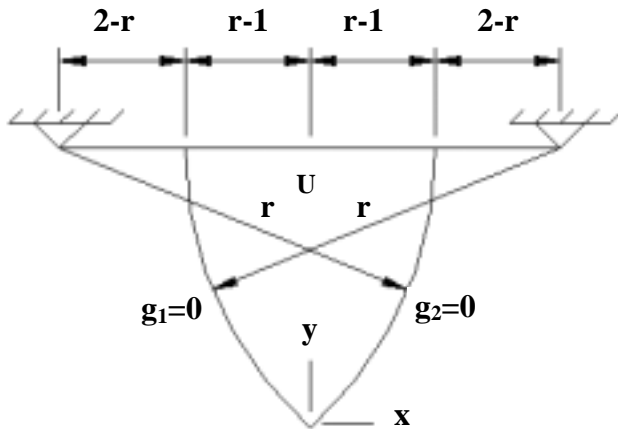


Fig. 2.5 Boundary with Radius Inside Supports

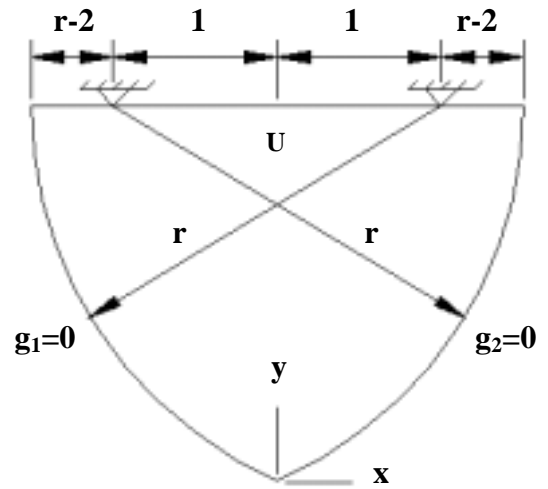


Fig. 2.6 Boundary with Radius Outside Supports

### 2.2.3 Analogy

The model resembles a bouncing ball in a valley or U shaped region with gravity acting

on it, which causes the ball to end

up at the bottom (Fig. 2.7) if no

other forces are applied. The ball

loses energy when it “impacts”

and bounces. When it is said that

the breakwater impacts, this is

defined as a cable becoming taut

and the breakwater reaching a

boundary  $G_1=0$  or  $G_2=0$ .

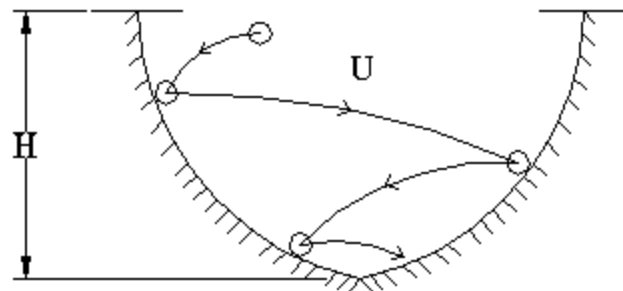


Fig. 2.7 Bouncing-Ball Analogy

### 2.3 Nondimensionalization

The variables used in the formulation of the problem have been nondimensionalized, so that the units will not be involved during this investigation. Length parameters were nondimensionalized by the cable spacing,  $S$ , and time by

$$\sqrt{S/g} \quad (2.8)$$

Mass is divided by itself and becomes unity. Uppercase letter symbols are used when terms have dimensions and lowercase letters are used to represent the nondimensionalized values. Thus, the parameters become

$$x=X/S \quad (2.8)$$

$$y=Y/S \quad (2.9)$$

$$r=R/S > 1 \quad (2.10)$$

$$h=H/S = \sqrt{r^2 - 1} \quad (2.11)$$

$$t = T\sqrt{g/S} \quad (2.12)$$

The nondimensionalized geometric parameters may be seen in Fig. 2.8.

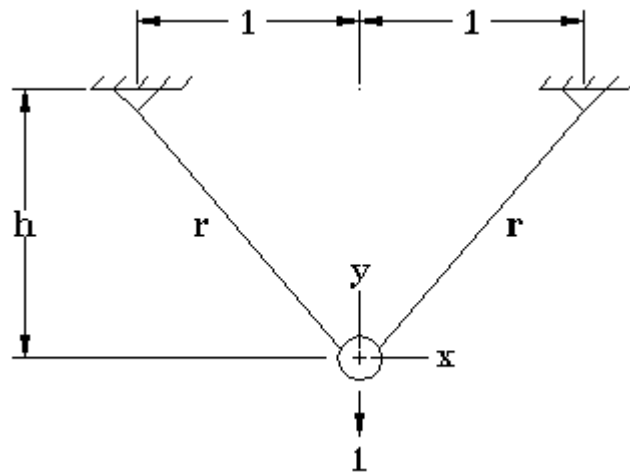


Fig. 2.8 Breakwater Configuration with Nondimensionalized Parameters

## 2.4 Equations of Motion

Inside the region, U, both cables are slack, and the only force acting on the breakwater during free vibration is gravity. Thus, simple Newtonian equations of motion are applicable:

$$F=ma \quad (2.13)$$

$$m \frac{d^2X}{dT^2} = 0 \quad (2.14)$$

$$m \frac{d^2Y}{dT^2} = -mg \quad (2.15)$$

After the nondimensionalization, the basic equations of motion (EOM's) become

$$\ddot{x} = 0 \quad (2.16)$$

$$\ddot{y} = -1 \quad (2.17)$$

where  $\bullet = \frac{d}{dt}$

The solutions for this formulation are

$$x(t) = x_o + \dot{x}_o t \quad (2.18)$$

$$\dot{x}(t) = \dot{x}_o \quad (2.19)$$

$$y(t) = y_o + \dot{y}_o t - \frac{1}{2} t^2 \quad (2.20)$$

$$\dot{y}(t) = \dot{y}_o - t \quad (2.21)$$

where the initial conditions at  $t=0$  are

$$x(0)=x_o, \dot{x}(0) = \dot{x}_o, y(0)=y_o, \dot{y}(0) = \dot{y}_o \quad (2.22)$$

### 2.4.1 Equations of Motion at Impact

At a time when one of the breakwater's cables becomes taut, referred to as an impact, the breakwater rebounds off a boundary and starts moving in a different direction. For this, new variables will be introduced. First a symbol will be introduced where the superscript

(-) means a variable has this value just before impact, and similarly (+) means that the variable has this value just after the impact transition time. At the time of impact, the solutions change as follows. The subscript, i, indicates that a parameter is at an impact. Thus, after an impact a new set of “initial conditions” is determined and takes the values just after impact,

$$t=t_i, x(t_i)=x_i^+, \dot{x}(t_i) = \dot{x}^+, y(t_i)=y_i^+, \dot{y}(t_i) = \dot{y}^+ \quad (2.23)$$

Then, until the next impact, the solutions are

$$x(t) = x^+ + \dot{x}^+(t - t_i) \quad (2.24)$$

$$y(t) = y^+ + \dot{y}^+(t - t_i) - \frac{1}{2}(t - t_i)^2 \quad (2.25)$$

For example, in the first time interval,

$$x(0)=x_o, \dot{x}(0) = \dot{x}_o, y(0)=y_o, \dot{y}(0) = \dot{y}_o \quad (2.26)$$

Until the first impact, if the initial point is in the interior of U,

$$x(t) = x_o + \dot{x}_o(t - t_i) \quad (2.27)$$

$$y(t) = y_o + \dot{y}_o(t - t_i) - \frac{1}{2}(t - t_i)^2 \quad (2.28)$$

where  $t_i=0$ . It is necessary to determine when “impacts” occur, and subsequent “initial conditions” after impacts.

## 2.5 Impact

Now a detailed derivation of impact response equations will be formulated to determine the new initial conditions after impact.

### 2.5.1 Definition of Impact

When it is said that a breakwater impacts, this is defined as a cable becoming taut. “Taut” in this sense means that the cable reaches its natural length. When the cable becomes taut it is said that the breakwater is hitting a fictitious boundary which is defined by the mathematical equations for  $G_1=0$  and  $G_2=0$ . Once one of the cables has become taut, an

impact is felt and the breakwater rebounds in the opposite direction. This is analogous to a ball bouncing down the valley, thus hitting a side and changing direction. The taut condition is determined when the value of  $G_1$  or  $G_2$  or both become zero. At this instant the breakwater is on the boundary. During the solution procedure the values of  $G_1$  and  $G_2$  are negative when the breakwater is inside the region. After the nondimensionalization and some rearranging of terms, the boundary equations take the form of  $g_1=0$  and  $g_2=0$ , where

$$g_1=(x-1)^2 + (y-h)^2 - r^2 \quad (2.29)$$

$$g_2=(x+1)^2 + (y-h)^2 - r^2 \quad (2.30)$$

The EOM's are valid as long as  $g_1<0$  and  $g_2<0$ .

### 2.5.2 Impact Response when $g_1=0$

Impact parameters will now be developed for  $g_1=0$ . Solving Equation 2.29 for  $y$  where  $g_1=0$  gives

$$y = h - \sqrt{r^2 - (x-1)^2} \quad (2.31)$$

Thus, to get the slope of the boundary at a given point, the derivative is taken:

$$\frac{dy}{dx} = \frac{x-1}{\sqrt{r^2 - (x-1)^2}} \quad (2.32)$$

#### 2.5.2.1 Angle $\phi$

Taking a small differential triangle formed by the local  $x$  and  $y$  axes (Figs. 2.9 and 2.10), the tangent to the arc at this point may be obtained by measuring the angle  $\phi$  from the horizontal. The differential length of the hypotenuse may be obtained from the Pythagorean Theorem. Knowing the derivative of the circular arc equation,  $g_1$ , and simple trigonometry,  $\sin\phi$  and  $\cos\phi$  are obtained. By dividing the terms by the applicable  $dy$  or  $dx$ , the  $\sin\phi$  and  $\cos\phi$  terms may be simplified as seen in Equations 2.33 and 2.34:

$$\sin \phi = \frac{dy}{\sqrt{dy^2 + dx^2}} = \frac{-(dy/dx)}{\sqrt{1 + (dy/dx)^2}} \quad (2.33)$$

$$\cos \phi = \frac{-dx}{\sqrt{dy^2 + dx^2}} = \frac{1}{\sqrt{1 + (dy/dx)^2}} \quad (2.34)$$

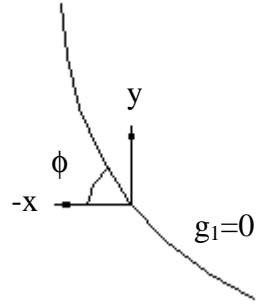


Fig. 2.9 Axes at Point on  $g_1=0$

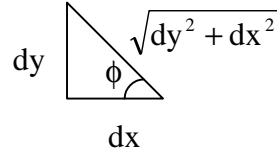


Fig. 2.10 Differential Triangle  
( $dx < 0, dy > 0$ )

### 2.5.2.2 Normal and Tangential Velocities at $g_1=0$

From simple geometry, the normal and tangential velocities may be obtained. By taking the vectors of the  $x$  and  $y$  velocities and then decomposing them into normal and tangential vectors, the normal and tangential velocities at a given point on the  $g_1=0$  arc may be obtained. The normal velocity is the velocity vector occurring longitudinal to the taut cable, while the tangential velocity is the velocity that occurs tangential to a point on the boundary. Conversely, by taking the normal and tangential velocity components in the  $x$  and  $y$  directions, the  $x$  and  $y$  velocities may be obtained. This derivation is shown graphically in Figs. 2.11 and 2.12 and given in Equations 2.35–2.38.

$$v_n = -\dot{x} \sin \phi - \dot{y} \cos \phi \quad (2.35)$$

$$v_t = -\dot{x} \cos \phi + \dot{y} \sin \phi \quad (2.36)$$

$$\dot{x} = -v_t \cos \phi - v_n \sin \phi \quad (2.37)$$

$$\dot{y} = v_t \sin \phi - v_n \cos \phi \quad (2.38)$$

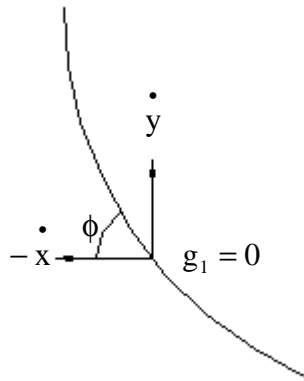


Fig. 2.11 Velocity Vectors at Point on  $g_1=0$

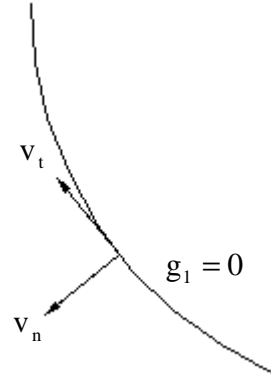


Fig. 2.12 Normal and Tangential Velocity Vectors

It must be noted that in this derivation, the normal velocity points outward from the region in its positive direction. This is done to aid in developing graphs to interpret the data from the case solutions. For example, as the breakwater is heading towards a boundary (i.e., in a positive direction) then its normal velocity just before impact will be positive.

### 2.5.3 Impact Response when $g_2=0$

Similar to the derivation of the  $g_1=0$  impact response, the impact parameters will now be developed for  $g_2=0$ . Solving Equation 2.30 for  $y$  where  $g_2=0$  :

$$y = h - \sqrt{r^2 - (x + 1)^2} \tag{2.39}$$

Thus, to get the slope of the boundary at a given point, the derivative is taken:

$$\frac{dy}{dx} = \frac{x + 1}{\sqrt{r^2 - (x + 1)^2}} \tag{2.40}$$

#### 2.5.3.1 Angle $\psi$

Likewise for  $g_2=0$ , by taking a small differential triangle formed by the local  $x$  and  $y$  axes (Figs. 2.13 and 2.14), the tangent to the arc at this point may be obtained by measuring the angle  $\psi$  from the horizontal. The differential length of the hypotenuse may be

obtained from the Pythagorean Theorem. Knowing the derivative of the circular arc equation,  $g_2$ , and simple trigonometry,  $\sin\psi$  and  $\cos\psi$  are obtained. By dividing the terms by the applicable  $dy$  or  $dx$ , the  $\sin\psi$  and  $\cos\psi$  terms may be simplified as given in Equations 2.40 and 2.41:

$$\sin \psi = \frac{dy}{\sqrt{dy^2 + dx^2}} = \frac{dy/dx}{\sqrt{1 + (dy/dx)^2}} \quad (2.40)$$

$$\cos \psi = \frac{dx}{\sqrt{dy^2 + dx^2}} = \frac{1}{\sqrt{1 + (dy/dx)^2}} \quad (2.41)$$

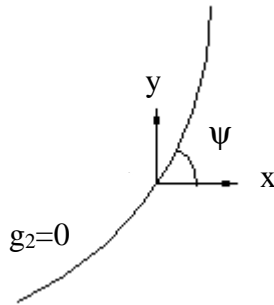


Fig. 2.13 Axes at Point on  $g_2=0$

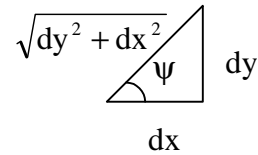


Fig. 2.14 Differential Triangle  
( $d_x>0, d_y>0$ )

### 2.5.3.2 Normal and Tangential Velocities at $g_2=0$

Similar to the left boundary derivation, from simple geometry, the normal and tangential velocities may be obtained. This derivation is shown graphically in Figs. 2.15 and 2.16 and given in Equations 2.42–2.45:

$$v_n = \dot{x} \sin \psi - \dot{y} \cos \psi \quad (2.42)$$

$$v_t = \dot{x} \cos \psi + \dot{y} \sin \psi \quad (2.43)$$

$$\dot{x} = v_t \cos \psi + v_n \sin \psi \quad (2.44)$$

$$\dot{y} = v_t \sin \psi - v_n \cos \psi \quad (2.45)$$

It must be noted that in this derivation, the normal velocity points outward from the region in its positive direction.

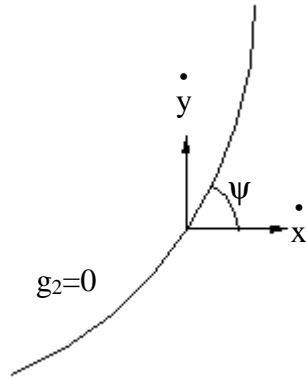


Fig. 2.15 Velocity Vectors at Point on  $g_2=0$

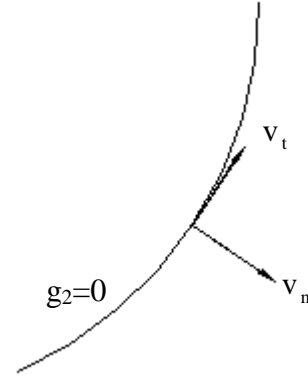


Fig. 2.16 Normal and Tangential Velocity Vectors

#### 2.5.4 Snap Loading Response

The breakwater feels a similar snap loading response if either the left or right boundary is hit. The only difference in the response is the equations for determining the normal and tangential velocities, which were explained previously. Snap loading in this project is referred to as an impact. This is when a cable becomes taut, and the loading in the cable at this instant is defined as the normal velocity (i.e., normal to the boundary). The mass of the breakwater may be multiplied by its change of velocity to give a resulting “impact force” or impulsive force. The normal velocity at impact is computed, just before the breakwater rebounds when the cable has become taut. When the breakwater impacts a boundary, some energy is dissipated. This dissipation of energy is absorbed by the mooring lines and is transferred to the supports. In practice the amount of energy dissipated depends on material and geometric properties of the mooring line. In this investigation, the affects of these properties are taken into account by a coefficient of restitution,  $e$  ( $0 < e < 1$ ), which is common to impact problems. This reduction factor is applied to the normal velocity at the time of impact. Thus, the normal velocity is reduced during impacts, which in turn reduces the magnitudes of the horizontal and vertical velocities of the breakwater. Equation 2.46 explains this mathematically:

$$v_n^+ = -ev_n^- \quad (2.46)$$

It is assumed that the tangential velocity,  $v_t$ , remains unchanged at the time of impact and that the only parameter affected by the rebound is the normal velocity. Though the tangential velocity remains unchanged, the x and y velocities do change because they are based on both the normal and tangential velocities after impact. At an impact time, the subscript i is used to denote an impact or the next initial condition. As seen previously, new x and y values are determined after impact and these become the new initial conditions for the next range of motions until the next impact. Thus, initial conditions are seen in Equation 2.23.

## 2.6 Convergence to a Boundary

As seen in boundary Equations 2.29 and 2.30, the breakwater is inside of the region when  $g_1$  and  $g_2$  are negative. As the solution proceeds through time, the breakwater might hit a boundary, which occurs when a cable becomes taut. Mathematically, this is shown by  $g_1$  or  $g_2$  becoming greater than or equal to zero. The ideal case is that the breakwater's position ends up directly on a boundary (i.e.,  $g_{1,2}=0$ ). However, for practical purposes, a finite time step is used in the solution and it is more likely that the breakwater's position will end up past the boundary at an impact. In this case the exact time at which the breakwater hits the boundary is required to keep the solution accurate, and thus an impact time must be converged upon. Several convergence methods exist. Originally, the “bracketing” method known as *Regula Falsi* (the method of false position) was used to converge the breakwater to an impact time on the boundary. However, the convergence used method was later changed to Newton's Method during this investigation. This method was chosen for its simplicity and its ability to converge quickly and accurately (Johnson and Riess 1982). Newton's Method is used to find a root of a function and has the following form:

$$t_{n+1} = t_n - \frac{g_{(1,2)}(t_n)}{g'_{(1,2)}(t_n)} \quad (2.47)$$

where

$$\dot{g}_1 = 2(x-1)\dot{x} + 2(y-h)\dot{y} \quad (2.48)$$

$$\dot{g}_2 = 2(x+1)\dot{x} + 2(y-h)\dot{y} \quad (2.49)$$

where

$x(t)$ ,  $\dot{x}(t)$ ,  $y(t)$ , and  $\dot{y}(t)$  are functions of time as seen in Equations 2.18-2.21. With either of these methods, the value of  $g$  was converged to a tolerance of  $10^{-6}$ , and the time at which this occurs becomes the impact time.

## 2.7 Solution Procedure

Once all of these parts were formulated, they were put together into a computer program which was developed to solve the problems being investigated. The program was written using the FORTRAN programming language. This program uses the equations of motion and solves for the breakwater's position and velocities at a given time. The solution procedure may be summarized as follows:

1. dimensions and other parameters are given
2. the breakwater is given initial position and velocities
3. the solution proceeds through time using the analytical solution of the equations of motion
4. when  $g_1$  or  $g_2$  equals zero or becomes positive (i.e., a cable has become "taut"), conditions are converged within tolerance (close to zero) using Newton's Method, and the tangential and normal velocities are determined from geometry
5. the normal velocity is reduced by a coefficient of restitution and the direction of motion is changed; this is the loss of energy and the rebound of the breakwater
6. new velocities are calculated and these conditions are made the new initial conditions, and the procedure starts over with step 3

## **2.8 Development of Alternate Modeling Program**

The solution discussed above is an analytical solution to the problems being investigated. Before the analytical solution was applied a numerical solution was used to solve the problems. When the analytical solution was formulated, the solution process used in this research was switched to using the analytical solution because it gave realistic and accurate results. However, it was understood that more complicated forms of this same problem may be investigated in the future and an analytical solution may not exist for such problems. Therefore, a numerical solution and is explained here.

### **2.8.1 Numerical Modeling Program**

The solutions to the differential equations discussed in the formulation section may be obtained by using a computer program written to model the motions of the point mass breakwater. A program written in FORTRAN programming language was used to obtain the solution of the ordinary differential equations (ODE's). The DIVPAG subroutine from IMSL (International Mathematical and Statistical Library) was used in solving the ODE's. DIVPAG requires the ODE's to be in first-order form, so as seen in the formulation, the ODE's to be solved are put in this form. The DIVPAG subroutine offers two numerical integration method options, the Adams-Moulton Method and Gear's Stiff Method. The Adams-Moulton Method was used in this numerical analysis.

## Chapter 3

# Free Motions of a Point-Mass Breakwater

### 3.1 Introduction

Before more complicated analyses are conducted, a simple study was necessary to see common responses of the breakwater and to check that the formulation was correct. In the first analyses, the breakwater was modeled as a point mass, which would undergo free motion. This point-mass breakwater (PMBW) is an infinitesimally small point of mass  $m$ . Free motions are those where the only force acting on the breakwater is gravity, which pulls the breakwater down. Thus, the problem investigated is a two-dimensional free vibration of a point mass which is restricted to a specified region. More realistic and complicated cases will be investigated in subsequent chapters.

### 3.2 Equations of Motion

The equations of motions (EOM's) developed in Chapter 2 will be used to model the motions of the PMBW in this problem. These EOM's are reviewed in Section 3.5.2.

### 3.3 Analyzed Cases

Several different cases were analyzed to investigate how the variation of different parameters affected the motions of the breakwater. For this problem, the parameters include the radius of the mooring cables,  $r$ , the coefficient of restitution,  $e$ , and initial  $x$  and  $y$  positions and velocities. These parameters and initial conditions are summarized in Table 3.1. This table shows the case number, which was used to identify each case; this number is a series of numbers taken from the initial conditions. In this problem, the case

number uses  $r, e, x(0), \dot{x}(0), y(0), \dot{y}(0)$  in this order to identify it. For example, the standard case has a case number of 194611. The standard case will be explained in detail later and is denoted by the shaded cells in Table 3.1 where  $v_x = \dot{x}(0)$  and  $v_y = \dot{y}(0)$ . Further, the initial conditions shown in this table are put into a series of groups. These groups were used to see how varying only one parameter would affect the breakwater's response. These series and the extra cases analyzed that do not necessarily fall directly into a series were used to decide ranges of parameters to be used in future analyses.

**Table 3.1. Parameters and Initial Conditions for Free Motions of a Point-Mass Breakwater**

<b>Case #</b>	<b>r</b>	<b>e</b>	<b>x</b>	<b>v<sub>x</sub></b>	<b>y</b>	<b>v<sub>y</sub></b>
<b>rexv<sub>x</sub>yv<sub>y</sub></b>						
<b>r</b>						
294611	2.5	0.9	0.4	0.6	1.0	-0.1
194611	1.5	0.9	0.4	0.6	1.0	-0.1
292010	2.5	0.9	0.2	0.0	1.0	0.0
192010	1.5	0.9	0.2	0.0	1.0	0.0
<b>e</b>						
114611	1.5	1.0	0.4	0.6	1.0	-0.1
194611	1.5	0.9	0.4	0.6	1.0	-0.1
174611	1.5	0.7	0.4	0.6	1.0	-0.1
154611	1.5	0.5	0.4	0.6	1.0	-0.1
174010	1.5	0.7	0.4	0.0	1.0	0.0
164010	1.5	0.6	0.4	0.0	1.0	0.0
154010	1.5	0.5	0.4	0.0	1.0	0.0
<b>x</b>						
194010	1.5	0.9	0.4	0.0	1.0	0.0
174010	1.5	0.7	0.4	0.0	1.0	0.0
173010	1.5	0.7	0.3	0.0	1.0	0.0
172010	1.5	0.7	0.2	0.0	1.0	0.0
171010	1.5	0.7	0.1	0.0	1.0	0.0
<b>r, e, x</b>						
2751010	2.5	0.75	1.0	0.0	1.4	0.0
272010	2.5	0.7	0.2	0.0	1.0	0.0
264010	2.5	0.6	0.4	0.0	1.0	0.0
261010	2.5	0.6	1.0	0.0	1.4	0.0
194611m (mirror)	1.5	0.9	-0.4	-0.6	1.0	-0.1

### 3.3.1 Standard Case

A standard case was developed for this problem as a starting point for the variation of parameters. The standard parameters and initial conditions for this PMBW problem are:

$$\begin{aligned} r &= 1.5 & e &= 0.9 \\ x(0) &= 0.4 & \dot{x}(0) &= 0.6 \\ y(0) &= 1.0 & \dot{y}(0) &= -0.1 \end{aligned} \tag{3.1}$$

The PMBW is given initial  $x$  and  $y$  positions, denoted by  $I$  in Fig. 3.1, in the top right corner of the region. This position was chosen because the only force in the system was the gravitational force, and thus if the PMBW was given an initial position near its equilibrium state then it would not likely have long-lasting motions. In other words, the PMBW has potential energy and no kinetic energy added to the system by some outside force. Theoretically the PMBW will settle to the bottom of the region because it loses energy every time it impacts a boundary. If the PMBW is given a low initial height, then it will settle quicker than if it is started higher, and the primary purpose of this problem is to investigate the response of the breakwater. The longer the PMBW continues moving, the more characteristic responses may be seen from its motion, and thus the PMBW will be started at a higher position.

### 3.4 Analysis of Data

The data collected was analyzed to see what types of behavior the PMBW exhibited during its period in motion. The primary method of evaluating the response of the PMBW was to produce and evaluate several types of graphs.

#### 3.4.1 Types of Graphs

By putting the data into graphical form, it was easy to interpret the responses of the PMBW. The trajectory plot is used to show the motion of the breakwater in a planar

form with the breakwater bouncing between two circular arc boundaries. The boundaries are definite (i.e., fixed in space) in the point-mass cases and are drawn on the plot. Figure 3.1 shows a typical trajectory plot with I denoting the initial point. Figure 3.2 shows a plot of normal velocity just before impact vs. time. This plot is used to show how the normal velocity (snap loading) tends to decrease throughout time due to a loss of energy. Vertical lines are drawn below the points (denoted by x's) corresponding to impacts with the right circular arc in Fig. 3.1, this was done to help show when they occur relative to impacts with the left circular arc (denoted by o's). After the first few impacts, the circles are higher than the x's and almost seem to lie on a smooth curve in this case. Theoretically, the motion will die out with an infinite number of impacts in a finite time. Other plots produced include: x and y vs. time for time histories; x and y velocity vs. x and y position, respectively, for phase diagrams; impact Poincaré plots; and total and kinetic energy vs. time plots. Though several graphs were produced, the trajectory and normal velocity before impact vs. time plots were the most useful for the analyses being performed. Some of the other plots are shown in the Appendix.

### **3.4.2 Observations**

After varying the different parameters of the problem, several characteristic phenomena were observed about the motions of a PMBW. The following is a summary of these observations.

The radius was the first parameter varied to see how the PMBW would respond. There does not appear to be a significant difference between the motions of a case that has a radius of 1.5 and a case that has a radius of 2.5. The only notable difference between the two radii is the ability for the PMBW to bounce around longer and travel about higher portions of the region more with the  $r=2.5$  cases. Figures 3.3 and 3.4 illustrate this difference in size and range of motions of the PMBW dependent upon the mooring line radius. Note that the Figs. 3.3 and 3.4 are approximately to scale.

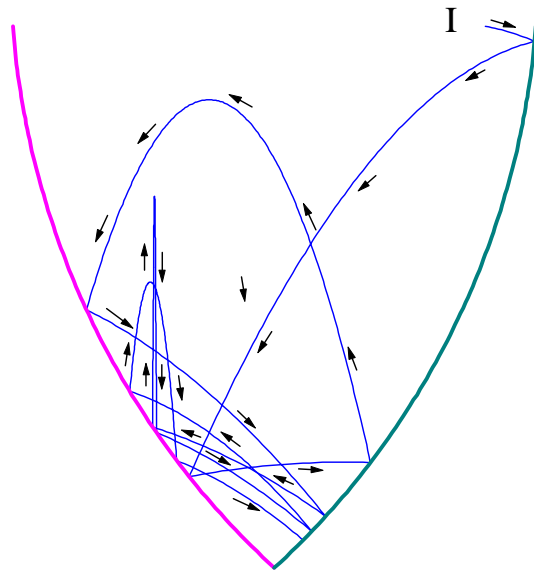


**Fig. 3.1. Typical Trajectory Plot, Standard Case**

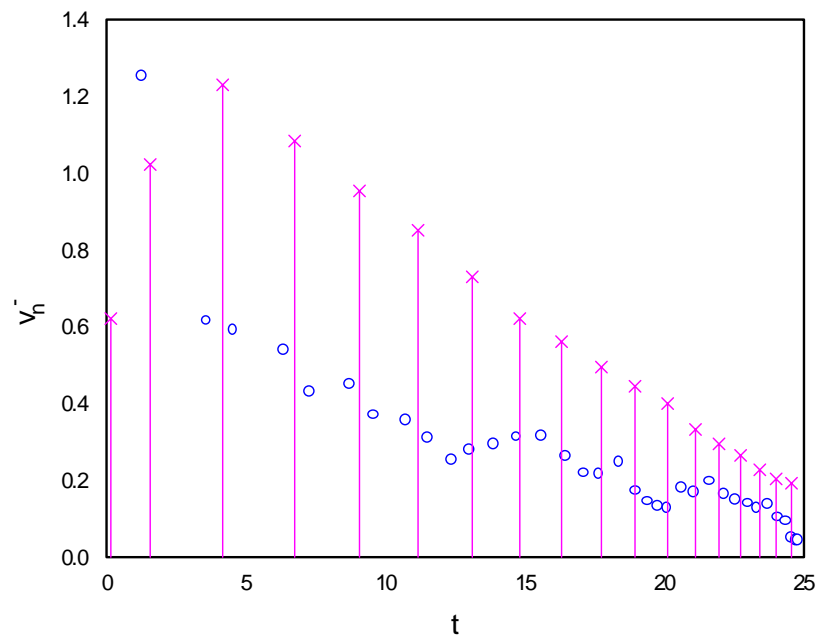


**Fig. 3.2. Typical Normal Velocity Before Impact vs. Time, Standard Case**

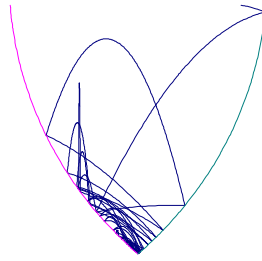


**Fig. 3.3. y vs. x, Case 194611 (r=1.5)**

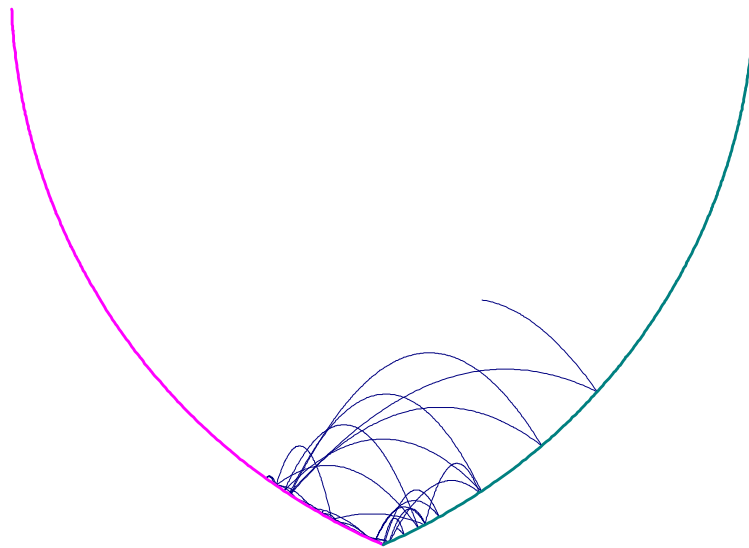


**Fig. 3.4. y vs. x, Case 294611 (r=2.5)**

The lower the coefficient of restitution, the quicker the PMBW dies out to the bottom of the region. This is demonstrated in Figs. 3.5-3.7, where it can be seen that as the coefficient of restitution is decreased from 0.9 to 0.7 to 0.5, the time it takes for the PMBW to lose enough energy to settle to the bottom of the region is reduced. The breakwater will travel around the region until it loses enough energy to die down. The graph of the case where  $e=1.0$  is not shown in this series, because in this case the PMBW retained so much energy that its motions caused it to go above the upper boundary,  $y=h$ , which indicates, in reality, that the breakwater hits the sea bed. The trajectory is shown in Fig. 3.8 and reaches  $y=h$  at point A. This motion is undesired and most likely not possible.

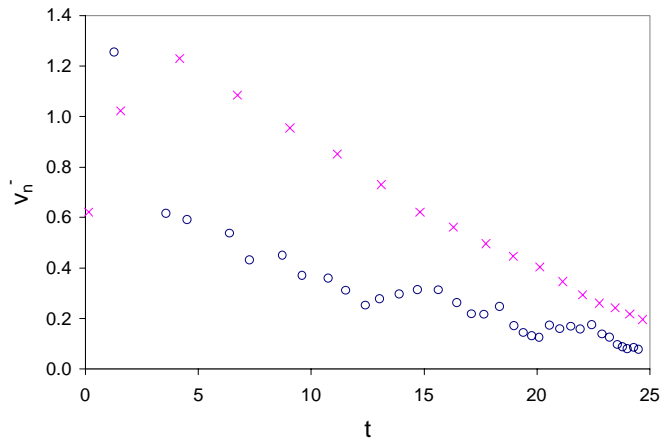


**Fig. 3.5.**  $v_n^-$  vs.  $t$ , Case 194611  
( $e=0.9$ )

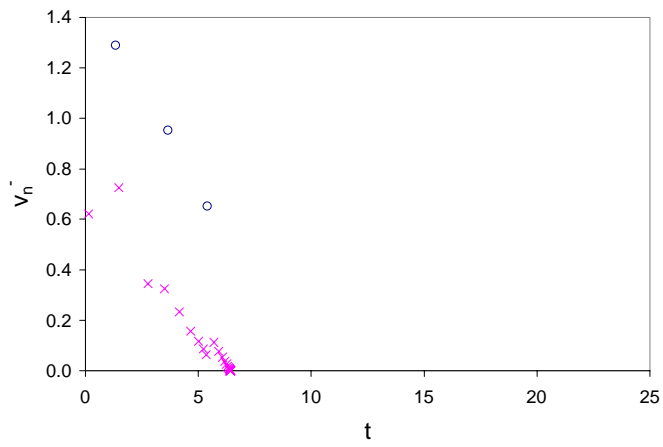


**Fig. 3.6.**  $v_n^-$  vs.  $t$ , Case 174611  
( $e=0.7$ )

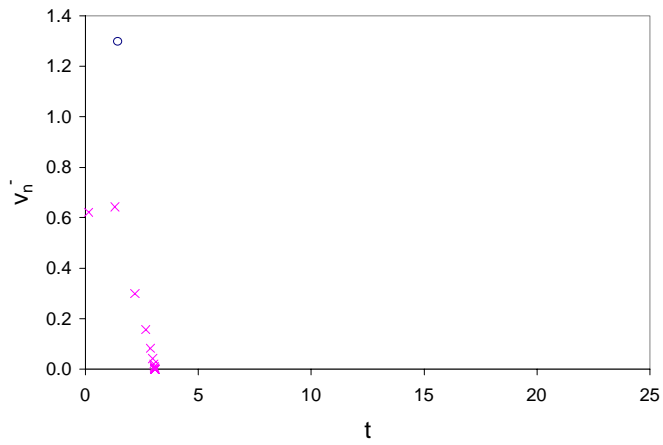


**Fig. 3.7.**  $v_n^-$  vs.  $t$ , Case 154611  
( $e=0.5$ )

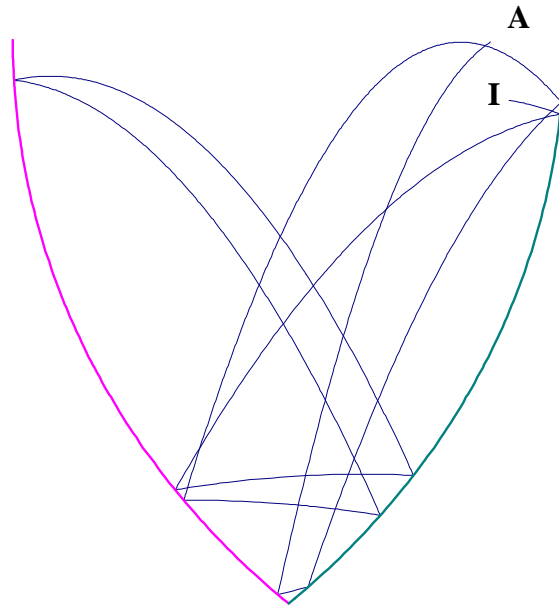


**Fig. 3.8. y vs. x, Case 114611 (e=1.0)**

When the breakwater is started on one side of the axis of symmetry, it tends to hit the boundary on the other side with a greater normal velocity than the boundary on the side on which it started. This is due to the curvature of the opposite boundary and the angle at which it strikes; when the PMBW hits the boundary at almost a right angle to the slope of the curve, the impact velocity is high. Conversely, the normal velocity would be low if the breakwater just grazes off of a boundary and does not hit it straight on, thus transferring less normal velocity. The magnitude of the normal velocity is dependent upon the direction of the PMBW trajectory relative to the tangent to the boundary curve where the breakwater hits. As seen in Fig. 3.2, the normal velocity usually decreases in magnitude because it loses energy as it impacts. However, the possibility of a PMBW with a normal velocity greater than a prior normal velocity exists. This is because if the breakwater travels downwards for a long time, it gains velocity from gravitational acceleration and possesses more kinetic energy and may have a large normal velocity at impact, even if the breakwater does not hit at a right angle and only grazes a boundary. The normal velocities tend to die down with time because of the coefficient of restitution, which removes energy from the system, as seen in a typical  $v_n$  vs.  $t$  plot in Fig 3.2. Some trials hardly get started before they die out due to initial conditions or to a low coefficient

of restitution. The above said phenomenon may be seen in comparing how the breakwater strikes a boundary in Fig. 3.1 to the magnitude of the normal velocity in Fig. 3.2. Section 3.5.3 discusses this phenomenon further.

The more energy you add to the system, like increasing the x and y velocities, the more excited the motion of the breakwater may be. This can be seen in Figs. 3.9 and 3.10, where in Fig. 3.9 the breakwater is started with some velocities while in Fig. 3.10 the breakwater is essentially dropped from rest. In Fig. 3.9 the PMBW moves about the region striking both boundaries, while the PMBW in Fig. 3.10 mainly sticks close to the right boundary because it has less horizontal velocity to cause it to strike the left boundary.

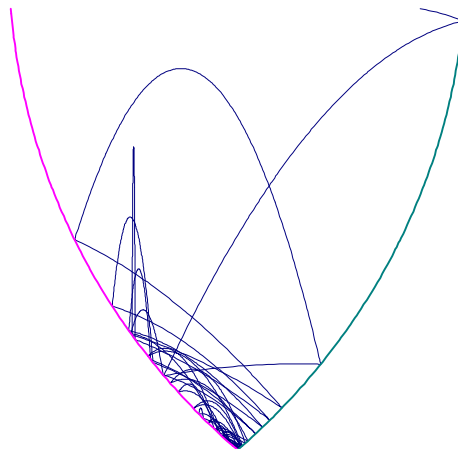


**Fig. 3.9. y vs. x, Case 194611**  
( $v_x = 0.6$ ,  $v_y = -0.1$ )

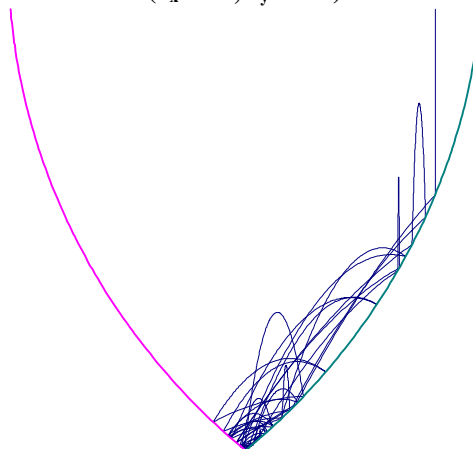


**Fig. 3.10. y vs. x, Case 194010**  
( $v_x = 0.0$ ,  $v_y = 0.0$ )

### **3.5 Verification of Computer Modeling Techniques**

After a solution procedure was developed and coded into a computer program, several cases were investigated. To verify that the formulation and coding were correct, a few checks were developed to determine the accuracy and versatility of the formulation. This was done using data collected from the cases investigated.

#### **3.5.1 Analytical vs. Numerical Solution**

As seen in Chapter 2, the bases for the motions of the PMBW are the classical physics equations of motion. For this first problem investigated, numerical integration was used to solve the equations of motion. However, a numerical solution is not necessary in this case since an analytical solution exists. A numerical solution was first developed for the first problem to give a check on the solution process and for reference to future researchers. One can solve for the motions of the PMBW by hand or with a numerical method. A comparison of the numerical solution to the analytical solution was investigated. This was done to determine the accuracy of the numerical modeling program using the DIVPAG subroutine from IMSL. The comparison of the two solution methods is best performed on the impact times. Most of the error will accumulate in the convergence rather than in the straight numerical integration of the free motions between impacts.

#### **3.5.2 Verification of Impact Times**

Once data was collected for a case using the numerical solution, in this instance the standard case, it was then compared with an analytical solution developed to determine the impact times. Two solution procedures were used and compared to the numerical solution. Both procedures used the same analytical solution formulation; the only difference was in the tools used to solve the analytical solution. These tools will be explained later. The following is the formulation of the impact time analytical solution.

To allow us to find the times at which a boundary is hit, the following formulation was developed. First, the EOM's for the free motion case, Equations 3.2-3.7, are combined with the equations for the  $g_1=0$  and  $g_2=0$  boundaries, Equations 3.12 and 3.13, as seen in Equation 3.14:

$$x = c_2 t + c_1 \qquad y = -\frac{1}{2} t^2 + c_4 t + c_3 \qquad (3.2, 3.3)$$

$$\dot{x} = c_2 \qquad \dot{y} = -t + c_4 \qquad (3.4, 3.5)$$

$$\ddot{x} = 0 \qquad \ddot{y} = -1 \qquad (3.6, 3.7)$$

where the constants for motion following  $t=t_i$  (initial time or impact time) are

$$c_1 = x_i - c_2 t_i \qquad c_3 = y_i - c_4 t_i + \frac{1}{2} t_i^2 \qquad (3.8, 3.9)$$

$$c_2 = \dot{x}_i \qquad c_4 = \dot{y}_i + t_i \qquad (3.10, 3.11)$$

The boundary equations  $g_1$  and  $g_2$  are

$$g_1 = (x-1)^2 + (y-h)^2 - r^2 \qquad g_2 = (x+1)^2 + (y-h)^2 - r^2 \qquad (3.12, 3.13)$$

Plugging  $x$  and  $y$  into the  $g_1=0$  equation gives

$$\left[ x_i + \dot{x}_i (t - t_i) - 1 \right]^2 + \left[ y_i + \dot{y}_i (t - t_i) - \frac{1}{2} (t - t_i)^2 - h \right]^2 = r^2 \qquad (3.14)$$

Rearranging and simplifying gives

$$\left[ x_i - \dot{x}_i t_i - 1 + \dot{x}_i t \right]^2 + \left[ y_i - \dot{y}_i t_i - \frac{1}{2} t_i^2 - h + (\dot{y}_i + t_i) t - \frac{1}{2} t^2 \right]^2 - r^2 = 0 \qquad (3.15)$$

After expanding, the following constants are defined:

$$A_1 = x_i - \dot{x}_i t_i - 1 \qquad (3.16)$$

$$B = \dot{x}_i \qquad (3.17)$$

$$C = y_i - \dot{y}_i t_i - \frac{1}{2} t_i^2 - h \qquad (3.18)$$

$$D = \dot{y}_i + t_i \qquad (3.19)$$

$$E = -\frac{1}{2} \qquad (3.20)$$

Similarly, plugging  $x$  and  $y$  into  $g_2=0$  gives

$$A_2 = x_i - \dot{x}_i t_i + 1 \quad (3.21)$$

The rest of the constants B, C, D, E are the same for  $g_2=0$  as for  $g_1=0$ .

Next, by plugging the constants back into the boundary equations for  $g_1=0$  and  $g_2=0$ , the general Equation 3.22 is developed:

$$g_{(1,2)} = C_0 + C_1 t + C_2 t^2 + C_3 t^3 + C_4 t^4 = 0 \quad (3.22)$$

where

$$C_0 = A_{(1,2)}^2 + C^2 - r^2 \quad (3.23)$$

$$C_1 = 2A_{(1,2)}B + 2CD \quad (3.24)$$

$$C_2 = B^2 + 2CE + D^2 \quad (3.25)$$

$$C_3 = 2DE \quad (3.26)$$

$$C_4 = E^2 \quad (3.27)$$

By solving Equation 3.22, the times when  $g_1=0$  and  $g_2=0$  may be computed. The impact time analytical solution is obtained from this equation by using the following procedure:

1. plug the initial conditions into the coefficient equations, Equations 3.16-3.21 and 3.23-3.27, for the particular boundary being investigated;
2. plug the coefficients into the fourth-order equation, Equation 3.22;
3. solve Equation 3.22 with a polynomial equation solver to get an impact time;
4. determine new “initial conditions” following this impact time and then the procedure starts over with step 1 to calculate the subsequent motion and the next impact time.

The first solution procedure used to solve for the impact times involved using Microsoft EXCEL to find the polynomial coefficients and the root finding program on a TI-85 hand calculator. The second solution procedure used Müller’s Method of the DZREAL subroutine in the IMSL library to find the root. Both methods used double precision to help control accuracy. These methods only looked at the conditions at the time of impact (i.e., a taut cable) and not at the conditions when both cables were slack because it is believed that during an impact is where the most errors will occur. The results of this

comparison may be seen in Table 3.2, where “Tol” refers to the tolerance and “Diff.” refers to the difference. Further, the values in the table have eight decimal places in order to save space; in actuality, the calculations were performed with numbers having 16 decimal places (double precision).

It must be mentioned that the impact times associated with the DIVPAG solution were computed using the *Regula Falsi* convergence method (Johnson and Riess 1982). From the table we can see that errors accumulate as time goes on. However, the methods of solving for the true impact times are accurate within acceptable tolerances and the numerical solution using DIVPAG matches well with the analytical solution. In Table 3.2 the shaded cells indicate a point where the accuracy drops one order of magnitude.

**Table 3.2. Comparison of Impact Times Calculated by Different Methods**

<b>Impact #</b>	<b>Impact Times, (DIVPAG) Tol=1.0E-6</b>	<b>Impact Times, (DZREAL) Tol=1.0E-12</b>	<b>Impact Times, (TI-85/Excel) Tol=unknown</b>	<b>Diff. DZREAL-DIVPAG</b>	<b>Diff. DIVPAG-TI-85</b>	<b>Diff. DZREAL-TI-85</b>
0	0.00000000	0.00000000	0.00000000			
1	0.15487522	0.15487524	0.15487524	1.2E-08	1.2E-08	2.7E-13
2	1.29044703	1.29044704	1.29044704	5.4E-09	5.4E-09	1.4E-13
3	1.56122317	1.56122317	1.56122317	2.1E-09	2.1E-09	3.4E-12
4	3.59966608	3.59966598	3.59966598	9.9E-08	9.9E-08	4.0E-11
5	4.17157260	4.17157267	4.17157267	7.1E-08	7.1E-08	2.8E-12
6	4.52925467	4.52925457	4.52925457	9.9E-08	9.9E-08	8.8E-11
7	6.38741123	6.38741097	6.38741097	2.6E-07	2.6E-07	3.3E-10
8	6.73907649	6.73907664	6.73907664	1.5E-07	1.5E-07	2.4E-12
9	7.28300933	7.28300867	7.28300867	6.6E-07	6.6E-07	1.2E-09
10	8.73095524	8.73095452	8.73095452	7.2E-07	7.1E-07	3.1E-09
11	9.05636623	9.05636656	9.05636656	3.3E-07	3.3E-07	2.0E-10
12	9.59914050	9.59913850	9.59913851	2.0E-06	2.0E-06	7.4E-09
13	10.76988925	10.76988608	10.76988608	3.2E-06	3.2E-06	6.0E-09
14	11.16521568	11.16521650	11.16521650	8.2E-07	8.2E-07	1.7E-09
15	11.53959696	11.53959143	11.53959144	5.5E-06	5.5E-06	1.1E-08
16	12.41141812	12.41140590	12.41140594	1.2E-05	1.2E-05	3.4E-08
17	13.03986820	13.03985781	13.03985784	1.0E-05	1.0E-05	2.3E-08
18	13.10760818	13.10761069	13.10761065	2.5E-06	2.5E-06	4.1E-08
19	13.91268806	13.91264917	13.91264933	3.9E-05	3.9E-05	1.6E-07
20	14.72034117	14.72030045	14.72030060	4.1E-05	4.1E-05	1.5E-07
21	14.81818740	14.81819959	14.81819948	1.2E-05	1.2E-05	1.1E-07
22	15.64892103	15.64878279	15.64878340	1.4E-04	1.4E-04	6.2E-07
23	16.30909588	16.30913839	16.30913814	4.3E-05	4.2E-05	2.4E-07
24	16.46689858	16.46670330	16.46670420	2.0E-04	1.9E-04	9.0E-07
25	17.10958634	17.10908788	17.10909025	5.0E-04	5.0E-04	2.4E-06
26	17.66412876	17.66356037	17.66356306	5.7E-04	5.7E-04	2.7E-06
27	17.73239474	17.73255352	17.73255277	1.6E-04	1.6E-04	7.5E-07
28	18.37584603	18.37433473	18.37434191	1.5E-03	1.5E-03	7.2E-06
29	18.94699238	18.94757767	18.94757495	5.9E-04	5.8E-04	2.7E-06
30	19.01118237	19.00810018	19.00811490	3.1E-03	3.1E-03	1.5E-05
31	19.41265035	19.40475649	19.40479420	7.9E-03	7.9E-03	3.8E-05
32	19.79233780	19.78092566	19.78098028	1.1E-02	1.1E-02	5.5E-05
33	20.10826357	20.09518713	20.09524977	1.3E-02	1.3E-02	6.3E-05
34	20.12473656	20.12721416	20.12720271	2.5E-03	2.5E-03	1.1E-05
35	20.61283111	20.58340792	20.58354735	2.9E-02	2.9E-02	1.4E-04
36	21.06461945	21.02023927	21.02045245	4.4E-02	4.4E-02	2.1E-04
37	21.12226038	21.13614937	21.13608828	1.4E-02	1.4E-02	6.1E-05
38	21.62245445	21.52829593	21.52873485	9.4E-02	9.4E-02	4.4E-04
39	21.95838994	22.00416803	22.00397907	4.6E-02	4.6E-02	1.9E-04

### 3.5.3 Verification of Rebound Angles

When the cable becomes taut, the  $x$  and  $y$  positions are assumed to remain the same before and after the impact. After the positions have been converged within the tolerance, then the velocities are changed according to the geometry of the angle at which the PMBW strikes the boundary. The magnitude of the normal velocity (snap loading) is based on the angle at which the boundary is hit. The more perpendicular the angle of strike, the higher the value of normal velocity. More extensively, as in the physics of an impact, the angles at which an object strikes and rebounds off another object should be on opposite sides of a perpendicular to the point on the boundary at which the object strikes. Thus, the following check was created to prove that the angles at which the breakwater strikes and rebounds off a boundary are on opposite sides of a perpendicular to the boundary. This shall be done by investigating the striking and rebounding angles of the boundary  $g_2=0$ . As seen in Figs. 3.11 and 3.12, the angle  $\psi$ , which is measured from the horizontal to the boundary, has  $\pi/2$  added to it to give an angle perpendicular to the boundary and measured from the horizontal. From this angle, striking and rebounding angles should be on either side of this perpendicular.

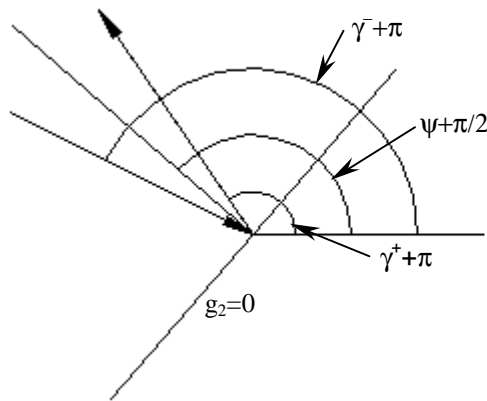


Fig. 3.11. Breakwater Striking Upwards

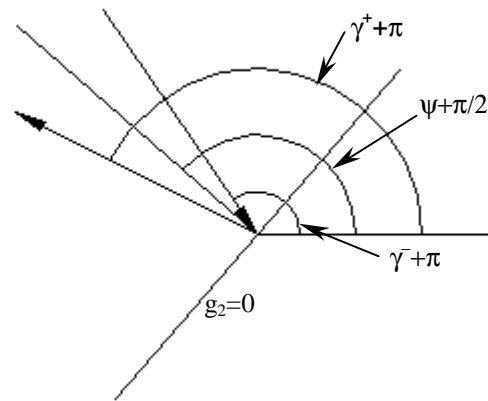


Fig. 3.12. Breakwater Striking Downwards

The superscript (-) denotes quantities just before impact and the superscript (+) denotes quantities just after impact.

To verify this conclusion, the following criteria must be met:

$$\bar{\gamma} + \pi > \psi + \pi/2 > \gamma^+ + \pi \quad (3.28)$$

where  $\psi$  may be obtained from Section 2.5.3.1 and

$$\bar{\gamma} = \tan^{-1} \left( \frac{\dot{y}^-}{\dot{x}^-} \right) \quad (3.29)$$

Similarly, to get  $\gamma^+$  just replace the (-) superscripts with (+) in Equation 3.29.

Table 3.3 shows results from an impact during the standard case.

**Table 3.3. Verification of Striking and Rebound Angles**

Impact Time	11.16521661				
	x	v <sub>x</sub>	v <sub>y</sub>	γ	γ+π
before ( - )	0.03969501	0.58081667	-0.62245686	-0.81999012	2.32160253
after ( + )	0.03969501	-0.54024265	0.54337590	-0.78828962	2.35330303
ψ	0.76582237				
ψ+π/2	2.33661870				
		Difference			
γ̄+π	2.32160253	0.015016166			
ψ+π/2	2.33661870				
γ <sup>+</sup> +π	2.35330303	0.016684334			
γ <sup>+</sup> /γ̄	0.900015867				

By obtaining the positions and velocities before and after the impact, one can calculate the values of  $\psi$ ,  $\bar{\gamma}$ , and  $\gamma^+$  and after adding the appropriate angles to these, one can compare the angles as measured from the horizontal x-axis. One can see that, in this case,  $\bar{\gamma} + \pi < \psi + \pi/2 < \gamma^+ + \pi$ . Furthermore, it can be seen, within some error, that  $\gamma^+/\bar{\gamma}$  is the coefficient of restitution, which is 0.9 for the standard case. Lastly, it may be noted that the angle between the velocity vector and the perpendicular is greater after impact than before. This is due to loss of energy based on the coefficient of restitution (i.e., the breakwater does not have the same energy before and after impact, so it will not rebound as high).

### 3.5.4 Verification of Impact Conditions

The trials were all started from the same side of the axis of symmetry and same y position, as seen in Table 3.1. If one were to start the trial on the opposite side by changing the signs of the x values of the initial conditions, then a mirror image of the trial would occur. This indicates that both of the derivations of the convergence and rebounding during an impact are correct. This mirroring is about the middle axis of the trajectory plot (Figs. 3.13 and 3.14) at  $x=0$  or the axis of symmetry for the valley trajectory plots between  $g_1=0$  and  $g_2=0$ .

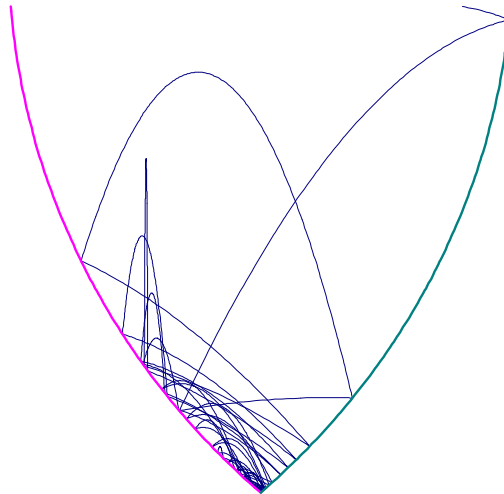


**Fig. 3.13. y vs. x, Standard Case (Case 194611)**

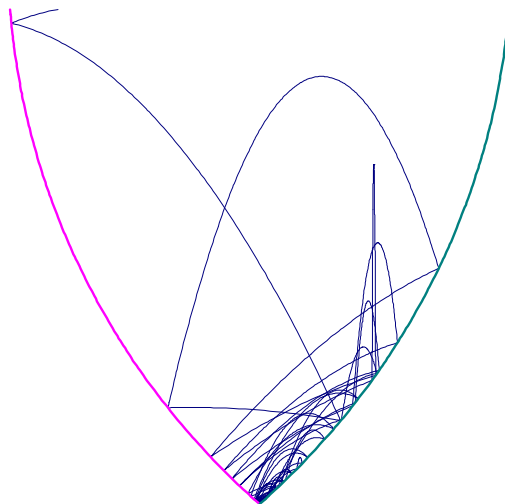


**Fig. 3.14. y vs. x, Mirror of Standard Case**

## Chapter 4

# Forced Motions of a Point-Mass Breakwater

### 4.1 Introduction

Now that a simple analysis has been performed and checked, a more complicated and realistic analysis will be conducted. For this problem the same formulation and geometry are used as in the first problem investigated, with the breakwater still modeled as a point mass. However, in this problem the point-mass breakwater (PMBW) is subjected to horizontal and vertical sinusoidal forcing used to model natural wave forcing (Fig. 4.1). This will cause the PMBW to respond more like an object that is actually subjected to the natural conditions of being in the ocean.

### 4.2 Wave Forcing

To model the horizontal and vertical sinusoidal forcing, consider the forces  $F_x$  acting in the x direction and  $F_y$  acting in the y direction in the x-y plane. These forces are acting on the PMBW as seen in Fig. 4.1. The forces shall be harmonic to simulate the periodic nature of wave particle motions in the ocean.

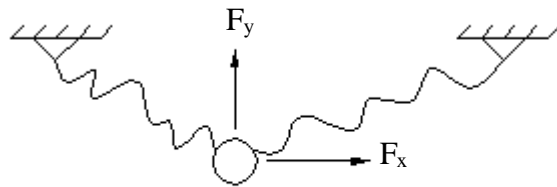


**Fig. 4.1. Breakwater with Horizontal and Vertical Forces**

### 4.2.1 Forcing Equations

The mathematical equations used to simulate the wave motions are as follows:

$$F_x = F_o \cos[\omega(T - T_x)] \quad (4.1)$$

$$F_y = v F_o \cos[\omega(T - T_y)] \quad (4.2)$$

where

$$T = \text{independent variable, time} \quad F_o = \text{amplitude of forcing} \quad (4.3, 4.4)$$

$$T_x = 0 \quad v = \text{amplitude reduction factor for } F_y \quad (4.5, 4.6)$$

$$T_y = T_x + \frac{\pi}{2\omega} \quad \omega = \text{forcing frequency} \quad (4.7, 4.8)$$

Notice that the only difference between the forcing in the x direction and the forcing in the y direction is the amplitude reduction factor, v, and a phase angle, T<sub>y</sub>. In nondimensional form,

$$x = X/S, y = Y/S, t = T \sqrt{g/S}, \Omega = \omega \sqrt{S/g}, f_x = F_x/(mg), f_y = F_y/(mg), f_o = F_o/(mg) \quad (4.9)$$

Equations 4.1 and 4.2 are plotted in nondimensional form against time in Figs. 4.2 and 4.3, where v=0.5. When Equations 4.1 and 4.2 are combined, they form an ellipse (Fig. 4.4). This elliptical forcing is a mathematical model of natural wave forcing. These forces are simply added into the ODE's (Equations 2.14 and 2.15) in the formulation in first-order form to be analyzed. The EOM's for this problem are

$$m \frac{d^2 X}{dT^2} = F_x \quad (4.10)$$

$$m \frac{d^2 Y}{dT^2} = -mg + F_y \quad (4.11)$$

Summarizing, the force in the x direction is:

1. F<sub>x</sub>, forcing in x direction by wave action

Forces in the y direction are:

1. g, forcing in the y direction by gravity
2. F<sub>y</sub>, forcing in the y direction by wave action

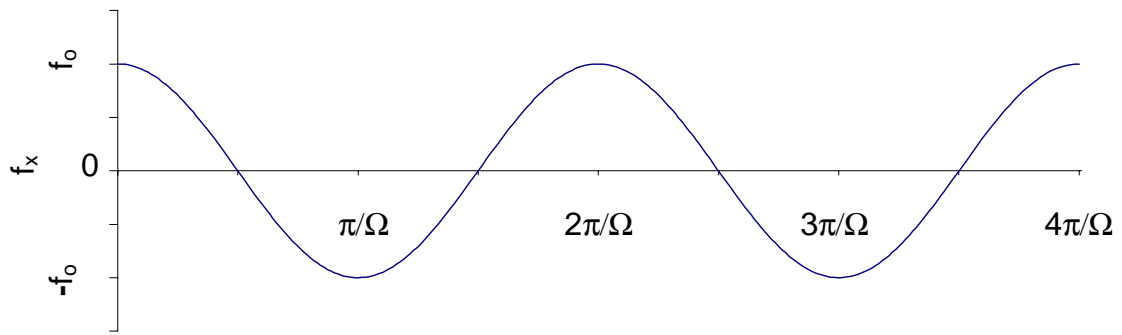


**Fig. 4.2. Horizontal Sinusoidal Forcing**

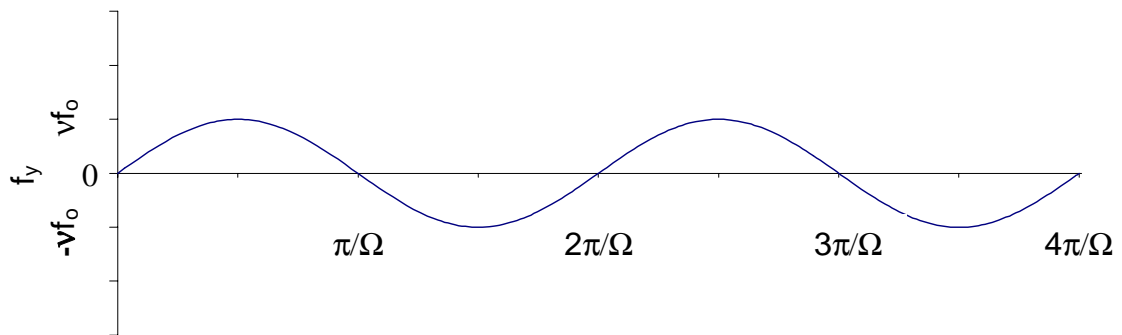


**Fig. 4.3. Vertical Sinusoidal Forcing**

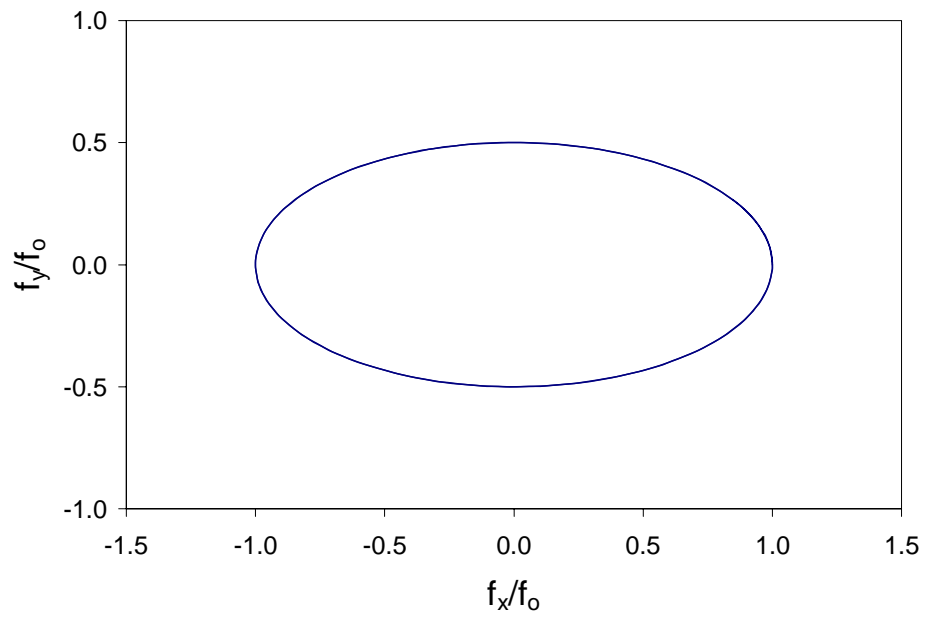


**Fig. 4.4. Combined Elliptical Forcing**

Nondimensionalizing the forcing equation gives the final form

$$\frac{d^2x}{dt^2} = f_x \quad (4.12)$$

$$\frac{d^2y}{dt^2} = -1 + f_y \quad (4.13)$$

with

$$f_x = f_o \cos[\Omega(t - t_x)] \quad [t_x = 0] \quad (4.14, 4.15)$$

$$f_y = v f_o \cos[\Omega(t - t_y)] \quad [t_y = \pi/(2\Omega)] \quad (4.16, 4.17)$$

Therefore

$$\ddot{x} = f_o \cos[\Omega(t - t_x)] \quad (4.18)$$

$$\ddot{y} = -1 + v f_o \cos[\Omega(t - t_y)] \quad (4.19)$$

#### 4.2.2 Analytical Solution

Now that the forcing functions have been formulated, the extra forces may be added into the analytical solution by integrating Equations 4.12 and 4.13 to obtain the x and y position and velocity equations similar to those obtained in the free vibration formulation. In this problem only a few modifications were applied to the previous method of solution. A numerical solution was developed for this case; however, it was found that an analytical solution may be determined for solving the forced case. It was felt that using an analytical solution would give better results than an approximate numerical solution. Thus, the solution procedure was modified to use the following analytical solution for the forced problem:

$$x = c_1 + c_2 t - \frac{f_o}{\Omega^2} \cos[\Omega(t - t_x)] \quad (4.20)$$

$$\dot{x} = c_2 + \frac{f_o}{\Omega} \sin[\Omega(t - t_x)] \quad (4.21)$$

$$y = c_3 + c_4 t - \frac{1}{2} t^2 - \frac{v f_o}{\Omega^2} \cos[\Omega(t - t_y)] \quad (4.22)$$

$$\dot{y} = c_4 - t + \frac{vf_o}{\Omega} \sin[\Omega(t - t_y)] \quad (4.23)$$

where

$$c_1 = x_i - c_2 t_i + \frac{f_o}{\Omega^2} \cos[\Omega(t_i - t_x)] \quad (4.24)$$

$$c_2 = \dot{x}_i - \frac{f_o}{\Omega} \sin[\Omega(t_i - t_x)] \quad (4.25)$$

$$c_3 = y_i - c_4 t_i + \frac{1}{2} t_i^2 + \frac{vf_o}{\Omega^2} \cos[\Omega(t_i - t_y)] \quad (4.26)$$

$$c_4 = \dot{y}_i + t_i - \frac{vf_o}{\Omega} \sin[\Omega(t_i - t_y)] \quad (4.27)$$

### 4.3 Analyzed Cases

These solutions were used and several different cases were analyzed to investigate how the varying of different parameters affected the responses of the breakwater. For this problem, the only additional parameters added to this solution are the forcing amplitude,  $f_o$ , the amplitude reduction factor,  $v$ , and the forcing frequency,  $\Omega$ . The parameters in this problem were varied to see any characteristic responses and the parameters and initial conditions considered in this problem are summarized in Table 4.1 where  $v_x = \dot{x}(0)$  and  $v_y = \dot{y}(0)$ . This table shows the case number, which was used to identify each case analyzed. This number is a series of numbers taken from the parameters and initial conditions. In this problem, the case number uses  $r, e, x(0), \dot{x}(0), y(0), \dot{y}(0)$ -  $f_o, v, \Omega$  in this order to identify the case. For example, the standard case has a case number of 190010-559. The standard case will be explained in detail later and is denoted by the shaded cells in Table 4.1. Further, the parameters and initial conditions shown in this table are grouped into series. These groups were used to see how variation of only one parameter would affect the breakwater's response.

**Table 4.1. Parameters and Initial Conditions for Forced Motions  
of a Point-Mass Breakwater**

<b>Case #</b>	<b>r</b>	<b>e</b>	<b>x</b>	<b>v<sub>x</sub></b>	<b>y</b>	<b>v<sub>y</sub></b>	<b>f<sub>o</sub></b>	<b>v</b>	<b>Ω</b>
<b>190010-559</b>	1.5	0.9	0.0	0.0	0.1	0.0	0.50	0.50	0.90
290010-559	2.5	0.9	0.0	0.0	0.1	0.0	0.50	0.50	0.90
190010-1059	1.5	0.9	0.0	0.0	0.1	0.0	1.00	0.50	0.90
120010-1050	2.5	0.9	0.0	0.0	0.1	0.0	1.00	0.50	0.90
<b>110010-559</b>	1.5	1.0	0.0	0.0	0.1	0.0	0.50	0.50	0.90
1950010-559	1.5	1.0	0.0	0.0	0.1	0.0	0.50	0.50	0.90
190010-559	1.5	0.9	0.0	0.0	0.1	0.0	0.50	0.50	0.90
180010-559	1.5	0.8	0.0	0.0	0.1	0.0	0.50	0.50	0.90
170010-559	1.5	0.7	0.0	0.0	0.1	0.0	0.50	0.50	0.90
<b>190010-359</b>	1.5	0.9	0.0	0.0	0.1	0.0	0.30	0.50	0.90
190010-559	1.5	0.9	0.0	0.0	0.1	0.0	0.50	0.50	0.90
190010-7559	1.5	0.9	0.0	0.0	0.1	0.0	0.75	0.50	0.90
190010-1059	1.5	0.9	0.0	0.0	0.1	0.0	1.00	0.50	0.90
190010-1559	1.5	0.9	0.0	0.0	0.1	0.0	1.50	0.50	0.90
<b>190010-5520</b>	1.5	0.9	0.0	0.0	0.1	0.0	0.50	0.50	2.00
190010-5515	1.5	0.9	0.0	0.0	0.1	0.0	0.50	0.50	1.50
190010-559	1.5	0.9	0.0	0.0	0.1	0.0	0.50	0.50	0.90
190010-5575	1.5	0.9	0.0	0.0	0.1	0.0	0.50	0.50	0.75
190010-555	1.5	0.9	0.0	0.0	0.1	0.0	0.50	0.50	0.50
<b>centered ellipse</b>									
115302-04575ng	1.5	1.0	0.05835	0.03048	0.1	0.02188	0.04	0.50	0.75
<b>f<sub>o</sub> (no-gravity)</b>									
110010-01575ng	1.5	1.0	0.0	0.00762	0.1	0.00547	0.01	0.50	0.75
110010-02575ng	1.5	1.0	0.0	0.01524	0.1	0.01094	0.02	0.50	0.75
110010-03575ng	1.5	1.0	0.0	0.02286	0.1	0.01641	0.03	0.50	0.75
110010-04575ng	1.5	1.0	0.0	0.03048	0.1	0.02188	0.04	0.50	0.75
110010-05575ng	1.5	1.0	0.0	0.03810	0.1	0.02735	0.05	0.50	0.75
<b>v (no-gravity)</b>									
110010-02175ng	1.5	1.0	0.0	0.01524	0.1	0.00219	0.02	0.10	0.75
110010-022575ng	1.5	1.0	0.0	0.01524	0.1	0.00547	0.02	0.25	0.75
110010-02575ng	1.5	1.0	0.0	0.01524	0.1	0.01094	0.02	0.50	0.75
110010-021075ng	1.5	1.0	0.0	0.01524	0.1	0.02188	0.02	1.00	0.75

### 4.3.1 Standard Case

A standard case was developed for this problem as a starting point for the varying of parameters. The standard parameters and initial conditions for this PMBW under forced motions are:

$$\begin{array}{lll} r=1.5 & e=0.9 & f_0=0.5 \\ x(0)=0.0 & \dot{x}(0) = 0.0 & v=0.5 \\ y(0)=0.1 & \dot{y}(0) = 0.0 & \Omega=0.9 \end{array} \quad (4.28)$$

For the forced PMBW problem, the cases studied have initial x and y positions near the bottom of the region (i.e., near the highest point of a floating breakwater). These cases are unlike the free vibration cases where the PMBW is released from the top of the region. This difference in position is due to the fact that the forced case has forces acting in several directions on the mass and it may move more freely than in the free motion case. The free motion case only has gravity acting down on the PMBW, hence the mass is released from a higher position to gain more energy (potential to kinetic) from falling a farther distance in order to cause the PMBW to go through a longer period of motion. Further, waves possess more energy near the surface of a body of water, thus to effectively attenuate wave energy, a breakwater would have to be near the surface of the water where its mooring cables are stretched to their extreme length. Thus, in practical usage a breakwater would not be near the ocean floor; it would be near the surface so it might effectively break up the waves passing by. So, it is better to model the breakwater at a point near the bottom of the region being investigated because this more accurately represents the location of an actual breakwater.

### 4.4 Analysis of Data

Cases were analyzed and data was collected to see what types of behavior the PMBW exhibited under forced motions. Again, several types of graphs were used to evaluate the responses of the PMBW.

#### 4.4.1 Observations

There does not seem to be any noticeable characteristic motion changes between the two radii investigated. The only major difference is that the 1.5 case has a sharper point at the region's bottom than the 2.5 case, as seen in Fig. 4.5. Further, as seen in Fig. 4.5, the nondimensional area of the region with a radius of 1.5 is 0.774 and the nondimensional area of the region with a radius of 2.5 is 4.954, which is more than six times larger than that of the  $r=1.5$  case. With a larger region and shallower boundary angles, the  $r=2.5$  case permits larger motions than that of the  $r=1.5$  case (Figs. 4.6 and 4.7). Note that these figures are not drawn to scale as in Fig. 4.5. Though the PMBW moves around the larger region and exhibits a larger range of movements, the  $r=2.5$  region is not attributed to any new motion phenomena. Thus, the radius  $r=1.5$  will be the primary focus of this investigation.

As seen in Figs. 4.8-4.12, as the coefficient of restitution,  $e$ , was varied from 1.0 to 0.95 to 0.9 to 0.8 to 0.7, the motions of the PMBW became less active as more energy was dissipated through the impacts occurring as the cables became taut. It must be noted that in Figs. 4.9-4.12 and subsequent trajectory plots, the lower portion of the region ( $0 \leq y \leq 0.1$ ) has been focused in on to see the motions of the breakwater in more detail. This behavior is further illustrated in Figs. 4.13-4.17 where the corresponding  $v_n^-$  vs.  $t$  plots show that the energy tends to decrease if  $e < 1$ . Note that Fig. 4.13 and Figs. 4.14-4.17 are not to the same time scale. The chaotic nature of the case where  $e=1.0$  may be attributed to the forcing adding energy to the system while gravity tries to draw the PMBW down. As  $e$  is decreased, more and more energy is lost from the system, causing the PMBW to move around the region less and in turn produces less snap loading. As time goes on, more energy is dissipated and gravity starts to control the motions of the breakwater and draws it down to the equilibrium state at the bottom of the region. Thus, the lower the  $e$  value, the less time the breakwater will move around the region before it settles to the bottom of the region because of the influence of gravity.

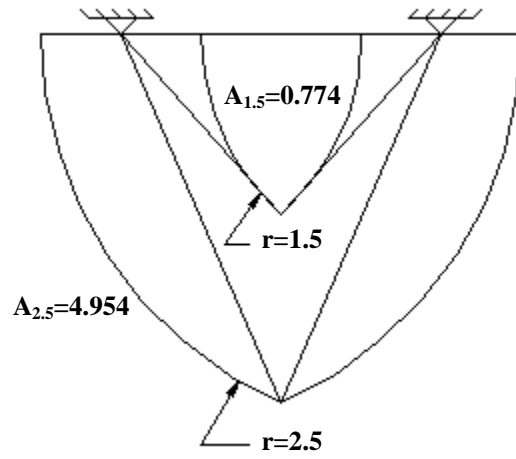


Fig. 4.5. Comparison of  $r=1.5$  and  $r=2.5$  Areas

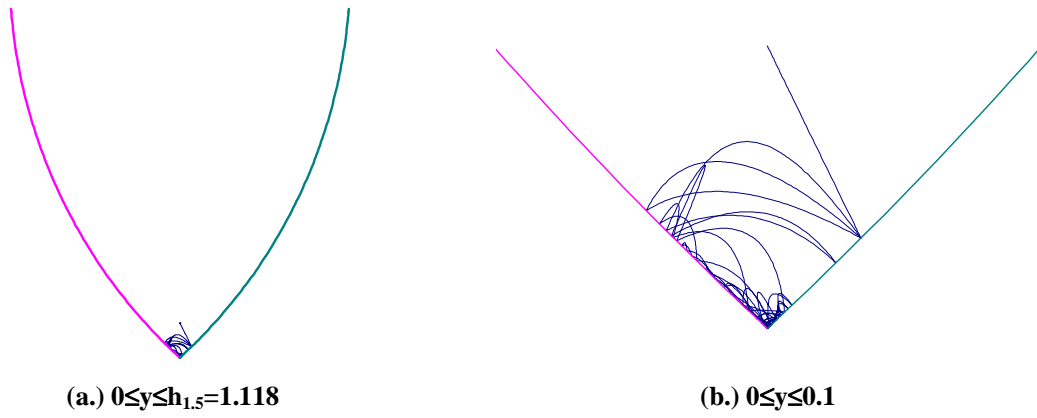


Fig. 4.6.  $y$  vs.  $x$ , Case 190010-559

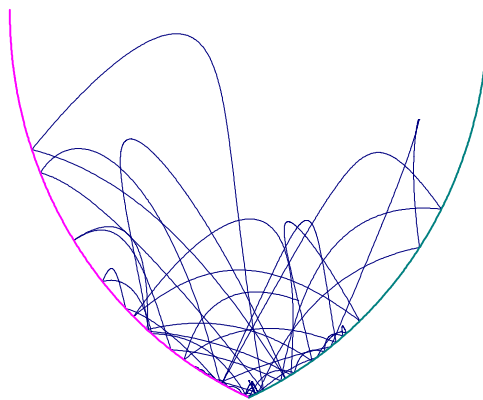
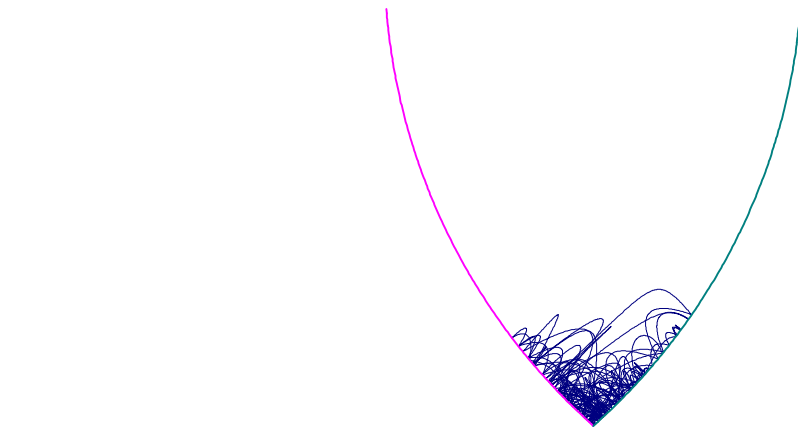
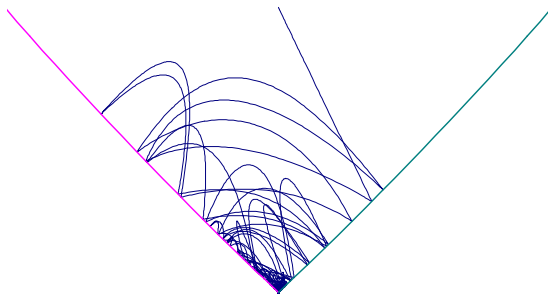


Fig. 4.7.  $y$  vs.  $x$ , Case 290010-559  
 $0 \leq y \leq h_{2.5} = 2.291$



**Fig. 4.8.  $y$  vs.  $x$ , Case 110010-559 ( $e=1.0$ )**



**Fig. 4.9.  $y$  vs.  $x$ , Case 1950010-559 ( $e=0.95$ )**

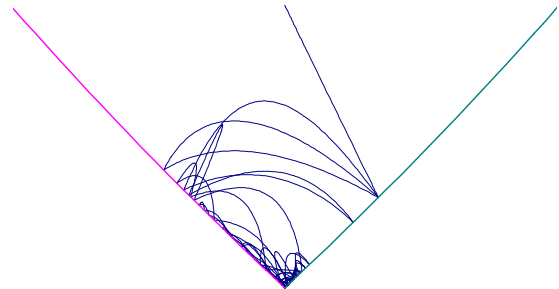


**Fig. 4.10.  $y$  vs.  $x$ , Case 190010-559 ( $e=0.9$ )**

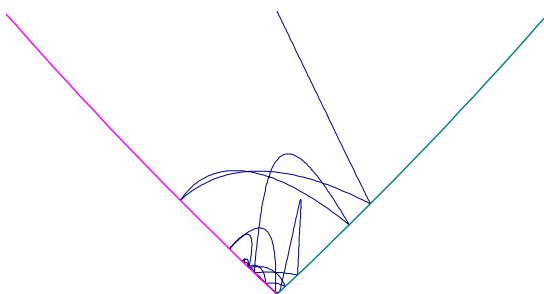


**Fig. 4.11.  $y$  vs.  $x$ , Case 180010-559 ( $e=0.8$ )**

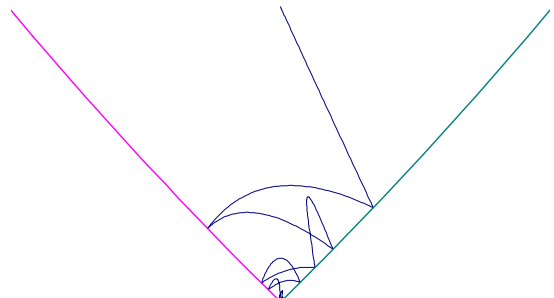


**Fig. 4.12.  $y$  vs.  $x$ , Case 170010-559 ( $e=0.7$ )**

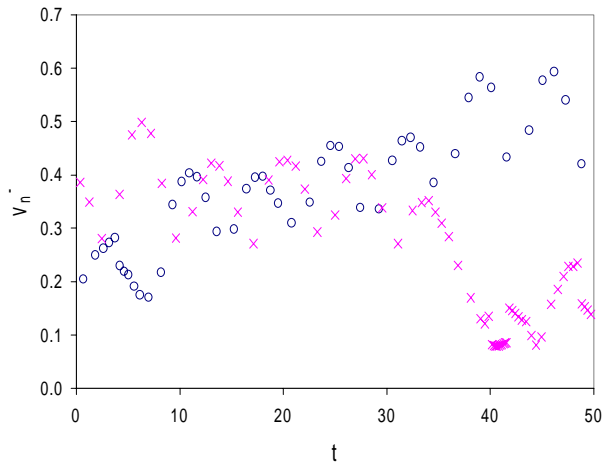


**Fig. 4.13.**  $v_n$  vs.  $t$ , Case 110010-559 ( $e=1.0$ )

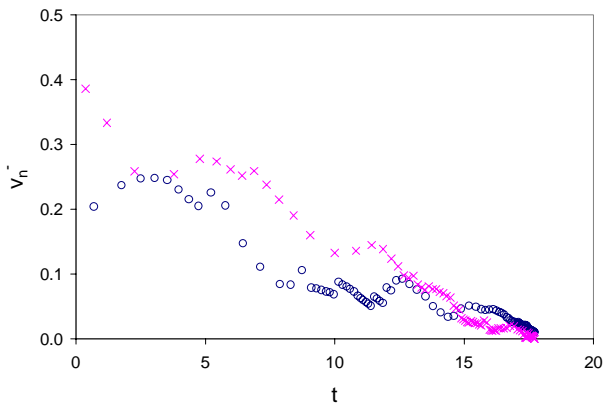


**Fig. 4.14.**  $v_n$  vs.  $t$ , Case 1950010-559 ( $e=0.95$ )

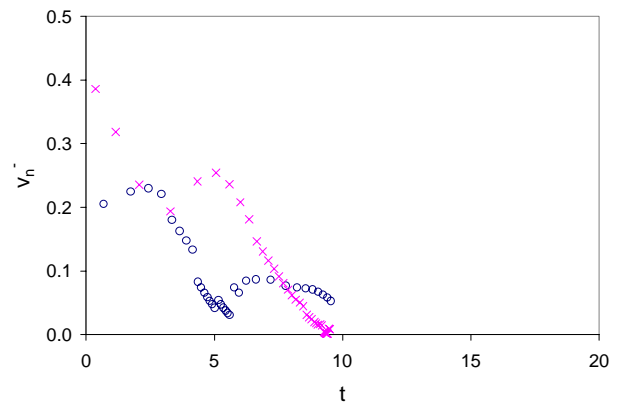


**Fig. 4.15.**  $v_n$  vs.  $t$ , Case 190010-559 ( $e=0.9$ )

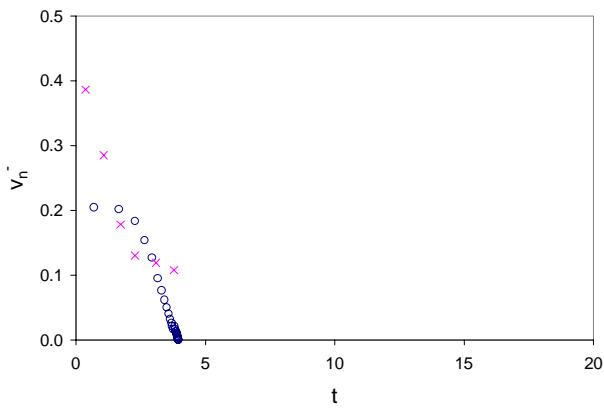


**Fig. 4.16.**  $v_n$  vs.  $t$ , Case 180010-559 ( $e=0.8$ )

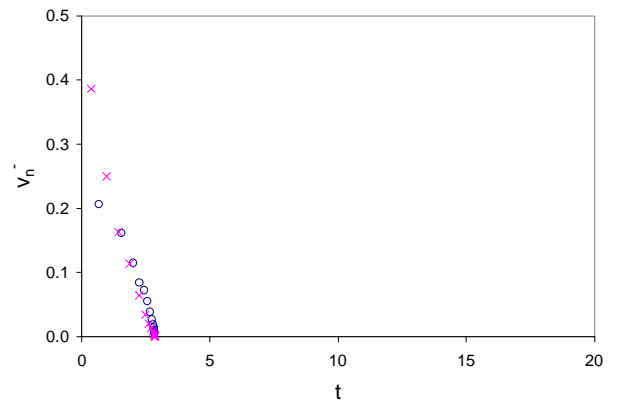


**Fig. 4.17.**  $v_n$  vs.  $t$ , Case 170010-559 ( $e=0.7$ )

The forcing parameter  $\Omega$  was varied to see its effect on the response of the PMBW under forced motions. Figures 4.18-4.22 show the trajectory plots of the data obtained from the cases which were run with  $\Omega$  varying from 0.5 to 0.75 to 0.9 to 1.5 to 2.0. Characteristic features do not noticeably appear from these plots; however, Figs. 4.23-4.27 show some interesting phenomena in the  $v_n^-$  vs. time plots. One interesting feature is seen in Fig. 4.23 around the time  $t=8$ . This is where three parallel lines of o's stick out. By looking at the trajectory and impact data, it can be deduced that this is caused by the PMBW bouncing down the  $g_1=0$  boundary and then striking the  $g_2=0$  boundary at the lowest point in the region with a large normal velocity. Then the PMBW rebounds and bounces down the  $g_1=0$  boundary and again strikes the  $g_2=0$  boundary, and the process repeats until the PMBW settles to the bottom of the region due to the effect of gravity.

As seen in the plots of various normal velocity just before impact versus time ( $v_n^-$  vs.  $t$ ) throughout this chapter, a pattern to the x's and o's may be noticed which is different than the patterns seen in the PMBW free motion chapter. Instead of having the normal velocities consistently higher on one boundary than the other, as seen in Fig. 3.2, in this problem they seem to have two types of patterns. The first pattern shows the boundary normal velocities converging and then diverging, which is referred to as a serpentine pattern and is seen in Figs. 4.23 and 4.26. The other pattern is one where the boundary normal velocities intertwine and seem to braid in and out of each other. This may be seen in Figs. 4.24, 4.25, and 4.27. These patterns are most likely due to the elliptical forcing in this problem which is continually changing direction. For example, say the PMBW is headed towards the right boundary and the forcing is acting in the same direction; then the normal velocity at impact will be high. Then after the rebound the PMBW is headed towards the left boundary but the forcing is acting in the opposite direction; then the normal velocity will be low when it strikes the left boundary, showing up on the graph as a separation in the braids. If both boundaries are struck in succession with similar conditions and the forcing has switched direction, the normal velocities may have the same value, indicated on the  $v_n^-$  vs.  $t$  graph as a point of convergence or overlapping.

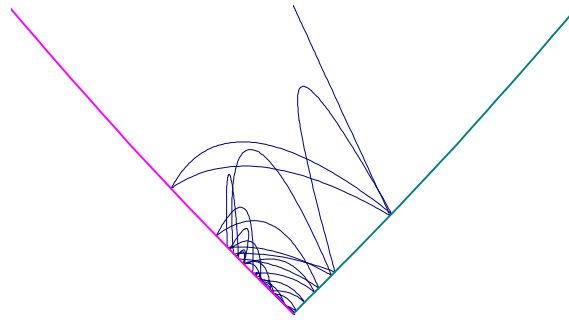


**Fig. 4.18.** y vs. x, Case 190010-555 ( $\Omega=0.5$ )

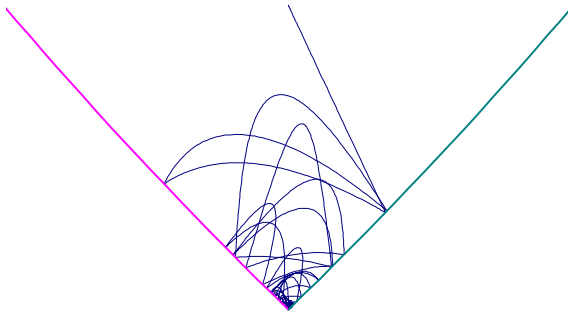


**Fig. 4.19.** y vs. x, Case 190010-5575 ( $\Omega=0.75$ )

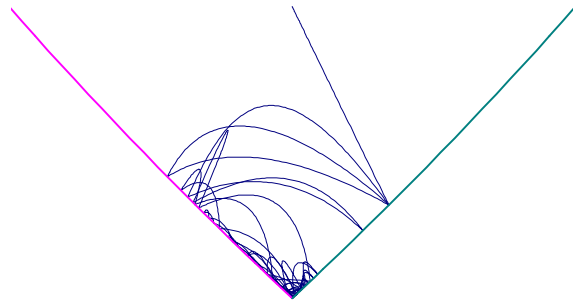


**Fig. 4.20.** y vs. x, Case 190010-559 ( $\Omega=0.9$ )

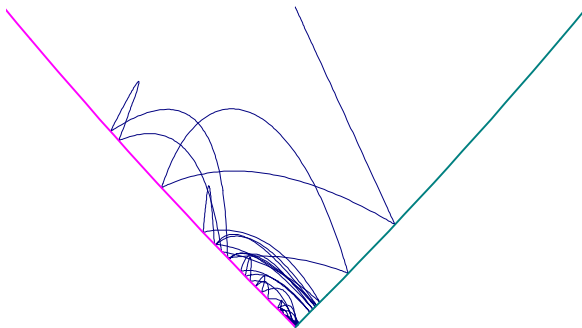


**Fig. 4.21.** y vs. x, Case 190010-5515 ( $\Omega=1.5$ )

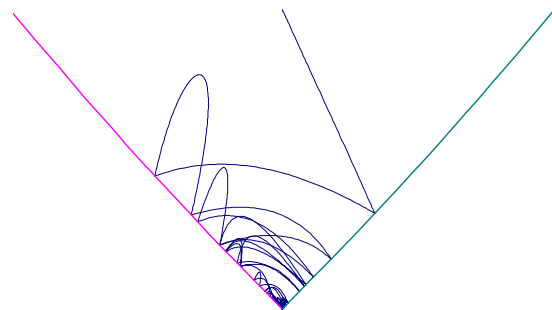


**Fig. 4.22.** y vs. x, Case 190010-5520 ( $\Omega=2.0$ )

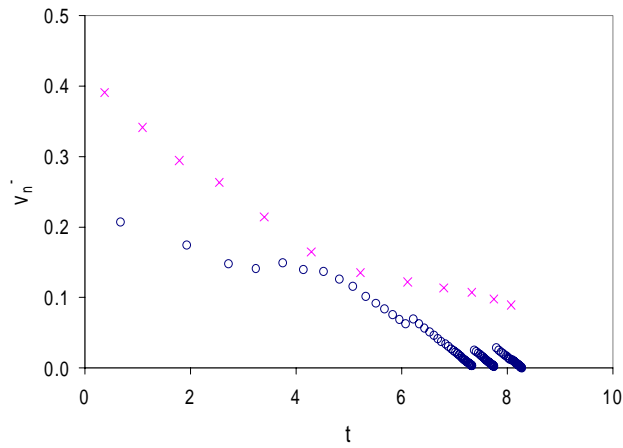


**Fig. 4.23.**  $v_n$  vs.  $t$ , Case 190010-555 ( $\Omega=0.5$ )

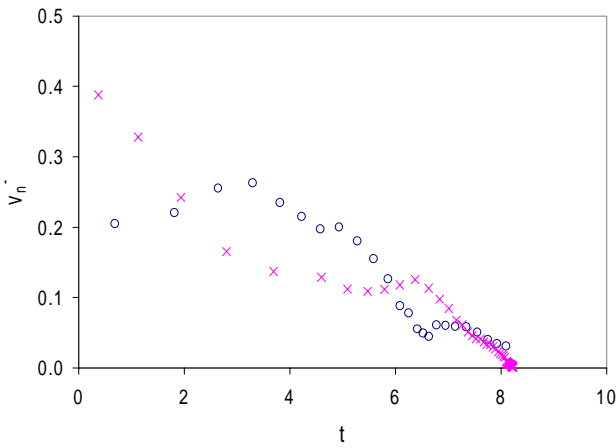


**Fig. 4.24.**  $v_n$  vs.  $t$ , Case 190010-5575 ( $\Omega=0.75$ )

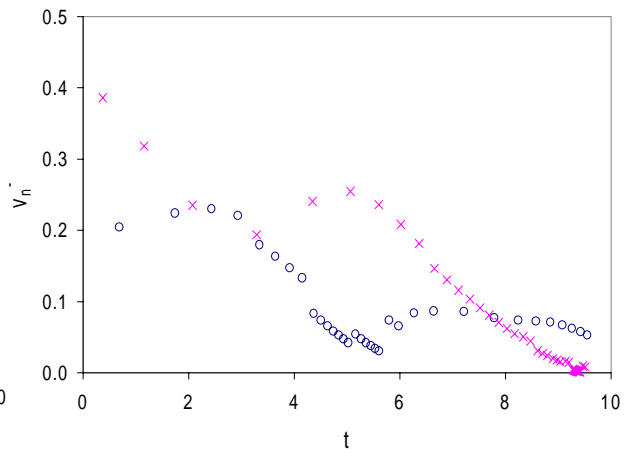


**Fig. 4.25.**  $v_n$  vs.  $t$ , Case 190010-559 ( $\Omega=0.9$ )

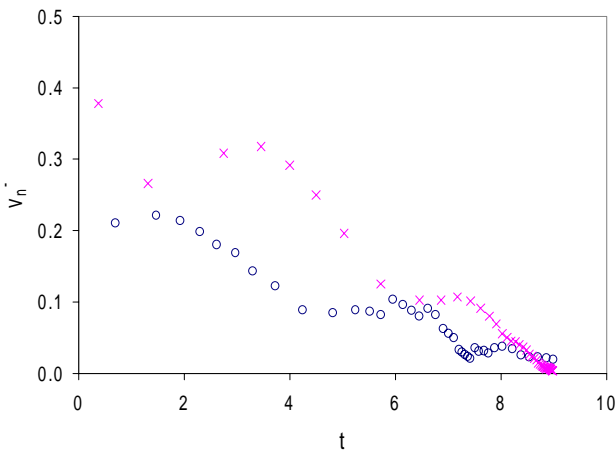


**Fig. 4.26.**  $v_n$  vs.  $t$ , Case 190010-5515 ( $\Omega=1.5$ )

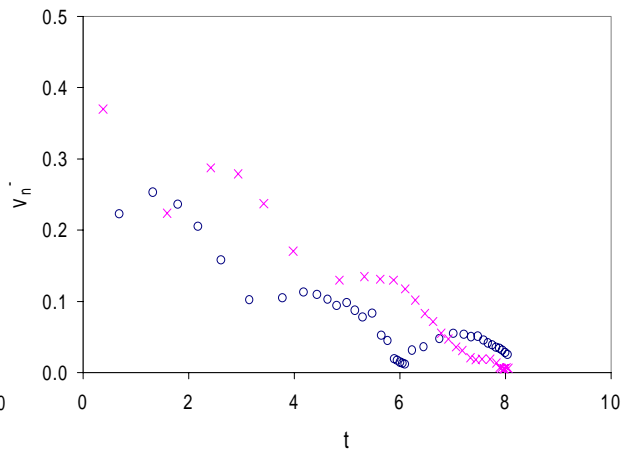


**Fig. 4.27.**  $v_n$  vs.  $t$ , Case 190010-5520 ( $\Omega=2.0$ )

#### 4.4.2 Critical Force

As the amplitude of the forcing,  $f_o$ , increases, the motions tend to become larger and last longer. This behavior is seen in Figs. 4.28-4.32 as  $f_o$  increases from 0.3 to 0.5 to 0.75 to 1.0 to 1.5. As seen, the amplitude of the forcing increases and this causes the breakwater to climb the sides of the region because there is more energy introduced to the system to cause this behavior. At some point the motions of the breakwater becomes less dependent upon the gravity component of the force and more dependent on the wave forcing component. This can be seen in Fig. 4.30, the  $f_o=0.75$  case, where the motions reach a higher value of  $y$  than in Fig. 4.29, the  $f_o=0.5$  case, but still die down towards the bottom because the gravity force is controlling. However, in the  $f_o=1.5$  case the forcing ultimately controls, and this is seen in Fig. 4.32 because the breakwater travels all around the region instead of staying near the bottom. It should be noted that trajectory plots of Figs. 4.28-4.32 are not plotted to the same scale. Figures 4.28–4.30 are plotted up to  $y=0.1$ , while Fig. 4.31 goes to  $y=0.4$ , and Fig. 4.32 to  $y=h$ .

Due to this occurrence, a new term will be introduced known as critical force,  $f_{cr}$ . The critical force is defined as the forcing amplitude which would cause the breakwater to hit the upper boundary ( $y=h$ ), which indicates that the forcing was so large that it controlled the motions of the breakwater and caused it to hit the sea floor. Plots of the critical force versus the coefficient of restitution,  $e$ , and the wave frequency,  $\Omega$ , were created (Figs. 4.33 and 4.34). These plots were produced by fixing all of the standard case conditions except  $e$  in Fig. 4.33 and  $\Omega$  in Fig. 4.34, and increasing  $f_o$  until the calculated  $y$  value reached the height  $h$ . It is seen in Figs. 4.33 and 4.34 that the critical force for the standard case is around 1.17. This means that when  $f_o=1.17=f_{cr}$  for the standard case conditions, the PMBW will hit the upper boundary  $y=h$ . This can be seen in Fig. 4.32 where  $f_o=1.5$  which is greater than  $f_{cr}=1.17$ , and thus the breakwater goes above  $y=h$  at the point denoted by A. Further, Figs. 4.33 and 4.34 show a decreasing nature of the critical force as the variables  $e$  and  $\Omega$  increase. However, the critical force solutions are not monotonic in nature; they contain some local maxima and minima.

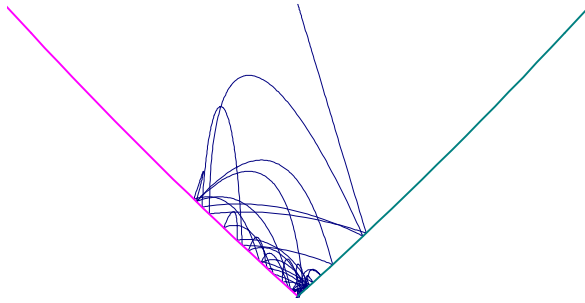


**Fig. 4.28. y vs. x, Case 190010-359 ( $f_0=0.3$ )**

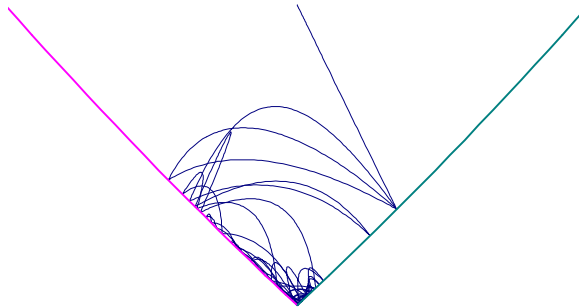


**Fig. 4.29. y vs. x, Case 190010-559 ( $f_0=0.5$ )**

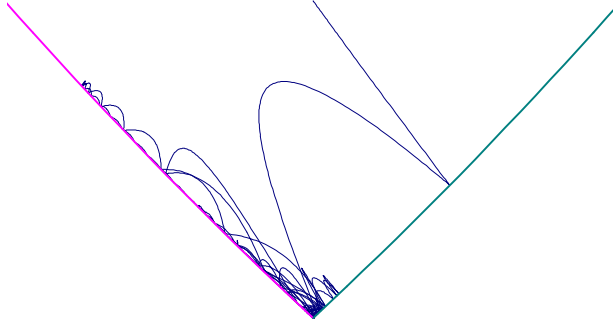


**Fig. 4.30. y vs. x, Case 190010-7559 ( $f_0=0.75$ )**

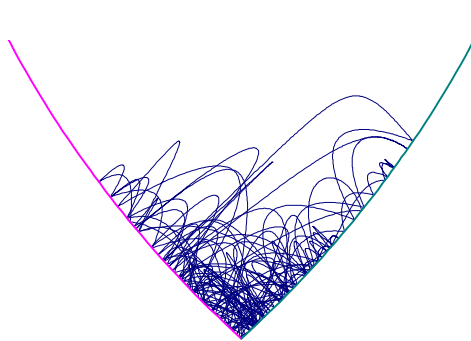


**Fig. 4.31. y vs. x, Case 190010-1059 ( $f_0=1.0$ )**

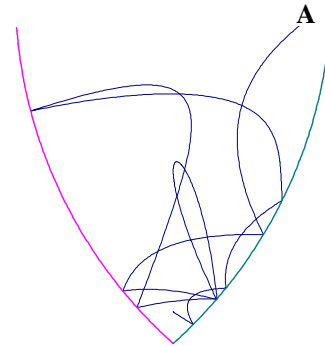


**Fig. 4.32. y vs. x, Case 190010-1559 ( $f_0=1.5$ )**

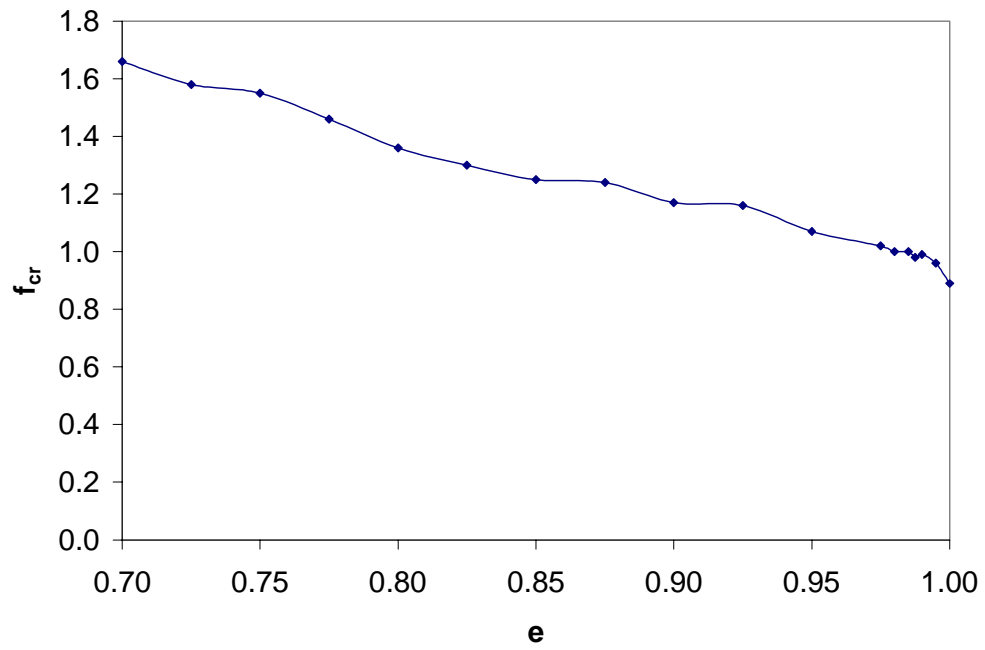


**Fig. 4.33. Critical Force vs.  $e$**

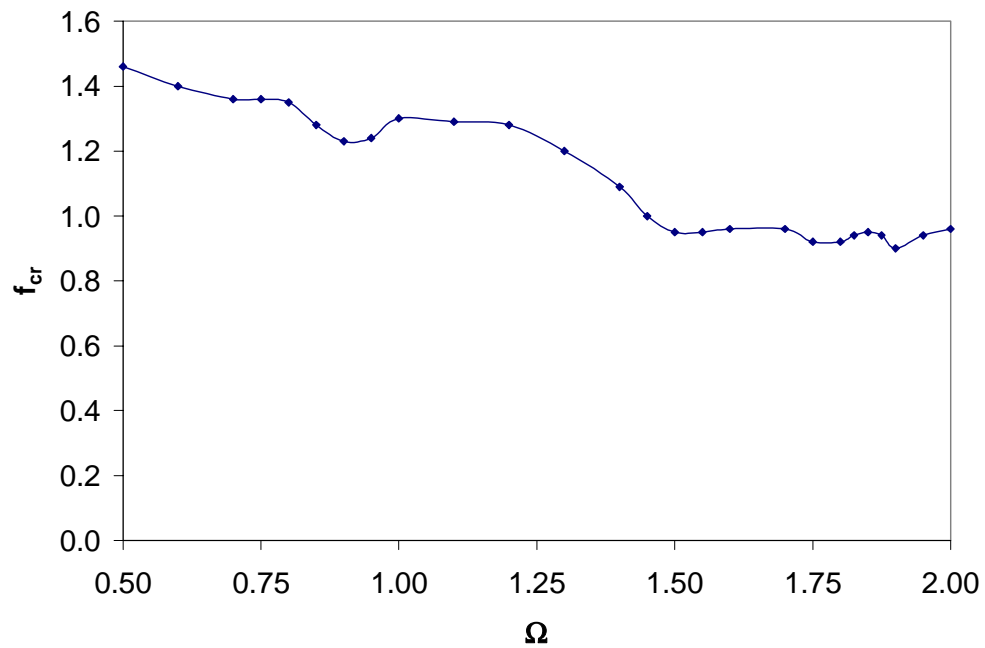


**Fig. 4.34. Critical Force vs.  $\Omega$**

### 4.4.3 Norms

Norm plots were also created for a set of given parameters. Norms for this problem are either maximum data points or summation of data. Four norms were investigated; three dealt with the normal velocity just before impact,  $v_n^-$ , and are as follows:

$$\rho_1 = \max_t(v_n^-) \quad (4.29)$$

$$\rho_2 = \sum_{t=0}^{10} v_n^- \quad (4.30)$$

$$\rho_3 = \sum_{t=0}^{\infty} v_n^- \quad (4.31)$$

The last was the maximum height,  $y_{\max}$ , which the PMBW attained during its period of motion. The data used in the determination of the norms was the same data used to produce the trajectory and normal velocity vs. time plots. The norms are plotted versus the magnitude of the forcing,  $f_o$ , for a given set of parameters (Figs. 4.35-4.37). The standard case parameters and initial conditions were used to create these plots with the exception of  $f_o$  which was the parameter varied. As seen in Fig. 4.35, the phenomenon of a critical forcing is reinforced. It can be seen that as the forcing is increased,  $y_{\max}$  increases to a point where the PMBW is just below the boundary height  $h$ , and the forcing is just below the predetermined value of  $f_{cr}$ . When the forcing is low, the initial height of  $y_o=0.1$  is  $y_{\max}$ ; this is due to gravity controlling the motions at this low forcing, and as the forcing increases, the response becomes more and more controlled by the forcing. Further, as the forcing amplitude,  $f_o$ , is increased, the norm  $\rho_1$  (Fig. 4.36) increases because more energy is introduced into the system and this causes the normal velocity just before impact to increase because the PMBW strikes the boundaries with more force. Finally, for this same reason, the cumulative norms  $\rho_2$  and  $\rho_3$  (Figs. 4.36 and 4.37) increase because more energy is moving the PMBW about. The chaotic nature increases as the forcing increases towards the critical force and may be attributed to the highly nonlinear nature of the problem. An increase in the forcing amplitude,  $f_o$ , does not necessarily cause the maximum height,  $y_{\max}$ , or the other norms to increase.

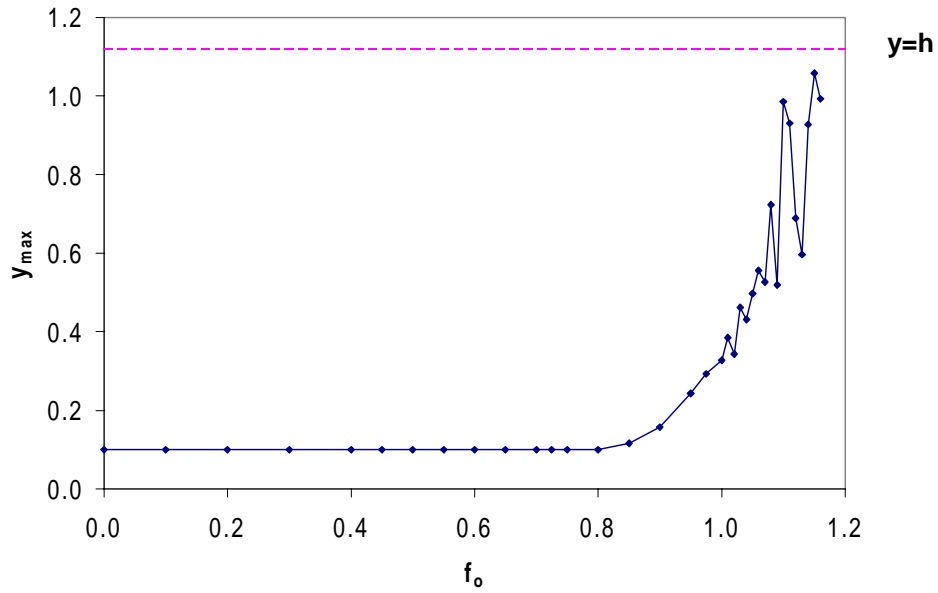


Fig. 4.35.  $y_{\max}$  vs.  $f_0$ , Norm Plot

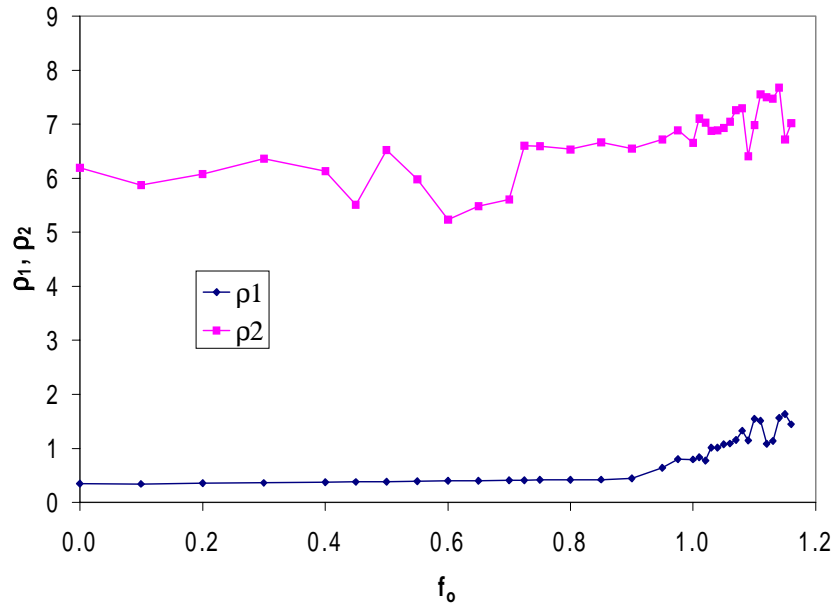


Fig. 4.36.  $\rho_1$  and  $\rho_2$  vs.  $f_0$ , Norm Plots

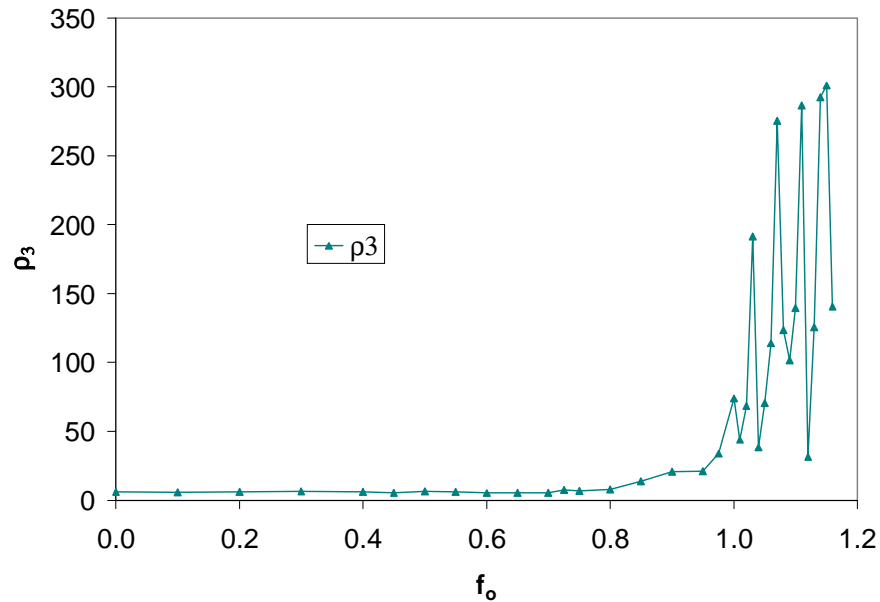


Fig. 4.37.  $\rho_3$  vs.  $f_0$ , Norm Plot

## 4.5 Special Cases

Several special cases were developed in order to observe the effects of varying the forcing parameters and to see if some special situations may arise under certain specific conditions.

### 4.5.1 No-Gravity Case

A special case where gravity and/or buoyant forces were neglected was investigated. This case simulates the property of a “neutrally buoyant” object in a fluid. This means that the gravity forces pulling down on an object exactly equal the buoyant forces that are making the object float up. This eliminates the gravitational force and leaves only the wave forces to act on the object. Several trials were conducted to see how varying the forcing parameters affected the motions of the PMBW, and these parameters are summarized in Table 4.1.

#### 4.5.1.1 No-Gravity Case Formulation

The EOM's used in this analysis are similar to those in section 4.2.2; however, the effects of gravity are neglected. The resulting solutions are summarized here:

$$x = c_1 + c_2 t - \frac{f_o}{\Omega^2} \cos[\Omega(t - t_x)] \quad (4.32)$$

$$\dot{x} = c_2 + \frac{f_o}{\Omega} \sin[\Omega(t - t_x)] \quad (4.33)$$

$$y = c_3 + c_4 t - \frac{vf_o}{\Omega^2} \cos[\Omega(t - t_y)] \quad (4.34)$$

$$\dot{y} = c_4 + \frac{vf_o}{\Omega} \sin[\Omega(t - t_y)] \quad (4.35)$$

where

$$c_1 = x_i - c_2 t_i + \frac{f_o}{\Omega^2} \cos[\Omega(t_i - t_x)] \quad (4.36)$$

$$c_2 = \dot{x}_i - \frac{f_o}{\Omega} \sin[\Omega(t_i - t_x)] \quad (4.37)$$

$$c_3 = y_i - c_4 t_i + \frac{vf_o}{\Omega^2} \cos[\Omega(t_i - t_y)] \quad (4.38)$$

$$c_4 = \dot{y}_i - \frac{vf_o}{\Omega} \sin[\Omega(t_i - t_y)] \quad (4.39)$$

However, for these equations to produce motions which resemble the applied wave forcing, the initial values of the terms  $c_2$  and  $c_4$  need to be zero. Thus, initial  $x$  and  $y$  positions,  $f_o$ ,  $v$ , and  $\Omega$  were chosen to satisfy these initial conditions. To accomplish this, the Equations 4.40 and 4.41 were used to get the initial  $x$  and  $y$  velocities. The values of these parameters and initial conditions may be seen in Table 4.1. It must be noted that the no-gravity cases investigated here were mistakenly given  $t_x=5.0$  during the analysis, contrary to the other cases analyzed. The results of this analysis were not significantly impacted because the  $t_x$  value was not equal to zero since this parameter is a phase shift. The only effect on the no-gravity cases would be that the forcing would start at a different point on the forcing ellipse. Thus, since the no-gravity motions follow the forcing, the

only effect would be that the motions in the trajectory plots would be shifted. Normally  $\dot{x}_o$  would be zero, but with  $t_x \neq 0$ , the values of  $\dot{x}_o$  do not equal zero as seen in Table 4.1. Since this does not affect the desired conclusion of the varying of the forcing parameters, it was deemed acceptable for the analysis. The values  $\dot{x}_o$  and  $\dot{y}_o$  are

$$\dot{x}_o = \frac{f_o}{\Omega} \sin[-\Omega t_x] \quad (4.40)$$

$$\dot{y}_o = \frac{vf_o}{\Omega} \sin[-\Omega t_y] \quad (4.41)$$

#### 4.5.1.2 No-Gravity Case Results

Table 4.1 shows the initial conditions used to produce the responses investigated. The initial conditions were produced from the analytical solution with the gravity terms neglected. In Figs. 4.38-4.42 the results of varying  $f_o$  can be seen, with  $f_o$  increasing from 0.01 to 0.02 to 0.03 to 0.04 and 0.05. As expected, when the amplitude of the forcing increases, the size of the elliptical motion increases. The elliptical path occurs because the only forces affecting the motions are the periodic forces which cause the PMBW to travel in an elliptical path produced by the elliptical forces previously discussed. Also, during this analysis, both the left and right mooring cables are slack. In Figs. 4.38-4.40, the size of the ellipse increases until it reaches a boundary where the impact (i.e., cable becoming taut) causes the motion to change direction, thus causing the loss of the elliptical pattern (Figs. 4.41 and 4.42). The ellipses occur off center because of the way the forcing functions start and how the initial conditions were chosen. As seen in Fig. 4.43 and Table 4.1, initial conditions can be chosen to make the trajectory occur about the axis  $x=0$ . The asymmetry seen in the previous figures arises from terms  $c_2$  and  $c_4$  which come about from the integral derivation of the EOM's used in the solution. By setting these constants to zero and staying zero throughout the analysis, an ellipse with its small axis along the line  $x=0$  may be obtained (Fig. 4.43).

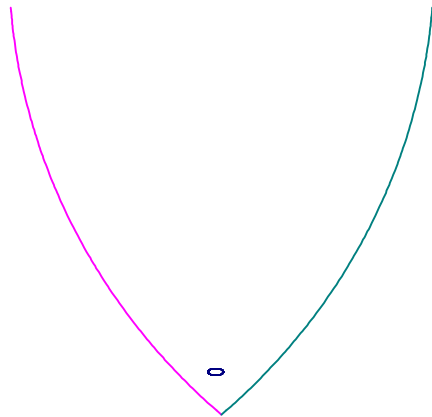


Fig. 4.38. y vs. x, Case 110010-01575ng  
( $f_0=0.01$ )

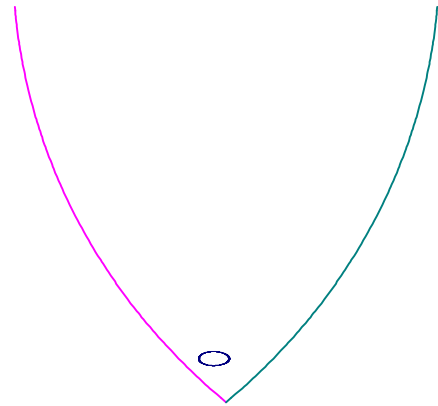


Fig. 4.39. y vs. x, Case 110010-02575ng  
( $f_0=0.02$ )

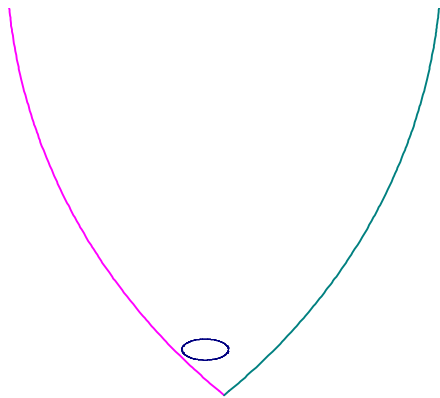


Fig. 4.40. y vs. x, Case 110010-03575ng  
( $f_0=0.03$ )

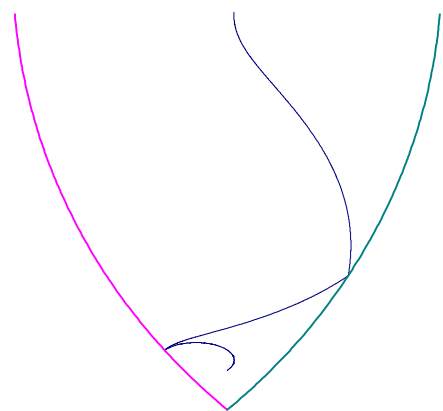


Fig. 4.41. y vs. x, Case 110010-04575ng  
( $f_0=0.04$ )

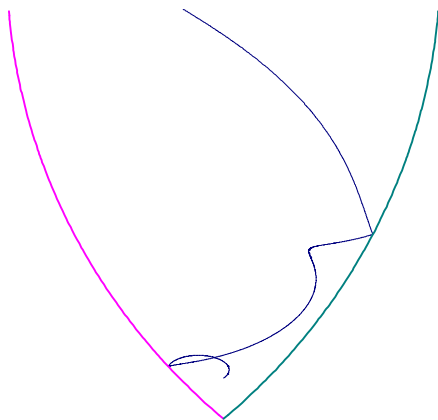


Fig. 4.42. y vs. x, Case 110010-05575ng  
( $f_0=0.05$ )

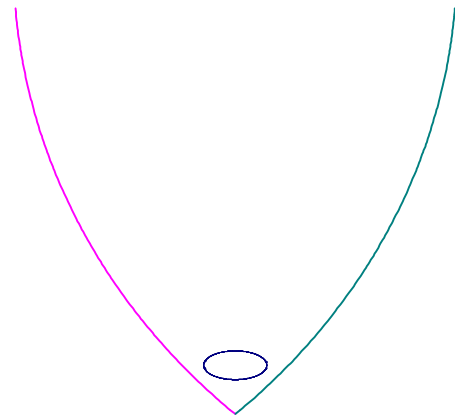
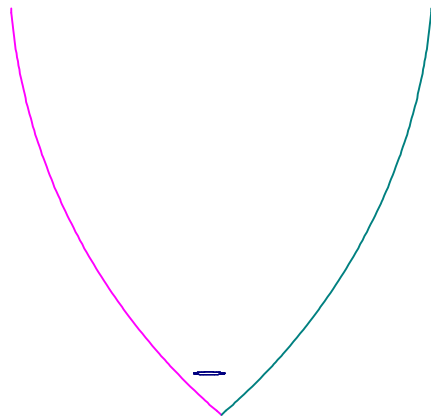
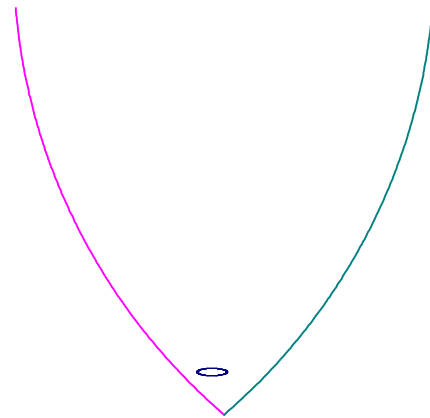


Fig. 4.43. y vs. x, Case 115302-04575ng  
(Centered Ellipse)

In Figs. 4.44-4.47, the amplitude reduction factor,  $v$ , varied from 0.1 to 0.25 to 0.5 to 1.0 and this causes the height-to-width ratio of the forcing ellipse to vary. Further initial conditions and parameters may be seen in Table 4.1. The parameter  $v$  is the constant that determines the ratio of  $f_y$  to  $f_x$  as seen in Equations 4.14 and 4.16. As  $v$  increases toward unity, the more circular the force ellipse becomes; this is because the  $x$  and  $y$  forcing amplitudes are becoming more equal as  $v$  gets closer to one. This trend is seen in Figs. 4.44-4.47 where a low value of  $v$  produces a flatter ellipse and a higher value of  $v$  produces a more circular ellipse.



**Fig. 4.44. y vs. x, Case 110010-02175ng  
( $v=0.1$ )**



**Fig. 4.45. y vs. x, Case 110010-022575ng  
( $v=0.25$ )**

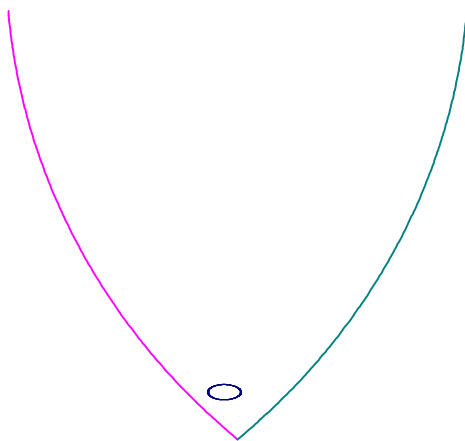


**Fig. 4.46. y vs. x, Case 110010-02575ng  
( $v=0.5$ )**

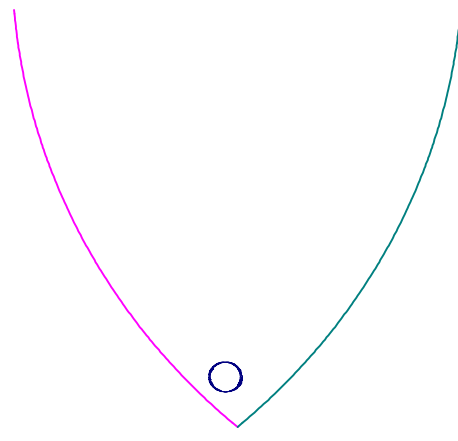


**Fig. 4.47. y vs. x, Case 110010-021075ng  
( $v=1.0$ )**

## 4.5.2 Harmonic Motion Case

The special case of harmonic motion of the forced motion problem was investigated to see if a periodic solution existed in which the motions of the PMBW trajectory would become harmonic.

### 4.5.2.1 Harmonic Motion Case Formulation

Constraints on the parameters and conditions were imposed in the formulation of this special case to see if a periodic solution could be induced. The following parameters were used in the derivation of the equations to find the solution and used to determine suitable initial conditions. This case included the effects of gravity. No energy was to be lost at impacts. Vertical forcing was inhibited and only horizontal forcing was allowed; thus, to induce this,

$$e=1.0 \quad t_x=0.0 \quad t_y=0.0 \quad v=0.0 \rightarrow f_y=0.0 \quad (4.42)$$

By imposing the above restrictions and making the initial time  $t_0=0$  and the time at the first impact  $t_1=\pi/\Omega$  (i.e., half the forcing period), further conditions at the first impact may be specified as

$$x_1=-x_0 \quad \dot{x}_1 = \dot{x}_0 \quad y_1=y_0 \quad \dot{y}_1 = \dot{y}_0 \quad (4.43)$$

with the mass starting on the left boundary.

Thus, the following equations were derived to obtain the initial conditions, which would induce a periodic solution from the previously stated solutions and restrictive conditions:

$$x_0 = 1 - \sqrt{r^2 - (h - y_0)^2} \quad (4.44)$$

$$f_0 = -x_0 \Omega^2 - \frac{\pi^2 (1 - x_0)}{4\sqrt{r^2 - (1 - x_0)^2}} \quad (4.45)$$

$$\dot{x}_0 = \frac{-2x_0 \Omega}{\pi} - \frac{2f_0}{\pi \Omega} \quad (4.46)$$

$$\dot{y}_0 = \frac{\pi}{2\Omega} \quad (4.47)$$

By choosing an initial height,  $y_0$ , and frequency,  $\Omega$ , then using Equations 4.44-4.47, the other initial conditions may be calculated in order to obtain a periodic solution. Table 4.2 shows the initial conditions used in the analysis of the periodic solution, and the figures in the following section show how the trajectories vary according to the varying of independent variables  $y_0$  and  $\Omega$ .

#### 4.5.2.2 Harmonic Motion Case Results

A standard case was developed for the special harmonic forcing case utilizing the restrictive parameters. The values of the parameters and initial conditions for the standard case may be seen in Table 4.2 (shaded). As seen in Fig. 4.48, as time increases, the small errors in the rounding and estimations of calculated values accumulate and the trajectories lose their nice periodic motion. Because a periodic solution is the desired outcome, plots such as seen in Fig. 4.49 were produced from the plots with the accumulated errors. The only difference between Figs. 4.48 and 4.49 is that Fig. 4.49 has had the data points cut out starting from the time at which the solution stopped being periodic, to show just the trajectory of the initial periodic solution without the accumulated errors. Figure 4.50 shows a nice example of this with the  $v_n^-$  vs. time graphs initially having the same  $v_n^-$  values for a while, as expected, but then after some time the velocities start to diverge as the error increases.

A standard case was run but with  $e=0.95$  instead of 1.0 to see the effects of  $e$  on the trajectory. As seen in Fig. 4.51, the first loop is similar to that of the periodic solution when  $e=1.0$ , but after the first impact the loop shape is lost due to the loss of energy. When the coefficient of restitution was allowed to be 0.99, the PMBW followed a similar pattern but went above the upper boundary  $y=h$ . Thus, a periodic solution will exist when  $e=1.0$ ; however, because energy is lost from the system when  $e \neq 1.0$ , the PMBW will not continue along this periodic path.

When  $\Omega$  is varied, the periodic trajectory of the PMBW decreases from a loop to an arc (Figs. 4.52-4.56). These figures show  $\Omega$  varying from 1.5 to 2.0 to 3.0 to 4.0 to 5.0, and the other parameters and initial conditions may be seen in Table 4.2. The length of the path between the boundaries decreases as the forcing frequency increases, thus, the mass is moving faster.

As the initial height on the left boundary,  $y_0$ , is increased, the trajectory just moves up, keeping the same type of shape (Figs. 4.57-4.60). The variable  $y_0$  is varied from 0.1 to 0.2 to 0.3 to 0.4 in the figures. There do not seem to be any notable characteristics, except that the trajectory is moving up. As  $y_0$  is increased, the trajectory will eventually strike the upper boundary  $y=h$ .

The harmonic motion case gives a good opportunity to show an impact Poincaré plot. The impact Poincaré plots used here show the value of velocity before impact versus position for either the vertical or horizontal direction. In Figs. 4.61 and 4.62 the x and y impact Poincaré plots are shown for the fspo3 case from Table 4.2 (Fig. 4.54). These plots put a dot corresponding to the impact velocity versus the position in the x and y directions. According to the formulation, the criteria of Equation 4.43 from Section 4.4.2 must be met for the harmonic motion solution to exist. Thus, only two dots, which are mirror images of one another, should show up on the x plot, and one dot would show up on the y plot. These criteria are met, as seen in Figs. 4.61 and 4.62.

**Table 4.2. Initial Conditions for Harmonic Motions of a Point-Mass Breakwater**

<b>Case Name</b>	<b>r</b>	<b>e</b>	<b>x</b>	<b>v<sub>x</sub></b>	<b>y</b>	<b>v<sub>y</sub></b>	<b>f<sub>o</sub></b>	<b>v</b>	<b>Ω</b>
fspstd	1.5	1.0	-0.10164	1.13320	0.1	1.04720	-2.44135	0.0	1.5
fspe99	1.5	0.99	-0.10164	1.13320	0.1	1.04720	-2.44135	0.0	1.5
fspe95	1.5	0.95	-0.10164	1.13320	0.1	1.04720	-2.44135	0.0	1.5
<b>Ω</b>									
fspstd	1.5	1.0	-0.10164	1.13320	0.1	1.04720	-2.44135	0.0	1.5
fspo2	1.5	1.0	-0.10164	0.84990	0.1	0.78540	-2.26348	0.0	2.0
fspo3	1.5	1.0	-0.10164	0.56660	0.1	0.52360	-1.75529	0.0	3.0
fspo4	1.5	1.0	-0.10164	0.42495	0.1	0.39270	-1.04382	0.0	4.0
fspo5	1.5	1.0	-0.10164	0.33996	0.1	0.31416	-0.12908	0.0	5.0
<b>y<sub>o</sub></b>									
fspstd	1.5	1.0	-0.10164	1.13320	0.1	1.04720	-2.44135	0.0	1.5
fspy2	1.5	1.0	-0.18626	1.35316	0.2	1.04720	-2.76923	0.0	1.5
fspy3	1.5	1.0	-0.25731	1.60953	0.3	1.04720	-3.21342	0.0	1.5
fspy4	1.5	1.0	-0.31698	1.92071	0.4	1.04720	-3.81237	0.0	1.5

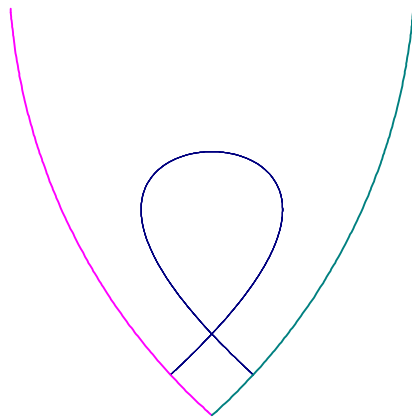


**Fig. 4.48. y vs. x, Standard Case with Errors (Case fspstd)**

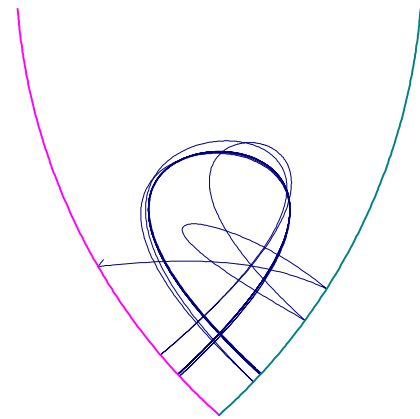


**Fig. 4.49. y vs. x, Standard Case (Case fspstd)**

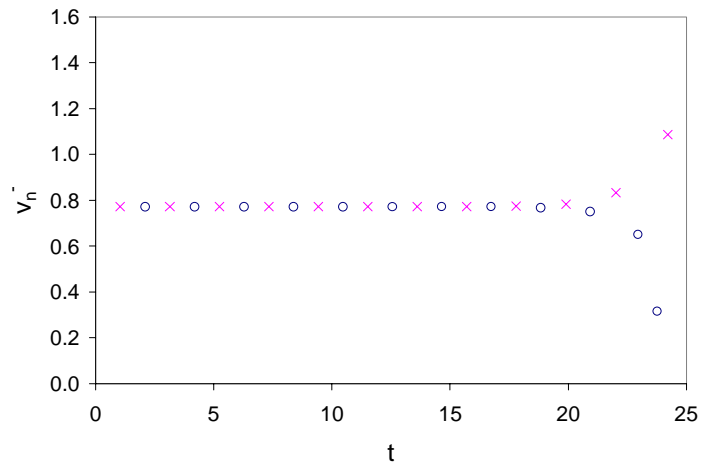


**Fig. 4.50. v<sub>n</sub> vs. t, Case fspo3**

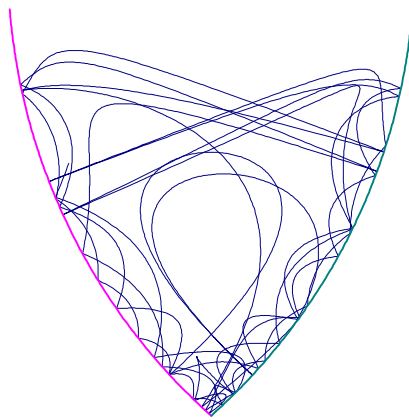


**Fig. 4.51. y vs. x, Case fspe95 (e=0.95)**

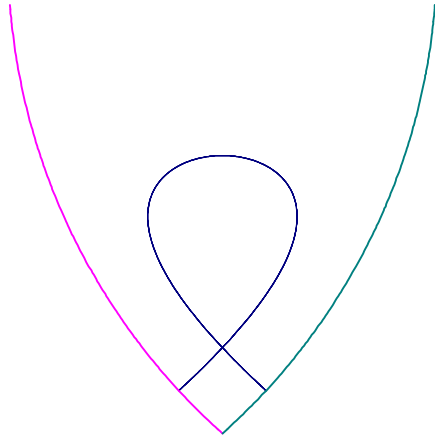


Fig. 4.52.  $y$  vs.  $x$ , Case fspstd ( $\Omega=1.5$ )

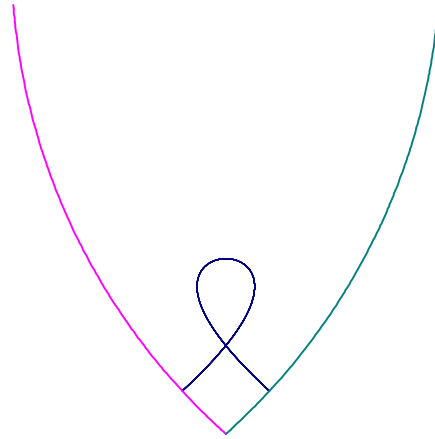


Fig. 4.53.  $y$  vs.  $x$ , Case fsp2 ( $\Omega=2.0$ )

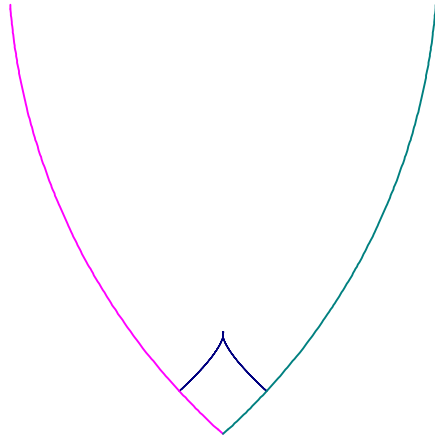


Fig. 4.54.  $y$  vs.  $x$ , Case fsp3 ( $\Omega=3.0$ )

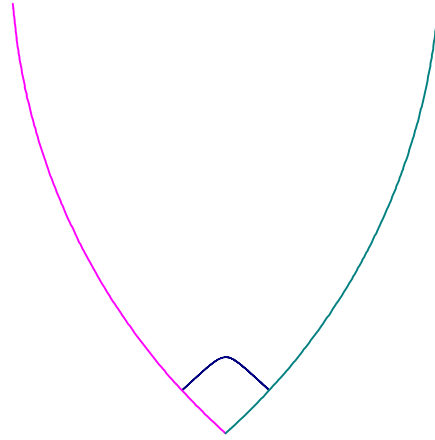


Fig. 4.55.  $y$  vs.  $x$ , Case fsp4 ( $\Omega=4.0$ )

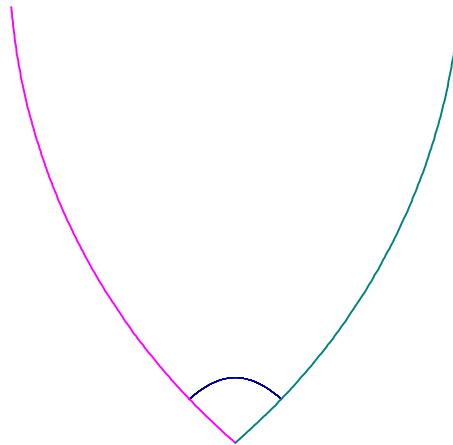
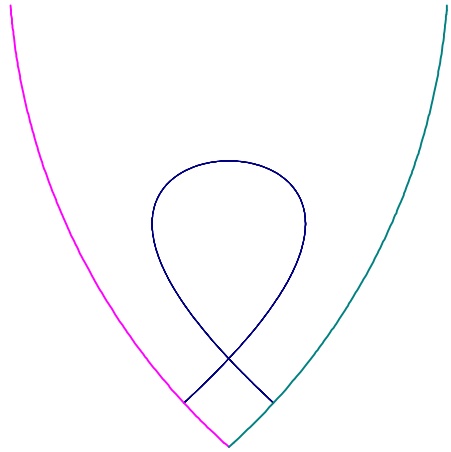
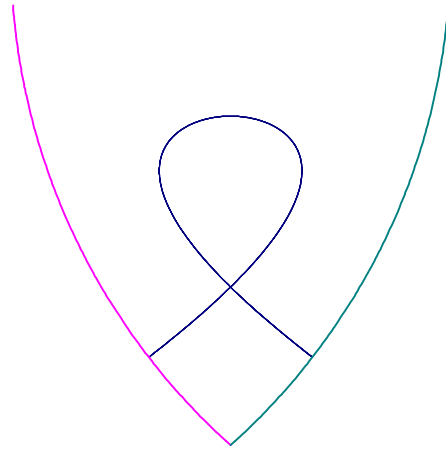


Fig. 4.56.  $y$  vs.  $x$ , Case fsp5 ( $\Omega=5.0$ )



**Fig. 4.57.**  $y$  vs.  $x$ , Case fspstd ( $y_0=0.1$ )



**Fig. 4.58.**  $y$  vs.  $x$ , Case fspy2 ( $y_0=0.2$ )

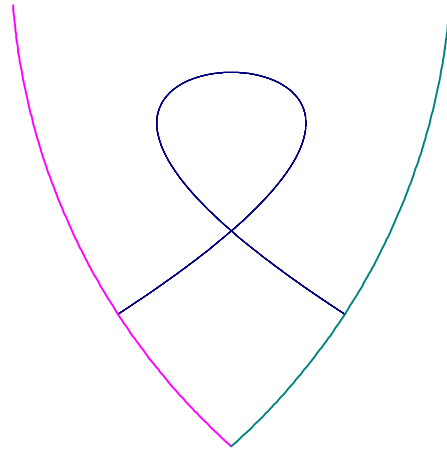


**Fig. 4.59.**  $y$  vs.  $x$ , Case fspy3 ( $y_0=0.3$ )

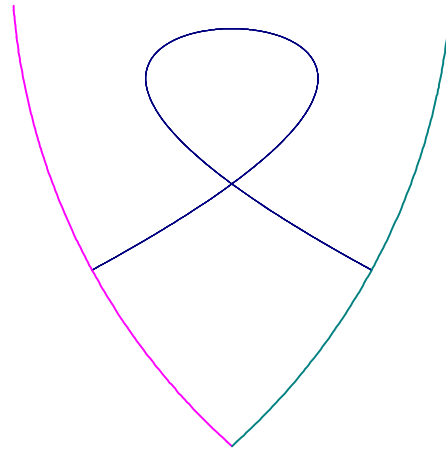


**Fig. 4.60.**  $y$  vs.  $x$ , Case fspy4 ( $y_0=0.4$ )

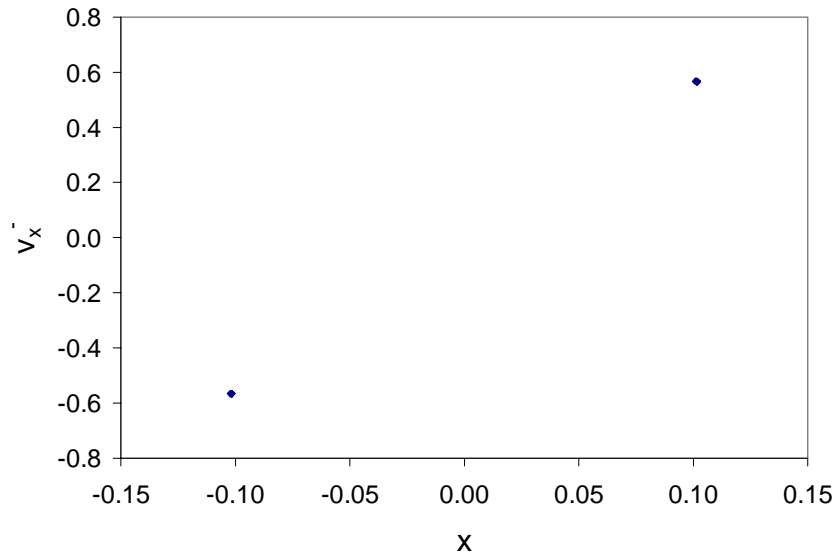


**Fig. 4.61. x Impact Poincaré Plot, Case fspo3**

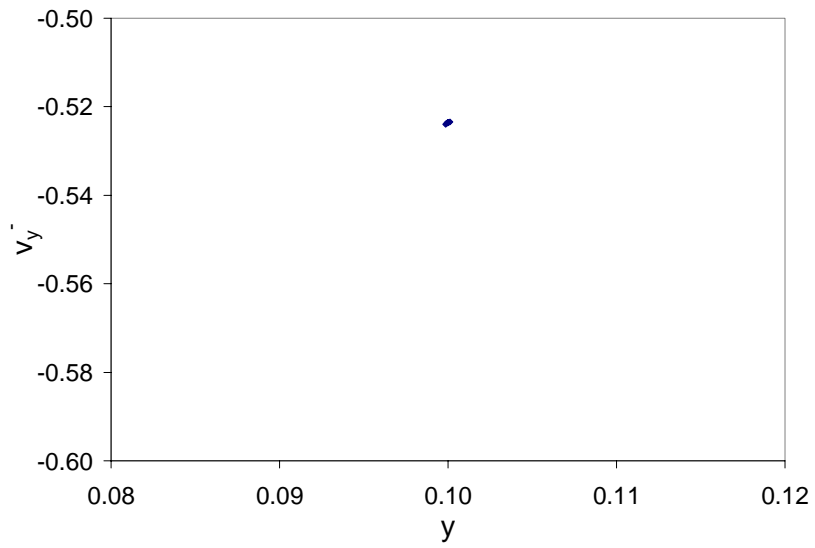


**Fig. 4.62. y Impact Poincaré Plot, Case fspo3**

## Chapter 5

# Free Motions of a Rigid-Body Breakwater

### 5.1 Introduction

In order to make the analyses of this problem more realistic, an in-depth rigid body analysis will be conducted. The point-mass case is a special case of the more general rigid-body case where the dimensions of the rigid body are infinitesimally small. The point-mass case needed to be performed before the rigid body investigation to make sure the formulation was correct. Now that a point-mass analysis has been performed and checked, the point-mass breakwater (PMBW) is now given dimensions and becomes a rigid-body breakwater (RBBW). To simplify the first RBBW analysis, free motions of the breakwater will be investigated as in the first problem.

### 5.2 Rigid-Body Model and Configuration

In this formulation, the generalized shape of the RBBW is a rectangle with a length dimension of  $A$  and a depth dimension of  $B$  as seen in Fig. 5.1. Also seen in Fig. 5.1 are labeled points of reference, which will be used later in the formulation of this problem. Points  $J$  and  $K$  are the left and right supports, respectively. Similarly, points  $V$  and  $W$  are the left and right mooring cable to

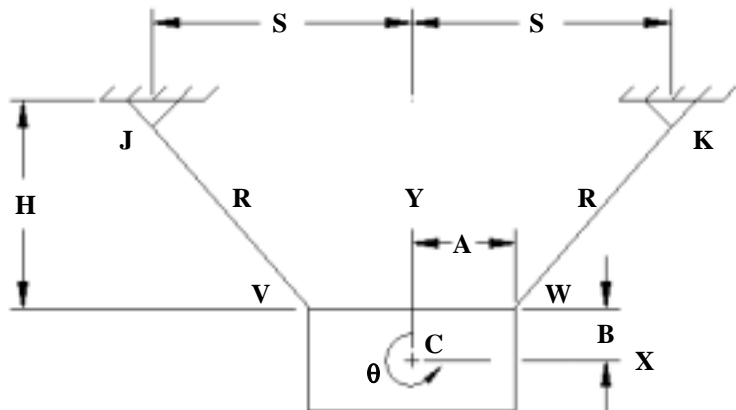


Fig. 5.1 Dimensional Parameters

breakwater connections, respectively. The point C is the center of mass of the RBBW. The coordinates X and Y define the position of this point in their positive directions, and the rotation,  $\theta$ , is measured counterclockwise about this point from the horizontal axis in its positive direction. The origin of the global X-Y axes is located at the center of the breakwater when it is at its lowest point, its equilibrium state with both cables taut.

Similar to the previous problems, the geometric configuration of the breakwater and its mooring system is arranged in such a manner that the components are symmetric. The two cables are of equal length and are suspended from the same height. Figure 5.1 shows the separation length of the supports as  $2S$ , and the “taut” (natural) length of each cable as  $R$ . “Taut” in this sense means the cable has been stretched out and has reached its natural length. In order for the breakwater to float, the following condition must be satisfied:

$$R > S-A \quad (5.1)$$

With these dimensions, the distance  $H$  from the supports J and K to the connection points V and W when the RBBW is at its lowest point (the equilibrium state) may be defined by

$$(S-A)^2 + H^2 = R^2 \quad (5.2)$$

or

$$H = \sqrt{R^2 - (S-A)^2} \quad (5.3)$$

Motions of the RBBW must remain below the height of the supports (i.e., the breakwater not hitting the sea floor). Therefore the following restriction on Y must be met:

$$Y \leq H+B \quad (5.4)$$

Section 5.2.2.1 discusses this in more detail after some more parameters have been defined. There are three degrees of freedom in this system:  $X(T)$ ,  $Y(T)$ , and  $\theta(T)$ , where  $T$  = time.

### 5.2.1 Rigid-Body Breakwater Shape

The RBBW is assumed to be symmetric vertically and horizontally about its center, C. Three shapes will be investigated. The first is a thin ring or circle of radius A with the cables connected at the level of the center of mass, as shown in Fig. 5.2.a. Thus  $B=0$  for this case and the shape may be thought of as a bar. The second shape is a solid square, with  $B=A$  and the cables connected at the upper corners (Fig. 5.2.b). In the third case the RBBW is solid and rectangular in cross-section (Fig. 5.2.c), with  $B \neq A$ . The shape of the RBBW does not matter, just the locations of the points C, V, and W. The mass moment of inertia,  $I_c$ , takes into account the shape of the RBBW. Thus, the mass moments of inertia, about the center of mass, are as follows:

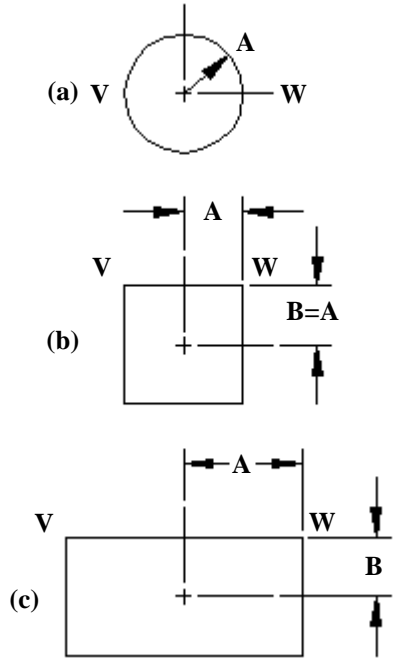


Fig. 5.2. Rigid-Body Breakwater Shapes

for the circular shape,

$$I_c = mA^2 \quad (5.5)$$

and for the square or rectangular shapes,

$$I_c = \frac{1}{3}m(A^2 + B^2) \quad (5.6)$$

### 5.2.2 Boundary Equation Formulation

In order to develop equations for the boundaries of the RBBW case, the positions of the connection points, V and W, must be determined. The following positions of V and W were developed with respect to the respective support points, J or K. To determine the position equations, the breakwater is moved slightly with either one, both, or no cables taut in the positive X, Y, and  $\theta$  directions. Thus, the general solution of the case with both cables slack is shown in Fig. 5.3.

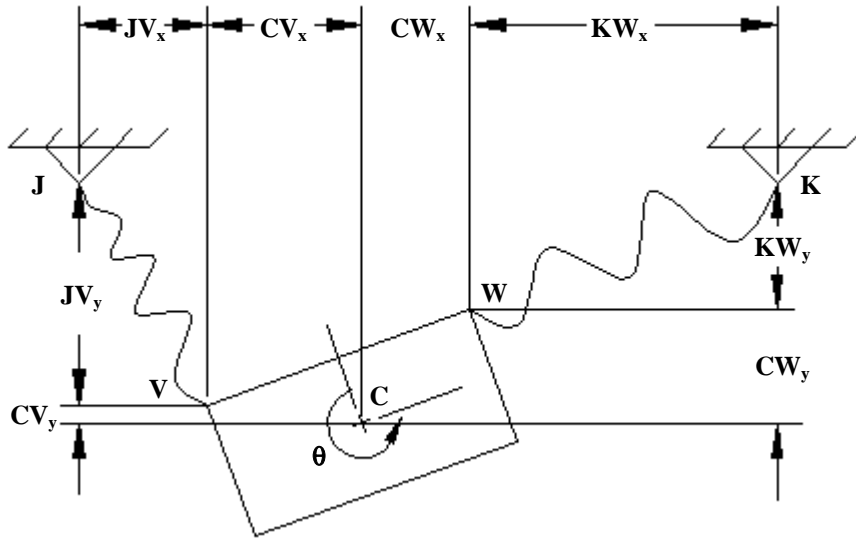


**Fig. 5.3 Dimensions with RBBW Moved in Positive Directions**

Remembering that positive X is to the right, positive Y is up, and positive  $\theta$  is counterclockwise, the following equations describe the positions of V and W with respect to J and K vertically and horizontally:

$$JV_x = S + X - A \cos \theta - B \sin \theta \quad (\text{horizontal distance between J and V}) \quad (5.7)$$

$$JV_y = H + B - Y + A \sin \theta - B \cos \theta \quad (\text{vertical distance between J and V}) \quad (5.8)$$

$$KW_x = S - X - A \cos \theta + B \sin \theta \quad (\text{horizontal distance between K and W}) \quad (5.9)$$

$$KW_y = H + B - Y - A \sin \theta - B \cos \theta \quad (\text{vertical distance between K and W}) \quad (5.10)$$

Now that these vertical and horizontal positions are known, the distances  $D_L$  and  $D_R$  may be calculated from the Pythagorean Theorem.

Therefore

$$D_L^2 = JV_x^2 + JV_y^2 \quad (\text{direct distance between J and V}) \quad (5.11)$$

$$D_R^2 = KW_x^2 + KW_y^2 \quad (\text{direct distance between W and K}) \quad (5.12)$$

Using Equations 5.7-5.10 in Equations 5.11 and 5.12 gives

$$D_L^2 = (S + X - A \cos \theta - B \sin \theta)^2 + (H + B - Y + A \sin \theta - B \cos \theta)^2 \quad (5.13)$$

$$D_R^2 = (S - X - A \cos \theta + B \sin \theta)^2 + (H + B - Y - A \sin \theta - B \cos \theta)^2 \quad (5.14)$$

where the following conditions must be satisfied:

$$D_L \leq R \quad (5.15)$$

$$D_R \leq R \quad (5.16)$$

Equations 5.13 and 5.14 gives the direct distances between the supports and the RBBW mooring cable connections at any time when the cables are slack. Thus, when a cable is taut and the conditions 5.15 and 5.16 are met, the equations describing the position of the RBBW between the boundaries may be developed similar to Section 2.2.2, using

$$G_1 = D_R^2 - R^2 \quad (5.17)$$

$$G_2 = D_L^2 - R^2 \quad (5.18)$$

Thus the motion of the breakwater must remain in the region where

$$G_1 \leq 0 \quad (G_1 \text{ equation}) \quad (5.19)$$

$$G_2 \leq 0 \quad (G_2 \text{ equation}) \quad (5.20)$$

Recalling from Chapters 3 and 4, the boundaries for these problems are definite (i.e., fixed in space) in the point-mass cases and are drawn on the trajectory plots. However, the boundaries are more like regions in the rigid-body cases because  $x$  and  $y$  give the position of the center of gravity, which is not at the attachment points of the cables, and hence the boundaries are not plotted on the trajectory plots for the rigid-body problems.

### 5.2.2.1 Upper Boundary Restriction

The upper boundary restriction discussed in Section 5.2 becomes complicated when the RBBW is not horizontal (i.e., RBBW is rotated by some angle,  $\theta$ ). Therefore, points V and W must remain below the upper boundary and must follow the following restrictions:

If the RBBW is circular,

$$Y < H-A \quad (5.21)$$

If the RBBW is rectangular,

$$JV_y > 0 \quad (5.22)$$

and

$$KW_y > 0 \quad (5.23)$$

These conditions insure that the RBBW is below the upper boundary (i.e., the sea floor).

### 5.2.2.2 Rotation Restriction

In the rigid-body cases, a restriction was placed on the amount of rotation allowed. With the RBBW now having dimensions and the possibility to rotate, it is possible for the RBBW to rotate excessively. This motion is not desirable, since in reality the cables may wrap around the breakwater or become entangled. Therefore, the restriction of limiting the RBBW to rotations of  $\pm\pi/2$  or less was imposed. In the solution procedure, if this limit was reached, then the solution would stop, indicating that the initial conditions and parameters were not suitable to keep the rotations within the specified range.

### 5.3 Nondimensionalization

The terms used in the formulation of the problem have been nondimensionalized, so that the units will not be involved during this investigation. Length parameters were nondimensionalized by the cable spacing,  $S$ , and time by

$$\sqrt{S/g} \quad (5.24)$$

Mass is divided out of the equations of free motion. Uppercase letter symbols are used when terms have dimensions and lowercase letters are used to represent the nondimensionalized values. Thus, the variables become

$$x=X/S \quad (5.25)$$

$$y=Y/S \quad (5.26)$$

$$r=R/S > 1-a \quad (5.27)$$

$$a=A/S \quad (5.28)$$

$$b=B/S \quad (5.29)$$

$$h=H/S = \sqrt{r^2 - (1-a)^2} \quad (5.30)$$

$$t = T\sqrt{g/S} \quad (5.31)$$

$$d_L=D_L/S \quad (5.32)$$

$$d_R=D_R/S \quad (5.33)$$

From these nondimensionalizations, Equations 5.13, 5.14, 5.17, and 5.18 become

$$d_L^2=(1+x-acos\theta-bsin\theta)^2+(h+b-y+asin\theta-bcos\theta)^2 \quad (5.34)$$

$$d_R^2 = (1-x-a\cos\theta+b\sin\theta)^2 + (h+b-y-a\sin\theta-b\cos\theta)^2 \quad (5.35)$$

$$g_1 = d_R^2 - r^2 \quad (5.36)$$

$$g_2 = d_L^2 - r^2 \quad (5.37)$$

## 5.4 Equations of Motion

Inside the bounded region, both cables are slack, and the only force acting on the RBBW during free vibration is gravity. Therefore the equations of motion (EOM's) are

$$m \frac{d^2 X}{dT^2} = 0 \quad (5.38)$$

$$m \frac{d^2 Y}{dT^2} = -mg \quad (5.39)$$

$$I \frac{d^2 \theta}{dT^2} = 0 \quad (5.40)$$

After the nondimensionalization, the basic EOM's become

$$\frac{d^2 x}{dt^2} = 0 \quad (5.41)$$

$$\frac{d^2 y}{dt^2} = -1 \quad (5.42)$$

$$\frac{d^2 \theta}{dt^2} = 0 \quad (5.43)$$

The solutions for this formulation are

$$x = c_1 + c_2 t \quad y = c_3 + c_4 t - \frac{1}{2} t^2 \quad \theta = c_5 + c_6 t \quad (5.44, 5.45, 5.46)$$

$$\dot{x} = c_2 \quad \dot{y} = c_4 - t \quad \dot{\theta} = c_6 \quad (5.47, 5.48, 5.49)$$

$$\ddot{x} = 0 \quad \ddot{y} = -1 \quad \ddot{\theta} = 0 \quad (5.50, 5.51, 5.52)$$

where  $\bullet = \frac{d}{dt}$  and

where the constants for motion following  $t=t_i$  (initial time or impact time) are

$$c_1 = x_i - c_2 t_i \quad c_3 = y_i - c_4 t_i + \frac{1}{2} t_i^2 \quad c_5 = \theta_i - c_6 t_i \quad (5.53, 5.54, 5.55)$$

$$c_2 = \dot{x}_i \qquad c_4 = \dot{y}_i + t_i \qquad c_6 = \dot{\theta}_i \qquad (5.56, 5.57, 5.58)$$

## 5.5 Rigid-Body Impact

Now a detailed derivation of impact response equations will be formulated to determine the new initial conditions after impact for the RBBW problems.

### 5.5.1 Definition of Rigid-Body Impact

Similar to the definition of “impact” discussed in Chapter 2, impact is defined when a cable becomes taut. “Taut” in this sense means that the cable reaches its natural length which in this problem is from a support to an attachment point on the RBBW, as seen in Figs. 5.4 and 5.5, and not to the center of mass as in the PMBW problems. When a cable becomes taut, it is said that the breakwater is hitting a fictitious boundary which is defined by the mathematical equations for  $g_1=0$  or  $g_2=0$  discussed in Section 5.2.2. Once one of the cables has become taut, an impact is felt and the breakwater rebounds in the opposite direction. However, it can be seen that now the boundaries depend on the size of the RBBW and the angle at which it is rotated before impact, and this complicates the impact response of the RBBW.

### 5.5.2 Formulation of Impact Response

The impact response of the RBBW is not the same as in the PMBW problems. Before, the impact conditions were

$$v_n^+ = -ev_n^- \qquad (5.59)$$

for the normal velocity, and no change in tangential velocity. However, with the rigid-body case, three impact conditions are needed and several modifications to the previous impact equations were required. It is no longer assumed that the tangential velocity,  $v_t$ , remains unchanged at the time of impact, because of the rotations involved. The rotation of the RBBW at the time of impact has a significant effect on the impact velocities. This is because if the center of mass of the RBBW is not in line with the normal velocity

vector of the taut cable, then a spinning will occur at the time of impact. This causes the RBBW to rotate in the opposite direction to the direction it was rotating before impact. This may be compared to the motions of a yo-yo, which unrolls down a string and then, acting like a pendulum, rotates around the end of the string and rolls back up (Bürger 1984). The mathematical models, which describe this behavior with respect to a RBBW, will now be described.

Equation 5.59 will continue to be used as the first impact condition. The second impact condition is that the resultant of the impulsive force during impact acts longitudinally along the taut cable. The third impact response is that the sudden change in the angular momentum of the RBBW relative to its center of mass is equal to the sum of the moments induced by the impulsive forces about the center of mass (Synge and Griffith 1959).

This may be stated mathematically by

$$I_c \Delta \dot{\theta} = \hat{M} \quad (5.60)$$

where

$$I_c \text{ is the moment of inertia about the center of mass} \quad (5.61)$$

$$\Delta \dot{\theta} \text{ is the change in angular velocity} \quad (5.62)$$

$$\hat{M} \text{ is the summation of the impulsive force moments} \quad (5.63)$$

$$(\wedge) \text{ means that the term is an impulsive action} \quad (5.64)$$

The specific terms associated with both boundaries for these conditions will be expanded upon during more detailed formulations in subsequent sections.

### 5.5.3 Impact Response when $g_1=0$

Impact parameters will now be developed for  $g_1=0$ . Solving Equation 5.36 for  $y$  where  $g_1=0$  gives

$$y = h + b - a \sin \theta - b \cos \theta - \sqrt{r^2 - (1 - x - a \cos \theta + b \sin \theta)^2} \quad (5.65)$$

Thus, to get the slope of the boundary at a given point, the derivative is taken:

$$\frac{dy}{dx} = \frac{(1-x-a\cos\theta+b\sin\theta)}{\sqrt{r^2-(1-x-a\cos\theta+b\sin\theta)^2}} \quad (5.66)$$

The angle,  $\phi$ , from Section 2.5.2.1 is the same for this case and is used in the following derivations. Seen in Fig 5.4, this angle is formed when the right cable is taut.

### 5.5.3.1 Normal and Tangential Velocities at $g_1=0$

By including the RBBW dimensions and its potential to rotate, and from the simple geometry in Section 2.5.2.2, the normal and tangential velocities may be obtained. In the RBBW problems, the point W is actually the point hitting the boundary, and not the center, C. The equations in this section are derived with respect to displacements from the center, but are actually with respect to the attachment points with some geometric transformations. Thus, the following equations were developed based on the position and velocity of point W when it strikes the boundary  $g_1=0$ :

$$v_x^- = \dot{x}^- - a\dot{\theta}^- \sin\theta - b\dot{\theta}^- \cos\theta \quad (5.67)$$

$$v_y^- = \dot{y}^- + a\dot{\theta}^- \cos\theta - b\dot{\theta}^- \sin\theta \quad (5.68)$$

$$v_n^- = -v_x^- \sin\phi - v_y^- \cos\phi \quad (5.69)$$

$$v_t^- = -v_x^- \cos\phi + v_y^- \sin\phi \quad (5.70)$$

### 5.5.3.2 Impact Solution for $g_1=0$

Now the impact condition equations and their solutions will be derived. By using the first condition, Equation 5.59, and Fig. 5.4, the impact equation becomes

$$-x^+ \sin\phi - y^+ \cos\phi + (CW_y \sin\phi - CW_x \cos\phi)\dot{\theta}^+ = -ev_n^- \quad (5.71)$$

where

$$CW_x = a \cos\theta - b \sin\theta \quad (5.72)$$

$$CW_y = a \sin\theta + b \cos\theta \quad (5.73)$$

Next, by applying the second condition to Fig. 5.4, the second impact equation is developed:

$$KW_y \dot{x}^+ - KW_x \dot{y}^+ = KW_y \dot{x}^- - KW_x \dot{y}^- \quad (5.74)$$

Finally, by again using Fig. 5.4, the following impulsive forces and moments may be derived:

$$\hat{F}_x = m\Delta \dot{x} = m(\dot{x}^+ - \dot{x}^-) \quad (5.75)$$

$$\hat{F}_y = m\Delta \dot{y} = m(\dot{y}^+ - \dot{y}^-) \quad (5.76)$$

$$\hat{M} = I_c \Delta \dot{\theta} = I_c (\dot{\theta}^+ - \dot{\theta}^-) \quad (5.77)$$

Summing the moments about the center, C, gives

$$-\hat{F}_x CW_y + \hat{F}_y CW_x - \hat{M} = 0 \quad (5.78)$$

Plugging Equations 5.75–5.77 into Equation 5.78 gives the third impact equation

$$-CW_y \dot{x}^+ + CW_x \dot{y}^+ - I_c \dot{\theta}^+ = -CW_y \dot{x}^- + CW_x \dot{y}^- - I_c \dot{\theta}^- \quad (5.79)$$

After grouping the terms of Equations 5.71, 5.74, and 5.79 with respect to the velocities after impact, the equations may be put into matrix form, giving the following impact velocity matrix equation:

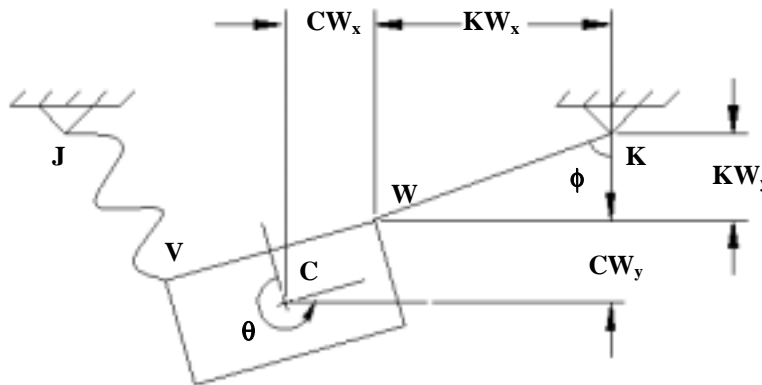


Fig. 5.4. Right Cable Taut with RBBW Moved in Positive Directions

$$\begin{bmatrix} a_{11} & a_{12} & a_{13} \\ a_{21} & a_{22} & a_{23} \\ a_{31} & a_{32} & a_{33} \end{bmatrix} \begin{bmatrix} \dot{x}^+ \\ \dot{y}^+ \\ \dot{\theta}^+ \end{bmatrix} = \begin{bmatrix} b_1 \\ b_2 \\ b_3 \end{bmatrix} \quad (5.80)$$

where

$$a_{11} = -\sin\phi \quad (5.81)$$

$$a_{12} = -\cos\phi \quad (5.82)$$

$$a_{13} = a \sin\theta \sin\phi + b \sin\theta \cos\phi - a \cos\theta \cos\phi + b \cos\theta \sin\phi \quad (5.83)$$

$$a_{21} = KW_y \quad (5.84)$$

$$a_{22} = -KW_x \quad (5.85)$$

$$a_{23} = 0 \quad (5.86)$$

$$a_{31} = -CW_y \quad (5.87)$$

$$a_{32} = CW_x \quad (5.88)$$

$$a_{33} = -I_c \quad (5.89)$$

$$b_1 = -e v_n^- \quad (5.90)$$

$$b_2 = KW_y \dot{x}^- - KW_x \dot{y}^- \quad (5.91)$$

$$b_3 = -CW_y \dot{x}^- + CW_x \dot{y}^- - I_c \dot{\theta}^- \quad (5.92)$$

Then, by using Cramer's Rule, the velocities after impact may be determined.

The analytical solution, along with the Newton's Method for convergence, will be used to analyze the cases in this problem. The solution procedure is similar to the previous problems with exceptions brought about by the inclusion of the rotational degree of freedom.

#### 5.5.4 Impact Response when $g_2=0$

Similar to the derivation of the  $g_1=0$  impact response, the impact parameters will now be developed for  $g_2=0$ . Solving Equation 5.37 for  $y$  where  $g_2=0$  gives

$$y = h + b + a \sin \theta - b \cos \theta - \sqrt{r^2 - (1 + x - a \cos \theta - b \sin \theta)^2} \quad (5.93)$$

Thus, to get the slope of the boundary at a given point, the derivative is taken:

$$\frac{dy}{dx} = \frac{1 + x - a \cos \theta - b \sin \theta}{\sqrt{r^2 - (1 + x - a \cos \theta - b \sin \theta)^2}} \quad (5.94)$$

The angle,  $\psi$ , from Section 2.5.3.1 is the same for this case and is used in the following derivations. Seen in Fig 5.5, this angle is formed when the left cable is taut.

#### 5.5.4.1 Normal and Tangential Velocities at $g_2=0$

By including the RBBW dimensions and its potential to rotate, and from the simple geometry in Section 2.5.3.2, the normal and tangential velocities may be obtained. In the RBBW problems, the point V is actually the point hitting the boundary and not the center, C. The equations in this section are derived with respect to displacements from the center, but are actually with respect to the attachment points with some geometric transformations. Thus, the following equations were developed based on the position and velocity of point V when it strikes the boundary  $g_2=0$ :

$$v_x^- = \dot{x}^- + a \dot{\theta}^- \sin \theta - b \dot{\theta}^- \cos \theta \quad (5.95)$$

$$v_y^- = \dot{y}^- - a \dot{\theta}^- \cos \theta - b \dot{\theta}^- \sin \theta \quad (5.96)$$

$$v_n^- = v_x^- \sin \psi - v_y^- \cos \psi \quad (5.97)$$

$$v_t^- = v_x^- \cos \psi + v_y^- \sin \psi \quad (5.98)$$

#### 5.5.4.2 Impact Solution for $g_2=0$

Now the impact condition equations and their solutions will be derived. By using the first condition, Equation 5.59, and Fig. 5.5, the impact equation becomes

$$\dot{x}^+ \sin \psi - \dot{y}^+ \cos \psi + (-CV_y \sin \psi + CV_x \cos \psi) \dot{\theta}^+ = -e v_n^- \quad (5.99)$$

where

$$CV_x = a \cos \theta + b \sin \theta \quad (5.100)$$

$$CV_y = -a \sin \theta + b \cos \theta \quad (5.101)$$

Next, by applying the second condition to Fig. 5.5, the second impact equation is developed:

$$JV_y \dot{x}^+ + JV_x \dot{y}^+ = JV_y \dot{x}^- + JV_x \dot{y}^- \quad (5.102)$$

Finally, by again using Fig. 5.5, the following impulsive forces and moments may be derived:

$$\hat{F}_x = m \Delta \dot{x} = m(\dot{x}^+ - \dot{x}^-) \quad (5.103)$$

$$\hat{F}_y = m \Delta \dot{y} = m(\dot{y}^+ - \dot{y}^-) \quad (5.104)$$

$$\hat{M} = I_c \Delta \dot{\theta} = I_c(\dot{\theta}^+ - \dot{\theta}^-) \quad (5.105)$$

Summing the moments about the center, C, gives

$$\hat{F}_x CV_y + \hat{F}_y CV_x + \hat{M} = 0 \quad (5.106)$$

Plugging Equations 5.103–5.105 into Equation 5.106 gives the third impact equation

$$CV_y \dot{x}^+ + CV_x \dot{y}^+ + I_c \dot{\theta}^+ = CV_y \dot{x}^- + CV_x \dot{y}^- + I_c \dot{\theta}^- \quad (5.107)$$

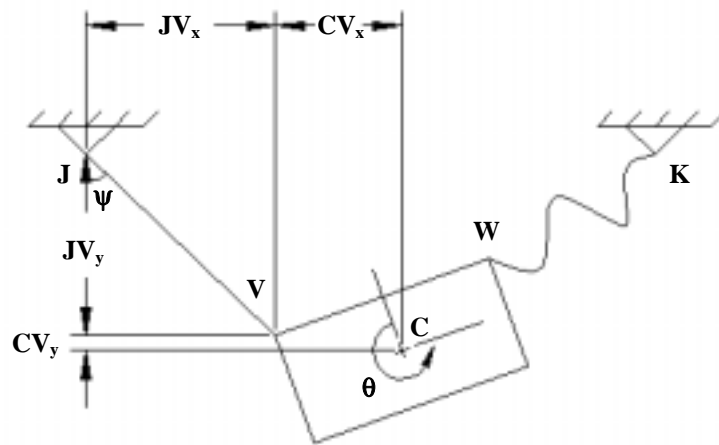


Fig. 5.5. Left Cable Taut with RBBW Moved in Positive Directions

After grouping the terms of Equations 5.99, 5.102, and 5.107 with respect to the velocities after impact, the equation may be put into matrix form, giving Equation 5.80 with

$$a_{11} = \sin\psi \quad (5.108)$$

$$a_{12} = -\cos\psi \quad (5.109)$$

$$a_{13} = a \sin\theta \sin\psi - b \cos\theta \sin\psi + a \cos\theta \cos\psi + b \sin\theta \cos\psi \quad (5.110)$$

$$a_{21} = JV_y \quad (5.111)$$

$$a_{22} = JV_x \quad (5.112)$$

$$a_{23} = 0 \quad (5.113)$$

$$a_{31} = CV_y \quad (5.114)$$

$$a_{32} = CV_x \quad (5.115)$$

$$a_{33} = I_c \quad (5.116)$$

$$b_1 = -ev_n^- \quad (5.117)$$

$$b_2 = JV_y \dot{x}^- + JV_x \dot{y}^- \quad (5.118)$$

$$b_3 = CV_y \dot{x}^- + CV_x \dot{y}^- + I_c \dot{\theta}^- \quad (5.119)$$

The analytical solution, along with the Newton's Method for convergence, will be used to analyze the cases in this problem. The solution procedure is similar to the previous problems with exceptions brought about by the inclusion of the rotational degree of freedom.

## 5.6 Convergence to a Boundary

Similar to the PMBW problems, Newton's Method will be employed to converge the RBBW to a boundary. The development of Newton's Method for this investigation is discussed in Section 2.6. In order to use Newton's Method, the derivatives of  $g_1$  and  $g_2$  are required. Using Equations 5.36 and 5.37, the derivatives with respect to time are found to be

$$\begin{aligned} \dot{g}_1 = & 2(1 - x - a \cos \theta + b \sin \theta)(-\dot{x} + a \dot{\theta} \sin \theta + b \dot{\theta} \cos \theta) \\ & + 2(h + b - y - a \sin \theta - b \cos \theta)(-\dot{y} - a \dot{\theta} \cos \theta + b \dot{\theta} \sin \theta) \end{aligned} \quad (5.120)$$

and

$$\begin{aligned} \dot{g}_2 = & 2(1 + x - a \cos \theta - b \sin \theta)(\dot{x} + a \dot{\theta} \sin \theta - b \dot{\theta} \cos \theta) \\ & + 2(h + b + y + a \sin \theta - b \cos \theta)(-\dot{y} + a \dot{\theta} \cos \theta + b \dot{\theta} \sin \theta) \end{aligned} \quad (5.121)$$

where

$x(t)$ ,  $\dot{x}(t)$ ,  $y(t)$ ,  $\dot{y}(t)$ ,  $\theta(t)$ , and  $\dot{\theta}(t)$  are seen in Equations 5.44-5.49.

Again, the value  $g$  was converged to a tolerance of  $10^{-6}$ , and the corresponding converged time becomes the impact time.

With the more general rigid-body solution now formulated, the FORTRAN program previously used may be modified to account for the changes in the solution and response at impact. This program may be used because the solution procedure discussed in Section 2.7 does not change for the RBBW problems.

## 5.7 Analyzed Cases

Several different cases were analyzed to investigate how the variation of different parameters affected the motions of the breakwater. With this problem, several more parameters and degrees of freedom (DOF's) are involved. These parameters and initial conditions are summarized in Table 5.1 where  $v_x = \dot{x}(0)$ ,  $v_y = \dot{y}(0)$ , and  $v_\theta = \dot{\theta}(0)$ . These include the size of the RBBW and the initial rotation and angular velocity of the RBBW. This table shows the case number, which was used to identify each case; this number is a series of numbers taken from the parameters and initial conditions. In this problem, the case number uses  $r$ ,  $e$ ,  $a$ ,  $b$ ,  $x(0)$ ,  $\dot{x}(0)$ ,  $y(0)$ ,  $\dot{y}(0)$ ,  $\theta(0)$ , and  $\dot{\theta}(0)$  in this order to identify it. For example, the standard case has a case number of 1910121100. The standard case will be explained in detail later and is denoted by the shaded cells in

Table 5.1. Further, the initial conditions shown in this table are put into a series of groups. These groups were used to see how varying only one parameter would affect the breakwater's response. The value of  $h$  is given Table 5.1 because, as seen in Equation 5.30, the value of  $h$  is based upon the size of the RBBW; thus, the size of the region is dependent on the RBBW size as well. This value will be shown for reference when looking at the trajectory plots.

**Table 5.1. Parameters and Initial Conditions for Free Motions  
of a Rigid-Body Breakwater**

<b>Case #</b>	<b>r</b>	<b>h</b>	<b>e</b>	<b>a</b>	<b>b</b>	<b>x</b>	<b>v<sub>x</sub></b>	<b>y</b>	<b>v<sub>y</sub></b>	<b>θ</b>	<b>v<sub>θ</sub></b>
<b>r</b>											
1910121100	1.5	1.200	0.9	0.1	0.0	0.1	0.2	0.1	-0.1	0.0	0.0
2910121100	2.5	2.332	0.9	0.1	0.0	0.1	0.2	0.1	-0.1	0.0	0.0
1911121100	1.5	1.200	0.9	0.1	0.1	0.1	0.2	0.1	-0.1	0.0	0.0
2911121100	2.5	2.332	0.9	0.1	0.1	0.1	0.2	0.1	-0.1	0.0	0.0
1921121100	1.5	1.269	0.9	0.2	0.1	0.1	0.2	0.1	-0.1	0.0	0.0
2921121100	2.5	2.369	0.9	0.2	0.1	0.1	0.2	0.1	-0.1	0.0	0.0
<b>e</b>											
1110121100	1.5	1.200	1.0	0.1	0.0	0.1	0.2	0.1	-0.1	0.0	0.0
1910121100	1.5	1.200	0.9	0.1	0.0	0.1	0.2	0.1	-0.1	0.0	0.0
1710121100	1.5	1.200	0.7	0.1	0.0	0.1	0.2	0.1	-0.1	0.0	0.0
1510121100	1.5	1.200	0.5	0.1	0.0	0.1	0.2	0.1	-0.1	0.0	0.0
<b>a,b=0 (circle)</b>											
1910121100	1.5	1.200	0.9	0.1	0.0	0.1	0.2	0.1	-0.1	0.0	0.0
1920121100	1.5	1.269	0.9	0.2	0.0	0.1	0.2	0.1	-0.1	0.0	0.0
1930121100	1.5	1.327	0.9	0.3	0.0	0.1	0.2	0.1	-0.1	0.0	0.0
<b>a=b (square)</b>											
1911121100	1.5	1.200	0.9	0.1	0.1	0.1	0.2	0.1	-0.1	0.0	0.0
1922121100	1.5	1.269	0.9	0.2	0.2	0.1	0.2	0.1	-0.1	0.0	0.0
1933121100	1.5	1.327	0.9	0.3	0.3	0.1	0.2	0.1	-0.1	0.0	0.0
<b>a&gt;b (rectangle)</b>											
1911121100	1.5	1.200	0.9	0.1	0.1	0.1	0.2	0.1	-0.1	0.0	0.0
1921121100	1.5	1.269	0.9	0.2	0.1	0.1	0.2	0.1	-0.1	0.0	0.0
1931121100	1.5	1.327	0.9	0.3	0.1	0.1	0.2	0.1	-0.1	0.0	0.0
<b>θ</b>											
1910121100	1.5	1.200	0.9	0.1	0.0	0.1	0.2	0.1	-0.1	0.00	0.0
19101211050	1.5	1.200	0.9	0.1	0.0	0.1	0.2	0.1	-0.1	0.05	0.0
1910121110	1.5	1.200	0.9	0.1	0.0	0.1	0.2	0.1	-0.1	0.10	0.0
19101211150	1.5	1.200	0.9	0.1	0.0	0.1	0.2	0.1	-0.1	0.15	0.0
<b>v<sub>θ</sub></b>											
1910121100	1.5	1.200	0.9	0.1	0.0	0.1	0.2	0.1	-0.1	0.0	0.00
19101211002	1.5	1.200	0.9	0.1	0.0	0.1	0.2	0.1	-0.1	0.0	0.02
19101211005	1.5	1.200	0.9	0.1	0.0	0.1	0.2	0.1	-0.1	0.0	0.05
1910121101	1.5	1.200	0.9	0.1	0.0	0.1	0.2	0.1	-0.1	0.0	0.10
<b>point mass</b>											
1900461100	1.5	1.118	0.9	0.0	0.0	0.4	0.6	1.0	-0.1	0.0	0.0

### 5.7.1 Standard Case

A standard case was developed for this problem as a starting point for the variation of parameters and initial conditions. The standard parameters and initial conditions for this RBBW problem are:

$$\begin{aligned} r &= 1.5 & e &= 0.9 \\ a &= 0.1 & b &= 0.0 \\ x(0) &= 0.1 & \dot{x}(0) &= 0.2 \\ y(0) &= 0.1 & \dot{y}(0) &= -0.1 \\ \theta(0) &= 0.0 & \dot{\theta}(0) &= 0.0 \end{aligned} \tag{5.122}$$

As in the point mass free motion case, the breakwater is started above its equilibrium height and off to one side. However, the RBBW, in this case, is not started from a large height as in the previous case. This is because it is felt that the modeling should be as realistic as possible and the RBBW would actually be near the bottom most of the time, as discussed in Section 4.3.1. Further, after running a few cases, it was found that the restriction of  $\theta \leq \pi/2$ , discussed in Section 5.2.2.2, was violated with  $y(0)=1.0$ , as in the first problem. The RBBW is given some  $x$  and  $y$  velocities to give it some initial push, since there are no external forces other than gravity acting on the RBBW. Further, it is felt that the rotational ability of the RBBW will add to its motions, and thus no initial rotation or rotational velocity is specified.

As seen in Table 5.1 and in the standard case parameters  $a$  and  $b$  (Equation 5.122) the RBBW will be modeled, most of the time, with a horizontal but not a vertical dimension. This condition may be thought of as a bar supported by two strings, and is meant to model the circular RBBW, as seen in Fig. 5.2.a, where the mooring lines are attached to the breakwater at the sides. Also seen in Table 5.1, other shapes including squares and rectangles, will be analyzed. The circular RBBW will be modeled as a thin ring with a nondimensional mass moment of inertia of

$$I_c = ma^2 \quad (5.123)$$

with  $m=1.0$ .

This is because the inflatable structures proposed may be modeled as a thin ring in cross section. A circular shape was chosen for the standard case because this is the shape most likely to be used in practice. The solid square and rectangular shapes of the RBBW will have a nondimensional mass moment of inertia of

$$I_c = \frac{1}{3}m(a^2 + b^2) \quad (5.124)$$

with  $m=1.0$ .

## 5.8 Analysis of Data

Cases were analyzed and data was collected to see what types of behavior the RBBW exhibited under free motions. Again, several types of graphs were used to evaluate the responses of the RBBW, but now the time history plot of rotation vs. time and the phase plane plot of angular velocity vs. rotation were also generated. Special attention must be paid to the fact that the RBBW has the ability to rotate. There might be a position of the RBBW where  $g_1$  and  $g_2$  are close to zero but the RBBW is not at the origin. This is due to the fact that the RBBW is free to rotate, thus giving it the possibility of tensioning both cables by rotating its center while not being at the origin. This situation occurred when the RBBW was near the origin and was treated as though the RBBW would settle to the equilibrium state because gravity is the only force acting and would tend to pull the RBBW down. It is not possible for the RBBW to rise out of this state because gravity is the only force acting. This situation will be discussed in more detail in Section 6.5.2 when wave forcing is added to the system. However, most of the solutions settled down towards the origin (i.e., the equilibrium state).

### 5.8.1 Observations

The radius was the first parameter varied to see how the RBBW would respond. There do not appear to be any significant differences between the motions of a case that has a radius of 1.5 and a case that has a radius of 2.5. The only notable difference between the

two radii is that the boundaries for the 1.5 radius have a sharper point at the bottom of the region than for the 2.5 radius case, which is shallower, as discussed previously. Figures 5.6 and 5.7 illustrate the difference in size and range of motions of the RBBW, dependent upon the mooring cable length (radius). Note that the Figs. 5.6 and 5.7 are plotted to a similar scale.

This response may also be seen in the varying of the dimensions  $a$  and  $b$ . As the dimensions increase, it may be seen that the bottom of the region becomes flatter. This flatness is further exaggerated by the increase of the radius (Figs. 5.8–5.11). Note that Figs. 5.6-5.11 are all plotted to the same scale for comparison purposes. This flatness can be seen in Fig. 5.1 where the size of the shape would cause the connection points,  $V$  and  $W$ , to move apart or together. Further, the smaller the dimensions, the more rotations occur. This is because the moment of inertia is less, and thus the resistance to rotation is less and the RBBW rotates more. Figures 5.12 through 5.14 show that when the dimension  $a$  is increased for a rectangular section from 0.1 to 0.2 to 0.3 with  $b=0.1$ , the magnitude and amount of rotation are decreased. Thus, larger dimensions give a larger moment of inertia and the more the rotation is being resisted. Numerically, the dimensional values with the associated nondimensional mass moments of inertia for the various shapes may be seen in Table 5.2.



**Fig. 5.6. y vs. x, Case 191012110**  
( $r=1.5$ ,  $a=0.1$ ,  $b=0.0$ )



**Fig. 5.7. y vs. x, Case 291012110**  
( $r=2.5$ ,  $a=0.1$ ,  $b=0.0$ )



**Fig. 5.8. y vs. x, Case 1911121100**  
( $r=1.5$ ,  $a=0.1$ ,  $b=0.1$ )

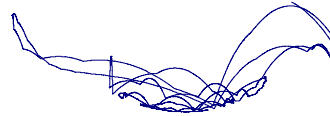


**Fig. 5.9. y vs. x, Case 2911121100**  
( $r=2.5$ ,  $a=0.1$ ,  $b=0.1$ )



**Fig. 5.10. y vs. x, Case 1921121100**  
( $r=1.5$ ,  $a=0.2$ ,  $b=0.1$ )



**Fig. 5.11. y vs. x, Case 2921121100**  
( $r=2.5$ ,  $a=0.2$ ,  $b=0.1$ )

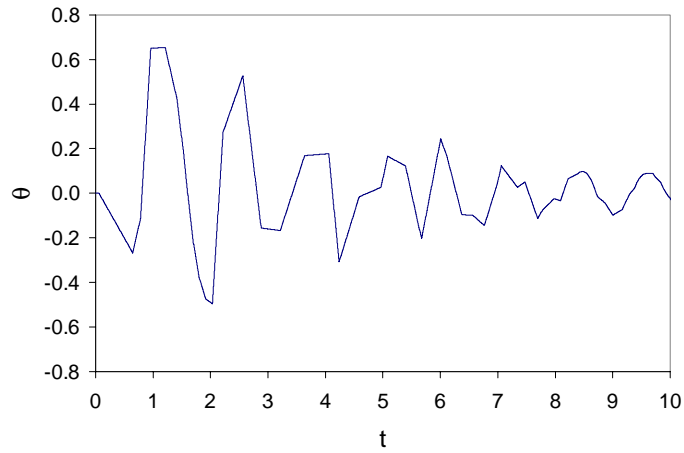


**Fig. 5.12.  $\theta$  vs.  $t$ , Case 1911121100 ( $a=0.1$ ,  $b=0.1$ )**

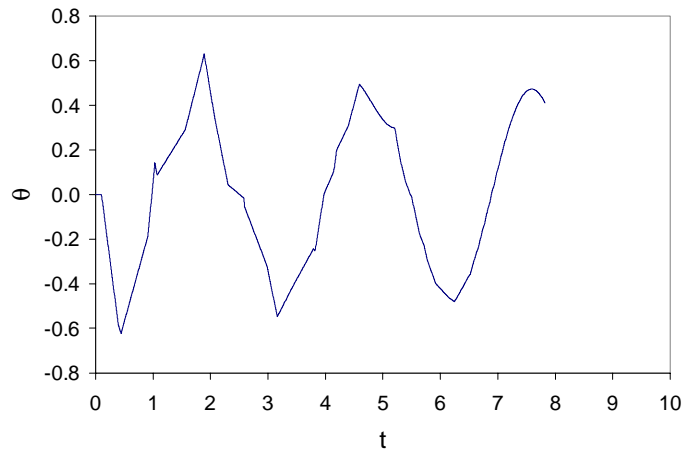


**Fig. 5.13.  $\theta$  vs.  $t$ , Case 1921121100 ( $a=0.2$ ,  $b=0.1$ )**

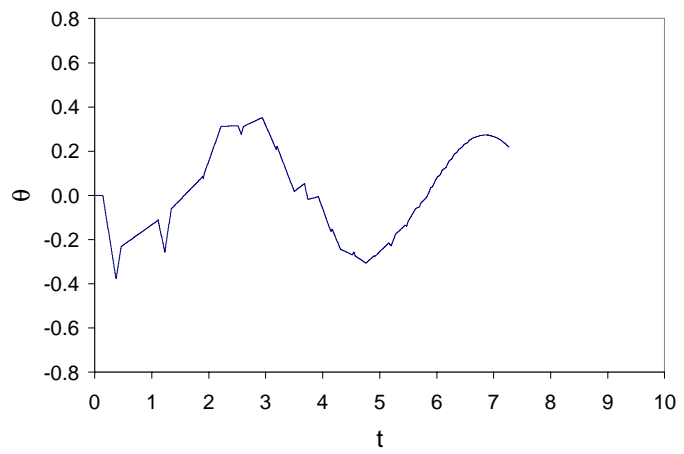


**Fig. 5.14.  $\theta$  vs.  $t$ , Case 1931121100 ( $a=0.3$ ,  $b=0.1$ )**

**Table 5.2 Moments of Inertia for Different Shapes**

shape	a	b	I
circle	0.1	0	0.010
	0.2	0	0.040
	0.3	0	0.090
square	0.1	0.1	0.007
	0.2	0.2	0.027
	0.3	0.3	0.060
rectangle	0.1	0.1	0.007
	0.2	0.1	0.017
	0.3	0.1	0.033

The variation of the coefficient of restitution,  $e$ , in this problem does not produce any noticeable characteristic differences from the phenomena previously discussed. Figures 5.15 through 5.18 show the normal velocity before impact vs. time plots for  $e$  ranging from 1.0 to 0.9 to 0.7 and to 0.5. The time scale in Fig. 5.15 is different than in Figs. 5.16-5.18. One point which should be noted is that during the solution of the  $e=1.0$  case, the rotation of the RBBW surpassed the  $\pi/2$  restriction. This is because no energy is lost, thus the motions are not damped out and excessive rotations become likely.

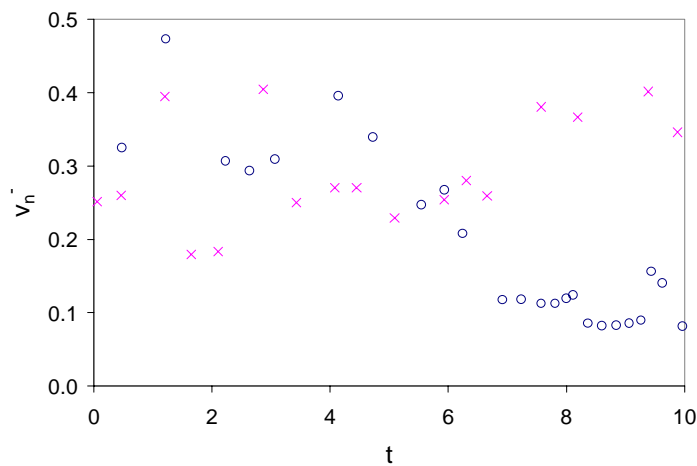


**Fig. 5.15.  $v_n$  vs.  $t$ , Case 1110121100 ( $e=1.0$ )**

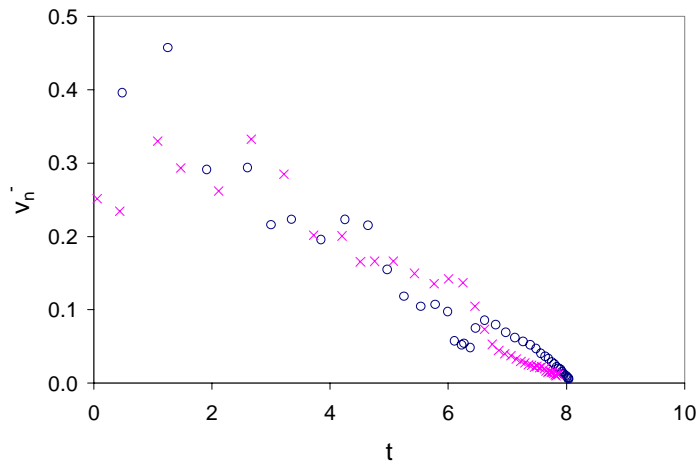


**Fig. 5.16.**  $v_n^-$  vs.  $t$ , Case 1910121100 ( $e=0.9$ )

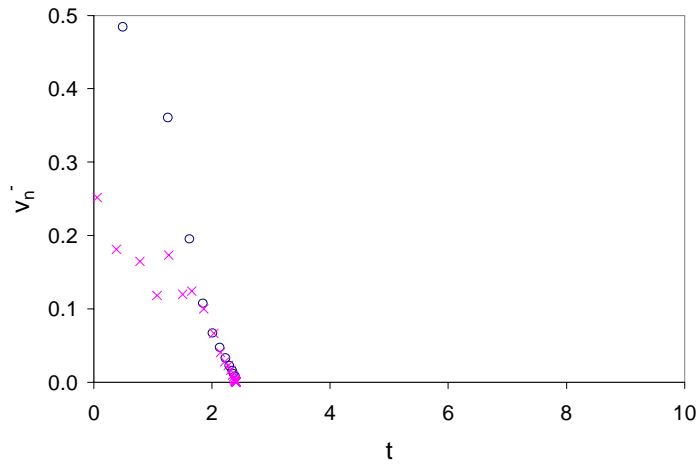


**Fig. 5.17.**  $v_n^-$  vs.  $t$ , Case 1710121100 ( $e=0.7$ )

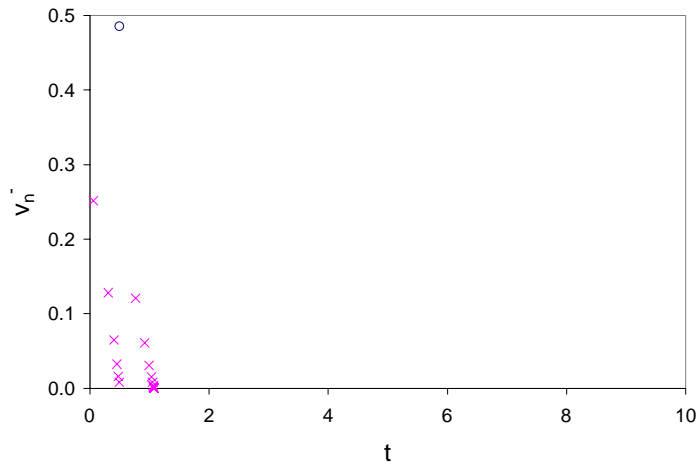


**Fig. 5.18.**  $v_n^-$  vs.  $t$ , Case 1510121100 ( $e=0.5$ )

There was no significant change in behavior when the initial values of  $\theta$  and  $\dot{\theta}$  were varied with the values seen in Table 5.1. However, intuitively it makes sense that if the initial rotation or rotational velocity were increased enough, the RBBW might rotate past its rotation restriction of  $\pi/2$  before it would settle to the bottom.

### 5.8.2 Point-Mass Case

When the size of the RBBW is set to zero, the solution for the PMBW is obtained. This was done as a check on the general RBBW solution. A modification was necessary in the impact equations because of problems in the mathematical solution of the matrix in Equation 5.80. The modification consisted of letting  $\dot{\theta}^+ = \dot{\theta}^-$  which is acceptable since  $\dot{\theta}$  does not appear in the special PMBW case of the RBBW case. A comparison of the trajectories may be seen in Figs. 5.19 and 5.20, where the standard case from the PMBW problem was analyzed. Some data points were selected randomly from the two solutions and have been compiled in Table 5.3 to show the equivalence. This comparison indicates that the PMBW case is just a special case of the more general RBBW solution.

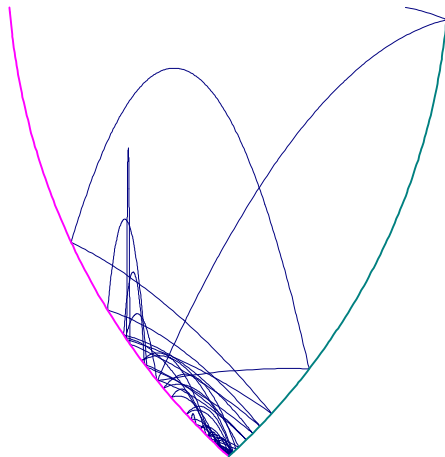


Fig. 5.19. y vs. x, PMBW-Case 194611

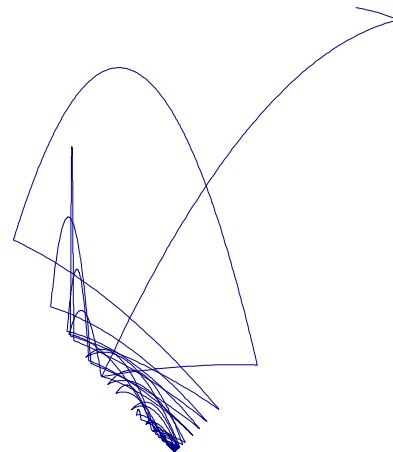


Fig. 5.20. y vs. x, RBBW-Case 1900461100

**Table 5.3 Comparison of Point-Mass Breakwater Solution with  
the Rigid-Body Breakwater Solution**

	<b>t</b>	<b>x</b>	<b>v<sub>x</sub></b>	<b>y</b>	<b>v<sub>y</sub></b>	<b>θ</b>	<b>v<sub>θ</sub></b>	<b>g<sub>1</sub></b>	<b>g<sub>2</sub></b>
<b>1<sup>st</sup> time step</b>									
<b>PMBW</b>	0.010000	0.406000	0.600000	0.998950	-0.110000	N/A	N/A	-1.882983	-0.258983
<b>RBBW</b>	0.010000	0.406000	0.600000	0.998950	-0.110000	0.0	0.0	-1.882983	-0.258983
<b>1<sup>st</sup> impact <sup>-</sup></b>									
<b>PMBW</b>	0.154875	0.492925	0.600000	0.972519	-0.254875	N/A	N/A	-1.974424	0.000000
<b>RBBW</b>	0.154875	0.492925	0.600000	0.972519	-0.254875	0.0	0.0	-1.974424	0.000000
<b>1<sup>st</sup> impact <sup>+</sup></b>									
<b>PMBW</b>	0.154875	0.492925	-0.576028	0.972519	-0.140248	N/A	N/A	-1.974424	0.000000
<b>RBBW</b>	0.154875	0.492925	-0.576028	0.972519	-0.140248	0.0	0.0	-1.974424	0.000000
<b>t=15.0</b>									
<b>PMBW</b>	15.000000	-0.018886	-0.197788	0.104275	0.397382	N/A	N/A	-0.184164	-0.259710
<b>RBBW</b>	15.000000	-0.018886	-0.197788	0.104275	0.397382	0.0	0.0	-0.184164	-0.259710
<b>last impact <sup>-</sup></b>									
<b>PMBW</b>	26.448888	-0.001603	0.085187	0.001436	-0.076411	N/A	N/A	0.000000	-0.006031
<b>RBBW</b>	26.448888	-0.001603	0.085187	0.001436	-0.076411	0.0	0.0	0.000000	-0.006031
<b>last impact <sup>+</sup></b>									
<b>PMBW</b>	26.448888	-0.001603	0.085184	0.001436	-0.076414	N/A	N/A	0.000000	-0.006031
<b>RBBW</b>	26.448888	-0.001603	0.085184	0.001436	-0.076414	0.0	0.0	0.000000	-0.006031

## Chapter 6

# Forced Motions of a Rigid-Body Breakwater

### 6.1 Introduction

Now the last and most realistic problem will be investigated. This problem treats the breakwater as a rigid body that undergoes periodic wave forcing. This problem is the most realistic because a breakwater truly has physical dimensions in reality and would behave as a rigid body. Furthermore, if a breakwater is in the sea, then it will feel the effects of waves acting on it and not just the effects of its own net buoyancy. It is believed that this model will be a fairly accurate representation of how a breakwater would behave when exposed to the natural ocean environment.

### 6.2 Equations of Motion

A combination of the equations of motion (EOM's) developed in Chapters 4 and 5 will be used to model the motions of the rigid-body breakwater (RBBW) in this problem. The analytical solution of the EOM's for  $x$  and  $y$  directions is reviewed in Section 4.2.2; while the analytical solution for the rotations may be seen in Section 5.4 (Equations 5.46, 5.49, 5.52, 5.55, and 5.58).

### 6.3 Analyzed Cases

These solutions were used and several different cases were analyzed to investigate how varying different parameters affected the motion responses of the breakwater. For this problem, no new parameters were added; just combinations of parameters and initial conditions from previous problems were used. This problem is basically a combination of Chapters 4 and 5. The EOM's and analytical solution from Chapter 4 are combined

with the rotations of the RBBW problem formulation from Chapter 5. The parameters in this problem were varied to see any characteristic responses, and the parameters and initial conditions considered in this problem are summarized in Table 6.1 where  $v_x = \dot{x}(0)$ ,  $v_y = \dot{y}(0)$ , and  $v_\theta = \dot{\theta}(0)$ . This table shows the case number, which was used to identify each case analyzed. This number is a series of numbers taken from the parameters and initial conditions. In this problem, the case number uses  $r$ ,  $e$ ,  $a$ ,  $b$ ,  $x(0)$ ,  $\dot{x}(0)$ ,  $y(0)$ ,  $\dot{y}(0)$ ,  $\theta(0)$ ,  $\dot{\theta}(0)$  -  $f_o$ ,  $v$ ,  $\Omega$  in this order to identify the case. For example, the standard case has a case number of 1910001000-559. The standard case will be explained in detail later and is denoted by the shaded cells in Table 6.1. Further, the parameters and initial conditions shown in this table are grouped into series. These groups were used to see how variation of only one parameter would affect the breakwater's response.

### 6.3.1 Stopping Criteria

During the solution process, some criteria were considered that would cause the solution to stop. These stopping criteria are conditions in which it is felt that the solution should not continue any further. Two of these criteria have already been discussed. The upper boundary restriction of Section 5.2.2.1 actually applies to all of the cases and was discussed in passing in the critical force section of Section 4.4.2. The RBBW has a different upper boundary formulation than the point-mass breakwater (PMBW) case where the PMBW is said to be beyond the upper bound when  $y > h$ . The RBBW upper boundary restriction is slightly different because the body is allowed to rotate; thus one side or corner would be out of the region before the center,  $c$ , would. Section 5.2.2.2 discusses the rotation restriction, which is more likely and easily achieved in the forced motion case than in the free motion case. This is because the forcing is elliptical in fashion, which can cause the RBBW to rotate with the forcing if the conditions are right and cause the RBBW to rotate excessively. This motion is not desirable since in reality the cables may wrap around the breakwater or become entangled. Therefore, the

restriction of limiting the RBBW to rotations  $\pm\pi/2$  or less was imposed. In the solution procedure, if this limit was reached, then the solution would stop and indicate that the initial conditions and parameters were not suitable to keep the rotations to a minimum.

It has been considered that the RBBW will settle to the bottom of the region when two criteria are met. The first criterion is that the normal velocity has become practically zero (i.e.,  $<1.0 \times 10^{-6}$ ). This indicates that the RBBW does not possess enough energy to rebound off of a boundary. The other criterion is that the height of the RBBW is very small (i.e.,  $< 5.0 \times 10^{-2}$ ). These two criteria together work on the premise that the RBBW will settle to the bottom of the region when its height is low and when it does not possess a substantial amount of energy to rebound to a height far above the origin. Also, it is assumed that the force amplitude used is below the critical force, and thus gravity will control and pull the RBBW down. Critical force, for this case, will be explained in Section 6.4.2.

When this situation arises, there is also the possibility that while the RBBW is settling to the bottom, both cables may become taut and the RBBW will start to rock back and forth. In the previous solution, this type of motion is not accounted for, only a situation where one cable becomes taut, and thus the previous solution is no longer valid and this solution is stopped. Therefore, a special formulation was developed to handle this rocking situation and will be discussed in detail in Section 6.5.2.

A similar situation where the previous solution is no longer valid and an alternate solution must be used is where one cable stays taut for a length of time. This situation is thought of as the breakwater sliding along the boundary and occurs when the normal velocity is practically zero and the RBBW is at a height where the breakwater is not considered to settle to the bottom of the region. Sliding occurs in the forcing case because the forcing acts as an elliptical force which is pushing the breakwater one direction and then it reverses and pushes the breakwater in the opposite direction. So, if a

breakwater happens to be near a boundary and is being pushed towards the boundary by the wave forcing, the breakwater may stay on the boundary until the wave forcing reverses direction and stops pushing the breakwater into the boundary. During this time the normal velocity is small, so the breakwater cannot rebound off of the boundary, and the breakwater may slide along the boundary (i.e., the breakwater arcing around the region with a cable being taut). In the previous solution, this type of motion is not accounted for, only a situation where the breakwater is instantaneously on the boundary and thus the previous solution is no longer valid and this solution is stopped. Therefore, a special formulation was developed to handle this sliding situation and will be discussed in detail in Section 6.5.1.

**Table 6.1. Parameters and Initial Conditions for Forced Motions of a Rigid-Body Breakwater**

<b>Case #</b>	<b>r</b>	<b>h</b>	<b>e</b>	<b>a</b>	<b>b</b>	<b>x</b>	<b>v<sub>x</sub></b>	<b>y</b>	<b>v<sub>y</sub></b>	<b>θ</b>	<b>v<sub>θ</sub></b>	<b>f<sub>o</sub></b>	<b>v</b>	<b>Ω</b>
<b>r</b>														
1910001000-359	1.5	1.200	0.9	0.1	0.0	0.0	0.0	0.1	0.0	0.0	0.0	0.3	0.5	0.9
2910001000-359	2.5	2.332	0.9	0.1	0.0	0.0	0.0	0.1	0.0	0.0	0.0	0.3	0.5	0.9
1911001000-359	1.5	1.200	0.9	0.1	0.1	0.0	0.0	0.1	0.0	0.0	0.0	0.3	0.5	0.9
2911001000-359	2.5	2.332	0.9	0.1	0.1	0.0	0.0	0.1	0.0	0.0	0.0	0.3	0.5	0.9
1921001000-359	1.5	1.200	0.9	0.2	0.1	0.0	0.0	0.1	0.0	0.0	0.0	0.3	0.5	0.9
2921001000-359	2.5	2.369	0.9	0.2	0.1	0.0	0.0	0.1	0.0	0.0	0.0	0.3	0.5	0.9
<b>e</b>														
1510001000-359	1.5	1.200	0.5	0.1	0.0	0.0	0.0	0.1	0.0	0.0	0.0	0.3	0.5	0.9
1710001000-359	1.5	1.200	0.7	0.1	0.0	0.0	0.0	0.1	0.0	0.0	0.0	0.3	0.5	0.9
1910001000-359	1.5	1.200	0.9	0.1	0.0	0.0	0.0	0.1	0.0	0.0	0.0	0.3	0.5	0.9
1110001000-359	1.5	1.200	1.0	0.1	0.0	0.0	0.0	0.1	0.0	0.0	0.0	0.3	0.5	0.9
<b>b=0 (circle)</b>														
1910001000-359	1.5	1.200	0.9	0.1	0.0	0.0	0.0	0.1	0.0	0.0	0.0	0.3	0.5	0.9
1920001000-359	1.5	1.269	0.9	0.2	0.0	0.0	0.0	0.1	0.0	0.0	0.0	0.3	0.5	0.9
1930001000-359	1.5	1.327	0.9	0.3	0.0	0.0	0.0	0.1	0.0	0.0	0.0	0.3	0.5	0.9
<b>a=b (square)</b>														
1911001000-359	1.5	1.200	0.9	0.1	0.1	0.0	0.0	0.1	0.0	0.0	0.0	0.5	0.5	0.9
1922001000-359	1.5	1.269	0.9	0.2	0.2	0.0	0.0	0.1	0.0	0.0	0.0	0.5	0.5	0.9
1933001000-359	1.5	1.327	0.9	0.3	0.3	0.0	0.0	0.1	0.0	0.0	0.0	0.5	0.5	0.9
<b>a&gt;b (rectangle)</b>														
1911001000-359	1.5	1.200	0.9	0.1	0.1	0.0	0.0	0.1	0.0	0.0	0.0	0.5	0.5	0.9
1921001000-359	1.5	1.269	0.9	0.2	0.1	0.0	0.0	0.1	0.0	0.0	0.0	0.5	0.5	0.9
1931001000-359	1.5	1.327	0.9	0.3	0.1	0.0	0.0	0.1	0.0	0.0	0.0	0.5	0.5	0.9
<b>f<sub>o</sub></b>														
1910001000-159	1.5	1.200	0.9	0.1	0.0	0.0	0.0	0.1	0.0	0.0	0.0	0.1	0.5	0.9
1910001000-259	1.5	1.200	0.9	0.1	0.0	0.0	0.0	0.1	0.0	0.0	0.0	0.2	0.5	0.9
1910001000-359	1.5	1.200	0.9	0.1	0.0	0.0	0.0	0.1	0.0	0.0	0.0	0.3	0.5	0.9
1910001000-459	1.5	1.200	0.9	0.1	0.0	0.0	0.0	0.1	0.0	0.0	0.0	0.4	0.5	0.9
1910001000-559	1.5	1.200	0.9	0.1	0.0	0.0	0.0	0.1	0.0	0.0	0.0	0.5	0.5	0.9
<b>Ω</b>														
1910001000-355	1.5	1.200	0.9	0.1	0.0	0.0	0.0	0.1	0.0	0.0	0.0	0.3	0.5	0.5
1910001000-3575	1.5	1.200	0.9	0.1	0.0	0.0	0.0	0.1	0.0	0.0	0.0	0.3	0.5	0.75
1910001000-359	1.5	1.200	0.9	0.1	0.0	0.0	0.0	0.1	0.0	0.0	0.0	0.3	0.5	0.9
1910001000-3515	1.5	2.332	0.9	0.1	0.0	0.0	0.0	0.1	0.0	0.0	0.0	0.3	0.5	1.5
1910001000-3520	1.5	1.200	0.9	0.1	0.0	0.0	0.0	0.1	0.0	0.0	0.0	0.3	0.5	2.0

### 6.3.2 Standard Case

A standard case was developed for this problem as a starting point for the variation of parameters and initial conditions. The standard parameters and initial conditions for this RBBW problem under wave forcing are:

$$\begin{aligned} r &= 1.5 & e &= 0.9 \\ a &= 0.1 & b &= 0.0 \\ x(0) &= 0.0 & y(0) &= 0.1 & \theta(0) &= 0.0 \\ \dot{x}(0) &= 0.0 & \dot{y}(0) &= 0.0 & \dot{\theta}(0) &= 0.0 \\ f_o &= 0.3 & v &= 0.5 & \Omega &= 0.9 \end{aligned} \tag{6.1}$$

As seen above in the standard initial conditions, the RBBW is started from a similar position as in the PMBW problem undergoing forced wave motions. Again, this position was chosen because it was felt to be more realistic to the true behavior of a breakwater. Further, the RBBW is started with no initial rotation or rotational velocity because in this forced motion case it is felt that the restriction of  $\theta \leq \pi/2$  might be violated if it were given initial rotational energy. The standard forcing parameters were kept the same as in the PMBW case except  $f_o$ . The forcing amplitude,  $f_o$ , of 0.5 used in the PMBW forced motion case was found to be greater than the critical force using the standard conditions for the RBBW case. Thus, as seen in Equation 6.1, the standard forcing amplitude used for the RBBW under forcing will be 0.3. The critical force for this problem will be discussed in detail in Section 6.4.2. Once the values were selected through judgement and experience, the parameters and initial conditions were varied about the standard case to see any characteristic response behavior to the varying of the values.

### 6.4 Analysis of Data

Cases were analyzed and data was collected to see what types of characteristic behavior the RBBW exhibited under forced motions. Again, several types of graphs were used to evaluate the responses of the RBBW, including rotation vs. time plots. With forcing now involved in the analysis, special attention must be paid to the fact that the RBBW might

start to slide along the boundary or rock at the bottom of the region, as discussed previously. Also, the stopping criteria discussed in Section 6.3.1 must be considered.

#### **6.4.1 Observations**

The radius (i.e., the length of the cables) was the first parameter varied to see how the RBBW under forced wave motions would respond. Similar to the other problems investigated, there does not appear to be a significant characteristic differences between the motions of a case that has a radius of 1.5 and a case that has a radius of 2.5. However, there are two notable differences between the two radii. First, the cases with a radius of 1.5 have a sharper point at the bottom than those of the 2.5 radius case, which is shallower and leads to a flatter pattern of motion at the bottom of the region, as discussed previously in Chapter 5. Figures 6.1 and 6.2 illustrate the difference in size and range of motions of the center of the RBBW, dependent upon the mooring cable radius. However, the motion in the graph of the 2.5 radius case is not complete, because of the second noticeable difference in the two radii. The 2.5 radius case reaches a rotation value of  $\pi/2$  before the motion settles to the bottom of the region as in the 1.5 radius case. All other parameters and initial conditions were kept the same for both cases. This excessive rotation indicates that the 2.5 case has a forcing amplitude greater than that of the critical force. The critical force for these two cases will be discussed in more detail in Section 6.4.2. Though this occurs, the characteristic nature of motions produced by the two radii may still be seen.

The same response of a flatter region may also be seen in the varying of the dimensions  $a$  and  $b$ . As the dimensions increase, it may be seen that the bottom of the region becomes flatter. This flatness is further exaggerated by the increase of the radius (Figs. 6.3–6.6). Note that Figs. 6.1-6.6 are all plotted to the same scale for comparison purposes. Figure 6.6, however, has some data cut off because of its large motions. Figure 6.7 shows the full range of motions for the case in Fig. 6.6 but plotted at a scale twice as big as the scale of Figs. 6.1-6.6. Also, by looking back at Fig. 5.1, it may be seen that as the distance

between the connection points, V and W, is increased, the flatter the bottom of the region becomes. Further, the smaller the dimensions, the greater the rotations. In other words, as the size of the breakwater increases, there is less potential to rotate. This is because if the moment of inertia is less, the resistance to rotation is less and the RBBW rotates more. Figures 6.8 through 6.10 show that when the dimension a is increased for a rectangular section from 0.1 to 0.2 to 0.3 with b=0.1, the magnitude and amount of rotation are increased but the frequency of large swings in the rotation decreases. What is meant by large swings in the rotation is that say the RBBW has a large value of  $\theta$  (i.e., near  $+\pi/2$ ) and then a short time later, has a small value of  $\theta$  (i.e., near  $-\pi/2$ ). This large difference in rotation in a short period of time would consume more of the energy of the breakwater than would several smaller swings in rotation. Further, larger dimensions give a larger moment of inertia and hence rotation is being resisted more and the large swings in the amount of rotation are decreased. Notice that as the graphs reach the end, the magnitudes of the rotations get smaller and the frequency increases, indicating that the breakwater is possibly approaching a rocking condition, discussed in Section 6.5.2. Numerically, the dimensional values with the associated nondimensional mass moments of inertia for the various shapes may be seen in Table 5.2.



**Fig. 6.1.**  $y$  vs.  $x$ , Case 1910001000-359  
( $r=1.5$ ,  $a=0.1$ ,  $b=0.0$ )

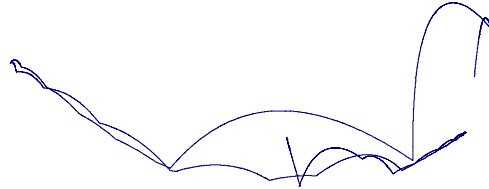


**Fig. 6.2.**  $y$  vs.  $x$ , Case 2910001000-359  
( $r=2.5$ ,  $a=0.1$ ,  $b=0.0$ )



**Fig. 6.3.**  $y$  vs.  $x$ , Case 1911001000-359  
( $r=1.5$ ,  $a=0.1$ ,  $b=0.1$ )



**Fig. 6.4.**  $y$  vs.  $x$ , Case 2911001000-359  
( $r=2.5$ ,  $a=0.1$ ,  $b=0.1$ )



**Fig. 6.5.**  $y$  vs.  $x$ , Case 1921001000-359  
( $r=1.5$ ,  $a=0.2$ ,  $b=0.1$ )

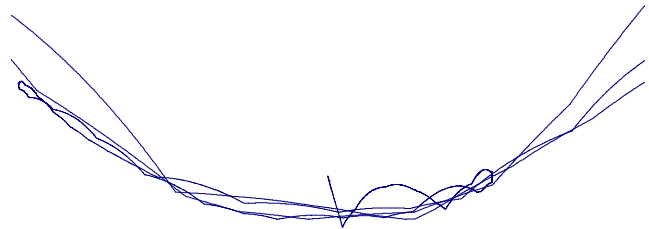


**Fig. 6.6.**  $y$  vs.  $x$ , Case 2921001000-359  
( $r=2.5$ ,  $a=0.2$ ,  $b=0.1$ )

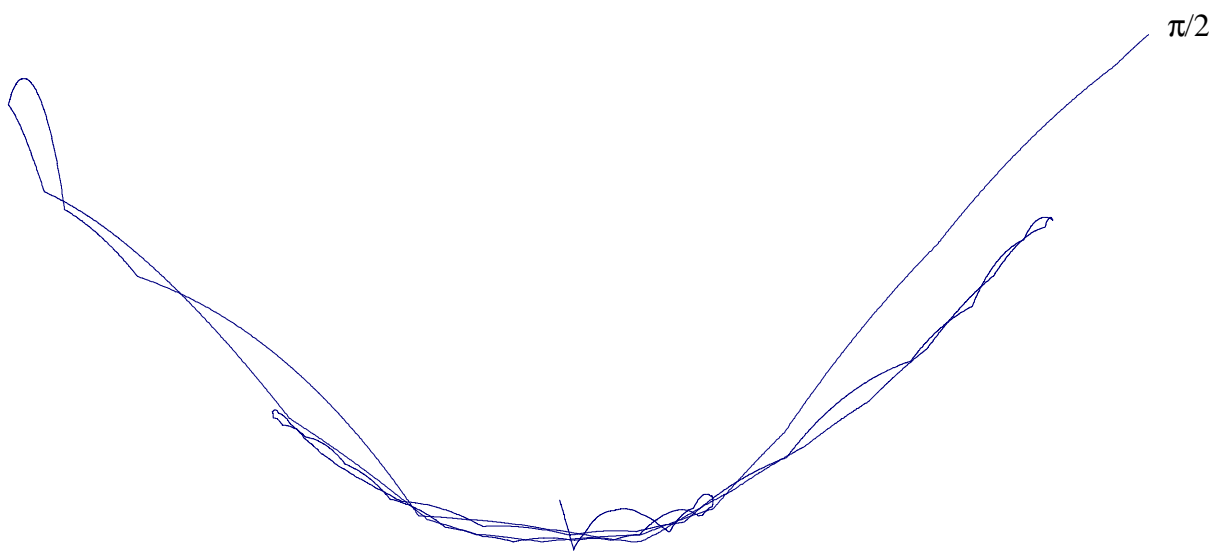


**Fig. 6.7. y vs. x, 2921001000-359**  
**(r=2.5, a=0.2, b=0.1)**  
**(twice scale)**

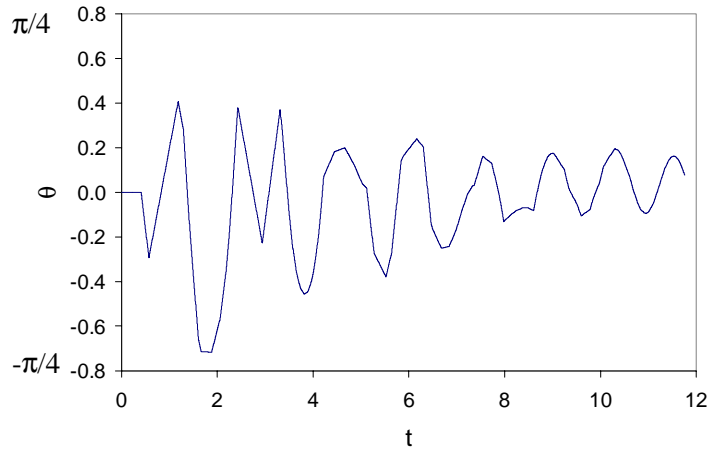


**Fig. 6.8.  $\theta$  vs.  $t$ , Case 1911001000-359  
( $a=0.1$ ,  $b=0.1$ )**

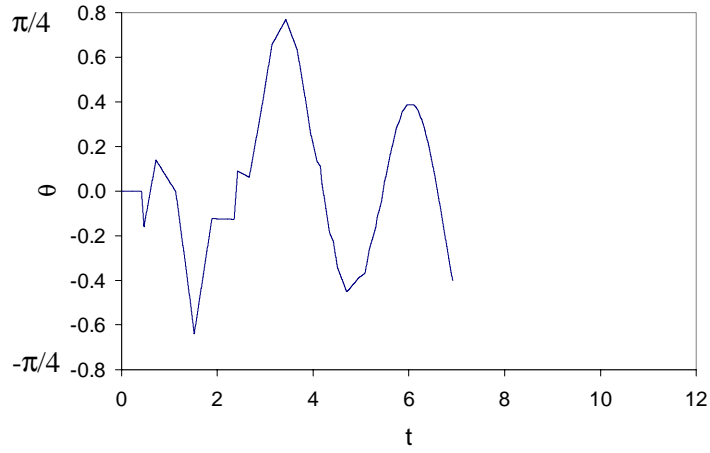


**Fig. 6.9.  $\theta$  vs.  $t$ , Case 1921001000-359  
( $a=0.2$ ,  $b=0.1$ )**

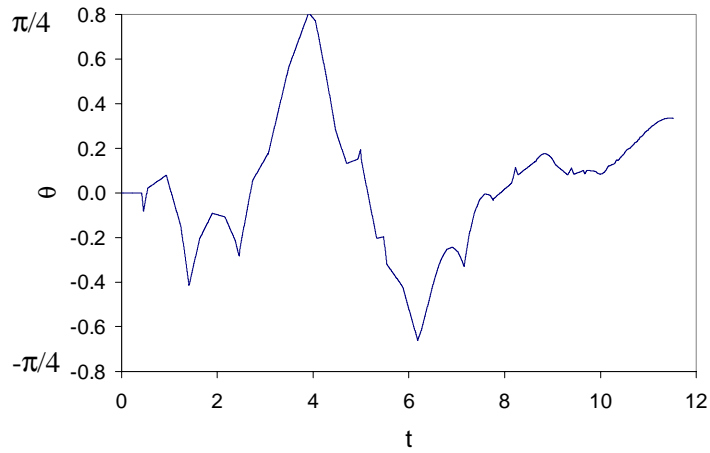


**Fig. 6.10.  $\theta$  vs.  $t$ , Case 1931001000-359  
( $a=0.3$ ,  $b=0.1$ )**

The variation of the coefficient of restitution,  $e$ , in this problem does not produce any noticeable characteristic differences from the characteristics previously discussed. As the coefficient of restitution was varied from 1.0 to 0.9 to 0.7 and to 0.5, the motions of the RBBW became less active as more energy was dissipated through the impacts occurring as the cables became taut. This behavior is illustrated in Figs. 6.11-6.14 where the corresponding  $v_n$  vs.  $t$  plots show that the energy tends to decrease if  $e < 1$ . The time scale in Fig. 6.11 is different than in Figs. 6.12-6.14. The chaotic nature of the case where  $e=1.0$  may be attributed to the forcing adding energy to the system while gravity tries to draw the RBBW downward. One point which should be noted is that during the solution of the  $e=1.0$  case, the rotation of the RBBW surpasses the  $\pi/2$  restriction and the solution is stopped. The trajectory plot of this case may be seen in Fig. 6.15. Further, Fig. 6.16 shows the rotation versus time plot for this case where the limit of  $\pi/2$  is indicated. This excessive rotation may be attributed to the fact that no energy is lost at the various impacts, and thus the motions are not damped out and excessive rotations become likely. As  $e$  is decreased, more and more energy is lost from the system, causing the RBBW to move less around the region and experience lower snap loading. As time goes on, more energy is dissipated and gravity starts to control the motions of the breakwater and draws it down to the equilibrium state at the bottom of the region. Thus, the lower the  $e$  value, the less time the breakwater will move around the region before it settles to the bottom of the region because of its loss of energy and the influence of gravity.

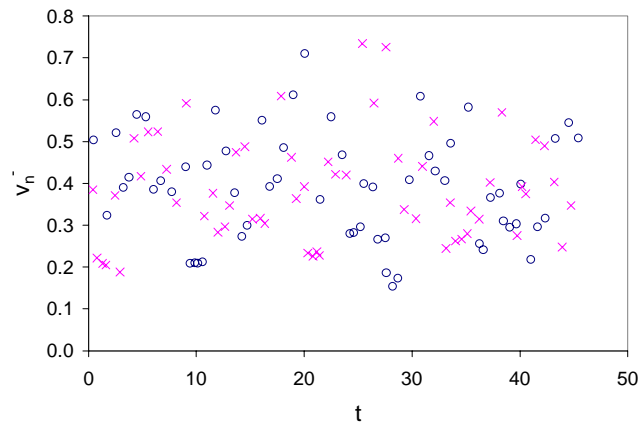


**Fig. 6.11.**  $v_n$  vs.  $t$ , Case 1110001000-359 ( $e=1.0$ )

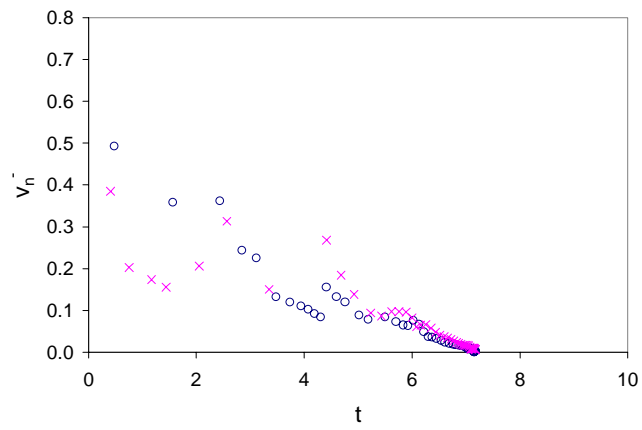


**Fig. 6.12.**  $v_n$  vs.  $t$ , Case 1910001000-359 ( $e=0.9$ )

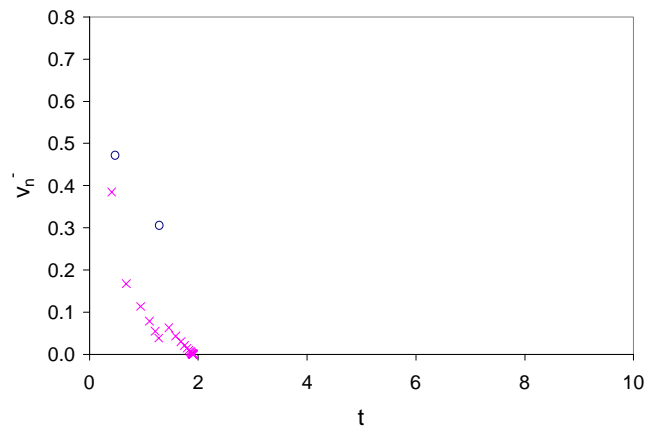


**Fig. 6.13.**  $v_n$  vs.  $t$ , Case 1710001000-359 ( $e=0.7$ )

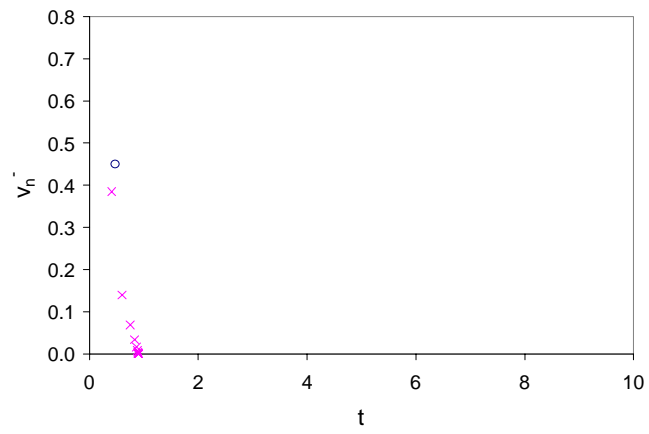


**Fig. 6.14.**  $v_n$  vs.  $t$ , Case 1510001000-359 ( $e=0.5$ )



**Fig. 6.15.**  $y$  vs.  $x$ , Case 1110001000-359 ( $e=1.0$ )

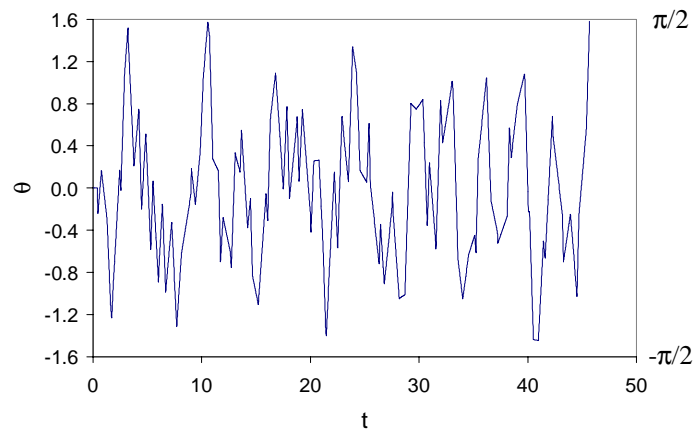


**Fig. 6.16.**  $\theta$  vs.  $t$ , Case 1110001000-359 ( $e=1.0$ )

As the force amplitude,  $f_o$ , was increased in steps of 0.1, it was seen that the rotation limit of  $\pi/2$  was first reached when  $f_o=0.5$ . However, when a smaller step of 0.01 in the variation of the force amplitude was used, it was found that the rotation limit was reached at 0.31. This force amplitude was found to be the critical force, which will be discussed in more detail in Section 6.4.2. The cases seen in Table 6.1 that have  $f_o$  less than 0.5 settle to the bottom of the region. This would indicate that these values are below the critical force, but this is not true since the critical force here is the first force which causes the breakwater to rotate past the rotation limit of  $\pm\pi/2$ . These cases settle to the bottom because it is possible for a case with a forcing amplitude greater than that of the critical force to have gravity control even though the rotation limit was reached at a lower forcing amplitude. This phenomenon is due to the many variables and degrees of freedom involved in the nonlinear solutions. This is why a detailed analysis of the critical force was performed.

The forcing parameter  $\Omega$  was varied to see its effect on the response of the RBBW under forced motions. The cases analyzed in this section used the standard case parameters and initial conditions except that the value of  $\Omega$  was varied from 0.5 to 0.75 to 0.9 to 1.5 to 2.0 to produce the data. No noticeable characteristic features appear in the trajectory plots, and they will not be shown. Figures 6.17-6.21 show the plots of  $\theta$  vs.  $t$  for these cases. In these plots it also appears that as the value of  $\Omega$  is increased, the magnitude of the rotations also increases though nonlinearly. The rotations increase until the rotation limit is exceeded, which occurs in the  $\Omega=2.0$  case, seen in Fig. 6.21. The  $v_n^-$  vs. time plots, seen in Figs. 6.22-6.26, also shows some interesting phenomena. One interesting feature is seen in Figs. 6.22, 6.24, and 6.26 where there are segments of only x's or only o's close to each other. By looking at the trajectory and impact data, it can be deduced that this is caused by the RBBW bouncing down a boundary for a while.

As seen in the various normal velocity just before impact versus time ( $v_n^-$  vs.  $t$ ) plots throughout this chapter, patterns of x's and o's may be noticed which are similar to

patterns previously seen in other problems. This problem appears to have all of the characteristic patterns discussed in earlier problems. Some of the plots have the normal velocities consistently higher on one boundary than the other, as seen in Fig. 6.22. This may indicate that the RBBW is grazing off one boundary with little normal velocity, and striking the other boundary more directly and producing a larger normal velocity before impact. Another pattern shows the normal velocities of the two boundaries converging and then diverging, like a serpentine pattern, as seen in Fig. 6.25. A similar pattern is seen where the normal velocities of the two boundaries intertwine in and out of each other similar to braiding. This may be seen in Figs. 6.23 and 6.24. These patterns are most likely due to the elliptical forcing which is continually changing direction. For example, say the RBBW is headed towards the right boundary and the forcing is acting in the same direction; then the normal velocity will be high at impact. Then after the rebound the RBBW is headed towards the left boundary but the forcing is acting in the opposite direction; then the normal velocity will be low when it strikes the left boundary, showing up on the graph as a separation in the braids. If both boundaries are struck in succession with similar conditions and the forcing has switched direction, then the normal velocities may have the same value, indicated on the  $v_n^-$  vs.  $t$  graph as a point of convergence or overlapping.

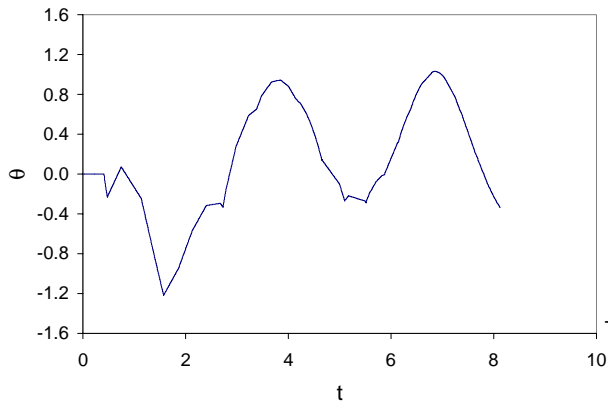


Fig. 6.17.  $\theta$  vs.  $t$ , Case 191001000-355 ( $\Omega=0.5$ )

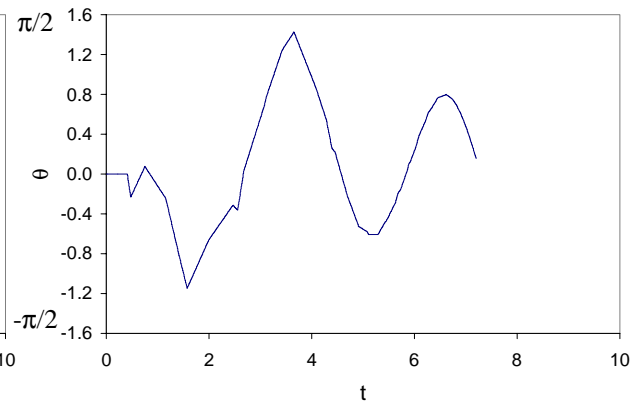


Fig. 6.18.  $\theta$  vs.  $t$ , Case 191001000-3575 ( $\Omega=0.75$ )

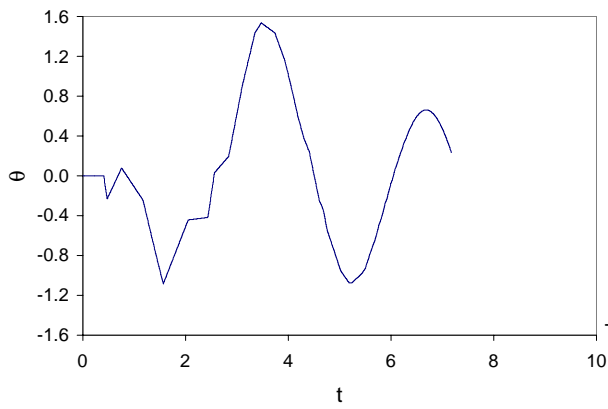


Fig. 6.19.  $\theta$  vs.  $t$ , Case 191001000-359 ( $\Omega=0.9$ )

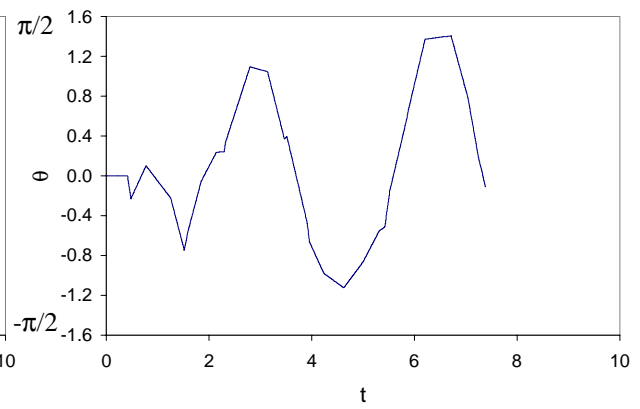


Fig. 6.20.  $\theta$  vs.  $t$ , Case 191001000-3515 ( $\Omega=1.5$ )

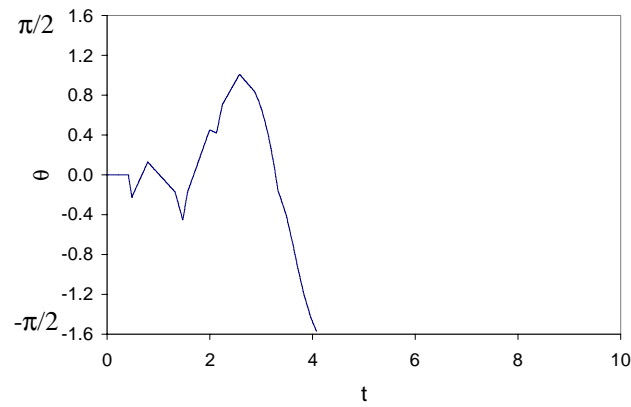


Fig. 6.21.  $\theta$  vs.  $t$ , Case 191001000-3520 ( $\Omega=2.0$ )

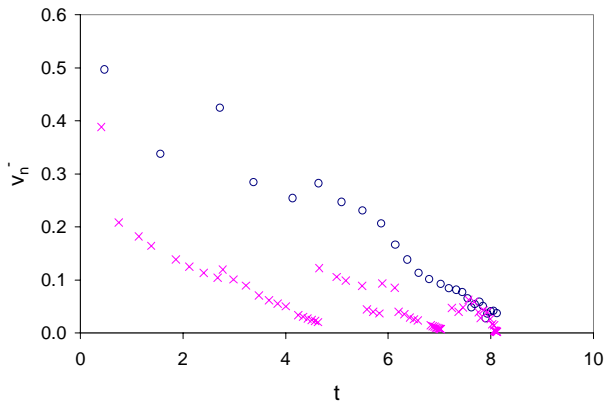


Fig. 6.22.  $v_n^-$  vs.  $t$ , Case 1910001000-355 ( $\Omega=0.5$ )

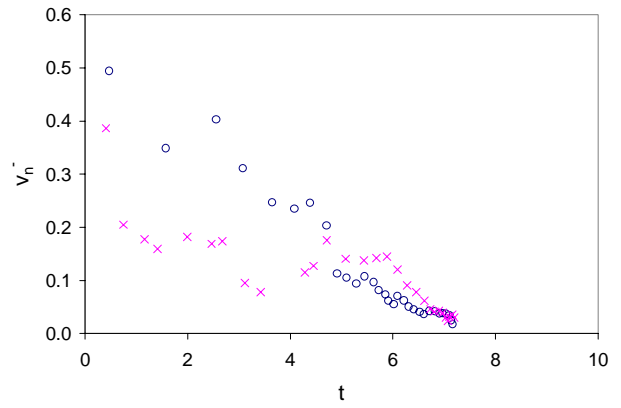


Fig. 6.23.  $v_n^-$  vs.  $t$ , Case 1910001000-3575 ( $\Omega=0.75$ )

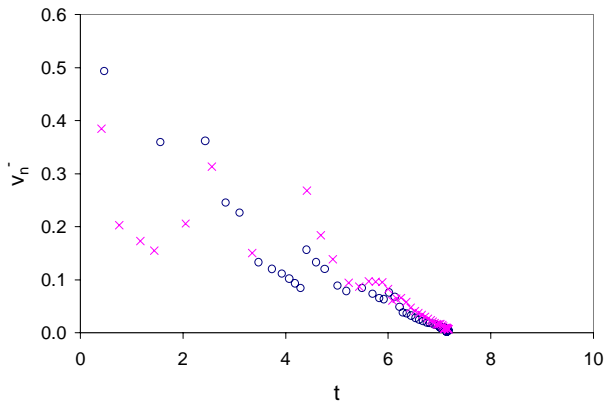


Fig. 6.24.  $v_n^-$  vs.  $t$ , Case 1910001000-359 ( $\Omega=0.9$ )

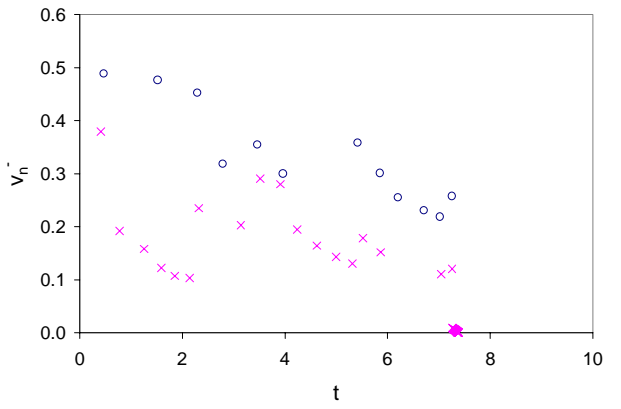


Fig. 6.25.  $v_n^-$  vs.  $t$ , Case 1910001000-3515 ( $\Omega=1.5$ )

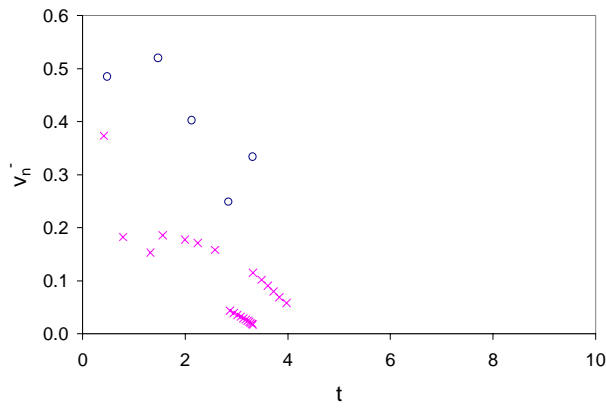


Fig. 6.26.  $v_n^-$  vs.  $t$ , Case 1910001000-3520 ( $\Omega=2.0$ )

## 6.4.2 Critical Force

The critical force was investigated in this problem and is similar in concept to that discussed previously in Section 4.4.2. The critical force was originally defined as the forcing amplitude,  $f_0$ , which would cause the breakwater to hit the upper boundary ( $y=h$ ), which indicates that the forcing was so large that it controlled the motions of the breakwater and caused it to hit the sea floor. Now that a more accurate and sensitive model is being investigated, this definition must be slightly modified. For the rigid-body analysis, the critical force turned out to be the force that causes the breakwater to rotate past  $\pm\pi/2$ . This limit was reached before the  $y=h$  limit because of the sensitivity of the RBBW to rotations. This limit is significant because if the breakwater rotates past this value the mooring lines may become entangled, which is undesirable.

Two critical force cases were investigated in depth for this problem, where plots of  $f_{cr}$  vs.  $e$  and  $\Omega$  were produced for both. Both analyses were performed with the circular shape of the standard case; however, two values of the length of the mooring lines,  $r=1.5$  and  $2.5$ , were used to see the effect on the critical force. These investigations were performed by fixing all of the case conditions and increasing  $f_0$  until  $\theta$  reached the limit of  $\pm\pi/2$ . The critical force for some other cases, where the size of the RBBW was varied, were determined under standard parameters (i.e.,  $e=0.9$  and  $\Omega=0.9$ ) to see what influence the size and shape of the breakwater has on the critical force.

Critical force results when varying the size of the RBBW with respect to the standard parameters and initial conditions may be seen in Table 6.2. It can be seen from the results summarized in this table that typically as the size of the RBBW is increased, as well as the mass moment of inertia, the higher the force amplitude has to be in order to cause the RBBW to rotate past the rotation limit. The exceptions to this conclusion, seen in the table, are most likely due to the fact that the problem being investigated is highly

nonlinear in nature from the many variables involved in the solution. Thus, one small change in the variables may cause a significant change in the results. The critical forces for the  $r=2.5$  cases tend to be less than the critical forces for the  $r=1.5$  cases. Again, this is most likely due to the larger area and flatter boundaries of the  $r=2.5$  cases. Another difference is seen between the circular and square or rectangular shapes. The circular shapes have lower critical forces than the square or rectangular shapes. The differences between the critical force of these different shapes may be due to the fact that the connection points are at different locations (Figs. 5.2a-c).

**Table 6.2 Critical Force Results of Different Size RBBW's with Different  $r$  Values and Same Standard Conditions**

<b>r=1.5</b>	<b>a</b>	<b>b</b>	<b>f<sub>cr</sub></b>	<b>r=2.5</b>	<b>a</b>	<b>b</b>	<b>f<sub>cr</sub></b>
<b>circle</b>	0.1	0	0.31	<b>circle</b>	0.1	0	0.10
	0.2	0	0.42		0.2	0	0.18
	0.3	0	0.40		0.3	0	0.30
<b>square</b>	0.1	0.1	0.32	<b>square</b>	0.1	0.1	0.28
	0.2	0.2	0.34		0.2	0.2	0.33
	0.3	0.3	0.60		0.3	0.3	0.35
<b>rectangle</b>	0.2	0.1	0.68	<b>rectangle</b>	0.2	0.1	0.27
	0.3	0.1	0.67		0.3	0.1	0.35

Plots of the critical force versus the coefficient of restitution,  $e$ , and the wave frequency,  $\Omega$ , were created (Figs. 6.27, 6.28, 6.29, and 6.30). These plots for the two different mooring line lengths were produced by fixing all of the standard case conditions (e.g.,  $a=0.1$ ,  $b=0.0$ ) except either  $e$  (Figs. 6.27, 6.29) or  $\Omega$  (Figs. 6.28, 6.30) was chosen, and  $f_0$  was increased until the calculated  $\theta$  value reached the rotation angle of  $\pm\pi/2$ . For the value of  $r=1.5$  it is seen in Figs. 6.27 and 6.28 that the critical force for the standard case ( $e=0.9$ ,  $\Omega=0.9$ ) is around 0.31. This means that when  $f_0=0.31=f_{cr}$  for the standard case conditions, the RBBW will rotate to an angle of  $\pm\pi/2$  sometime during its motions. This is why a force amplitude of 0.3 was used as the standard amplitude, because any  $f_0$  above 0.31 is above the critical force and the RBBW may rotate past the rotation restriction. In the  $r=2.5$  analysis, it may be seen in Figs. 6.29 and 6.30 that the critical force for the

given conditions is around 0.10. This means that when  $f_o=0.10=f_{cr}$  for the conditions, the RBBW will rotate to an angle of  $\pm\pi/2$ . This is why when the force amplitude of 0.3 was used during the analysis of the case in Table 6.1, the RBBW rotated past the rotation restriction, because  $f_o>f_{cr}$ . The critical force decreased from 0.31 in the  $r=1.5$  case to a value of 0.10 as the size of the region increased. This is because there is more area for the breakwater to move around and more possibility for the breakwater to rotate excessively.

Further, Figs. 6.27-6.29 show a decreasing nature of the critical force as the variables  $e$  and  $\Omega$  increase. However, Fig. 6.30 shows that the value of  $f_{cr}$  is basically increasing with  $\Omega$ . This may be attributed to the fact that the  $r=2.5$  region is larger and as the frequency increases the RBBW may be pushed around more rather than impacting a boundary which typically causes the breakwater to rotate excessively. It is also seen that the critical force plots are not monotonic in nature; they contain some local maxima and minima, and thus special attention must be paid to the critical force for the situation being investigated.

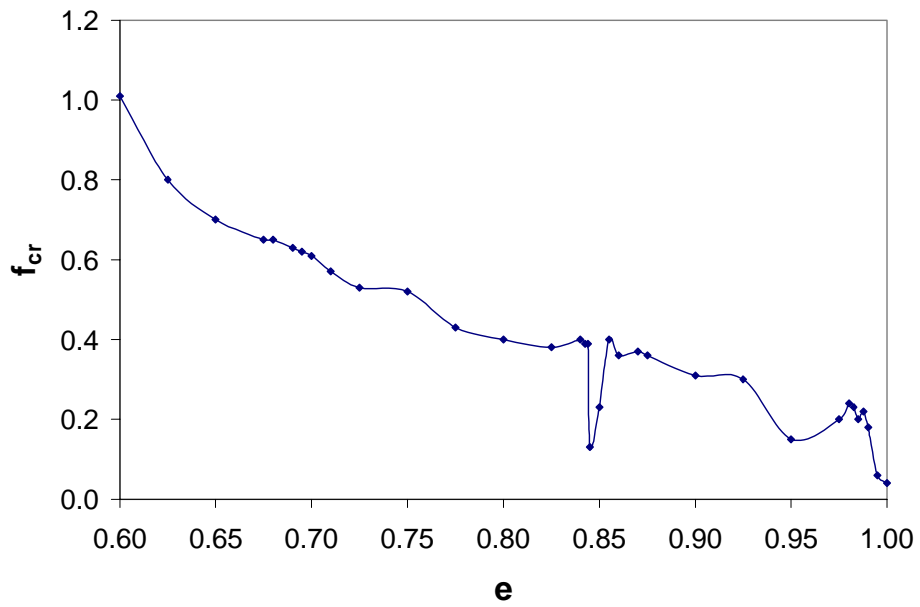


**Fig. 6.27. Critical Force vs.  $e$  ( $r=1.5$ )**

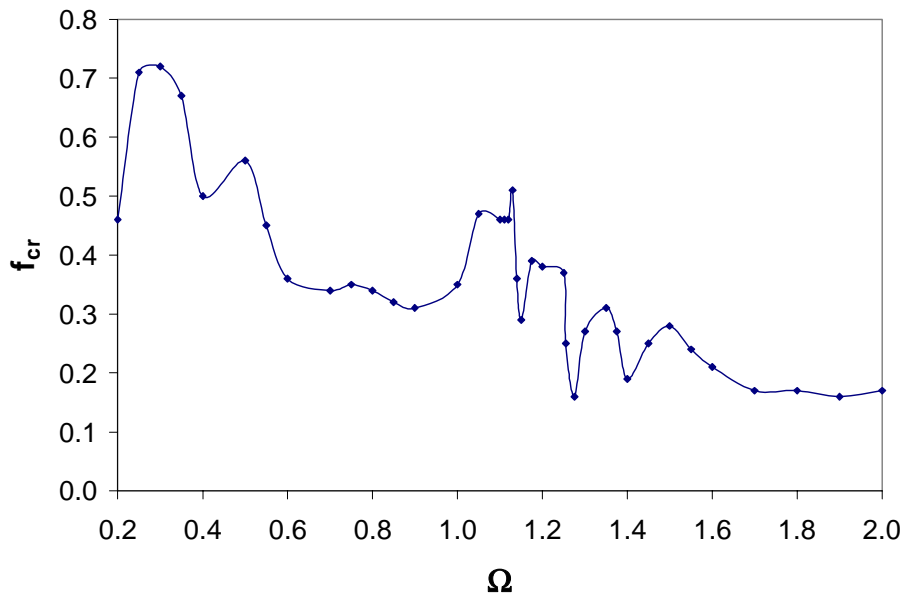


**Fig. 6.28. Critical Force vs.  $\Omega$  ( $r=1.5$ )**

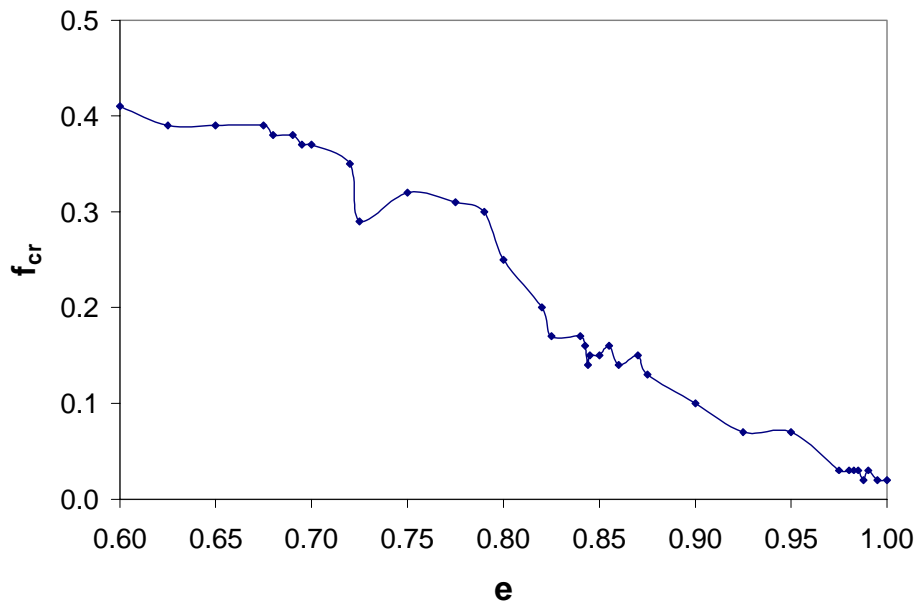


**Fig. 6.29. Critical Force vs. e (r=2.5)**

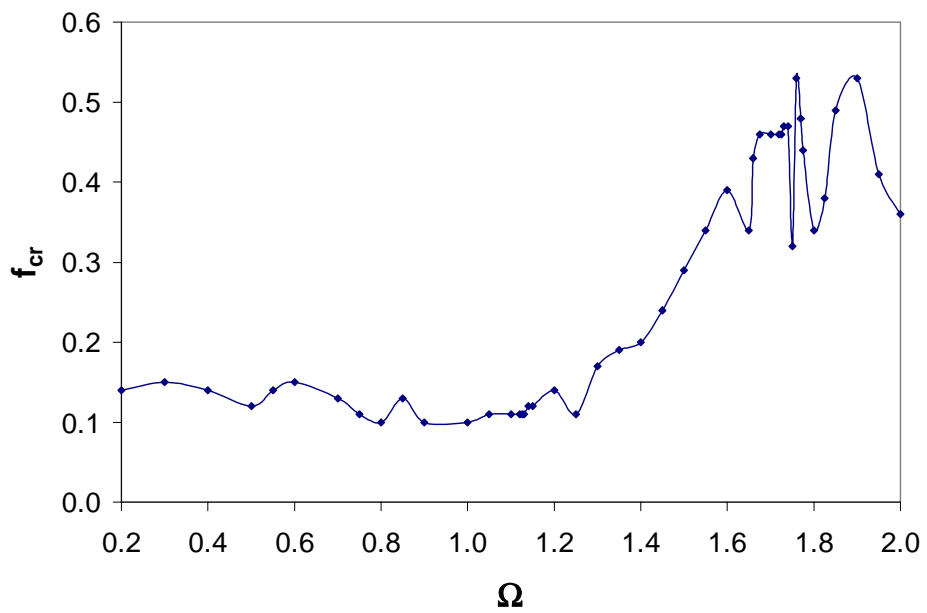


**Fig. 6.30. Critical Force vs. Ω (r=2.5)**

### 6.4.3 Norms

The norm plots created for this problem were done so with a set of given data for two cases where  $r=1.5$  and  $r=2.5$ . Norms for this problem are either maximum data points or summation of data. Five norms were investigated in this problem; three dealt with the normal velocity just before impact,  $v_n^-$ , as follows:

$$\rho_1 = \max_t(v_n^-) \quad (6.2)$$

$$\rho_2 = \sum_{t=0}^{10} v_n^- \quad (6.3)$$

$$\rho_3 = \sum_{t=0}^{\infty} v_n^- \quad (6.4)$$

The other two dealt with the maximum height,  $y_{\max}$ , and rotation,  $\theta_{\max}$ , which the RBBW attained during its period of motion. The data used in the determination of the norms was the same data used to produce the trajectory and normal velocity vs. time plots. The norms are plotted versus the magnitude of the forcing,  $f_o$ , for a given set of parameters in Figs. 6.31-6.38. The standard case parameters and initial conditions (Equation 6.1) were used to create these plots with the exception of the  $f_o$  parameter which was varied to the value of the critical force for that case. Figures 6.31-6.34 are the norm plots for the  $r=1.5$  case while Figs. 6.35-6.38 are the norm plots for the  $r=2.5$  case.

As seen in Figs. 6.31 and 6.35, the phenomenon of a critical forcing is reinforced. It can be seen that as the forcing is increased,  $|\theta|_{\max}$  increases to the rotation limit of  $\pi/2$ , and the corresponding force amplitude is at the predetermined value of  $f_{cr}$ . When the forcing is low, the initial height of  $y_o=0.1$  is  $y_{\max}$  (Figs. 6.32 and 6.36). This is due to gravity controlling the motions at this low forcing. As the forcing increases, the response becomes more and more controlled by the forcing and the maximum height attained by the RBBW may increase. However, in the  $r=2.5$  case,  $y_{\max}$  never gets above the initial height before the rotation restriction is reached. This is most likely due to the fact that

the bottom of the  $r=2.5$  region is flatter than that of the  $r=1.5$  case, thus there is more area for the breakwater to travel about and more possibility for it to rotate excessively.

As the force amplitude,  $f_o$ , is increased, the  $\rho_1$  norms (Figs. 6.33 and 6.37) tend to stay constant. This is different than the behavior seen in the PMBW under forcing (Section 4.4.3) where the value of  $\rho_1$  increased as the force amplitude increased. The norm  $\rho_1$  may have kept a constant value in this problem because of the rotations being introduced into the RBBW response at the time of impact (Equations 5.69, 5.70, 5.97, and 5.98). More likely, though, as seen in Equation 6.2, this norm is the greatest normal velocity value throughout the motions of the RBBW and the normal velocity is usually at a maximum around the first impact, as can be seen in Figs. 6.22-6.26. However, in the RBBW case the breakwater has dimensions unlike the PMBW case, and thus the RBBW is closer to the boundaries even when started from the same initial position because of these dimensions. As the forcing increases, the PMBW travels a farther distance than the RBBW does to hit a boundary for the first impact. Therefore, the PMBW will gain more velocity from the wave forcing than the RBBW would because it travels farther. Thus, it may be concluded that the norm  $\rho_1$  may stay constant in the RBBW case because of its rotations and dimensions.

The cumulative norms  $\rho_2$  and  $\rho_3$  (Figs. 6.33, 6.34, 6.37, and 6.38) exhibit some interesting behavior. In the  $r=1.5$  analysis,  $\rho_2$  and  $\rho_3$  appear to stay constant at lower values of  $f_o$  and decrease while acting erratically at higher values of  $f_o$  (Figs. 6.33 and 6.34). By examining the  $\theta$  vs. time plots for the cases used to produce these norms, it was found that the magnitude and frequency of jumping or swinging between extreme values stay low and constant at low values of  $f_o$  and then increase at higher values of  $f_o$ . This increase in rotational movement would transform some of the translational energy into rotational energy, and thus decrease the velocity with which a boundary is hit. Therefore, as the value of  $f_o$  increases, the magnitude of rotations increases (Fig. 6.31)

which causes large swings in  $\theta$  over time, and the impact energy which is derived from the velocities of the breakwater is reduced; this is reflected in the  $\rho_2$  and  $\rho_3$  plots.

In the  $r=2.5$  analysis,  $\rho_2$  and  $\rho_3$  appear to decrease as the value of  $f_0$  increases and then appear to increase and then decrease again while acting erratically at higher values of  $f_0$  (Figs. 6.37 and 6.38). The same rotation phenomenon is exhibited here; however, in this case, the swings in rotation extremes increase and then start decreasing and increase again, giving the dipping nature seen in Figs. 6.37 and 6.38. The interesting behavior seen in these plots indicates that there may be some optimum value of wave forcing amplitude for these cases where the wave energy may be dissipated most effectively. But the unpredictable and erratic response seen in these norm plots may only be explained and most likely attributed to the highly nonlinear nature of the problem. An increase in the forcing amplitude,  $f_0$ , does not necessarily cause the norms to increase in a nice geometric pattern.

In Figs. 6.33 and 6.34 and also in Figs. 6.37 and 6.38, it may be noticed that the plots of  $\rho_2$  and  $\rho_3$  are similar because the data are almost equal for both sets of norms. They stay the same because the time,  $t$ , does not get above  $t=10$  in most cases before the RBBW settles to the bottom. The limit of  $t=10$  for  $\rho_2$  comes from Equation 6.3. This phenomenon indicates that the RBBW dissipates wave energy within a short period. However, it reaches a critical force at a lower force than the PMBW. This is because the critical forces are defined in different manners and the RBBW is more sensitive to its critical force definition than the PMBW. A true comparison of the PMBW case with the RBBW can not be made since the PMBW is infinitesimally small with no rotations and the RBBW has a shape and the ability to rotate. Therefore, because these are differences between the two models, a direct comparison can not be made because the proportional effects of the differences are not known.

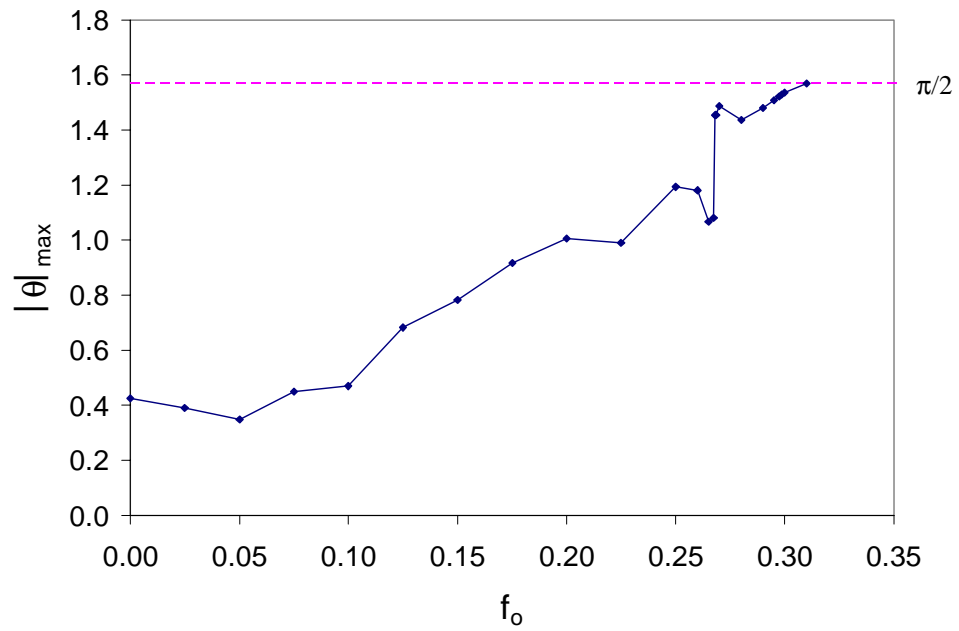


Fig. 6.31.  $|\theta|_{\max}$  vs.  $f_o$ , Norm Plot ( $r=1.5$ )

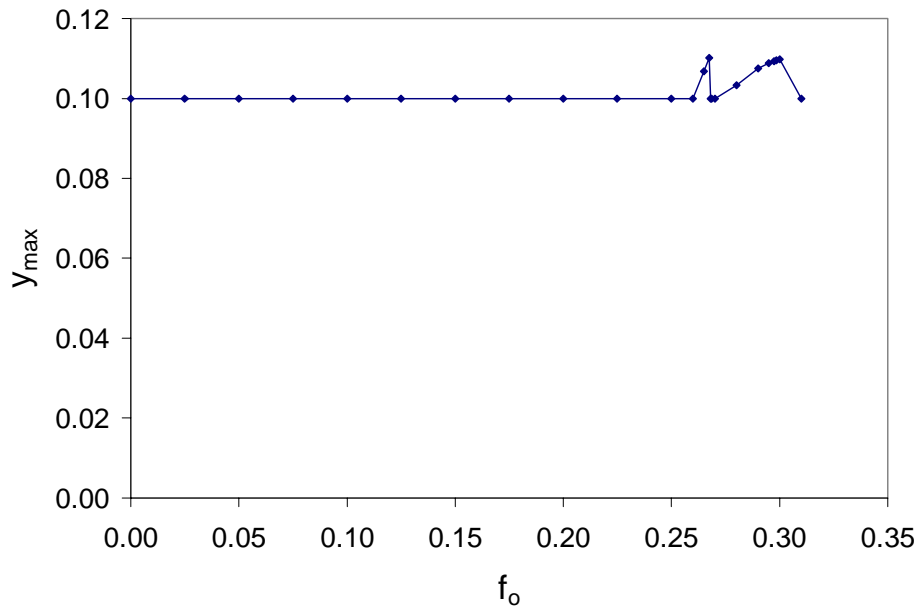


Fig. 6.32.  $y_{\max}$  vs.  $f_o$ , Norm Plot ( $r=1.5$ )

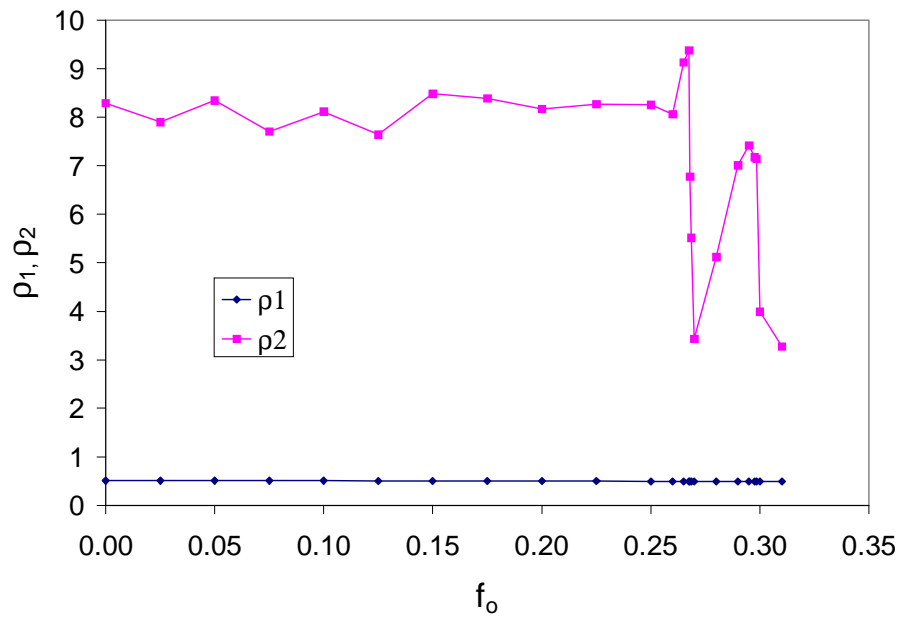


Fig. 6.33.  $\rho_1$  and  $\rho_2$  vs.  $f_0$ , Norm Plot ( $r=1.5$ )

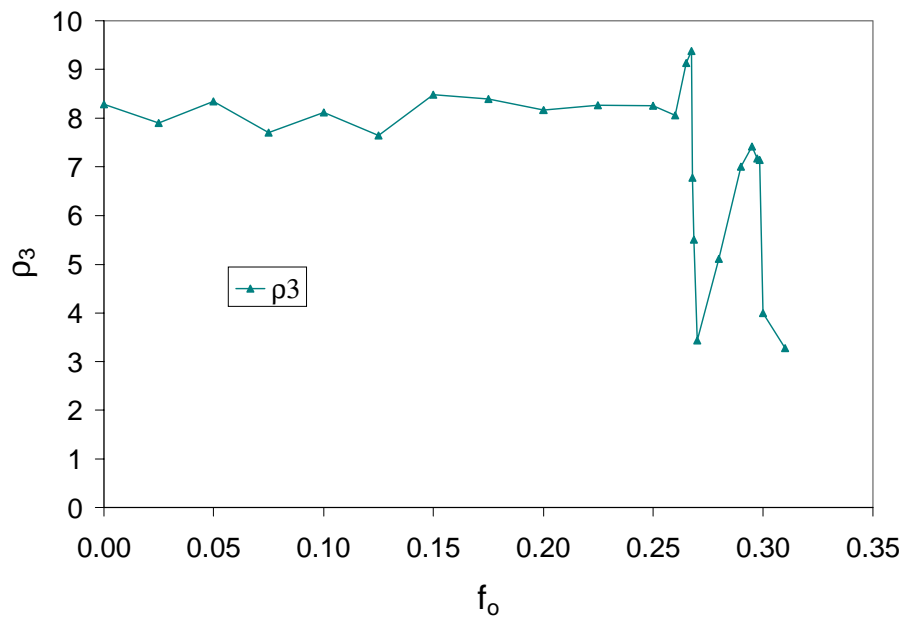
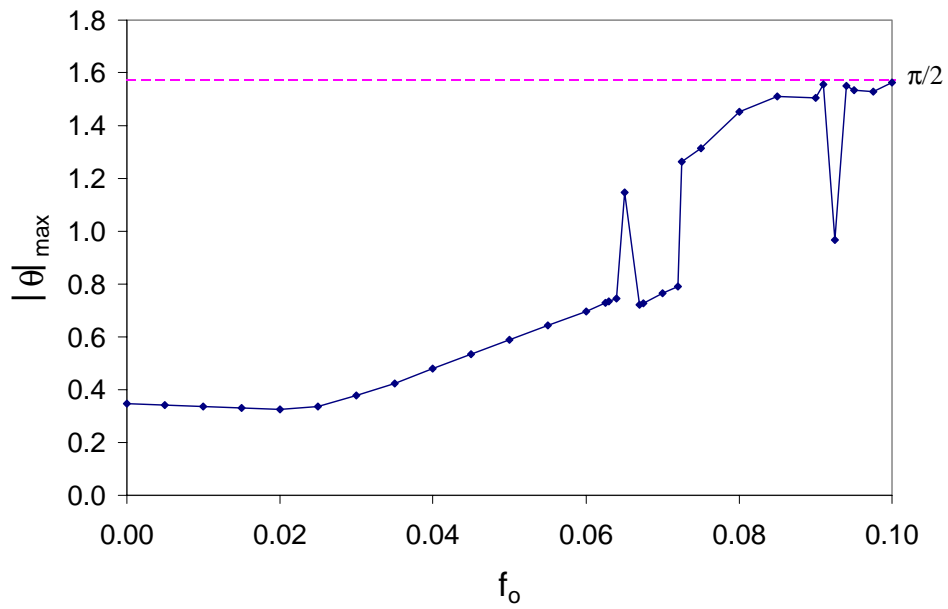
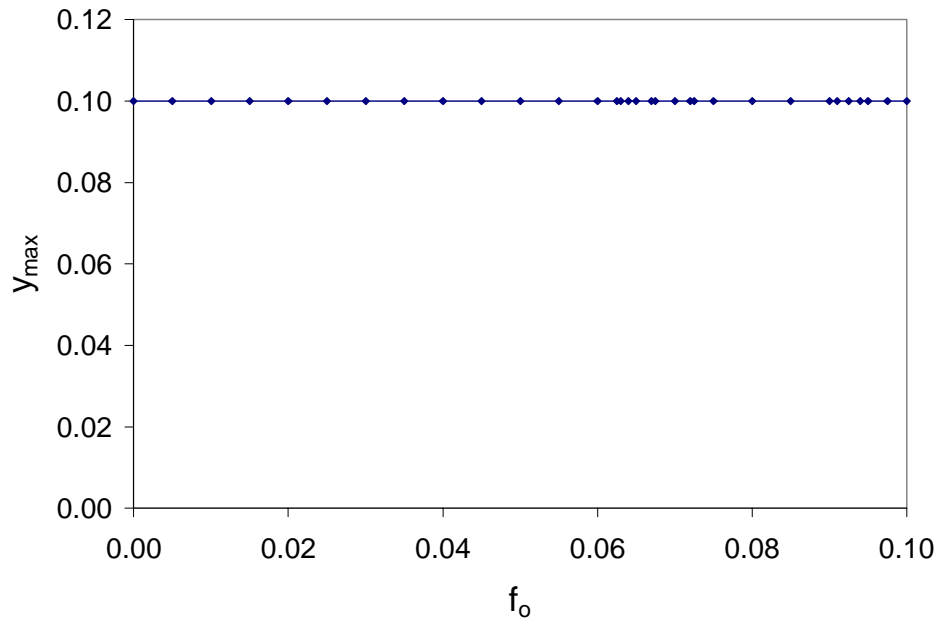


Fig. 6.34.  $\rho_3$  vs.  $f_0$ , Norm Plot ( $r=1.5$ )



**Fig. 6.35.**  $|\theta|_{\max}$  vs.  $f_0$ , Norm Plot ( $r=2.5$ )



**Fig. 6.36.**  $y_{\max}$  vs.  $f_0$ , Norm Plot ( $r=2.5$ )

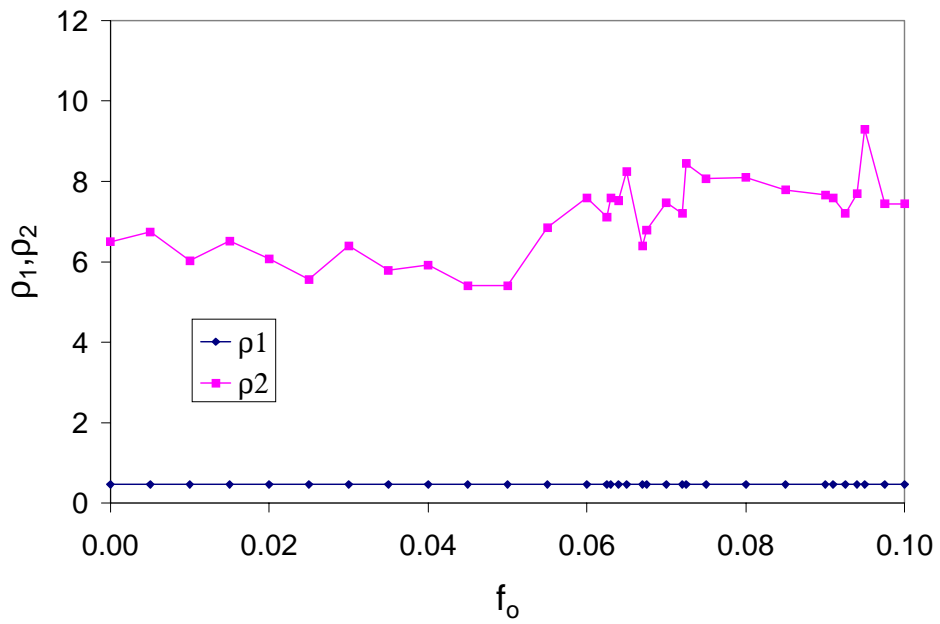


Fig. 6.37.  $\rho_1$  and  $\rho_2$  vs.  $f_0$ , Norm Plot (r=2.5)

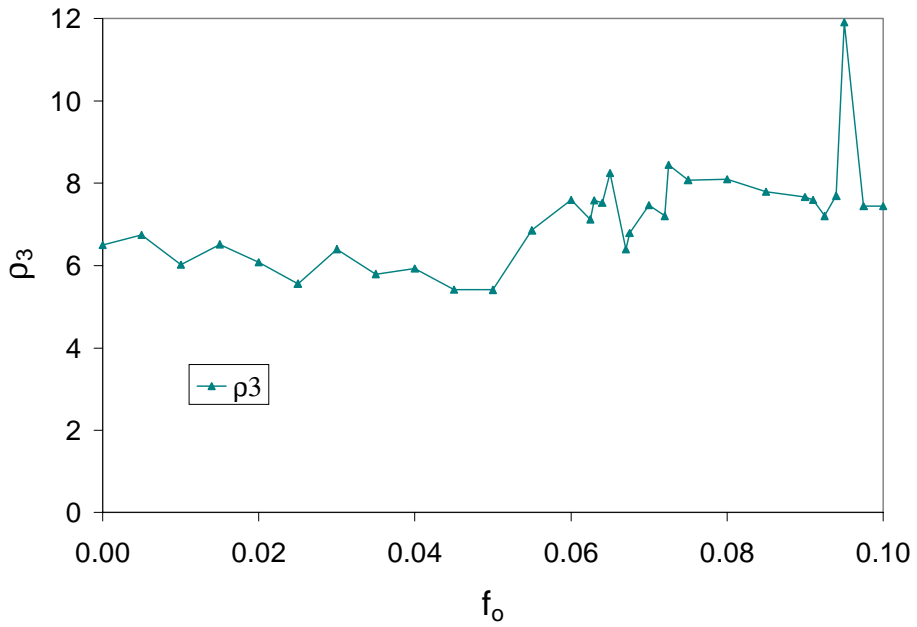


Fig. 6.38.  $\rho_3$  vs.  $f_0$ , Norm Plot (r=2.5)

## **6.5 Special Cases**

During the analyses discussed previously, it was found that the RBBW exhibits three types of motion. These motions include slack motions where the RBBW moves about the region with both cables taut. Another motion noticed is referred to as “sliding” motion where the breakwater may slide down a boundary with one cable staying taut. There is also a motion referred to as “rocking” where both cables stay taut and the breakwater simply rocks back and forth near the bottom of the region. These motions were found to exist separately, but also combinations of motions may act together during a solution. For example, a breakwater may be going through slack motions and then the wave forcing pushes it against a boundary and it slides to the bottom of the region. Then it may begin to rock at the bottom and then come out of rocking and slide up a boundary and then come off into a slack motion. It is very possible to have a combination of several of these motions occurring in one solution case. An example of this may be seen in the following sections. The slack motions have been discussed in detail throughout this thesis, and now the two new special motions will be investigated. These two special cases are more likely to occur in nature than the other special cases investigated in Section 4.5.

### **6.5.1 Sliding Case**

A special case that was investigated was a situation when one cable stays taut for some period of time while the other is slack, causing the breakwater to “slide” along a boundary. This situation may be caused by the elliptical wave motions pushing a breakwater into a boundary, along with the normal velocity not being large enough to cause the breakwater to rebound. The breakwater may stay on the boundary (i.e., slide along the boundary) until the wave forcing reverses direction, thus stopping the breakwater from being pushed into the boundary. In the slack motion solution, this type of motion is not accounted for, only a situation where the breakwater instantaneously hits

and rebounds off of a boundary. Thus, the previous solution is no longer valid. Therefore, a special solution for this sliding motion will now be formulated.

### 6.5.1.1 Sliding Case Formulation

The motions of the sliding motion case resemble that of a double pendulum. The double pendulum motions arise from a cable becoming taut and acting like the upper leg of the pendulum, with the rigid-body breakwater making up the lower leg of the double pendulum. This may be seen in Figs. 6.39 and 6.40. Meirovitch (1970) discusses the motions of a double pendulum in terms of Lagrange's Equations. Thus, the formulation of the sliding motion situation for any RBBW shape may be derived using geometry and Meirovitch's double pendulum formulation. The geometry for the  $g_1=0$  and  $g_2=0$  boundaries respectively may be seen in Figs. 5.4 and 5.5, where the dimensions are in terms of  $x$  and  $y$ , and the corresponding geometry where the dimensions are in terms of angles  $\alpha$  and  $\beta$  may be seen in Figs. 6.39 and 6.40.

The derivation of the left cable being taut and the breakwater sliding along the  $g_2=0$  (right boundary) boundary will be developed first. From the geometry of  $g_2=0$  and  $g_1<0$ , seen in Fig. 6.40, the following relationships may be derived in terms of the rotation angles  $\alpha$  and  $\beta$ :

$$x = r \sin \alpha + a \sin \beta - b \cos \beta - 1 \quad (6.5)$$

$$\dot{x} = r \dot{\alpha} \cos \alpha + a \dot{\beta} \cos \beta + b \dot{\beta} \sin \beta \quad (6.6)$$

$$y = h + b - r \cos \alpha - a \cos \beta - b \sin \beta \quad (6.7)$$

$$\dot{y} = r \dot{\alpha} \sin \alpha + a \dot{\beta} \sin \beta - b \dot{\beta} \cos \beta \quad (6.8)$$

$$\theta = \beta - \frac{\pi}{2} \quad (6.9)$$

$$\dot{\theta} = \dot{\beta} \quad (6.10)$$

Rearranging these equations, one can get  $\alpha$ ,  $\dot{\alpha}$ ,  $\beta$ , and  $\dot{\beta}$  in terms of  $x$ ,  $\dot{x}$ ,  $y$ ,  $\dot{y}$ ,  $\theta$ , and  $\dot{\theta}$ :

$$\alpha = \arcsin[(1 + x - a \cos \theta - b \sin \theta) / r] \quad (6.11)$$

$$\dot{\alpha} = \frac{\dot{x} + a \dot{\theta} \sin \theta - b \dot{\theta} \cos \theta}{h + b - y + a \sin \theta - b \cos \theta} \quad (6.12)$$

$$\beta = \frac{\pi}{2} + \theta \quad (6.13)$$

$$\dot{\beta} = \dot{\theta} \quad (6.14)$$

Equations 6.11 through 6.14 give the initial conditions for sliding in terms of angles  $\alpha$  and  $\beta$ . To get the equations of motion (EOM's) in terms of the angles  $\alpha$  and  $\beta$ , we use Lagrange's Equations:

$$L = \text{KE} - \text{PE} \quad (6.15)$$

$$\frac{d}{dt} \left( \frac{\partial L}{\partial \dot{q}} \right) - \frac{\partial L}{\partial q} = Q_q \quad (6.16)$$

where the coordinate  $q$  represents  $\alpha$  or  $\beta$  here and  $Q_q$  is a generalized force (here a moment corresponding to  $\alpha$  or  $\beta$ ). The kinetic energy of the system comes from rigid-body dynamics and is as follows:

$$\text{KE} = \frac{1}{2} m \left( \dot{x}^2 + \dot{y}^2 \right) + \frac{1}{2} I_c \dot{\theta}^2 \quad (6.17)$$

After substituting in the equations for  $\dot{x}$ ,  $\dot{y}$ , and  $\dot{\theta}$  which are in terms of  $\alpha$  and  $\beta$ ,

$$\text{KE} = \frac{1}{2} \left[ r^2 \dot{\alpha}^2 + (I_c + a^2 + b^2) \dot{\beta}^2 + 2ra \dot{\alpha} \dot{\beta} \cos(\beta - \alpha) + 2rb \dot{\alpha} \dot{\beta} \sin(\beta - \alpha) \right] \quad (6.18)$$

The potential energy of the system comes from the breakwater's height and is as follows:

$$\text{PE} = mgy \quad (6.19)$$

After substituting in the equation for  $y$  which is in terms of  $\alpha$  and  $\beta$ , and since nondimensionalization replaces  $mg$  by 1,

$$PE = h - r \cos \alpha - a \cos \beta - b \sin \beta \quad (6.20)$$

By substituting Equations 6.18 and 6.20 into Equation 6.15, the Lagrangian is developed. Specializing Equation 6.16 for the situation being investigated, the following equation is developed:

$$\frac{d}{dt} \left( \frac{\partial KE}{\partial \dot{q}} \right) - \frac{\partial KE}{\partial q} + \frac{\partial PE}{\partial q} = Q_q \quad (6.21)$$

By the use of the principle of virtual work, the values of  $Q_\alpha$  and  $Q_\beta$  may be derived:

$$\delta W = Q_\alpha \delta \alpha + Q_\beta \delta \beta \quad (6.22)$$

Figure 6.41 shows how the forces and the displacements are arranged about the taut cable and RBBW. This gives the virtual work done by the forces as

$$\delta W = f_x \delta x + f_y \delta y \quad (6.23)$$

From Equations 6.5 and 6.7, the virtual displacements  $\delta x$  and  $\delta y$  may be written as

$$\delta x = r \cos \alpha \delta \alpha + a \cos \beta \delta \beta + b \sin \beta \delta \beta \quad (6.24)$$

$$\delta y = r \sin \alpha \delta \alpha + a \sin \beta \delta \beta - b \cos \beta \delta \beta \quad (6.25)$$

The nondimensional values of  $f_x$  and  $f_y$  may be seen in Equations 4.14 and 4.16, respectively.

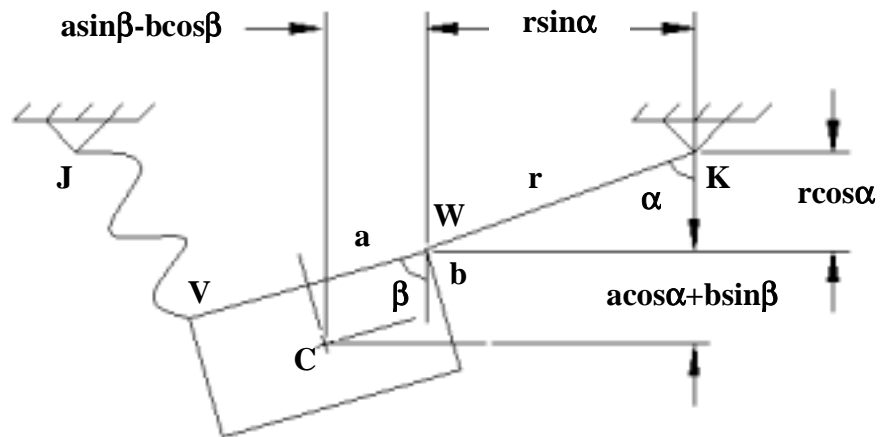


Fig. 6.39. Right Cable Taut with Dimensions in Terms of  $\alpha$  and  $\beta$

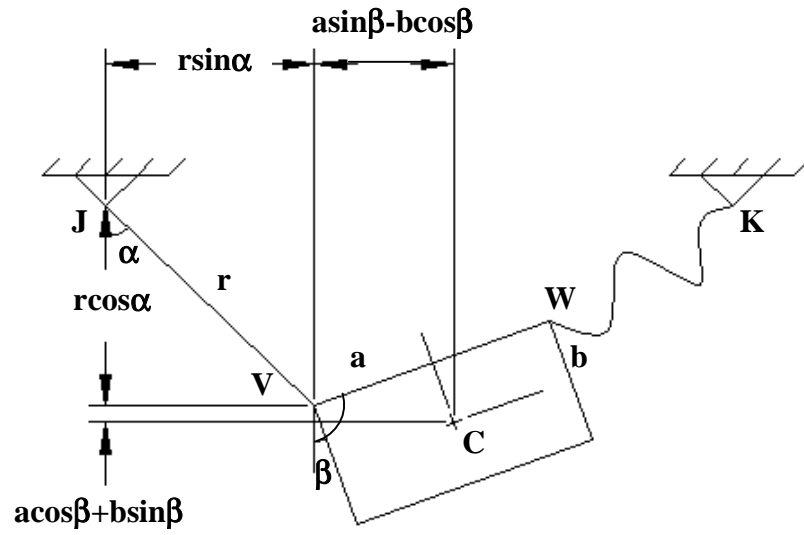


Fig. 6.40. Left Cable Taut with Dimensions in Terms of  $\alpha$  and  $\beta$

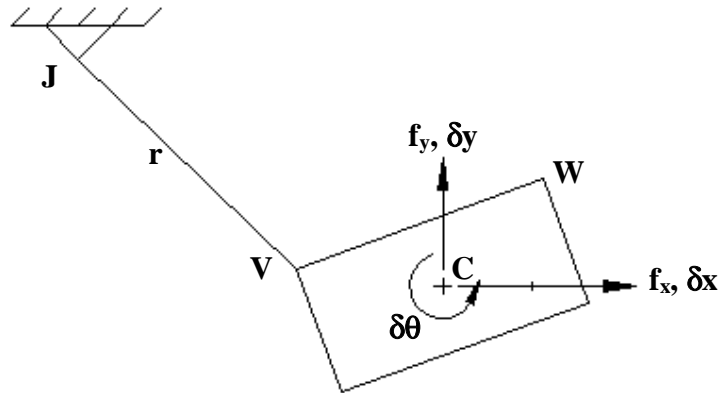


Fig. 6.41. Left Cable Taut with Forces and Virtual Displacements Shown

By plugging Equations 6.24 and 6.25 into Equation 6.23 and then by simplifying, rearranging, and comparing to Equation 6.22, the values of  $Q_\alpha$  and  $Q_\beta$  are as follows:

$$Q_\alpha = f_x r \cos \alpha + f_y r \sin \alpha \quad (6.26)$$

$$Q_\beta = f_x (a \cos \beta + b \sin \beta) + f_y (a \sin \beta - b \cos \beta) \quad (6.27)$$

By using Equations 6.18, 6.20, 6.26, and 6.27 in Lagrange's Equations (Equation 6.21) and then by rearranging and grouping the terms, the following generalized equations are obtained:

$$a_{11} \ddot{\alpha} + a_{12} \ddot{\beta} = B_1 \quad (6.28)$$

$$a_{21} \ddot{\alpha} + a_{22} \ddot{\beta} = B_2 \quad (6.29)$$

where

$$a_{11} = r^2 \quad (6.30)$$

$$a_{12} = ra \cos(\beta - \alpha) + rb \sin(\beta - \alpha) \quad (6.31)$$

$$a_{21} = a_{12} \quad (6.32)$$

$$a_{22} = I_c + a^2 + b^2 \quad (6.33)$$

$$B_1 = ra \dot{\beta}^2 \sin(\beta - \alpha) - rb \dot{\beta}^2 \cos(\beta - \alpha) - r \sin \alpha + Q_\alpha \quad (6.34)$$

$$B_2 = -ra \dot{\alpha}^2 \sin(\beta - \alpha) + rb \dot{\alpha}^2 \cos(\beta - \alpha) - a \sin \beta + Q_\beta \quad (6.35)$$

By using Cramer's Rule, the values of  $\ddot{\alpha}$  and  $\ddot{\beta}$  may be determined. However, a numerical technique was needed to solve the equations. A program written in FORTRAN was used to obtain the solution of these ordinary differential equations (ODE's). The DIVPAG subroutine from IMSL was applied. DIVPAG requires the ODE's to be in first-order form. The solutions were used to obtain the  $x$ ,  $\dot{x}$ ,  $y$ ,  $\dot{y}$ ,  $\theta$ , and  $\dot{\theta}$  values from Equations 6.5-6.10.

This solution is valid as long as the left cable is in tension (i.e., taut). Therefore, a formulation is required so that it is known when the cable loses tension. This formulation will also use Lagrange's Equations, but now the constraint of  $g_2=0$  will be imposed on this solution and will be in terms of  $x$ ,  $y$ , and  $\theta$  where these terms are equal to  $q$ . This idea may be seen in Meirovitch (1970), and the solution is as follows:

$$\frac{d}{dt} \left( \frac{\partial L}{\partial \dot{q}} \right) - \frac{\partial L}{\partial q} = Q_q + \lambda \frac{\partial g_2}{\partial q} \quad (6.36)$$

Using Equations 5.37, 6.18, and 6.20, and the generalized forces

$$Q_x = f_x \quad (6.37)$$

$$Q_y = f_y \quad (6.38)$$

$$Q_\theta = 0 \quad (6.39)$$

the following equations are obtained:

$$\ddot{x} = f_x + \frac{2\lambda(1+x-a\cos\theta-b\sin\theta)r}{r} \quad (6.40)$$

$$\ddot{y} = f_y - 1 + \frac{2\lambda(y-h-b-a\sin\theta+b\cos\theta)r}{r} \quad (6.41)$$

$$I_c \ddot{\theta} = 2\lambda[(1+x)(a\sin\theta-b\cos\theta) + (h+b-y)(a\cos\theta+b\sin\theta)] \quad (6.42)$$

where  $\lambda$  is known as the Lagrange multiplier. Interpreting Equations 6.40 and 6.41, it is found that the axial compression in the cable is  $2\lambda r$ . Thus, when the cable goes into compression (i.e., loses tension), the above solution is no longer valid and the analytical solution for no sliding should resume. For this to occur,  $\lambda > 0$ . Then, using Equations 6.5, 6.7, and 6.9, one can write Equation 6.42 in terms of  $\alpha$  and  $\beta$ :

$$I_c \ddot{\beta} = 2\lambda r [a \sin(\beta - \alpha) - b \cos(\beta - \alpha)] \quad (6.43)$$

Thus, sliding will stop when the cable loses tension ( $\lambda > 0$ ) and this will happen when the following condition arises:

$$\ddot{\beta} [a \sin(\beta - \alpha) - b \cos(\beta - \alpha)] > 0 \quad (6.44)$$

A similar derivation for the case where the right cable is taut and the breakwater is sliding along the  $g_1=0$  (left boundary) boundary may be performed. The geometry of  $g_1=0$  and  $g_2<0$  may be seen in Fig. 6.39. Thus the fundamental equations in this derivation are as follows:

$$x = 1 - r \sin \alpha - a \sin \beta + b \cos \beta \quad (6.45)$$

$$\dot{x} = -r \dot{\alpha} \cos \alpha - a \dot{\beta} \cos \beta - b \dot{\beta} \sin \beta \quad (6.46)$$

$$y = h + b - r \cos \alpha - a \cos \beta - b \sin \beta \quad (6.47)$$

$$\dot{y} = r \dot{\alpha} \sin \alpha + a \dot{\beta} \sin \beta - b \dot{\beta} \cos \beta \quad (6.48)$$

$$\theta = \frac{\pi}{2} - \beta \quad (6.49)$$

$$\dot{\theta} = -\dot{\beta} \quad (6.50)$$

Rearranging these equations, one can get  $\alpha$ ,  $\dot{\alpha}$ ,  $\beta$ , and  $\dot{\beta}$  in terms of  $x$ ,  $\dot{x}$ ,  $y$ ,  $\dot{y}$ ,  $\theta$ , and  $\dot{\theta}$ :

$$\alpha = \arcsin[(1 - x - a \cos \theta + b \sin \theta) / r] \quad (6.51)$$

$$\dot{\alpha} = \frac{\dot{x} - a \dot{\theta} \sin \theta - b \dot{\theta} \cos \theta}{y - h - b + a \sin \theta + b \cos \theta} \quad (6.52)$$

$$\beta = \frac{\pi}{2} - \theta \quad (6.53)$$

$$\dot{\beta} = -\dot{\theta} \quad (6.54)$$

From a similar virtual work derivation as before,

$$Q_\alpha = -f_x r \cos \alpha + f_y r \sin \alpha \quad (6.55)$$

$$Q_\beta = -f_x (a \cos \beta + b \sin \beta) + f_y (a \sin \beta - b \cos \beta) \quad (6.56)$$

The solution procedure discussed above for the values of  $\alpha$ ,  $\dot{\alpha}$ ,  $\beta$ , and  $\dot{\beta}$  is the same for this derivation with Equations 6.55 and 6.56 replacing Equations 6.26 and 6.27 (i.e., the sign in front of  $f_x$  changes). This solution is valid as long as Equation 6.44 is satisfied.

Both of the sliding solutions discussed above are valid as long as a cable is under tension, and when tension is lost the solution reverts back to the previous slack condition solution. However, the situation may arise where the breakwater slides down a boundary and strikes the origin, thus making both cables taut. This situation is handled by using the initial conditions from the sliding case and applying these values to the normal impact equations discussed in Section 5.5.

### **6.5.1.2 Sliding Case Results**

During the analysis of this problem, some of the cases analyzed would go into a sliding condition and would stay on a boundary for some period of time. This motion can not be handled by the previously used analytical solution, thus the numerical solution above was developed to handle this situation because it would not be accurate to simply stop the analysis if this motion would occur. When a RBBW goes into a sliding motion, the breakwater may slide either up a boundary, down a boundary, or simply rotate about a connection point while one cable is taut, essentially rotating the center of the breakwater into the region. All three of these motions were seen in the example discussed later. Since none of the solutions analyzed in Table 6.1 exhibited the special motion of sliding, some cases where this motion occurred were found from several additional analyses performed. Because of the large number of analyses conducted, not all will be shown; only an example which best depicts the behavior of a RBBW undergoing sliding will be illustrated, but the conclusions were drawn from all analyses.

It was found through many analyses that there is no set pattern to predict what parameters and initial conditions would cause a RBBW to go into a sliding condition. Sliding occurred for all of the RBBW shapes, for both radii, and at various parameters and conditions used throughout this investigation. Thus, no conclusion can be drawn as to why a breakwater would go into sliding in one case but not another. The only way to say that a breakwater would slide is when the normal velocity is very low, and this can not be

determined prior to an analysis being conducted. The highly nonlinear nature of the problem plays a major role in the occurrence of sliding.

Looking at the physical application of the problem to an actual breakwater in the sea, one can imagine that any shape, size, or configuration of a floating moored object might feel this sliding effect at some time during its life. Further, any one of the many variables involved in this type of problem might lead to a sliding condition. As seen in Fig. 6.42, if waves are pushing a breakwater in one direction long enough, one cable may be slack while the other is taut for a period of time. This might result from waves coming into the breakwater at a very high frequency and the breakwater may not be able to respond in an opposite direction. This might also be true if a very large breakwater is absorbing a lot of waves because of its size. These are just two examples of how any number of conditions might lead to a breakwater sliding (i.e., one cable being taut) and this can not be predicted.

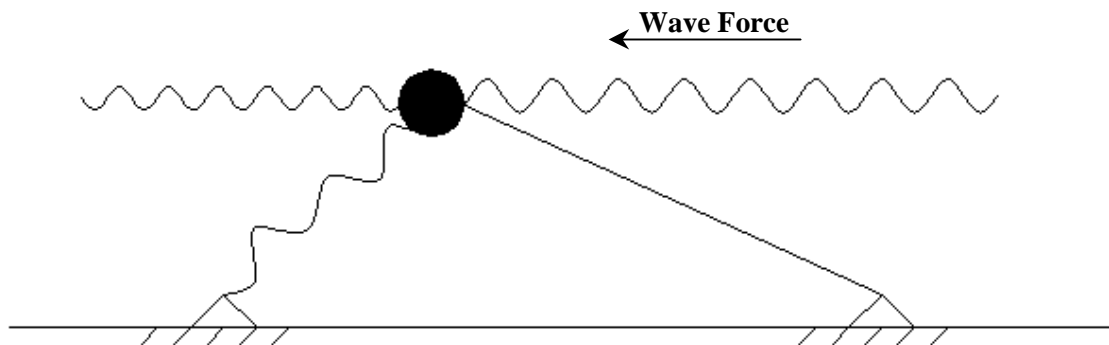


**Fig. 6.42. Breakwater with One Cable Taut (Sliding) Being Pushed by Waves**

The following is an example of one of the many cases where the sliding motion occurred sometime during the motion of the RBBW. The parameters and initial conditions used to produce this case are as follows:

$$\begin{array}{lll}
 r=1.5 & e=0.9 & \\
 a=0.1 & b=0.0 & \\
 x(0)=0.0 & y(0)=0.1 & \theta(0)=0.0 \\
 \dot{x}(0) = 0.0 & \dot{y}(0) = 0.0 & \dot{\theta}(0) = 0.0 \\
 f_0=0.27 & v=0.5 & \Omega=0.9
 \end{array} \tag{6.57}$$

This case exhibited sliding where the RBBW would slide down a boundary with one cable taut until it reached a point where both cables became taut, and then it rebounded back up a boundary (Fig. 6.43). The situation where a RBBW would impact the opposite boundary with one cable already taut (i.e.,  $g_1=g_2=0$ ) was handled by simply using the convergence part of the solution method to converge to the time where the breakwater would impact the other boundary. After this impact, using the standard impact conditions, the breakwater would rebound back up off of the opposite boundary and would continue to slide. While sliding back up the boundary, the RBBW would switch direction and travel back down the boundary again. This switching of direction may be caused by gravity taking over the motions, or the elliptical wave forcing switching direction but keeping the RBBW pushed into the boundary. Essentially, the RBBW bounced up and down with one cable taut. The RBBW in this case did not settle to an equilibrium state. Instead, an interesting situation arose where the RBBW rotates about the connection point defining the boundary of which it is sliding. This would bring the center of the RBBW and the other boundary into the region until the breakwater reaches a condition where it is on both boundaries (i.e., both cables taut), and the RBBW begins to rock and the sliding ceases. Point R in Fig. 6.43 denotes where this occurs in the trajectory. Figure 6.43 shows the trajectory of motion for the example case investigated. Like the point R, other important points of the case are noted on the plot. The starting point is indicated with an I. The point where sliding starts is denoted with an S. One of

the many points where the breakwater reaches a point where  $g_1=0$  and  $g_2=0$  and rebounds off of one boundary is denoted by G. Finally, the point where the RBBW would normally settle to an equilibrium state is denoted with an E. It should be noted that the sliding in this case starts on the left side and then moves to the right side while the RBBW is sliding down the  $g_2=0$  boundary (normally on the right side). This is because the boundaries are not definite as in the PMBW problems and the rotations of the RBBW make it possible to have a region for a boundary where the  $g_1=0$  and  $g_2=0$  could overlap, as seen in this case. The cases investigated would stop sliding by settling to the bottom of the region, reaching the rotation limit, or starting to rock. This example started to rock, and thus the rocking situation will now be described.

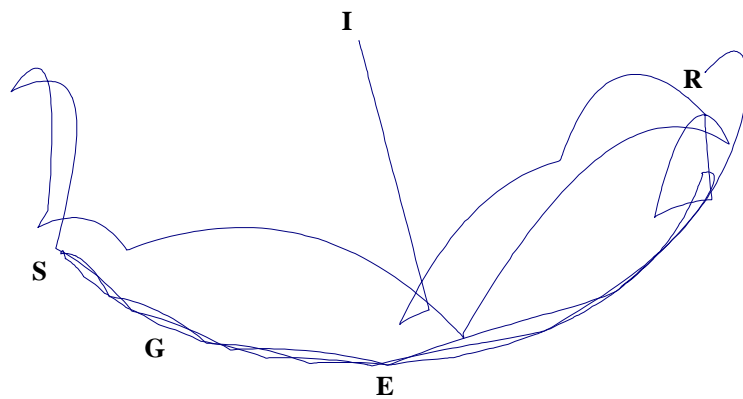


**Fig. 6.43. y vs.x, Case 1910001000-2759, Plot Showing Sliding**

## 6.5.2 Rocking Case

Rocking is another special motion seen in the rigid-body breakwater under wave forcing. A rocking situation may occur if the motions of the RBBW settle to the bottom of the region and the wave forcing is not influential enough to carry the breakwater out of this condition. In other words, the rocking case is simple in that if the wave forcing influence is small enough, the breakwater may not become excited enough to have one of its cables lose tension and it may simply rock (i.e., both cables stay taut and the breakwater rocks back and forth). This situation makes an interesting problem for investigation. A mathematical formulation was derived to model the motions of the RBBW while both cables were taut and the breakwater is rocking. This formulation uses the initial data from an analyzed case where the RBBW goes into a rocking condition during the analysis. The rocking formulation describes the motion and conditions where the RBBW comes out of rocking if in fact it does before settling to an equilibrium state. The formulation of the case where  $b=0$  (i.e., the circular shape) will be derived because it is this shape in which this investigation is most interested. Also, the mathematics involved in the case where  $b \neq 0$  become extremely complex and are not practical to solve for this investigation.

### 6.5.2.1 Rocking Case Formulation

In the analysis of the RBBW under free motions, when a condition where rocking was probable (i.e.,  $g_1=g_2=0$  and  $y \neq 0$ ), it was assumed that the breakwater would settle to the bottom of the region in a short period of time. This assumption may not be true for the RBBW under forced motions. This is because, unlike the free motion problem where the only force acting on the RBBW was gravity, the present problem being investigated has an elliptical force acting on the RBBW which may pull the breakwater out of an equilibrium state after some rocking. Thus, it is important to have a method to solve this type of condition if this situation arises.

Similar to the derivation of the sliding case, Lagrange's Equations will be used in this derivation to describe the motions of the RBBW during a rocking situation. The configuration for the rocking situation may be seen in Fig. 6.44. This configuration shows the geometry for a situation where  $g_1=0$  and  $g_2=0$  and where the dimensions are in terms of  $x$ ,  $y$ , and  $\theta$ . Thus, the formulation of the rocking motion situation for a circular RBBW shape may be derived using geometry, seen in Fig. 6.44, and Lagrange's Equations.

With  $b=0$  in this special case, the boundary condition equations become

$$g_1 = (1 - x - a \cos \theta)^2 + (h - y - a \sin \theta)^2 - r^2 = 0 \quad (6.59)$$

$$g_2 = (1 + x - a \cos \theta)^2 + (h - y + a \sin \theta)^2 - r^2 = 0 \quad (6.60)$$

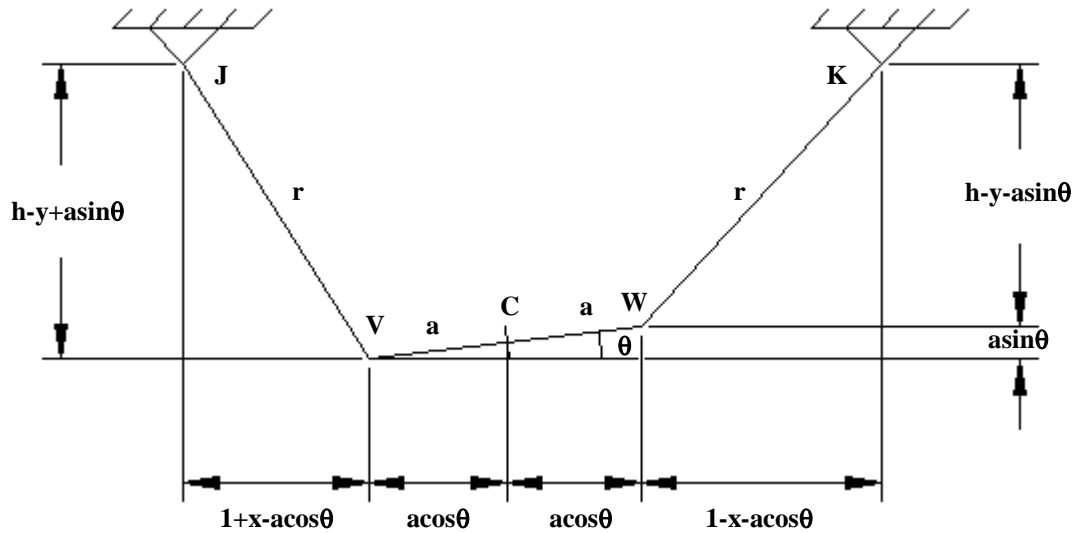


Fig. 6.44. Circular RBBW Rocking Configuration

By examining these equations, it may be seen that the problem really has only one degree of freedom. Thus,  $x$  and  $y$  can be written in terms of  $\theta$ . Expanding  $g_1$  and  $g_2$  and then subtracting these equations from one another, the following expression for  $x$  in terms of  $y$  and  $\theta$  is obtained:

$$x = \frac{(y - h)a \sin \theta}{(1 - a \cos \theta)} \quad (6.61)$$

By expanding and adding Equations 6.59 and 6.60, and using Equation 6.61, the following expression for  $y$  in terms of  $\theta$  is obtained:

$$y = h + \frac{(a \cos \theta - 1)\sqrt{r^2 - 1 - a^2 + 2a \cos \theta}}{\sqrt{1 + a^2 - 2a \cos \theta}} \quad (6.62)$$

The  $y$  value in Equation 6.61 may be replaced by Equation 6.62 to give  $x$  in terms of only  $\theta$ . With the  $x$  and  $y$  equations in terms of  $\theta$ , Equation 6.16 becomes

$$\frac{d}{dt} \left( \frac{\partial L}{\partial \dot{\theta}} \right) - \frac{\partial L}{\partial \theta} = Q_\theta \quad (6.63)$$

From the principle of virtual work, the following generalized force equation may be developed:

$$\delta W = Q_\theta \delta \theta = f_x \delta x + f_y \delta y + f_\theta \delta \theta \quad (6.64)$$

However, since there is no applied moment, the value of  $f_\theta \delta \theta = 0$  and the differential form of Equation 6.64 becomes

$$Q_\theta = f_x \frac{dx}{d\theta} + f_y \frac{dy}{d\theta} \quad (6.65)$$

The generalized force (Equation 6.65) for Equation 6.63 may be developed from Equations 4.14, 4.16, 6.61, and 6.62. Equations 6.17 and 6.19 give the kinetic and potential energies, respectively, for the Lagrangian of Equation 6.15 also to be used in Equation 6.63. This Lagrange Equation leads to an expression for  $\ddot{\theta}$  as a function of  $\theta$  and  $\dot{\theta}$ . Again, a numerical technique was needed to solve the equations. A program written in FORTRAN was used to obtain the solution of this ordinary differential

equation (ODE). The DIVPAG subroutine from IMSL was applied. DIVPAG requires the ODE to be in first-order form. The solutions were used to obtain the new values of  $\dot{x}$ ,  $\dot{y}$ ,  $\dot{\theta}$ , and  $\dot{\theta}$  for the next analysis.

In order to derive the condition for both cables to be taut, the following equations are developed from Lagrange's Equations in terms of  $x$ ,  $y$ , and  $\theta$ :

$$\ddot{x} = f_x + 2\lambda_1(-1 + x + a \cos \theta) + 2\lambda_2(1 + x - a \cos \theta) \quad (6.66)$$

$$\ddot{y} = f_y - 1 + 2\lambda_1(y - h + a \sin \theta) + 2\lambda_2(y - h - a \sin \theta) \quad (6.67)$$

$$I_c \ddot{\theta} = 2\lambda_1 a [(1 - x) \sin \theta - (h - y) \cos \theta] + 2\lambda_2 a [(1 + x) \sin \theta + (h - y) \cos \theta] \quad (6.68)$$

where  $\lambda_1$  and  $\lambda_2$  are Lagrange multipliers and are dependent upon time. Interpreting Equations 6.66 and 6.67, it is found that the axial compression in the right cable is  $2\lambda_1 r$  and the axial compression in the left cable is  $2\lambda_2 r$ . To determine if the RBBW is still in a rocking condition, the differential equations above (Equations 6.66-6.68) need to be solved with the algebraic equations for  $g_1=0$  and  $g_2=0$  (Equations 6.59 and 6.60, respectively) for  $x(t)$ ,  $y(t)$ ,  $\theta(t)$ ,  $\lambda_1(t)$ , and  $\lambda_2(t)$ . When one or both cables go into compression (i.e., lose tension), the above solution is no longer valid. There are three situations in which this may occur. If  $\lambda_1 > 0$  and  $\lambda_2 > 0$ , (i.e., both cables slack) then the analytical solution should be applied. If either  $\lambda_1 > 0$  and  $\lambda_2 < 0$  (i.e., right cable slack) or  $\lambda_1 < 0$  and  $\lambda_2 > 0$  (i.e., left cable slack), then the sliding solution should be applied.

### 6.5.2.2 Rocking Case Results

A rocking situation usually results when an analyzed case dissipates enough energy to cause the RBBW to not be able to get out of a region near the equilibrium state because gravity has pulled the breakwater near this state. While near the bottom of the region, the mooring lines of the RBBW may become taut for a period of time while the breakwater is rotating back and forth (i.e., rocking) due to its rotational ability. However, the RBBW may not settle to an equilibrium state in this problem. The RBBW may gain the ability to

climb out of a rocking situation and start sliding up one boundary or go back into a fully slack condition. This is because the RBBW is undergoing directional elliptical wave forcing. Either of these situations made it necessary to develop the above formulation in order to see if a RBBW indeed attains equilibrium or comes out of rocking.

Picking up where the case in Section 6.5.1.2 left off, the rest of the situation of that example will now be discussed. In that case the rocking only lasted a short period of time before one cable lost tension and the breakwater began to slide again. After the second sliding occurred, the breakwater settled to the bottom of the region. This is an example of where the RBBW comes out of rocking before settling to the bottom of the region. Now a case where the RBBW settles to an equilibrium state will be investigated. The parameters and initial conditions used to produce this case are as follows:

$$\begin{array}{lll}
 r=1.5 & e=0.9 & \\
 a=0.1 & b=0.0 & \\
 x(0)=0.0 & y(0)=0.1 & \theta(0)=0.0 \\
 \dot{x}(0) = 0.0 & \dot{y}(0) = 0.0 & \dot{\theta}(0) = 0.0 \\
 f_0=0.1 & v=0.5 & \Omega=0.9
 \end{array} \tag{6.69}$$

This case exhibited rocking where the RBBW would stay near the equilibrium state for a period of time with both cables being taut (i.e.,  $g_1=g_2=0$ ). Figure 6.45 shows the trajectory of motion for the example case investigated. This case is a continuation of the analytical solution of the case 1910001000-159 in Table 6.1. After the motions start to die out during the solution of the case, the RBBW does not have enough energy to rebound off of the boundaries. Further, since the forcing is low and the fact that the RBBW reaches a position where  $g_1$  and  $g_2$  are practically zero, the rocking solution is applicable. Once the RBBW enters rocking, the influence of the wave forcing is not significant enough for the RBBW to come off of the boundaries. Once in this situation, the horizontal component of the wave forcing takes control of the motions and continuously pushes the breakwater in a rocking motion. As before, some important points are noted on Fig. 6.45. The starting point is indicated with an I. Point R denotes

the point where rocking begins. The point where the RBBW settles near the equilibrium state is denoted with an E. It may be noticed in this figure that the region where the impact boundaries can exist may be seen. This region lies between the sharp points of the trajectory plot, which show where one cable becomes taut and the RBBW rebounds off of a boundary and the circular arc formed by both cables being taut and the breakwater rocking. The sharp points are above the circular arc formed by the rocking situation, indicating that the RBBW must have been rotated when it struck the boundary. If it were rotated perfectly in alignment with the boundary then, it would produce a point very close to the circular arc. The nice circular arc of the rocking shows that when both cables are taut, the only variable affecting the boundary is the rotation and the arc is formed from the breakwater being in its lowest region with  $\theta$  changing. Thus, a region where boundaries can exist extends from a rotated RBBW with one cable taut situation to a situation where both cables are taut and the RBBW is rotating (rocking).

Thus, rocking may occur in two different manners and may end in two different manners as well. Rocking may begin when a RBBW is sliding and then hits the opposite boundary; if the breakwater does not have enough energy to get back off of the boundary, it would begin rocking. Another instance where rocking may begin is when a RBBW settles to the bottom of the region and does not have enough energy to get out of this settling and the breakwater starts to rock at the bottom of the region. Rocking may end if the situation arises that the elliptical wave forcing can pull the RBBW free from the rocking. After the breakwater is freed it may start to slide again or go into the slack region. Ultimately, the final stopping of the rocking condition would be if the RBBW would simply settle and end up in the equilibrium state. Rocking may occur in almost any case where the conditions are right, but the forcing amplitude has a significant effect on whether and for how long rocking will occur. The lower the value of  $f_0$ , the more likely the breakwater will stay in a rocking condition. Whatever the manner by which a RBBW starts to rock or stops rocking, the situation where rocking occurs during the motions of a RBBW is significant and therefore has been analyzed.

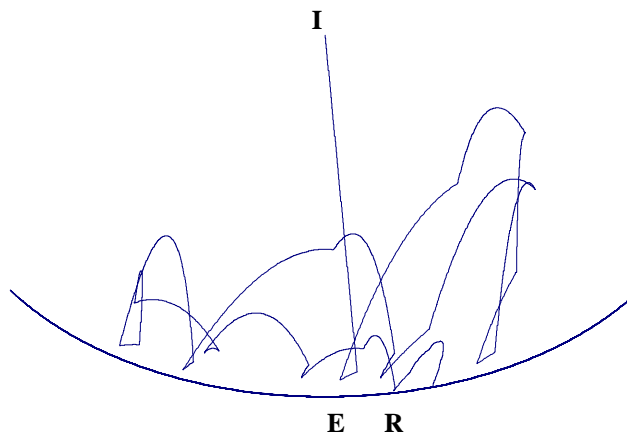


**Fig. 6.45.  $y$  vs.  $x$ , Case 1910001000-159, Plot Showing Rocking**

## Chapter 7

### Summary, Conclusions, and Recommendations

#### 7.1 Summary and Conclusions

An investigation into the snap loading of cables used in the mooring system of a breakwater was carried out in this thesis. Four problems were investigated, which had the breakwater modeled in two manners undergoing two forms of forcing. Each problem consisted of several cases, which were created by varying parameters and initial conditions for those cases. The first problem investigated had the breakwater modeled as a point mass which would undergo free vibration. The second problem was with the breakwater still modeled as a point mass, but it was subjected to elliptical forcing, which is a mathematical model to simulate natural wave forcing. The third problem investigated involved free motions like the first problem, but the point-mass breakwater was given dimensions and became a rigid-body breakwater with free motions. The fourth and final problem investigated was a rigid body undergoing forced wave motions. The third and fourth problems are very similar to the first and second except that angular positions and velocities are added. These angular variables modify the breakwater's response at impact; however, the solution procedure stays the same. To get a feel for the typical responses a breakwater exhibits before a more mathematically complicated rigid-body model was investigated, a point-mass breakwater was analyzed first, which is a simpler model to handle mathematically. The rigid-body breakwater undergoing forced wave-like motions is thought to be the most realistic of the problems investigated.

A solution was developed and employed on the problems using FORTRAN. Using either an analytical or numerical solution proved acceptable for analyzing the problems. The

results of the analyses were examined in many graphical forms and interpreted in several ways. Microsoft Excel was used to plot and evaluate the data collected.

Several assumptions were utilized to perform the analysis of these highly nonlinear problems. First, the problems were analyzed in a planar fashion and the breakwater was modeled in cross-section. The breakwater was modeled in an upside-down configuration, with the breakwater hanging by two support cables. The mooring lines were assumed to be inextensible and their weight, inertia, bending resistance, and axial resistance in compression were all neglected. The only dissipation of energy in this investigation occurred at a boundary impact (i.e., when a cable reaches its natural length) where a coefficient of restitution was used. No other damping was considered in this investigation, including fluid damping and internal resistance of the cables. Added-mass effects of the fluid also were neglected. The wave forcing is mathematically modeled as a perfectly elliptical force in the vertical plane, acting as a simple harmonic function of time. In reality waves are not regular motions; they are a combination of several varying waves. The rigid-body breakwaters were either modeled as thin-walled circular structures or solid square or rectangular types.

Certain conditions were analyzed as standard conditions, and the parameters and initial conditions of the cases analyzed were varied off of this starting point. The standard conditions were chosen to induce some desired responses but were mostly arbitrary with some judgement involved. The researcher used this judgement to try to predict the actual nature of a breakwater under real conditions. There are many variables involved in this analysis. It would be impossible and not worthwhile to investigate the infinite number of cases generated from the high number of variables; thus, the cases that were analyzed represent a small portion of a larger set of variables. Therefore, all of the analyses performed during this investigation were done so with a given set of parameters and conditions corresponding to the best guess for the situation being investigated.

From the varying of the parameters and initial conditions and the interpretation of the results of the analyses carried out, several conclusions may be drawn. First, the length of the mooring line (i.e., the nondimensional radius,  $r$ ) determines how deep the breakwater is moored relative to the distance between the mooring anchorages. During this investigation, changes in this value did not seem to produce any large changes in characteristic behavior. The only effect upon the behavior of the breakwater was that with a greater radius the area of the region of possible motion is larger and there is less of a point at the bottom of the region. With this larger area and flatter bottom, the breakwater may move about the region longer before settling to the bottom. But this may also lead to the point-mass breakwater going above the top of the region or the rigid body rotating excessively.

It has been seen through this investigation that the value of the coefficient of restitution,  $e$ , has a severe impact on the snap loading (i.e., normal velocity before impact) and the extent of motions of the breakwater. As the coefficient of restitution is decreased from unity, more energy is dissipated at the time of impact and the motions of the breakwater are suppressed. It is suggested that cables with a low value of  $e$  be used to help attenuate wave motions most effectively.

Another manner in which the snap loading or normal velocity before impact is decreased is from the effect that the size and shape have on the motion of the breakwater. It was noticed that the size and shape have a definite effect on how well a breakwater will dissipate wave energy. It was found that a point-mass breakwater dissipates less energy than a rigid-body breakwater because a rigid body utilizes its rotational resistance (i.e., the mass moment of inertia) to indirectly dissipate some of the translational energy. This is accomplished because in the point-mass investigations the breakwater is infinitesimally small and thus has no rotational ability or resistance. All of the energy of a point mass goes into translational energy and the normal velocity before impact develops from the translational velocities of the breakwater at impact. However, a rigid body has rotational

ability and thus a rotational velocity as well as a rotational inertia. Some of the energy that would go into translation is converted into rotational energy and is resisted by the moment of inertia. Thus, when a breakwater strikes a boundary, it does so with less energy because the rotations are decreasing the translational energy.

Another effect of the size of the breakwater is on the shape and size of the region in which the breakwater may move about. When the breakwater is modeled as a point mass, the area of possible motion has definite boundaries. However, when the breakwater is modeled as a rigid body, the boundaries become more like regions than definite arcs because of the rotations involved in the rigid-body investigations. Also, as the size of the breakwater increases, the flatter the bottom of the region becomes because of how the breakwater is configured with the connecting ends of the cables spreading apart as the size of the breakwater increases.

The problems investigated are initial-value problems; thus the initial position of the breakwater has an obvious effect upon the motions. During the point-mass breakwater investigations, when the breakwater was analyzed under free motions, it was started initially from a height near the top of the region. This was done to give the breakwater more energy so that it would move about the region more before settling to the bottom. This settling would happen because no energy was being introduced into the system, and thus gravity controlled the motion. During the other analyses, the breakwater was given an initial position near the equilibrium state. This was done because it is felt that this is a better representation of how the breakwater would truly behave in reality. The breakwater is subjected to a gravitational force, used to model the net buoyant force in an actual floating breakwater, which would tend to pull the breakwater downwards, near the equilibrium state. The inability to accurately predict the motions of the breakwater at a certain time during the life of the breakwater make the starting position and time totally arbitrary for a given analysis. In other words, there is no way of knowing precisely how a breakwater will behave at any point in its life because of the unknown past history and

the highly nonlinear nature of its motions. Further, the many variables involved in its modeling will also contribute to an inaccurate prediction, thus it might be said that the starting position may be anywhere in the region and the starting time of zero may be thought of as a time during the breakwater's life. The decision to start the point-mass breakwater under free vibration case at a higher position was just to allow the investigators to get a sense of the range of motions and responses during an initial analysis; this height was later refined. Though the predicting of an exact starting point is impossible, an intuitive conclusion may be drawn from the fact that the breakwater will stay near the bottom of the region in reality. This is why when the other, more accurate problems were investigated, the breakwater was given an initial position near the equilibrium state.

An interesting phenomenon was noticed while performing the forced motion analyses; this is the concept of the critical force. The critical force has been defined in two manners during this investigation. The first definition arose from the point-mass breakwater case. Here, the critical force is defined as the forcing amplitude which would cause the breakwater to hit the upper boundary ( $y=h$ ), which indicates that the forcing was so large that it controlled the motions of the breakwater and caused it to hit the sea floor. The second critical force came about from the rigid-body breakwater analysis. Here, the critical forcing was defined as the force that causes the breakwater to rotate more than  $\pm\pi/2$ . This limit is reached before the  $y=h$  limit in this problem and is significant in the sense that if the breakwater rotates past this value, the mooring lines may become entangled, which is undesirable. Further, in this situation the analysis discussed in this thesis is invalid. It was seen that the critical force solutions as a function of the coefficient of restitution or the forcing frequency are not monotonic in nature; they contain some local maxima and minima. The breakwater will be most effective in attenuating waves when the forcing amplitude is below the critical force for a given set of conditions. All of the forcing parameters are important to the response of the breakwaters. As stated above, the critical force is an important consideration in an

analysis and is dependent upon the parameters used in the analysis. Thus, a slight variation in these parameters may cause a point-mass breakwater to hit the upper boundary or cause the rigid-body breakwater to rotate excessively. A breakwater should be designed to prevent these excessive motions.

The special situations where either sliding or rocking or both occur during the motions of a breakwater were considered. These special motions were found to occur in several combinations and may arise during any analysis if the conditions are right. These motions were more likely to occur in the rigid-body investigations because of the rigid body's rotational ability. Both sliding and rocking occurred when the normal velocity before impact was very low. With sliding, in addition to a low normal velocity before impact, if the wave forcing was pushing a breakwater into a boundary (i.e., one cable is taut) then the breakwater may begin to slide on the boundary. This motion would last until the wave forcing changed direction and pulled the breakwater off of the boundary or the other cable became taut and the breakwater started to rock. With rocking, in addition to a low normal velocity before impact, if the breakwater was near the bottom of the region and both cables became taut, the breakwater may begin to rock. This motion would cease when the forcing would cause either one or both of the cables to become slack. Thus, the breakwater may begin to slide or go into slack motions after rocking. Rocking was found to occur at low values of forcing amplitude, but is possible during any analysis if the conditions are right. In fact, both of these special motions were found to occur at almost any set of parameters and conditions if the conditions are right to induce the motions. Thus, an analysis that includes slack motions, sliding motions, and rocking motions is necessary because it is hard to predict when one or both of the special situations may occur.

The life of a mooring line is affected by the number of times it experiences a transition from a slack condition to a taut condition (i.e., impacting a boundary), and by the magnitude of the normal velocity (i.e., snap load). Numerical results of these important

points may be seen in the previously discussed norms for the different problems investigated. Therefore the type of analysis presented here, using a simple impact model of snap loading, may be useful in assessing fatigue of mooring lines for various types of moored structures, as well as for other applications of cables, e.g., suspension and cable-stay bridges, cable-suspended roof systems, toelines, tethers, and guy wires.

In conclusion, the rigid-body breakwater, which undergoes wave forcing, was believed to be the more realistic model used during this investigation, because of the significant effects that rotations have on the breakwater's response. A rigid-body model of a moored breakwater was thought to have the ability to transform translational energy into rotational energy and thus reduce snap loading at higher values of forcing amplitude because of the rotations involved. The rigid-body model was found to be more sensitive to its definition of critical force than the point-mass model. However, because the shape, the ability to rotate, and the definition of critical force all differed between the two models, a direct comparison of results can not be made. Further, it was found that energy was dissipated most effectively by use of mooring lines with a low coefficient of restitution.

## **7.2 Recommendations**

There are several refinements and extensions that may be made to the models used in this investigation. It is recommended that these refinements be made and the research in this thesis be continued so that a more accurate model may be used to investigate the snap loading of cables used in moored breakwaters. Below are some of the suggested refinements to the models.

Most importantly, a more accurate analysis may be conducted to include parameters that were either neglected in assumptions or simplified to make the analysis conducted in this thesis easier. First, an analysis may be performed which would include the fluid inertia

and damping forces induced by the breakwater and its mooring lines moving through the fluid.

Next, the “impact” or sudden tensioning of a slack cable used in this thesis may be modeled as a non-instantaneous action. In other words, a mooring line may be modeled as an extensible cable. This could be accomplished by treating the cable as a very stiff spring which would take time to deform instead of instantaneously rebounding. Further, the inertia, internal energy dissipation abilities, weight, bending resistance, and axial resistance of the cables may be included in the mooring line model.

The breakwater may be modeled right side up instead of the simplification used in this thesis of upside-down. Further, the configuration may be made unsymmetrical where the spacing is not identical and is varied. This would cause the cable lengths to be varied as well.

The breakwater may be modeled in its true three-dimensional form. This would include cables on both sides of both ends of the cylindrical or 3-D rectangular breakwater. Also a cable may be attached to the ends of the breakwater for added lateral stability. All of the motion responses of these cables may be analyzed in three dimensions.

The wave forcing may be modeled more accurately to what it truly is in nature. This means that the wave forcing is dependent upon position. Actual wave motions decrease with depth. The model used in this thesis has the wave forcing the same at any position. Further, waves may not be harmonic, as they were assumed to be in this investigation. A wave model that best depicts the natural nonharmonic motions of waves should be used.

A non-rigid inflatable breakwater model may be investigated. An inflatable breakwater would have the ability to deform as well as move around under wave forcing. This deformation would be just another manner in which energy may be dissipated from

waves. Investigations may show that a deformable inflatable breakwater is better at dissipating wave energy than a rigid-body breakwater.

Lastly, either a scale or a full-scale model of a moored breakwater may be constructed to experimentally, rather than analytically, investigate the responses of a breakwater. The experimental results from the physical models may be compared with the results from this study and other studies conducted in the future.

## References

- Ansari, K.A. (1980). "Mooring with Multicomponent Cable Systems." *Journal of Energy Resources Technology*, Vol. 102, pp. 62-69.
- Archilla, J.C. (1999). "Three-Dimensional Nonlinear Dynamics of a Moored Cylinder to be Used as a Breakwater." *M.S. Thesis*, Virginia Polytechnic Institute and State University, Blacksburg, Virginia.
- Bathe, K.J. (1982). *Finite Element Procedures in Engineering Analysis*, Prentice-Hall, Englewood Cliffs, New Jersey.
- Bernitsas, M. and Garza-Rios, L.O. (1996). "Effect of Mooring Line Arrangement on the Dynamics of Spread Mooring Systems." *Journal of Offshore Mechanics and Arctic Engineering*, Vol. 118, pp. 7-20.
- Brekke, J.N. and Gardner, T.N. (1988). "Analysis of Brief Tension Loss in TLP Tethers," *Journal of Offshore Mechanics and Arctic Engineering*, Vol. 110, 43-47.
- Bürger, W. (1984). "The Yo-yo: A Toy Flywheel." *American Scientist*, Vol. 72, pp.137-142.
- Carver, R.D., Markle, D.G., Dubose, W.G., and Jensen, R.E. (1987). "Slope Float Breakwater Study, Oregon Inlet, North Carolina," Technical Report CERC 87-5, U.S. Army Corps of Engineers, Coastal Engineering Research Center, Vicksburg, Mississippi.

Chaplin, C. and Del Vecchio, C. (1992). "Appraisal of Lightweight Moorings for Deepwater." *24<sup>th</sup> Offshore Technology Conference*, Houston, Texas, Vol. 3, pp. 189-198.

Dercksen, A. and Hoppe, L.F.E. (1994). "On the Analysis of Mooring Systems using Synthetic Ropes." *26<sup>th</sup> Offshore Technology Conference*, Houston, Texas, Vol. 3, pp. 255-263.

DeYoung, B. (1978). "Enhancing Wave Protection with Floating Tire Breakwaters." Information Bulletin 139, Sea Grant I, New York State College of Agriculture and Life Sciences, Ithaca, New York.

Driscoll, R. and Biggins, L. (1993). "Passive Damping to Attenuate Snap Loading on a ROV Umbilical Cable." *Oceans'93*, IEEE, New York, Vol. I, p. 409.

Driscoll, R. and Nahon, M. (1996). "Mathematical Modeling and Simulation of a Moored Buoy System." *Oceans'96*, IEEE, New York, Vol. I, p. 517-523.

D'Souza, R.B., Dove, P.G.S., and Kelly, P.J. (1993). "Taut Leg Spread Moorings: a Cost-Effective Stationkeeping Alternative for Deepwater Platforms." *25<sup>th</sup> Offshore Technology Conference*, Houston, Texas, Vol. 3, pp. 41-55.

Gaythwaite, J.W. (1987). "Floating Breakwaters for Small Craft Facilities." *Journal of the Boston Society of Civil Engineers Section/ASCE*, Vol. 2, No. 1, pp. 89-108.

Goeller, J.E. and Laura, P.A. (1971). "Analytical and Experimental Study of the Dynamic Response of Segmented Cable Systems." *Journal of Sound and Vibration*, Vol. 18, pp. 311-329.

Hales, L.Z. (1981). "Floating Breakwaters: State-of-the Art Literature Review," Technical Report No. 81-1, U.S. Army Corps of Engineers, Coastal Engineering Research Center, Fort Belvoir, Virginia.

Huang, S. and Vassalos, D. (1993). "A Numerical Method for Predicting Snap Loading of Marine Cables." *Applied Ocean Research*, Vol. 15, pp. 235-242.

Huang, S. and Vassalos, D. (1995). "Analysis of Taut-Slack Marine Cable Dynamics." *OMAE 1995*, Vol. I-B, ASME, New York, pp. 401-406.

IMSL MATH/LIBRARY (1991). "IVPAG/DIVPAG." *FORTTRAN Subroutines for Mathematical Applications*, Houston, Texas, pp. 755-771.

IMSL MATH/LIBRARY (1991). "ZREAL/DZREAL." *FORTTRAN Subroutines for Mathematical Applications*, Houston, Texas, pp. 943-948.

Irvine, H. M. (1981). *Cable Structures*, MIT Press, Cambridge, Massachusetts.

Johnson, L.W. and Riess, D.R. (1982). *Numerical Analysis*, 2<sup>nd</sup> ed. Addison-Wesley Publishing Company, Reading, Massachusetts.

Kelly, H. (1999). Discussion about Floating Breakwaters. Naval Facilities Engineering Command, Norfolk, Virginia, July 1999.

Laura, P.A. and Goeller, J.E. (1971). "On the Dynamic Behavior of a Cable System in a Recovery Operation." *Journal of the Acoustical Society of America*, Vol. 49, pp. 615-621.

Leonard, J.W. (1988). *Tension Structures: Behavior and Analysis*, McGraw-Hill, New York.

Liu, F.C. (1973). "Snap Loads in Lifting and Mooring Cable Systems Induced by Surface Wave Conditions." Technical Note N-1288, Naval Civil Engineering Laboratory, Port Hueneme, California.

Lo, A. (1982). *Nonlinear Dynamic Analysis of Cable and Membrane Structures*. Ph.D. Dissertation. Oregon State University, Corvallis, Oregon.

Mays, T.W. (1997). "Three-dimensional Analysis of Moored Cylinders used as Breakwaters." *M.S. Thesis*, Virginia Polytechnic Institute and State University, Blacksburg, Virginia.

Mays, T.W., Plaut, R.H., and Liapis, S.I. (1999). "Three-dimensional Analysis of Submerged, Moored, Horizontal Rigid Cylinders used as Breakwaters." *Ocean Engineering*, Vol. 26, pp. 1311-1333..

McCartney, M. (1985). "Floating Breakwater Design." *Journal of Waterway, Port, Coastal, and Ocean Engineering*, Vol. 111, pp. 304-318.

Meirovitch, L. (1970). *Methods of Analytical Dynamics*, McGraw-Hill, New York.

Milgram, J.H., Triantafyllou, M.S., Frimm, F., and Anagnostou, G. (1988). "Seakeeping and Extreme Tensions in Offshore Towing." *The Society of Naval Architects and Marine Engineers Transactions*, Vol. 96, pp. 35-72.

Niedzwecki, J.M. and Thampi, S.K. (1991). "Snap Loading of Marine Cable Systems." *Applied Ocean Research*, Vol. 13, pp. 2-11.

Patel, M.H., Lyons, G.J., and Wilne, T. (1994). "Hydroelasticity of Tensioned Buoyant Platform Tethers at Low and Negative Tension." *Hydroelasticity in Marine Technology*, O. Faltinsen et al., eds., A.A. Balkema, Rotterdam, pp. 17-30.

Patel, M.H. and Park, H.I. (1995). "Tensioned Buoyant Platform Tether Response to Short Duration Tension Loss." *Marine Structures*, Vol. 8, pp. 543-553.

Plaut, R.H., Archilla, J.C., and Mays, T.W. (1999). "Snap Loading in Mooring Lines During Large Three-dimensional Motions of a Cylinder." Under review.

Scalzi, J.B., Podolny, W., Jr., and Teng, W.C. (1969). *Design Fundamentals of Cable Roof Structures*, United States Steel Corporation, Pittsburgh, Pennsylvania.

Shin, H. (1991). "Analysis of Extreme Tensions in a Snapping Cable." *Proceedings of the 1<sup>st</sup> International Offshore and Polar Engineering Conference*, Vol. II, pp. 216-221.

Skop, R.A. (1988). "Mooring Systems: a State-of-the-art Review." *Journal of Offshore Mechanics and Arctic Engineering*, Vol. 110, pp. 365-372.

Souza de Cursi, J.E. (1992). "Stress Unilateral Analysis of Mooring Cables." *International Journal for Numerical Methods in Engineering*, Vol. 34, pp. 279-302.

Suhara, T., Koterayama, W., Fukuzo, T., and Hiyama, H. (1981). "Dynamic Behavior and Tension of Oscillating Mooring Chain," *Offshore Technology Conference*, Houston, Texas, Vol. 2, pp. 415-425.

Synge, J.L. and Griffith, B.A. (1959). *Principles of Mechanics*, McGraw-Hill Book Company, Inc. 3<sup>rd</sup> ed. New York.

Szelangiewicz, T. (1996). "Loads in Mooring Lines of the Mooring Positioning System of a Vessel." *Proceedings of the Sixth International Offshore and Polar Engineering Conference*, Vol. II, pp. 233-240.

Tsinker, G. (1995). *Marine Structures Engineering: Specialized Applications*, Chapman and Hall, New York.

Vassalos, D. and Huang, S. (1996). "Dynamics of Small-Sagged Taut-Slack Marine Cables," *Computers and Structures*, Vol. 58, No. 3, pp. 557-562.

# Appendix A

## A.1 Other Types of Graphs

The data collected was analyzed to see what types of behavior the breakwater exhibited during its period in motion. The primary method of evaluating the response of the breakwater was to produce and examine several types of graphs. The trajectory and normal velocity before impact vs. time plots were primarily used in this investigation. However, several other plots were produced during the investigation and typical examples of these will now be discussed. The additional plots include:  $x$  vs. time,  $y$  vs. time, and  $\theta$  vs. time for time histories;  $\dot{x}$  vs.  $x$ ,  $\dot{y}$  vs.  $y$ , and  $\dot{\theta}$  vs.  $\theta$  for phase diagrams; impact Poincaré plots; and total and kinetic energy vs. time plots. The following plots were produced from the standard conditions of the point-mass breakwater (PMBW) and rigid-body breakwater (RBBW) under free motions, as seen in Chapters 3 and 5, respectively.

The time histories describe the position of the breakwater during the time in which it moves about the region. A typical time history of the horizontal position  $x$  of the breakwater (Fig. 2.2) may be seen in Fig. A.1. In this plot it may be seen that the position is oscillating about the  $x=0$  axis as expected from the geometrical configuration of the breakwater and it settles down to zero with time. Also, this plot is piecewise linear in nature because of the linear analytical solution developed in Chapter 2. A typical time history of the vertical position  $y$  of the breakwater may be seen in Fig. A.2. In this plot it may be seen that the position stays above the  $y=0$  axis as required and settles to zero with time. Also, this plot is piecewise quadratic in nature because of the quadratic analytical solution developed in Chapter 2. Time history plots of the rotation angle  $\theta$  of the breakwater may be seen in Chapters 5 and 6.

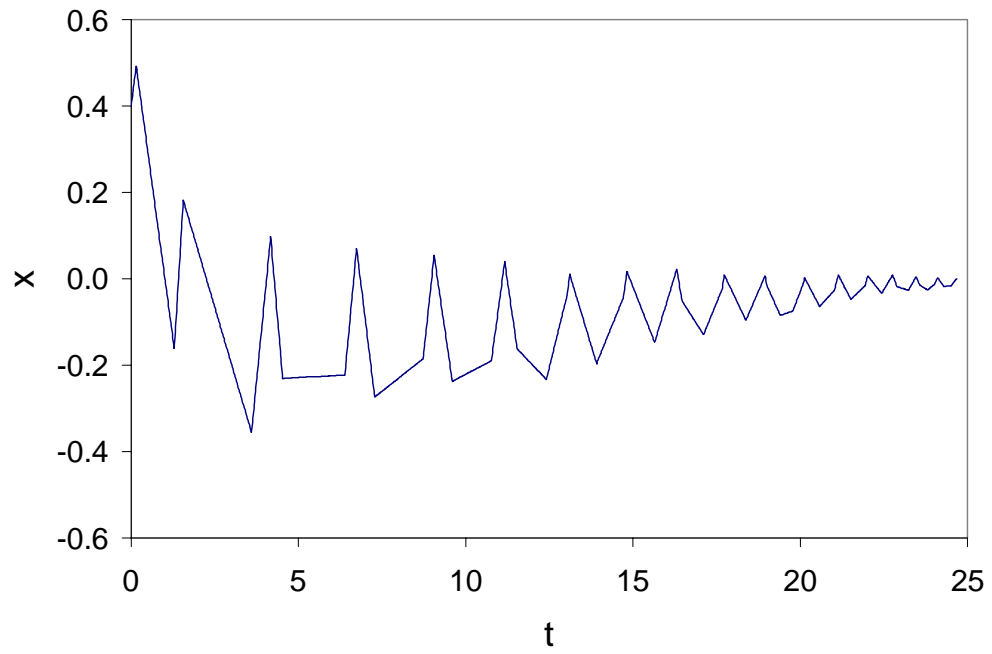


**Fig. A.1.  $x$  vs.  $t$ , PMBW Standard Case**

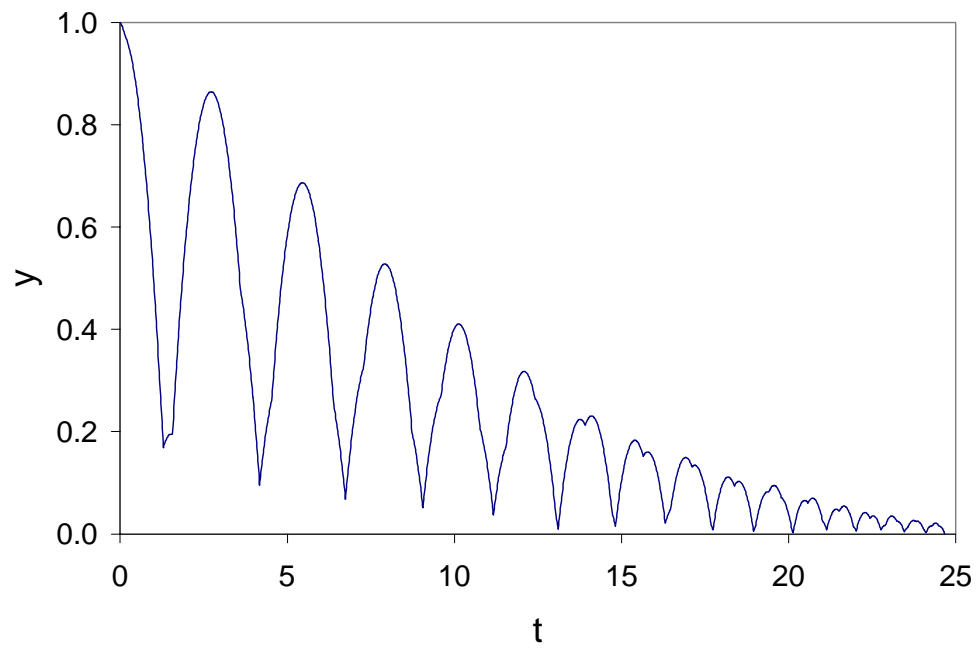


**Fig. A.2.  $y$  vs.  $t$ , PMBW Standard Case**

A phase plane plot is a plot where the velocity in one direction is plotted against the position in the same direction. These plots were produced for the  $x$ ,  $y$ , and  $\theta$  velocities and displacements. Figures A.3 and A.4 are the  $x$  and  $y$  phase plane plots for the standard case conditions of the PMBW under free motions from Chapter 3, respectively. Since rotations are not involved in the point-mass problem, Fig. A.5 was used to show a rotation phase plane plot and was produced from the standard case of the RBBW under free motions of Chapter 5.

The phase plane plot of the  $x$  velocity versus  $x$  position may be seen in Fig. A.3. It may be seen that in this plot the values of  $x$  and  $\dot{x}$  are decreasing towards the middle of the plot which occurs when the breakwater settles its motions. This is because as time goes on, energy is dissipated and the position and velocity go to zero. The position and velocity in the  $x$  direction may be either positive or negative as defined by the problem formulation, which explains why the motions go towards the center of the graph. The abrupt vertical jumps in the graph indicate that the breakwater has impacted a boundary, and since it was assumed that the position of the PMBW does not change during an impact, the velocity changes sign and abrupt jumps appear. Between the jumps, the velocity  $\dot{x}$  is constant because of the analytical solution in Chapter 2. Similar jumps may be seen in the  $\dot{y}$  vs.  $y$  phase plane (Fig. A.4). In this case, though the velocity may be positive or negative, the position can only be positive because of the geometrical formulation of the problem, and thus the motion settles towards the center of the left side of the plot. The  $y$  position between impacts is quadratic with respect to the velocity  $\dot{y}$  because of the analytical solution.

The phase plane plot of  $\dot{\theta}$  versus  $\theta$  (Fig. A.5) is similar to Fig. A.3. This plot should settle towards the center, but Fig. A.5 shows that the plot stops before it reaches the center of the plot where position and velocity both equal zero. This is because at this

point  $g_1=g_2=0$  but the breakwater is rotated and not settled to the equilibrium state. However, in the RBBW under free motions it was assumed that the breakwater would go into a rocking motion at this point and then settle to the bottom of the region. Again, the vertical jumps are caused by the position not changing during an impact and the velocity changing direction, and the analytical solution for  $\theta$  is linear between impacts so that  $\dot{\theta}$  is constant.

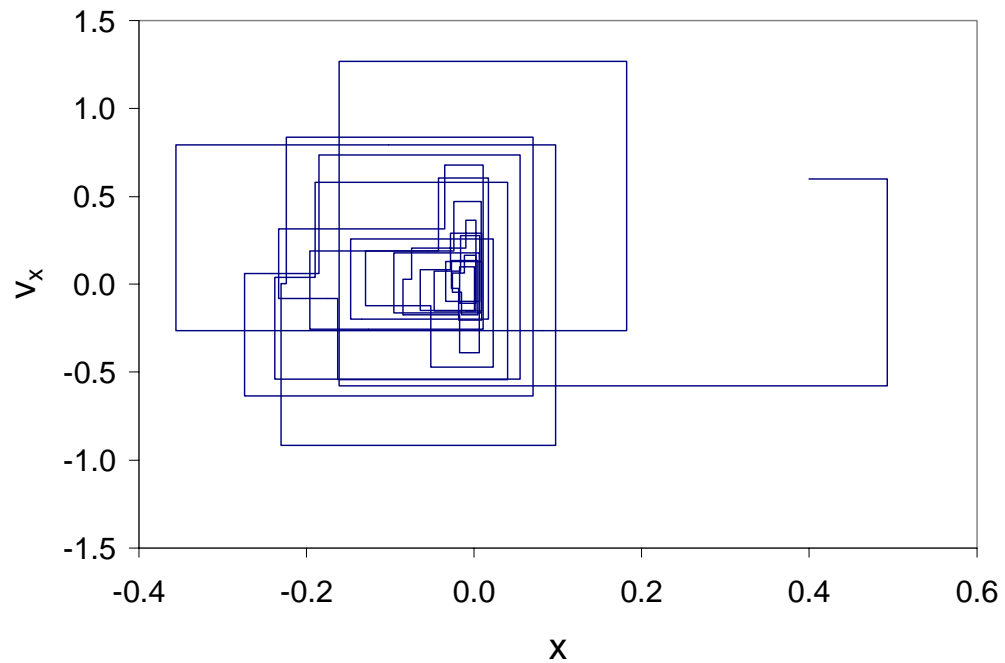


**Fig. A.3.  $v_x$  vs.  $x$ , PMBW Standard Case**

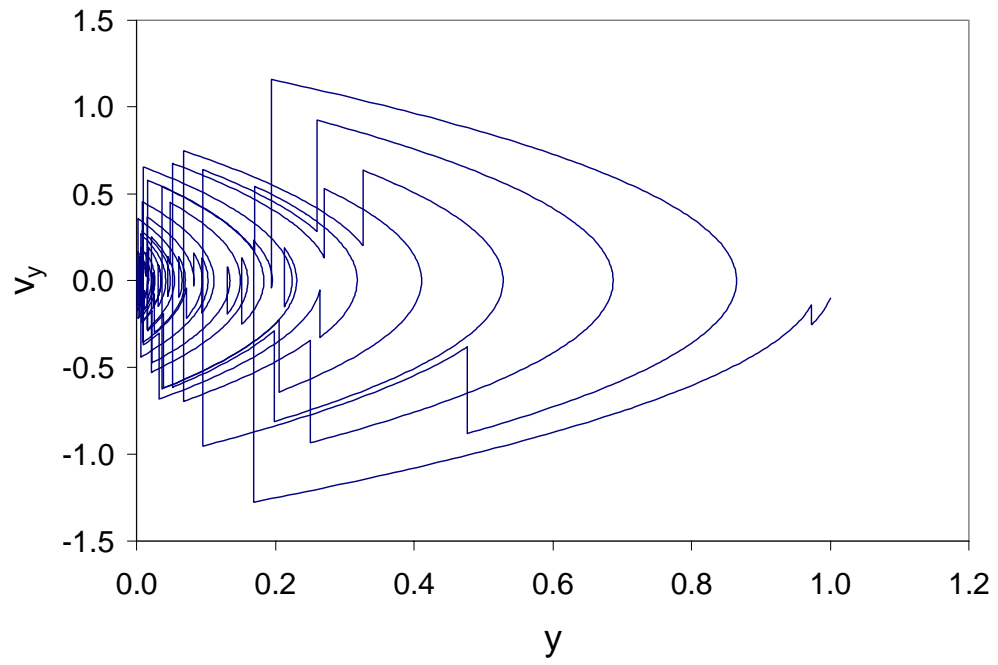


**Fig. A.4.  $v_y$  vs.  $y$ , PMBW Standard Case**

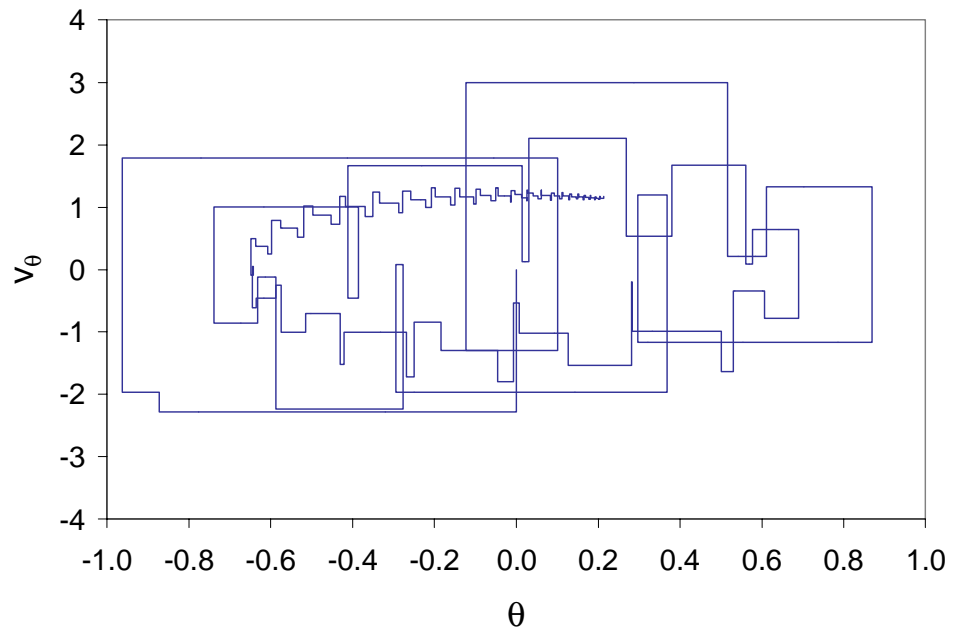


**Fig. A.5.  $v_\theta$  vs.  $\theta$ , RBBW Standard Case**

An impact Poincaré plot is a plot of the velocity just before impact versus the position at the time of impact. The impact Poincaré plot puts a dot corresponding to the impact velocity versus the position in the  $x$ ,  $y$ , and  $\theta$  directions. The  $x$  and  $y$  impact Poincaré plots for the free motion PMBW problem with standard conditions are shown in Figs. A.6 and A.7, respectively. The  $\theta$  impact Poincaré plot for the free motion RBBW problem with standard conditions is shown in Fig. A.8. Corresponding to Fig. A.5, the dots do not converge to the point  $(\theta, v_\theta)=(0,0)$ . In the plots, as time goes on, the impact velocities tend to decrease in magnitude, and  $x$  and  $y$  approach zero. This is indicated by the dots clustering towards the zeros on the plots.

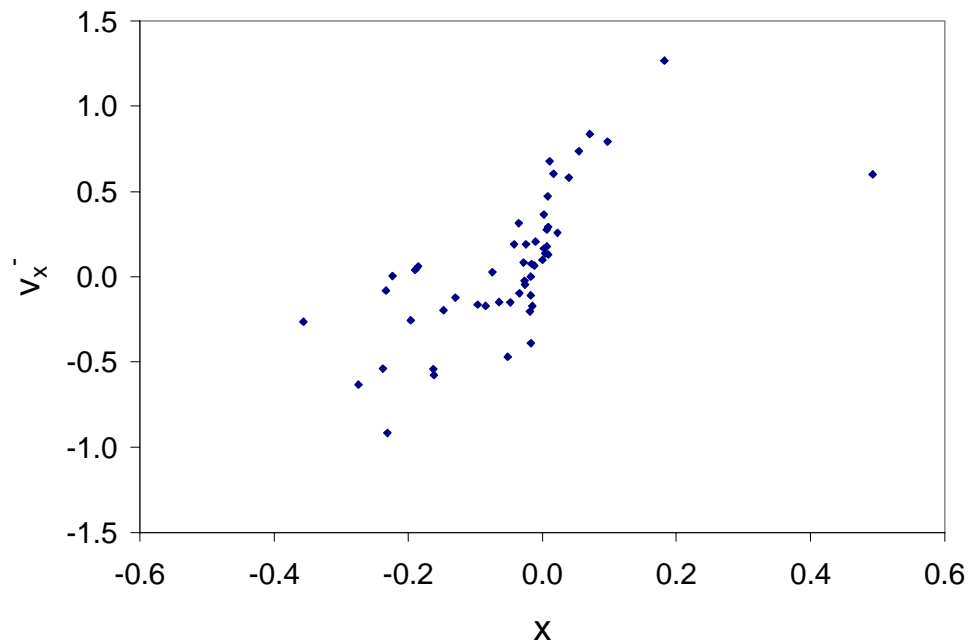


**Fig. A.6. x Impact Poincaré Plot, PMBW Standard Case**

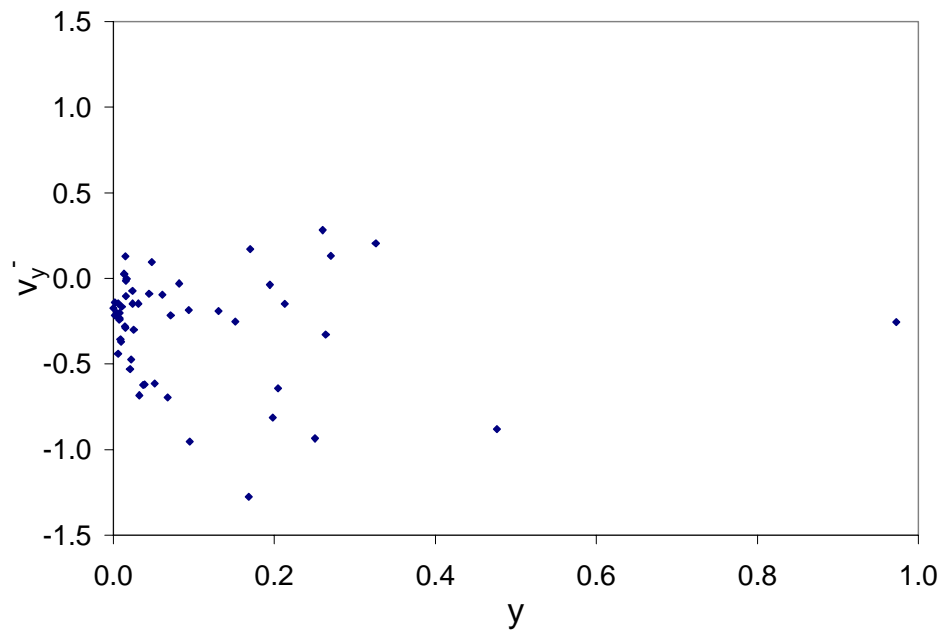


**Fig. A.7.  $y$  Impact Poincaré Plot, PMBW Standard Case**

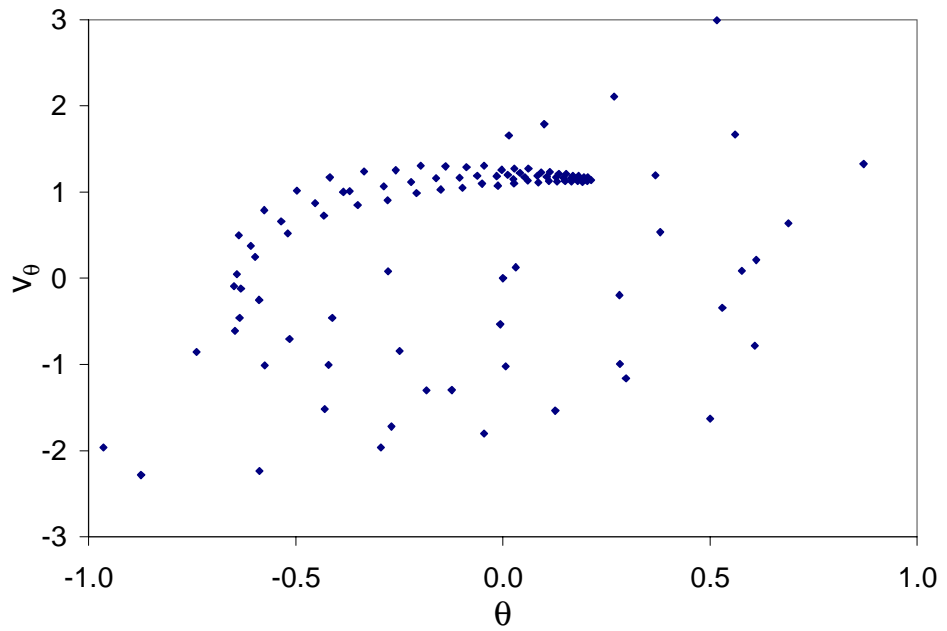


**Fig. A.8.  $\theta$  Impact Poincaré Plot, RBBW Standard Case**

The total energy and the kinetic energy were both plotted against time for the cases analyzed in this investigation and are shown in Figs. A.9 and A.10, respectively. These are typical plots where the energy in the system is decreasing as the breakwater dissipates energy during impacts and starts to settle to the equilibrium state. Figures A.9 and A.10 were produced from the data collected from the free motion PMBW standard case and exhibit this decreasing nature.

The plots of the cases where forcing was introduced were very similar to the plots discussed here when the motions tended to settle. The motion between impacts is not linear or quadratic because of the introduced sinusoidal forcing. The plots discussed here show the typical nature of the response of the breakwater during its motions.

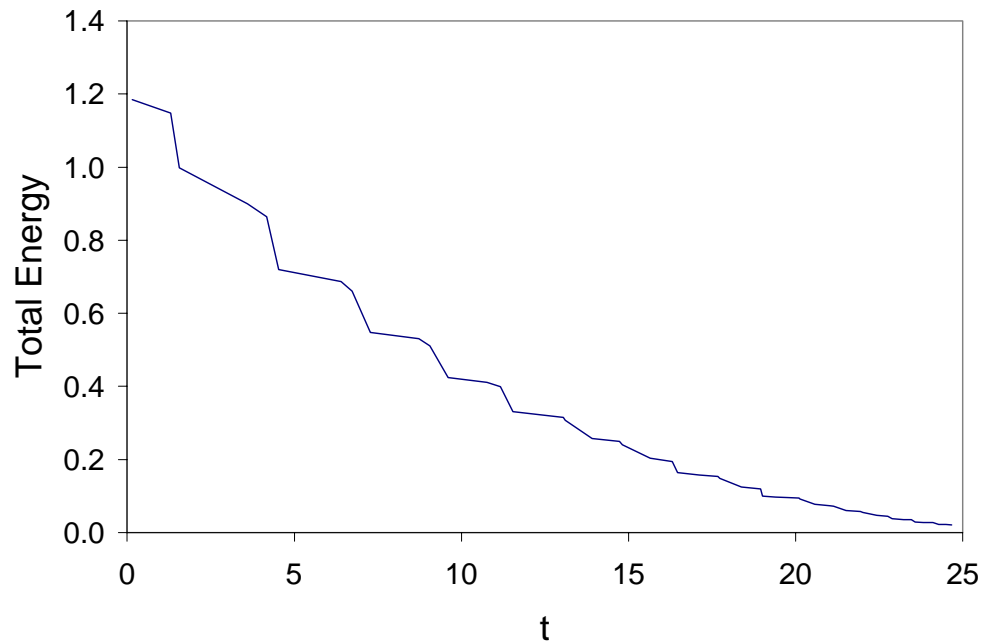


**Fig. A.9. Total Energy vs. t, PMBW Standard Case**

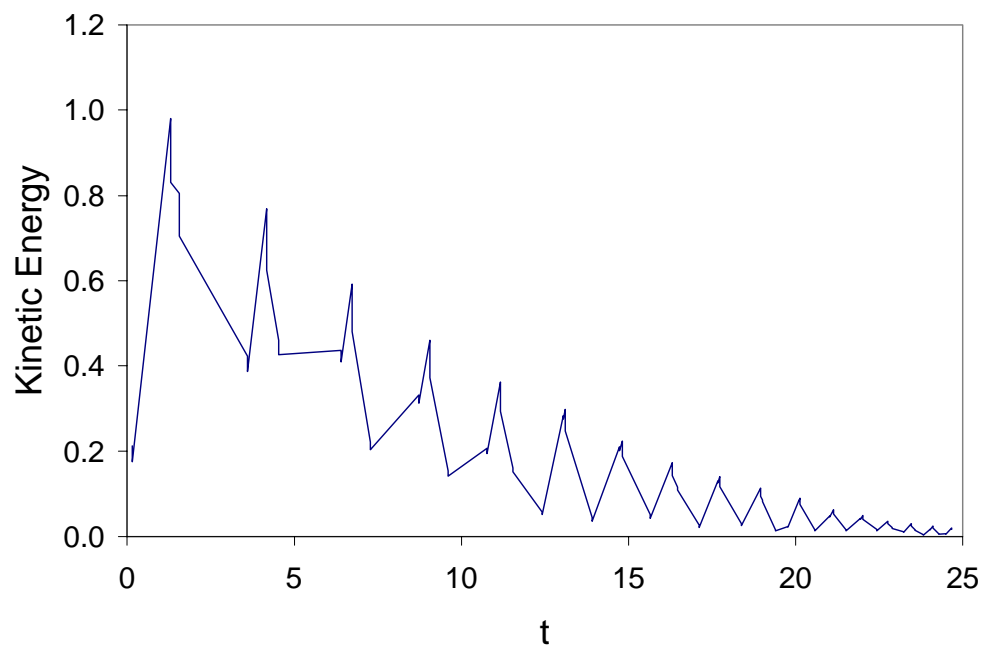


**Fig. A.10. Kinetic Energy vs. t, PMBW Standard Case**

## Vita

Anthony Lee Farmer was born on December 5, 1975 in Portsmouth, Virginia. He lived in Chesapeake, Virginia, attending Western Branch High School, until 1991 and then moved to Orange County, Virginia. In June of 1994 he graduated from Orange County High School in Orange, Virginia. He attended Piedmont Virginia Community College in Charlottesville, Virginia until 1996 when he transferred to Virginia Polytechnic Institute and State University. While attending Virginia Tech, he completed his Bachelor of Science Degree in May of 1998. He continued his engineering education by receiving a Master of Science in Civil Engineering degree at Virginia Tech in December of 1999. Shortly after finishing his graduate studies, Anthony will begin working for the Naval Facilities Engineering Command in Norfolk, Virginia.

---

Anthony L. Farmer